ELECTRON-OPTICAL CAMERAS WITH ULTRAHIGH TIME RESOLUTION IN ONE AND TWO SPATIAL DIMENSIONS

Richard Thomas Eagles BSc, ARCS.

A Thesis submitted for the degree of Doctor of Philosophy of the University of London and for the Diploma of Membership of Imperial College

Optics Group
Blackett Laboratory
Imperial College of
Science and Technology
London SW7 2BZ

September 1986

Abstract

A prototype electron-optical image converter vacuum tube, utilizing a sweep/compensation framing technique, has been implemented into an experimental picosecond framing camera; the Picoframe I. Picoseond risetime voltage gradients derived from laser illuminated photoconductive element devices have been employed in operating the camera in a single frame mode. Framed images of 130-200ps duration, demonstrating a dynamic spatial resolution of up to 10 lp/mm at the photocathode have been observed.

Framing operation using the voltage-gradients produced by a series chain of avalanche transistors has yielded single framed image durations of ~200ps and a dynamic spatial resolution of 7 lp/mm (at photocathode). A shorted stub transmission line pulse forming network has been used to generate ~2ns (FWHM) kilovolt amplitude triangular waveforms, facilitating double sweep operation of the Picoframe I. Doublet framed images each exposed for ~200ps and temporally separated by 1.2ns, with a dynamic spatial resolution of $\leq$ 10 lp/mm (at photocathode) were recorded in this mode.

A theoretical study of the paths followed through the Picoframe design by the energetic secondary electrons emitted from an x-ray sensitive photocathode has been made. Deficiencies in the imaging capabilities of the design under such conditions are revealed, and a modified design compatible with imaging x-ray photocathode secondary electrons is presented.

The performance of a repetitively operating Photochron IV-M streak camera is discussed. Hypershort optical pulses from a colliding pulse mode-locked CW ring dye laser were observed with a temporal resolution of 2.3ps. The contributory factors responsible for degrading the temporal resolution from the theoretically predicted value of ~0.5ps are reviewed.

CONTENTS

Abbreviations

ICHSP	International Congress on High Speed Photography
ICHSPP	International Congress on High Speed Photography and Photonics
SPIE	Society of Photo-Instrumentation Engineers
Adv EEP	Advances in Electronics and Electron Physics

CHAPTER 1

An Introduction to streak and framing cameras

1.1 General Introduction

The generation of ultrashort [1] and hypershort [2,3,4] optical pulses by the phase-coupling of laser cavity modes (mode-locking) is now an established procedure [5]. Pulses as short as 27fs duration have been generated directly by careful control of the cavity parameters in a colliding pulse mode-locked (CPM) dye laser [6,7]. Applying extracavity pulse compression, using a combination of group velocity dispersion and self phase modulation in optical fibres, optical pulses as short as 8fs have been produced [8].

The ability to generate such optical pulses has provided a valuable tool to probe many ultrafast physical processes. New fields of investigation now require diagnostic instruments capable of providing information on a picosecond timescale [9]. In many instances where the temporal-evolution of intensity in a laser induced reaction or pulse is of prime interest, and not the specific spatial origin of the intensity, one-dimensional imaging is sufficient. In other cases the spatial distribution of intensity in a reaction is an important parameter and a two-dimensional time-resolved diagnostic is therefore required. Two important linear-response diagnostic instruments capable of time-resolved imaging on a picosecond timescale in one and two spatial dimensions are the electron-optical streak and framing camera respectively. The design, operation and evaluation of state-of-the-art instrumentation in this field forms the subject matter of this thesis.

1.2 Introduction to the electron-optical streak camera

One of the most commonly used linear methods of recording the temporal intensity profile of an optical pulse is the photodiode/oscilloscope combination. Fast photodiodes typically have a risetime of $\leq$ 20ps [10] and modern fast real-time oscilloscopes a risetime of $\sim$50ps (direct access Tektronix 7104), providing an overall resolution of around 55ps. If the luminous event is repetitive, as in the case of a CW mode-locked laser, a sampling technique may be employed. Commercial sampling heads have a resolution of $\leq$ 25ps (Tektronix S4) yielding an overall temporal resolution of around 35ps.

A dramatic improvement in temporal resolution is achieved by utilizing non-linear optical effects [11] to generate correlation functions. These include; two photon fluorescence [12], three photon fluorescence [13], second harmonic generation (SHG) [12] and third harmonic generation [14]. Autocorrelation techniques [15] based on SHG have demonstrated excellent temporal resolution into the femtosecond regime [16]. Unfortunately the correlation function yielded by all these techniques is always symmetric regardless of the input pulse profile. Thus unambiguous determination of the intensity profile and duration is prohibited. However these non-linear techniques currently represent the only means of measuring the hypershort femtosecond pulses now being generated.

The only currently available linear diagnostic instrument permitting unambiguous interpretaion on the picosecond and subpicosecond timescale is the electron-optical streak camera. The one-dimensional imaging characteristics of the instrument allows the simultaneous recording of intensity profile and

spatial [17] or spectral [18] information along its spatial axis (slit). As a device its superior sensitivity, demonstrated by fluorescence studies [19], linearity of response and wide spectral coverage (IR/visible/vuv/x-ray) [20,21] through the choice of photocathode, has enabled it to find many applications as a picosecond diagnostic. These include; direct duration measurement of mode-locked laser pulses [22], time-resolved spectroscopic studies of molecular dynamics in liquids [23] and optical excitations in solids [24], time-domain measurements of pulse propagation in optical fibres [17], investigation of semiconductor diode lasers [25], temperature [26] and viscosity [19] dependence of excited state dye fluorescence lifetimes, studies of biological samples [27] and as a laser produced plasma diagnostic in laser-induced fusion research [28].

Instruments possessing picosecond resolution have been reported for some years now. However until the latest generation of femtosecond image tubes with sub-picosecond resolution (~0.8ps) had only been reported for illumination close to the photocathode cut-off frequency [29,30]. The Photochron IV femstosecond single-shot streak camera has demonstrated a deconvolved temporal resolution of 700fs [31] and a recently reported magnetically focused streak tube has claimed a temporal resolution of 440fs [32].

1.2.1 Principle of operation

Based on a proposal by Zavoiski and Franchenko [33] the operating principle of the electron-optical streak camera is illustrated in fig. 1.1. An optical signal under study is incident upon a narrow slit that is imaged via a relay lens onto the photocathode of the instrument.

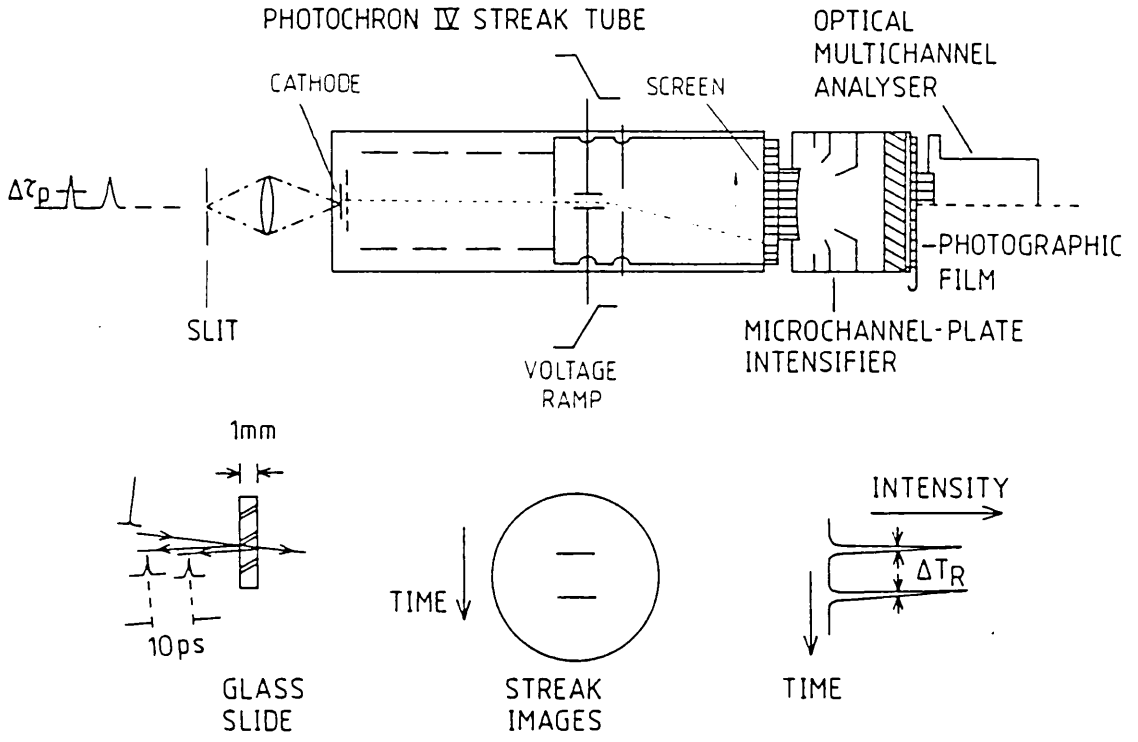

Fig. 1.1 Operating principle of the electron-optic streak camera

Liberated photoelectrons are accelerated and focused by an electron-optic lens [34] onto a luminescent phosphor screen where the electron signal is reconverted into an optical signal for subsequent recording. A linear time-varying voltage ramp applied to a pair of deflector plates inside the instrument, sweeps the slit image across the screen. Provided the photocathode response is linear the spatial extent of the streaked image on the phosphor is directly related to the duration of the incident light signal. For calibration purposes an ultrashort light pulse is often split into two equal components, and a known path difference introduced between them before being incident on the camera. The streaked output then consists of two replica pulses of known temporal separation.

1.2.2 Spatial resolution

In common with all imaging systems the image quality in an electron-optic tube is limited by the geometrical aberrations of the lens. The most important of these are astigmatism and field curvature [34]; as image tubes generally incorporate a planar phosphor screen any curvature of the image plane will degrade the spatial resolution. Modern computer aided design techniques [35] have made it possible to minimize these effects and image tubes exhibiting better than 50 line pairs per millimeter (lp/mm) static spatial resolution at photocathode are typical [36]. Most current streak tubes employ rotationally symmetric electrostatic focusing [36,37,38]. Although magnetic focusing has generally been more popular in the past, it has recently been adopted in a new tube design [32]. A quadrupolar lens has been reported [39] which permits independent control of the focusing in the spatial and temporal dimensions. An x-ray sensitive tube employing this type of electron lens has a predicted temporal resolution of 2ps [40], although this has still to be experimentally demonstrated.

High intensity irradiation of the photocathode has been shown to result in degradation of the spatial resolution [41], an effect often referred to as 'blooming'. It has been proposed that this is caused by a potential perturbation across the surface of the cathode as a result of the high photocurrent extracted [42]. Depending on the cathode type either a diverging or converging microlens is produced causing the image to become defocused at the screen [43]. The effect is reduced by limiting the photocurrent drawn from the photocathode by provision of a high gain intensification stage. There is some evidence to suggest the phenomenon may be minimized by fabrication of low surface resistivity

photocathodes (< 10Ω/square) [41], so reducing the potential perturbation for a given photocurrent.

1.2.3 Temporal resolution

The ultimate temporal resolution of electron-optical chronoscopy is governed by the photocathode response time. General theoretical considerations have indicated that for the multialkali cathodes commonly employed the inherent response time of this photoeffect should be $\leq 10^{-14}$s [44]. A more practical temporal resolution limitation results from the fact that due to pair production and lattice scattering [45], emitted electrons emerge from the photocathode with a small but finite energy distribution. This is typically ~0.6eV for multi-alkali type photocathodes not illuminated close to threshold or cut-off. The absolute degree of energy spread is a function of the particular photocathode, illumination wavelength, cathode workfunction and other cathode properties dictated by the type and method of processing. This is in effect an electron chromatic aberration which, unlike in conventional glass optics, cannot be completely eliminated by lens design.

The result of this chromatic aberration is that electrons emerging simultaneously from a common point on the photocathode do not exhibit identical transit times to their respective image point; an effect termed 'temporal dispersion'. Consequently upon application of a linear voltage ramp to the deflectors the electrons will be deflected to slightly different screen positions as later electrons experience a greater deflection. Provided the camera slit is narrow and can be ignored (<<dynamic spatial resolution of the camera) this will result in a slit image of width δx. For a given sweep speed v this will result in a

contribution T to the temporal resolution given by:

$$T = \frac{\delta x}{v}$$

For low sweep speeds approaching zero the temporal resolution is obviously poor, for extremely high sweep speeds deflection distortion effects [35] degrade the spatial resolution and again the temporal resolution is poor. Between the two extremes there exists an optimum sweep speed [35,46] for maximum temporal resolution.

In general the finite spread in photoelectron emission energy cannot be eliminated and it will degrade the temporal resolution of the instrument. Early workers in this field [22] realising that the detrimental effects of temporal dispersion accrued mainly in the vicinity of the cathode, introduced a high extraction field in that region to rapidly accelerate the photoelectrons, thus minimizing the effect. This facility, generally provided by a high potential mesh electrode in close proximity to the cathode, is commonly employed in all picosecond streak tubes today. Although this technique yielded a dramatic improvement in temporal resolution (30ps to $\leq$ 2ps) further resolution enhancement requires that the temporal dispersion in the whole imaging system, not just the cathode-mesh region, be minimized [47].

In the special case of illumination close to the long wavelength cut-off of a photocathode the energy distribution of the emitted photoelectrons is low. Under such conditions streak cameras exhibit their optimum temporal resolution. A Photochron II camera activated with an S20 photocathode (sensitivity 0.4 - 0.8 μm) and illuminated by 752nm wavelength light exhibited a deconvolved temporal resolution of 0.8ps [30].

The intrinsic response time of an electron-optical streak camera, generally referred to as the instrumental function (ΔT_{inst}), is limited by the electron temporal dispersion (due to the initial energy distribution of the emitted photoelectrons) and by the inherent aberrations of the imaging electron-optics and deflection system. These two components are termed the physical (ΔT_{phys}) and technical (ΔT_{tech}) temporal resolution respectively. The former is composed of the individual contributions to the temporal dispersion throughout the imaging region (i.e. cathode-mesh region contribution, focusing region contribution ... etc). The latter is defined by the time taken to sweep the electron beam through one resolution element at the screen i.e.,

$$\Delta T_{tech} = \frac{1}{\xi v}$$

where v is the sweep speed and ξ is the dynamic spatial resolution in the streak direction. Both referred to the screen.

In the past the instrumental function of a streak image tube has been estimated by combining together these contributory factors by application of the Guassian approximation [22,48], usually in the form

$$\Delta T_{inst} = \sqrt{(\Delta T_{phys})^2 + (\Delta T_{tech})^2}$$

Under the approximation all the individual components are assumed to be discrete, quasi-independent contributions of equal weight. Although this has been a useful approximation it has been found insufficient to describe fully the instrumental function of sub-picosecond tube designs [49]. Thus a more elegant, physically representative Modulation Transfer Function method (see section 5.2.3) has been developed. Experimentally the instrumental

function is usually determined by evaluating the FWHM response of the instrument to a delta function intensity input pulse [50].

1.2.4 Time resolution limited dynamic range

When analysing picosecond and femtosecond optical phenomena with an electron-optical streak camera to achieve a recordable image intensity significant photocurrents must be drawn from the photocathode. Consequently current densities of $\sim$100mA/cm^2 can exist inside the tube [51]. It has been observed [45,51,52] that under such conditions the temporal resolution deteriorated despite good spatial resolution being maintained along the slit. (At very high input intensities photocathode effects do degrade the spatial resolution, see section 1.2.2). The range of intensity over which the degradation in temporal resolution remains within acceptable limits is referred to as the time resolution limited (TRL) dynamic range.

The lower intensity limit of the dynamic range is dictated by the noise level of the system. The upper intensity limit is defined [53] to occur when the measured pluse duration (T_m) becomes 20% larger than the duration of the input pulse (T_i), within the limitations of the camera resolution. TRL dynamic range is then defined as the ratio of the upper and lower intensity limits:

$$\text{TRL dynamic range} = \frac{I(T_m = 1.2T_i)}{I_{noise}}$$

It is well established that the TRL dynamic range is a function of incident pulse duration [45]. The shorter the incident pulse the greater the photocurrent drawn from the photocathode and the lower the dynamic range. Experimental evaluation of the

dynamic range of a number of different streak tubes has been undertaken by a number of workers [45,54-57], but with poor consistency in their results. A number of theories [51,58,59] based on space charge effects in or near the photocathode have failed to provide a complete description of the phenomenon.

A recent extensive theoretical analysis [60] of space charge effects over the entire imaging region for the Photochron family of streak tubes has demonstrated good agreement with observation. The mode of temporal broadening may be understood by consideration of the electron packet emitted when a picosecond light pulse is incident on a narrow slit focused at the photocathode. Since the spatial extent of the packet is only a few microns Coulombic repulsion will tend to accelerate the leading electrons but retard the trailing ones, causing the packet to expand spatially. At the deflectors this spatial spread is transformed into a temporal spread at the phosphor screen. The effect becomes progressively worse with higher current densities.

This detailed theoretical analysis confirmed that temporal broadening accumulates over the whole electron path through the image tube and not just in the vicinity of the cathode as had been previously suggested [59]. It is notable, however, that space-charge temporal broadening is most significant in regions of low potential where the electrons are moving slowly. Hence this effect is more severe in the vicinity of the cathode region and in other low potential regions.

Recent results have shown [61] that the use of a fine-mesh electrode in close proximity to the photocathode does not seem to have any significant detrimental effect upon the lower limit

of the dynamic range as had been reported earlier [62]. However the method of photocathode activation does seem to affect the dynamic range to some extent [61]. In-situ processed photocathodes often results in alkali metal contamination of electrode surfaces inside the tube which leads to a higher noise level and hence reduced TRL dynamic range. Remotely processed photocathodes do not result in this type of contamination and are to be preferred as lower noise systems.

1.2.5 Dynamic slit curvature

At high sweep speeds curvature of the slit image has been noted [51]. This effect, known as either 'dynamic slit curvature' or 'temporal distortion', results from the difference in time of flight between on and off axis electrons emitted from the photocathode. Off-axis electrons take longer to arrive at the sweep deflectors and hence experience a larger deflection. The further off-axis an electron is emitted the greater this effect will be. Hence off-axis electrons suffer increased deflection and strike the phosphor screen further along the time axis resulting in a curved image. The main causes of this transit time difference are:

(1) The physical distance travelled by off-axis electrons is slightly longer than that for on-axis electrons.

(2) Particularly in the initial stages of the focusing region electrons emitted on-axis reach a particular velocity earlier than their off-axis counter-parts as they intersect the equipotential lines earlier.

These effects are illustrated in fig.1.2 for a three cylinder electron lens. Effect (2) becomes less significant as the

electrons approach the anode due to the closely spaced axial potentials in that region being virtually normal to the axis.

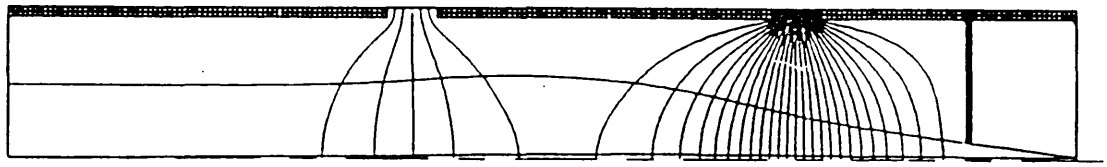

Fig.1.2 On and off axis electron trajectories

The effect of dynamic slit curvature can be detrimental to the temporal resolution particularly when a linear image sensor is employed as a read out device (see section 1.2.8). These devices consist of a series of closely spaced adjacent sensors, hence a curved slit image might cover more sensor elements than would be the case for a linear image. This would result in broadening of the recorded pulse-width. It is common practice to limit this effect by restricting the spatial extent of the camera slit, although this inevitably results in some degradation of the signal-to-noise ratio [45].

Dynamic slit curvature may be minimized and theoretically eliminated by equalising the time of flight for on and off axis photoelectrons. Two basically similar approaches have been investigated. Kinoshita et al [63] have designed and fabricated an image tube incorporating a concave photocathode in place of the more common planar variety. The radius of curvature is calculated such that the off-axis electrons do not have as far to travel, thus reducing their time of flight. This tube has demonstrated a temporal resolution of 2ps without noticeable image curvature. However, since the mesh electrode remains planar the cathode-to-mesh electric field is no longer uniform. A more elegant approach

incorporating a curved cathode and mesh configuration has been reported by Niu [64]. A prototype version of this tube has a reported temporal resolution of 2.7ps without apparent temporal distortion [65]

1.2.6 Single-shot operation

When it is desirable to record an isolated optical transient the electron-optical streak camera may be operated in a single-shot mode. A single fast linear voltage ramp is applied to the sweep deflectors in synchronism with the luminous event. To minimize any undesirable space-charge effects, and so maintain dynamic range, the streak tube photocurrent is limited. It is then necessary to incorporate a high gain intensification stage (see section 1.2.9) to ensure recordable image intensities.

1.2.6.1 Generation of deflection voltage ramps.

To ensure optimal time resolution streak recording it is necessary to derive high speed linear voltage ramps. Since the phosphor screen of an image tube is typically about 50mm in diameter, at high sweep speeds the viewable time window might only correspond to a few hundred picoseconds. Thus reliable synchronisation of the voltage ramp is essential to ensure the optical event is recorded. Any temporal error in the generation of the voltage waveform is referred to as jitter, and this should always be much less than the available time window.

A variety of voltage ramp generations have been employed with single-shot streak camera systems. The laser triggered spark gap [51,66] can generate kilovolt pulses with ~150ps rise-times. Unfortunately the trigger jitter of around 1ns is intolerable and these devices are now rarely used. A kryton tube (EG & G KN22/B) can produce $\leq$ 8kV pulses rising in < 1ns, but again the jitter

is poor. Hybrid avalanche transistor/kryton circuits [67] show improved jitter characteristics of ~100ps but this is still relatively large. Modern avalanche transistor circuits [68] have recently demonstrated improvements in sweep speed and linearity with trigger jitters of around 20ps now commonly attainable. This performance combined with their ease of use makes them versatile and convenient sweep generators. Their action is described more fully in section 4.2.

The fastest source of voltage ramps currently available is the laser illuminated photoconductive element (Auston switch) [69]. These devices are capable of switching kilovolt pulses in a few ten's of picoseconds with picosecond jitter. This has ensured their application in picosecond streak cameras [70] and ultrahigh speed gated devices [71] a full discussion of these devices is presented in section 3.2.

1.2.7 Repetitive operation

Although single-shot streak cameras are ideally suited for operation with passively mode-locked pulsed lasers they do not offer the best interface for CW mode-locked lasers. It had been recognised as early as 1972 [51] that there were considerable advantages to be gained in terms of sensitivity and signal-to-noise ratio by synchronising the operation of a streak camera to a repetitive luminous event. In principle low intensity streaks (with correspondingly low photocurrents) resulting from low power laser pulses or low intensity laser induced fluorescence or luminescence, are superposed at the screen so accumulating a recordable image intensity. In such a scheme the temporal and spatial resolution capabilities of the instrument are retained although any jitter between the applied sweep voltage ramps and

the incident luminous phenomenon will limit the temporal resolution of the system.

Techniques for deriving the deflection voltage ramps for single-shot cameras are not suitable for repetitive operation due to their long recovery time. A convenient method by which a repetitive sequence of voltage ramps can be derived is to apply a high frequency ($\sim$100MHz) sinusoidal voltage to the deflectors of the image tube. The central half of the peak-to-peak amplitude departs for linearity by less than 5% and lasts for approximately 1/6th of the period. An illustration showing the principle of operation of a repetitively operating streak camera is presented in fig. 1.3

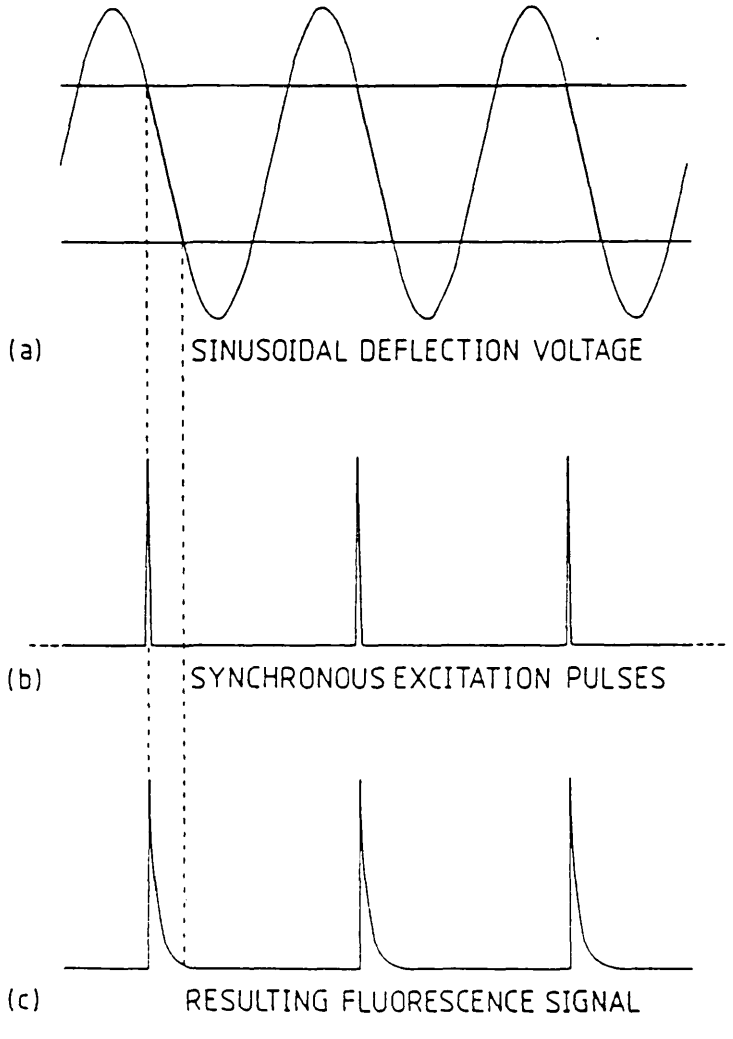

Fig.1.3 Principle of the repetitively operating streak camera

The advantages of repetitive operation are:

(1) Compatibility with CW mode-locked lasers.

(2) The accumulation of streak images often alleviates the requirement for further image intensification.

(3) The low-photocurrents associated with individual streak images minimizes any detrimental space-charge effects on the temporal resolution and dynamic range.

(4) Accumulation of images results in excellent signal-to-noise ratio characteristics.

(5) Photoelectronic read-out devices are readily employed to yield real-time monitoring.

The first experimental demonstration of a repetitively operating or 'Synchroscan' streak camera was reported by Hadland et al [72] in 1974. A modified Hadland 600 streak camera successfully imaged about ten superposed pulses from a mode-locked Nd:YAG oscillator. Since then repetitively operating streak cameras have been successfully employed in conjuction with both synchronously and passively mode-locked lasers [73]. To date the best temporal resolution demonstrated for a camera operating in this mode is 1.2ps [74]. This was achieved with a Photochron IIA camera system operating at 164MHz observing the pulses from a passively mode-locked ring dye laser. It should be noted that when a repetitively operating camera is employed with a synchronously pumped laser system the temporal resolution has been found to be degraded. This is thought to be due to interference effects between the laser mode-locking system and the camera deflection system or jitter in the synchronously pumped laser [73]. The operation of a repetitively operating Photochron IV-M streak camera is discussed in chapter 6.

When only intensity information is required a constant velocity circular scan [72] technique may be employed in place of the previously described linear scan. This is achieved by driving two pairs of orthogonally orientated deflectors in phase quadrature and has the advantage that initial synchronisation to the optical event is unnecessary as recording may start at any time. Streak recording does however necessitate the use of photographic film or specially designed photoelectronic read-out devices [75]. A circular scan Photochron IIC camera is currently being evaluated for implementation into a spaceborne laser ranging system [76].

1.2.8 Read-out devices

In the past the most commonly used streak recording medium was high speed photographic film. However this medium suffers from a number of disadvantages in that it requires chemical processing before being scanned by a microdensitometer to yield quantitative results. Additionally in the normal operating intensity range of a streak camera system, below the onset of detrimental space-charge effects, it forms the only system component to exhibit a non-linear response. Thus each film must be individually calibrated. Its use imposes a limitation on the dynamic range [45].

Increasingly photoelectronic read-out systems are being employed to provide linear real-time representation of streak image output. Considerable use has been made of vidicon [77] camera tubes. Basically, the operation consists of focusing an electron image of the observed optical scene (e.g. streak image) onto a charge-storage target. Luminous areas of the image cause local discharge of the target which is then detected by a slowly scanning electron beam. A number of such devices have been incorporated into streak camera read-out systems.

These include an image isocon TV tube interfaced to a microprocessor display unit [78] and silicon intensified target (SIT) cameras connected to either a one [80] or two [81] dimensional optical multichannel analyser (OMA). Solid state integrated photodiode arrays (Reticon^{TM}) have also been employed coupled to an oscilloscope for read-out purposes [82].

Advances in metal-oxide-semiconductor (MOS) technology has resulted in the development of charge coupled devices (CCD) [83]. These are essentially analogue shift registers composed of a number of gate electrodes deposited in sequence on a substrate material. Incident light quanta generate charge packets which collect under the electrodes to generate a replica of the variation in light intensity. These charge packets may then be read out by the application of suitable clocking waveforms to yield an analogue video signal.

Linear array CCD devices have been intimately coupled to the fibre-optic faceplates of streak image tubes and interfaced with signal processing electronics to provide compact real-time read-out systems [35]. A CCD device incorporated inside the vacuum envelope of a streak tube as an electron detector has been reported [85], this was only partially successful as the device suffered damage during photocathode activation and demonstrated a relatively low dynamic range of 10.

Although electronic read-out systems greatly facilitate the ease of use of streak camera systems, their spatial resolution has generally been poor. The measured static spatial resolution of a SIT vidicon optically coupled to a streak tube was 6 lp/mm at 15% modulation [80]. This can impose a limitation on the temporal resolution of the camera system. Modern solid-state sensors

do seem to exhibit improved resolution characteristics. Recent analysis of a number of fibre-optically coupled CCD/intensifier combinations has demonstrated that at 6 lp/mm static resolution the modulation can lie between 30% to 70% depending on the manufacturer of the CCD device [86]. It is expected that continued technological improvements in the field of solid-state read-out sensors will ensure their wide application in picosecond and femtosecond streak camera systems.

1.2.9 Image intensification

Historically several different types of image intensifier have been used in conjunction with electron-optical streak tubes. These include; magnetically focused cascade intensifiers [51], electrostatically focused cascade intensifiers [67] and channel plate intensifiers [45]. Various undesirable features of the first two types, such as high current and voltage demands necessitating ancillary cooling and the need to apply inefficient lens coupling to at least one end, has made them virtually obsolete in this application. Where image intensification is necessary most modern cameras incorporate channel plate intensifiers.

Channel plate intensifiers are composed of narrow bore ($\sim 12\mu m$) glass tubules with a length to diameter ratio of around 100. The inside surface is composed of a high resistance layer able to sustain a uniform electric field along its length provided by electrodes at either end. Electrons entering a channel strike the wall and cause secondaries to be emitted. These in turn strike the wall further along the cylinder and are thus amplified in an avalanche fashion. Many of these channels stacked together in a parallel mosaic structure form a microchannel plate (MCP).

For good spatial resolution it is an obvious requirement that the channels have small diameter and dense packing. Current manufacturing technology can produce channel diameters of around 12μm with open area ratio of approximately 0.6:1

Microchannel plates may be incorporated into two basic types of intensifier; inverting or proximity focused. In the inverting type an image relayed onto a photocathode is focused by an inverting electron-optical lens onto the MCP input. The output is in close proximity to a phosphor screen. In the proximity focused type the photocathode and phosphor screen are in close proximity to the MCP input and output respectively. A moderately high electric field between the MCP and the photocathode ensures good focusing. Devices with useful diameters of up to 40mm are available. This second type, despite the advantage of being extremely compact and essentially distortion-free, can suffer from a number of disadvantages. The most serious of these occurs when ions generated in the channel, due to contaminents, feed back and eventually destroy the photocathode. To inhibit this MCP channels usually have an angle of around 12° to the tube axis, and two MCP's are often configured in a chevron geometry.

The gain depends upon the applied potential, the channel length-to-diameter ratio and the secondary emission characteristics of the channel wall [87]. At a potential difference of a few kilovolts gains of up to 10^5 are achievable with the advantage that by adjusting the potential the gain may be controlled without affecting the focusing properties. Microchannel plates can be easily gated by modulating the applied voltage which thus allows optically contacted photographic film image recording without fogging [45].

A severe limitation of the MCP intensifier is channel saturation [88]. If secondary electrons are stripped from a channel wall faster than the charging current can replenish them, the gain for later electrons will be reduced until the channel has had sufficient time to recover. This has been found to limit the dynamic range at high gain levels because of the reduction in the linearity of the system [45].

Since the multiplication process is independent of the initial event yielding the first slow incident electron, MCP's may be employed to amplify any spatial distribution of electrons [88]. This has resulted in the direct incorporation of a MCP intensifier inside a streak image tube to provide a compact camera system [74]. Although this has proved suitable for repetitively operating streak cameras, gain saturation has been determined to limit the performance of single-shot systems [74]. There is therefore an advantage to be had by exploiting the phosphor decay time by fibre-optic coupling of an external intensification stage; this reduces the instantaneous current demand on the MCP.

1.3 A review of two-dimensional time resolved imaging

1.3.1 Introduction

Picosecond optical pulses have been amplified to terawatt peak powers [89] in linear amplifier chains. The ability to generate such pulses has made the possibility of controlled thermonuclear fusion a reality as the confinement time: density product criteria of Lawson [90] can in principle be achieved. High energy laser pulses are absorbed in the outer surface of spherical fuel pellets (e.g. Microballoons) in such a way as to produce at the centre a small volume of highly compressed, high-temperature

plasma, with an inertial confinement time of $\sim 10^{-11}$s [91]. The investigation of these laser produced plasma interactions are the subject of intense study at various National ladoratories.

Although picosecond streak cameras and other diagnostic instruments have provided valuable time-resolved information, there remains an urgent requirement to supplement this one-dimensional data with two-dimensional temporally resolved images of imploding microballoon targets. Such a 'framing' camera would find useful application in the study of implosion dynamic [28].

Since the luminous events of interest are generally unique transients many of the factors already discussed for single-shot streak cameras (e.g. spatial resolution, deflection voltage generation, image intensification) apply to these framing camera systems. Instruments permitting two-dimensional time-resolved imaging in the nanosecond regime have been available for some years, (e.g. IMACON 790*), but the development of picosecond resolution instruments has proved illusive despite concerted research effort. The primary instrumental requirements of a picosecond framing camera are; (1) frame exposure time $\leq$ 100ps, (2) inter-frame periods $\leq$ 250ps, (3) dynamic spatial resolution $\geq$ 10 lp/mm and (4) the potential for x-ray/visable/NIR spectral coverage. To satisfy the above requirement several different approaches have been explored, but is is generally agreed that the problem has not yet been solved. These techniques are now reviewed.

1.3.2 Mechanical techniques

At relatively low temporal resolution (ms) the recording medium is generally scanned passed the image. In order to attain improved resolution (μs-ns) it is preferable for the recording medium to remain stationary and the image be moved over it. This can be achieved with a rotating mirror or prism.

* Hadland Photonics Ltd., Bovingdon, Herts.

However, the basic problem with all mechanical systems is inertia. In order to obtain shorter time analysis it is necessary to move the mechanical components faster, thus to overcome the inertia ever increasing force must be applied. Eventually the stress limit of the materials forming the components is reached; that is when the atoms composing the mirror or prism are torn away by the centrifugal forces at the edge becoming comparable with the atomic binding force. For a rotating mirror camera this restricts the temporal resolution in the framing mode to $\sim 10^{-8}$ s [44]. However this limit assumes perfect materials; when the best structual materials currently available are used the limiting framing resolution is $\sim 10^{-7}$ s (e,g. CORDIN* model 114).

1.3.3 Electro-optic devices

Instead of accelerating whole bodies of material, individual molecules can be reorientated by an external time-dependent electric field to provide a shuttering action. Kerr [92], Pockels' [93] and Faraday cells provide a more delicate approach to light control. Electrically driven Kerr cells can operate with exposures of 0.5ns [94], the main limitation being the generation of high voltage(~10kV) fast risetime (~100ps) pulses. Shutters based on the optical Kerr effect make use of the large electric field associated with high-power laser pulses to induce transparency. A CS_2 Kerr cell optical shutter has successfully demonstrated a frame exposure duration of 5ps limited by the gating optical pulse [95]. Multiple frames were achieved by operating the shutter in conjunction with a slow electron-optical streak camera.

There is evidence to suggest that by a suitable choice of active medium the technique may be extended to the femtosecond

* CORDIN, Salt Lake City, Utah, USA.

regime [96]. However poor transmission efficiences of only a few percent and the lack of suitable mediums to cover the whole spectral range from IR to x-ray somewhat restricts the usefulness of this technique

1.3.4 Electron-optical techniques

Many approaches to ultrahigh speed image gating utilize electron-optical image converter tubes. The mass of an electron is extremely small and they thus have a low inertia which is favourable to high-speed operation. Additionally they are easily deflected by electromagnetic fields.

1.3.4.1 Gated image tubes

A common approach to ultrafast framed imaging is to gate an image converter tube on and off with a high speed voltage pulse. The simplist type of image converter tube is the proximity focused type consisting of a closely spaced photocathode and phosphor screen. An electric field between them extracts the photoelectrons from the photocathode which impinge on the phosphor screen providing a one-to-one image correspondence with low distortion. Good spatial resolution can be achieved with a moderate luminous gain of about 30 for a single stage device.

The use of these devices in the field of high speed photography was reported in the late 1960's with the Laboratories d'Electronique et al Physique appliquee at Limeil, France, developing tubes initially capable of ~1ns gating [97]. Incorporation of the photocathode into a transmission line configuration and decreasing the cathode surface resistance to around 10Ω/square by the deposition of a semi-conductive transparent substrate resulted in a proximity focused tube capable of 300ps gating periods

[98]. A major limitation of this tube was the high voltage (12kV) fast risetime (~150ps) gating pulse required. The only source capable of generating such a pulse was a 4-electrode spark gap which suffered a considerable jitter of around 700ps.

Another restraint suffered by this type of device is that for brief exposures ($\leq$1ns) of weak luminous phenomena it is difficult to generate sufficient photons to yield satisfactory image recording on photographic film. The deposition of luminescent phosphor's directly onto fibre-optic faceplates, permitting optically contacted film recording, improved photon collection efficiency but limited luminous gain remained a problem. Cascading several proximity focused tubes together provided a short term answer but this resulted in cumbersome, instruments with poor noise characteristics.

The development of MCP electron multipliers around 1960 resulted in small, rugged, proximity focused intensifiers being produced (see section 1.2.9). These bi-planar 'wafer' like devices may be gated in four possible ways; (i) photocathode gating, (ii) MCP gating, (iii) phosphor gating, (iv) combined MCP - phosphor gating. The gating pulse energy requirements for options (ii), (iii) and (iv) are significantly greater than for option (i) which is usually adopted in practice. Using option (i) gating voltage swings of <200V are typical, but the closely spaced photocathode - MCP arrangement presents a moderately high capacitative load which is likely to degrade the risetime of the gating voltage pulse. Extinction ratios exceeding 10^6 can be achieved, although if the rise and fall times of the gating pulse are comparable to the pulse-width defocusing with resultant image degradation will occur [99].

It is now common for the photocathode-MCP interface to form

part of a transmission line arrangement for optimal impedance matching. An x-ray sensitive gated MCP intensifier was reported by Fleurot et al [100] in 1982. This was gated using option (iv) and an open time of ~250ps with a dynamic spatial resolution of ~8 lp/mm was demonstrated. Unfortunately the 7kV gating pulse again suffered poor jitter which made operation at this fast gating speed difficult. By sacrificing image size five pinholes could be employed to image the x-ray luminous event five times across the photocathode. This facility was mainly used in conjunction with spectral filters to examine luminous events in different spectral regions.

More recently another x-ray sensitive, proximity focused, gated MCP intensifier tube has demonstrated an exposure time of $\leq$ 100ps [71]. Again the photocathode formed part of a 50Ω transmission line. To minimize the problem of jitter and provide an ultrafast risetime gating voltage pulse a laser illuminated photoconductive element (see section 3.2) was employed.

A major limitation of gated image tubes is their inability to generate a sequence of time resolved images. The conventional approach to this problem has been to employ several such devices together synchronised to operate in succession. This has been achieved on a nanosecond timescale [101] but has yet to be achieved in the picosecond regime.

Lieber [102] presented a novel scheme for a 'plategate' picosecond framing shutter using MCP technology. A passive, non-intensifying MCP with straight channels is utilized as an electron collimator [103]. The large aspect ratio (length - to - bore diameter), typically around 100, restricts the acceptance angle of the device such that a shuttering action is effected by a slight

deflection of an electron beam from axial propagation. The eletron beam is deflected by a composite stack of ribbon deflectors and microchannel tubules to achieve the required deflection sensitivity for a picosecond response time. Frame duration as short as 1ps are predicted but have yet to be shown in practice.

1.3.4.2 Image dissection techniques

A particularly ingenious approach to the generation of a single fast two-dimensional frame by making use of the good temporal resolution available in streak cameras was proposed by Baldwin [104]. The technique, implemented into an experimental system by Cheng et al [105], uses a fibre-optic image dissector to dissect a two-dimensional picture line by line and place each line consecutively end to end so as to form a single linear array. This encoded information is then focused onto the slit of a streak camera and swept in the normal manner. The streaked image is recorded and processed by computer to decode the two-dimensional image. In the prototype design a 20ps frame was recorded using a 7x7 element dissector yielding a relatively poor spatial resolution of only 2 lp/mm. The inherent spatial resolution limit along the camera slit (~100 pixels) is a restraint on the image resolution. This scheme may be extended to the x-ray spectrum by placing a thin subnanosecond plastic scintillator infront of the dissector, although the requirement for data processing is an undesirable feature.

A recently updated image dissection technique employing a conventional streak tube has been reported by Niu [106]. The input slit of the camera is replaced by a two-dimensional grid matrix to select out specific object points. After streak operation the recorded output is digitized prior to data processing.

Five framed images each exposed for 13ps and demonstrating a dynamic spatial resolution of 6 lp/mm (at photocathode) have been reported for this technique. The considerable effort involved in decoding the streak information represents the main disadvantage of this method of framing.

An image dissection framing technique which avoids the requirement for elaborate computational processing has been investigated by Kalibjlain [101]. His design of dissector/restorer image tube basically consists of two streak tubes one after the other. The front dissector section consists of a modified RCA C737435 tube with the phosphor screen replaced by a series of slit apertures. This is followed by the restorer section consisting of compensator deflectors, an electron lens, the restorer deflectors and a phosphor screen. The principle of operation is illustrated in fig.1.4, which has been reproduced from reference 107. A luminous event imaged at the photocathode generates an electron image which is focused at the slit aperture plane.

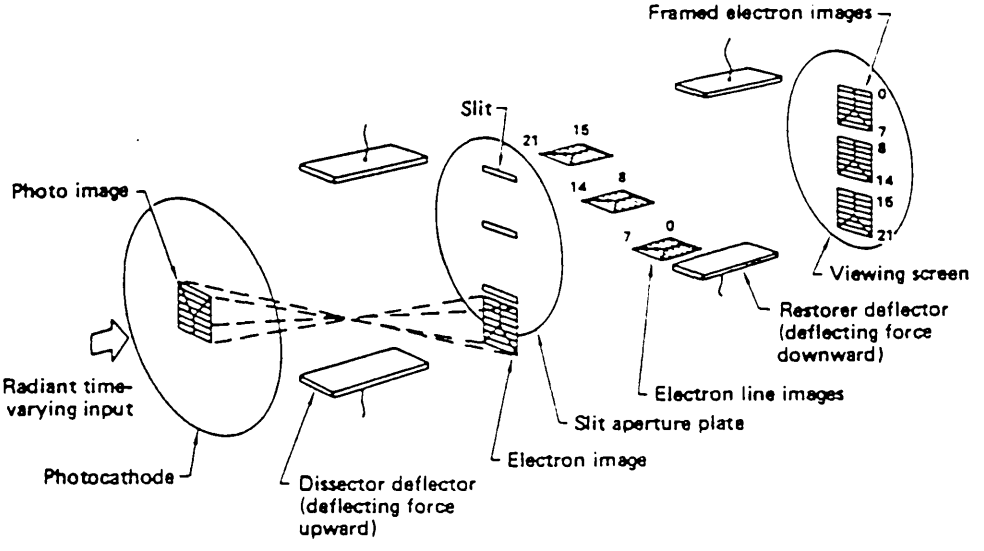

Fig.1.4 Principle of operation of the dissector/restorer tube.

A time-varying linear voltage ramp is applied to the dissector deflectors which sweeps the image over the slit apertures dissecting it line by line. Compensating deflectors remove the induced transverse velocity spread and then the restorer deflectors reform the framed image line by line.

A prototype tube demonstrated a triplet 2.5mm x 2.5mm frame capability with a frame duration of 135ps and spatial resolution of 7 lp/mm. [107] The ramp generator employed in generating these results suffered from extremely poor jitter (> 1ns) so more recent work [108] has concentrated on reducing the jitter to around 10ps and increasing the object format to 3.2mm x 4.5mm. Under these conditions three 250ps exposure frames with a dynamic spatial resolution of about 5 lp/mm were generated.

The main limitations of this approach result from the highly complex nature of the device. This incorporates two independent electron lenses and three different sets of deflectors, which must each be accurately synchronised with respect to the others. Additionally the restorer section electron optic results in increased image distortion.

1.3.4.3 Shaped deflection waveform techniques

Electron-optical, pin-hole image converter tubes have been satisfactorily employed in the streak mode readily achieving picosecond and even subpicosecond resolution. Conventional commercial framing cameras have employed this type of tube in the framing mode. A staircase type voltage waveform is applied to the deflector plates which successively moves the image to different positions across the screen. Exposures being obtained during the plateau regions. In some cases the beam is blanked off during the movement but in many cases this is considered unnecessary

as the exposure between images is relatively low.

The IMACON 675 employs the English Electric P855 image converter tube illustrated in Fig.1.5

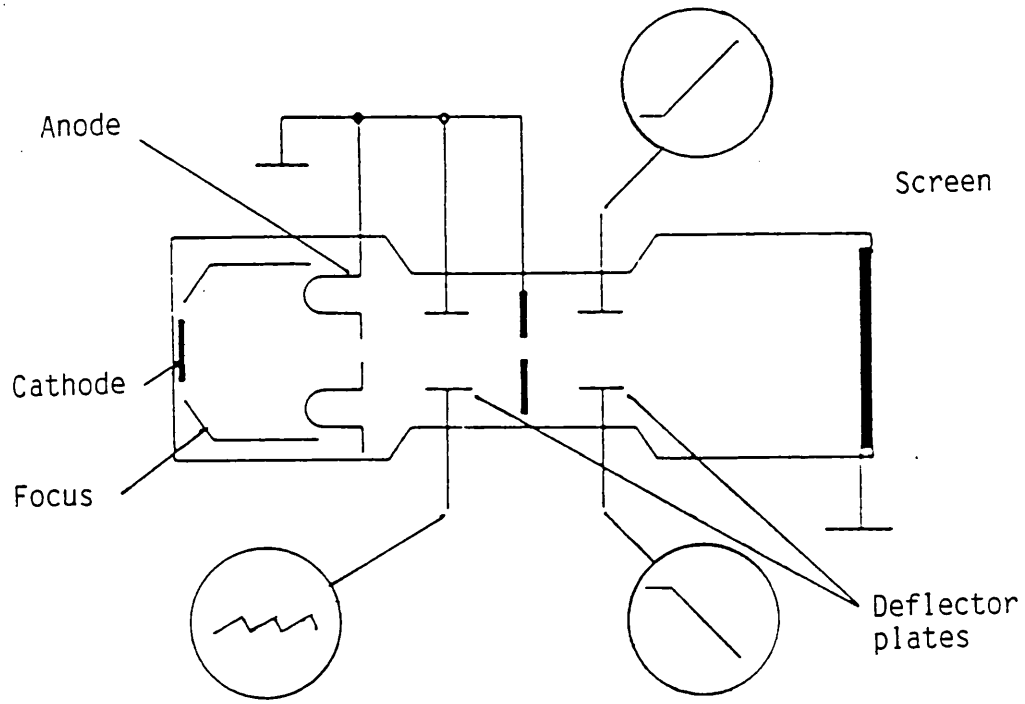

Fig.1. 5 Framing operation with a 'stair-case' deflection waveform

Framing operation is achieved by continuously supplying a saw tooth waveform to the first set of deflectors. When the camera is triggered a linear deflection waveform is applied to the second set of deflectors. The amplitudes of the two waveforms are arranged such that the rising edge of the saw tooth is cancelled by the linear ramp, thus resulting in a staircase deflection waveform at the screen. In principle a staircase waveform supplied directly to one pair of deflectors would function in the same manner, however the two-deflector arrangement considerably simplifies the drive electronics.

This type of framing camera has a limited time resolution because of the transit time of the electrons through the deflector

plates. This is because each part of the electron beam between the plates experiences a different amount of deflection depending on the distance left to travel through the deflectors. Thus even on application of a step voltage profile to the deflectors it will not be until one transit time later that all the electrons are deflected to the same screen position. This transit time is typically about 400ps and in practice the inter-frame time must be some three to four times longer to achieve a moderate spatial resolution. Consequently the minimum inter-frame time for the P855 tube is around 2ns. The IMACON 675 is capable of frame exposures of ~1ns at a modest spatial resolution of $\leq$ 3 lp/mm [109].

The generation of shorter duration frames by the provision of faster risetime deflector waveforms is prohibited by the deflector transit time. It is not feasible to merely shorten the length of the deflectors; this would require dramatically higher amplitude voltage waveforms which are not readily generated with sub-nanosecond profile specifications.

The approach taken by Hall [110] has been to adapt the P855 image tube for the incorporation of a travelling wave deflection structure (TWDS) in place of the parallel plate deflectors. The deflection voltage signal is propagated in a helical transmission line such that its passage along the axis of the tube is synchronised to the passage of the electron beam. Essentially the deflector plates are split into a series of shorter deflectors fed sequentially so as to reduce the effective deflector transit time to around 50ps whilst maintaining a similar sensitivity. The TWDS can readily be impedance matched to the driving circuitry for optimal performance.

An x-ray sensitive version of the P855 incorporating a TWDS has been operated in framing mode using deflection voltage ramps derived from a laser illuminated, silicon photoconductive element operated in the un-saturated mode. This instrument has demonstrated a quadruplet frame capability with an exposure duration of 350ps, inter-frame time of ~0.5ns and dynamic spatial resolution of 4 lp/mm [110]. The moderate spatial resolution is attributed to blurring when the image moves into and out of its stationary position. An electron beam blanking system is now being considered.

1.4 The Picoframe framing tube

To satisfy the rigorous demands on a new framing camera system for laser plasma interaction diagnostics, a new image tube has been developed specifically for the purpose. The pin-hole electron-optics of the familiar streak image tube has been retained, but the framing scheme has been redesigned to circumvent deflector transit time restraints. The basic concept has some features which are similar to a design proposed by Walters et al [111] and subsequently developed by Huston et al [112]. This design was demonstrated in the nanosecond regime and implemented into the commercial IMACON 790 camera [113]. The original tube was basically a variant of the P855 streak tube driven continuously with a high frequency sinusoid, generating two frames per cycle. Since it was necessary to operate in the quasi-linear region of the sinusoid the exposure duration was limited to approximately 1/6th of the inter-frame time. At high speed the non-linearities in the driving waveform degraded the spatial resolution to a poor 2 lp/mm.

The new tube design designated 'Picoframe', has been developed using computer aided design techniques specifically

as a framing image tube. Ultrahigh speed operation has been attained through the use of fast linear voltage deflection ramps produced by laser illuminated photoconductive elements and modern avalanche transitor sweep generator circuits. The principle of operation, design considerations and prototype construction are discussed in chapter 2. Experimental evaluations in single and multiple frame modes are presented in chapters 3 and 4.

1.5 Conclusion

The principle of operation and limitations of ultrafast electron-optical streak cameras have been discussed. These instruments currently provide the only linear intensity diagnostic on the picosecond and subpicosecond timescales, combined with a one-dimensional imaging capability. They are already used in many areas of picosecond diagnostics and with the advent of truly femtosecond resolution instruments it is expected that they will be even more widely employed.

The temporal resolution of an electron-optical streak camera is mainly limited by the finite energy distribution of the electrons emitted from the photocathode. Femtosecond resolution instruments incorporate high photocathode extraction fields, and maximized potentials throughout the imaging region, to reduce the effects of this spread. Under dynamic conditions the camera performance suffers two principle restraints; TRL dynamic range and dynamic slit curvature. At high photocurrents coulombic replusion between the constituent photoelectrons of a charge packet, emitted by a photocathode under picosecond/subpicosecond pulse illumination, causes the packet to spread spatially and so the temporal resolution becomes degraded.

The intensity range over which this effect is minimal is termed the TRL dynamic range. Dynamic slit curvature results from non-isochronism of electron trajectories through the electron-optic. Electrons emitted from off-axis cathode positions take longer to reach the deflectors. They are subsequently deflected further along the time axis resulting in a curved slit image.

The streak camera may be operated in two modes; single-shot and repetitive. Under single-shot conditions detrimental space-charge effects are usually limited by the provision of a high gain intensification stage. This usually takes the form of a fibre-optically coupled MCP intensifier. Repetitive operation exhibits high sensitivity and excellent signal-to-noise ratio characteristics. This mode is ideally suited for use with CW mode-locked lasers.

Advances in laser-induced thermonuclear fusion research have necessitated the development of picosecond camera systems providing imaging in two-spatial dimensions. Most modern approaches to the development of such cameras utilize image converter tubes due to their good sensitivity, wide spectral coverage and ease of use.

A number of different schemes have been reviewed. Gated tubes can provide the required short exposure durations with good spatial resolution but lack a true multiple frame capability. Image dissection techniques are able to generate a sequence of framed images, but require either undesirable data processing of the output or complex instrument design, generally with poor spatial resolution. The incorporation of a travelling wave deflection structure into a conventional image tube has shown some promise. However the generation of ultrahigh speed

staircase waveforms with sufficiently fast rising edges and flat plateaux, is technically demanding. As yet only moderate temporal and spatial resolution have been demonstrated.

A new image tube, the 'Picoframe', has been designed specifically for the purpose of picosecond framing. It employs a multiple frame generation technique that has been devised to be compatable with the ultrafast risetime voltage ramps available from laser illuminated photoconductive elements. The development of a new camera system based on this tube forms the bulk of the subject matter presented in this thesis.

References - Chapter 1

[1] H W Mocker and R J Collins,
Appl. Phys. Lett., 7, 270 (1965).

[2] L M Mollenauer and R H Stolen,
Optics Lett., 9. 13 (1984).

[3] J A Valdmanis, R L Fork and J P Gordon,
Optics Lett., 10. 131 (1985).

[4] B Nikolaus and D Grischkowsky,
Appl. Phys. Lett., 43, 228 (1983).

[5] G H C New,
Rep. Prog. Phys., 46, 877 (1983).

[6] R L Fork, B I Greene and C V Shank,
Appl. Phys. Lett., 38, 671 (1981).

[7] W Dietel, J J Fontaine and J C Diels,
Optics Lett., 8, 4 (1983).

[8] C V Shank.
as reported in New Scientist, April (1985).

[9] See for instance Vol 4, 14 and 23 of the
Springer-Verlag series on Chemical Physics.

[10] W Lenth et al,
Appl. Phys. Lett., 46(2), 191 (1985).

[11] D J Bradley,
'Ultrashort Light Pulses', Chapter 1, Ed. S L Shapiro,
2nd Edition, Springer-Verlag (1984).

[12] H.E Rowe and T Li,
IEEE J. Quant. Elect., QE-6, 49 (1970).

[13] P M Rentzepis, C J Mitschele and A C Saxman,
Appl. Phys. Lett., 17, 122 (1970).

[14] R C Eckardt and C H Lee,
Appl. Phys. Lett., 53, 425 (1969).

[15] A Kalpaxis et al,
Rev. Sci. Instrum., 53, 960 (1982).

[16] C V Shank, R L Fork, R Yen, R H Stolen and W J Tomlinson,
Appl. Phys. Lett., 40, 761 (1982)

[17] J P Wilson, W Sibbett and R G May,
'Picosecond Phenomena III', Ed K B Eisenthal, Springer-
Verlag series in Chemical Physics 23, New York, p149 (1982).

[18] R S Marjoribanks et al,
Optics Comm., 44, 113 (1982)

[19] J R Taylor, M C Adams and W Sibbett,
J Photochem., 12, 127 (1980).

[20] A J Cormier, W Margulis, W Sibbett and J R Taylor,
Optics Comm., 48(i), 61 (1983).

[21] D J Bradley et al,
Optics Comm., 15, 231 (1975).

[22] D J Bradley, B Liddy and W E Sleat,
Optics Comm., 2 (8), 391 (1971).

[23] C Kalpouzos et al,
'Picosecond Phenomena III', Ed K B Eisenthal, Springer-Verlag series in Chemical Physics 23, New York, p221 (1982).

[24] J G Fuyimoto, T K Yee and M M Salour,
Appl. Phys. Lett., 39, 12 (1981).

[25] J Chen, W Sibbett and J I Vukusic,
Elect. Lett., 18, 12 (1982).

[26] J R Taylor, M C Adams and W Sibbett,
Appl. Phys. Lett., 35, 590 (1979).

[27] See for example, 'Biological events probed by ultrafast laser spectroscopy', Ed. R R Alfano,
Academic Press, New York (1982).

[28] M H Key,
Phil. Trans. R Soc., London, A-298, 351 (1980).

[29] D J Bradley and W Sibbett,
Appl. Phys. Lett., 27, 382 (1975)

[30] PG May and W Sibbett,
Appl. Phys. Lett., 43, 624 (1983).

[31] M R Baggs, R T Eagles, W Margulis, W Sibbett and W E Sleat,
Adv. EEP, 64B, 617 (1985)

[32] K Kinoshita, N Hirai and Y Suzuki,
Proc. 16th ICHSPP, SPIE 491, 63 (1984).

[33] E K Zavoiskii and S D Fanchenko,
Sov. Physics Dotladay, 1, 285 (1956).

[34] O Klemperer and M E Barnett,
'Electron Optics', Cambridge University Press,
3rd Edition (1971).

[35] M R Baggs
Ph.D Thesis, University of London (1983).

[36] W Sibbett, H Niu and M R Baggs,
Proc. 15th ICHSPP, SPIE 348, 271 (1982).

[37] S W Thomas, G R Tripp and L W Coleman,
Proc 10th ISCHSP, p 127 (1972).

[38] A Lieber,
Proc. 13th ICHSPP, SPIE 189, 521 (1978).

[39] G Clement, C Loty, J P Roux and C Chancel,
Proc. 11th ICHSP, p 130 (1974).

[40] A Girard et al,
Proc. 16th ICHSPP, SPIE 491, 58 (1984).

[41] V Korobkin, AA Malyutin and M Ya Schelev,
Proc. 9th ICHSP, p 232 (1970).

[42] R Kalibjian,
J Appl. Phys., 46, 4875 (1975).

[43] R Kalibjian and G G Peterson,
Proc. 15th ICHSPP, SPIE 348, 195 (1982)

[44] E K Zavoisky and S D Franchenko,
Appl. Optics., 4(9), 1155 (1965).

[45] S F Bryant,
Ph.D Thesis, University of London (1978).

[46] K Kinoshita, T Kate and Y Suzuki,
Proc. 14th ICHSPP, p 119 (1980).

[47] H Niu and H Zhang,
Proc. 16th ICHSPP, SPIE 491, 669 (1984).

[48] V V Korabkin, B M Stepanov, S D Franchenko and M Ya Schelev,
Opt. Quant. Electron., 10, 367 (1978).

[49] H Niu, W Sibbett and M R Baggs,
Rev, Sci. Instrum., 53 (5), 563 (1982).

[50] Workshop on picosecond streak cameras Moderator: N Fleurot,
Proc. 16th ICHSPP, SPIE 491, 374 (1984).

[51] W Sibbett,
Ph.D Thesis, The Queen's University of Belfast,(1973).

[52] D J Bradley et al,
Adv EEP, 33B, 1145 (1972).

[53] Dynamic range measurement definition, Chairman S W Thomas,
Proc. 13th ICHSPP, SPIE 189, 838 (1978).

[54] W Friedman, S Jackel, W Seka and J Zimmermann,
Proc. 12th ICHSPP, SPIE 97, 544 (1976).

[55] P Dooley, V I Little, S Sim and S Majumdar,
Proc. 12th ICHSPP, SPIE 97, 80 (1976).

[56] S W Thomas and G E Philips,
Proc. 13th ICHSPP, SPIE 189, 471 (1978).

[57] D R Hull and N J Freeman,
J. Phys. E., 13, 685 (1980).

[58] S Majumdar,
Proc. 12th ICHSPP, SPIE 97, 24 (1976).

[59] R Kalibjian,
Proc. 13th ICHSPP, SPIE 189, 452 (1978).

[60] H Niu and W Sibbett,
Rev. Sci Instrum., 52, 1830 (1981).

[61] S W Thomas and R L Peterson,
Proc. 15th ICHSPP, SPIE 348, 190 (1982).

[62] S W Thomas and G E Philips,
Proc. 13th ICHSPP, SPIE 189, 471 (1978).

[63] K Kinoshita, N Hirai and Y Tsuchiya,
Proc. 15th ICHSPP, SPIE 348, 222 (1982).

[64] H Niu,
Proc. 15th ICHSPP, SPIE 348, 231 (1982).

[65] H NIU and H Zhang,
Proc. 16th ICHSPP, SPIE 491, 669 (1984).

[66] A J Alcock, M C Richardson and M Ya Schelev,
Proc. 9th ICHSP, p 191 (1970).

[67] W E Sleat,
Ph.D Thesis, The Queen's University of Belfast (1973).

[68] M C Jackson, R D Long, D Lee and N J Freeman,
Laser and Particle Beams, 4, 145 (1986).

[69] D H Auston,
Appl. Phys. Lett., 26, 101 (1975).

[70] W Margulis,
Ph.D Thesis, University of London (1981).

[71] A K L Dymoke - Bradshaw. J D Kilkenny and J Westlake,
Adv. EEP 64B, 531 (1985).

[72] R Hadland, K Helbrough and A E Huston,
Proc. 11th ICHSP, p107 (1974).

[73] W Sibbett,
Proc. 15th ICHSPP, SPIE 348, 15 (1982), and refs. therein.

[74] W Sibbett, W E Sleat, J R Taylor and J P Willson,
Proc. 15th ICHSPP, SPIE 348, 217 (1982).

[75] C B Johnson et al,
Appl. Optics, 19, 3491 (1980).

[76] W Sibbett, W E Sleat and W Krausse,
Proc. ESA Workshop on Space Laser Applications and
Technology, ESA SP-202, 171 (1984).

[77] See for instance, 'Photoelectronic Imaging Devices', Vol.2. Ed. L.M Biberman and S Nudelman, Plenum Press, New York - London (1971).

[78] C Cavailler, N Fleurot, D Mazatud and R Verrecchia, Proc. 14th ICHSPP, p347 (1980).

[80] D J Bradley, S F Bryant and W Sibbett, Rev. Sci. Instrum., 51,824 (1980).

[81] Y Tsuchiya, C Horiguchi, H Iida and K Kamiya, Proc. 14th ICHSPP, p 350 (1980).

[82] J C Cheng et al, Proc. 12th ICHSPP, SPIE, 97, 311 (1976).

[83] J Seymour, 'Electronic Devices and Components', Chapter 6, Pitman, London (1984).

[84] S W Thomas, R L Griffith and W R McDonald, Proc. 16th ICHSPP, SPIE 491, 101 (1984).

[85] P B Weiss, P Black, H Oona and L Sprouse, Proc. 16th ICHSPP, SPIE 491, 679 (1984).

[86] C Cavailler et al, Proc. 16th ICHSPP, SPIE 491, 693 (1984).

[87] B W Manky, A guest and R T Holmshaw, Adv. EEP, 2 (1969).

[88] P Schagen, 'Advances in Image Pickup and Display', Ed. B Kazan, Academic Press, New York, Vol 1, (1974).

[89] H G Ahlstrom, 'Physics of Laser Fusion', Vol. II, Lawrence Livermore National Laboratory, USA. UCRL - 53106 (1982).

[90] J D Lawson, Proc. Phys. Soc. B70, 6 (1957).

[91] J Nicholls, L Wood, A Thiessen and G Zimmerman, Nature, 239, 139 (1972).

[92] M Blanchet, Proc. 6th ICHSP, p313 (1962).

[93] R E Rowlands and J L Wentz, Proc. 9th ICHSP, p51 (1970).

[94] M Blanchet, Proc. 9th ICHSP, p112 (1970)

[95] M C Richardson and K Sala, Appl. Phys. Lett., 23, 420 (1973).

[96] J Etchepare, G Grillon, A Migus, J L Martin and G Hamoniaux, Appl. Phys. Lett., 43, 406 (1983).

[97] G Eschord and R Polaert, Adv. EEP, 28B, 989 (1969).

[98] E Laviron and C Delmare, Proc. 9th ICHSP, p198 (1970).

[99] A S Lundy and A E Iverson, Proc. 15th ICHSPP, SPIE 348, 178 (1982).

[100] N Fleurot, J P Gex, M Rostaning and R Sauneuf, Proc. 15th ICHSPP, SPIE 348, 772 (1982).

[101] A J Lieber and H D Sutphin, Rev Sei Instrum, 42, 1663 (1971).

[102] A J Lieber and H d Sutphin, Appl. Optics, 18, 745 (1979).

[103] A J Lieber et al, Nuclear Instrums. and methods, 127, 87(1975).

[104] M W Baldwin, Bell System Tech Jour., 19, 563 (1940).

[105] J C Cheng, L G Multhauf and G R Tripp, Proc. 12th ICHSPP, SPIE 97, 218 (1976).

[106] H Niu, T Chao and W Sibbett, Rev. Sci. Instrum., 52, 1190 (1981).

[107] R Kalibjian, Rev. Sci. Instrum., 49(7), 891 (1978).

[108] R Kalibjian and S W Thomas, Rev. Sci. Instrum., 54(12), 1626 (1983).

[109] IMACON 675 technical literature, Hadland Photonics Ltd., Bovingdon, Herts., UK.

[110] N Finn, T A Hall and E McGoldrick, Appl. Phys. Lett., 46(8), 731 (1985).

[111] F Walters, R A Chippendale, R P Bown, Proc. 6th ICHSP, p357 (1962).

[112] A E Huston, Appl. Optics, 3(11), 1231 (1964).

[113] A E Huston, Proc. Electro - Optics '71 Int. Conf., p344 (1971).

CHAPTER 2

The Picoframe framing camera

2.1 Introduction

It has already been stated that particularly in the field of laser - induced compression of matter there is a requirement for a two - dimensional time resolved imaging diagnostic. The velocities involved in the laser induced implosions of micro-balloon targets dictate that for a spatial resolution of 10 lp/mm frame exposure durations of ~100ps are necessary [1]. These requirements represent roughly an order of magnitude improvement on currently available commercial instruments. A new sweep/ compensation type image converter tube has been designed to fulfil these rigorous demands. This design fabricated into a prototype device, designated 'Picoframe I', has been incorporated into an experimental camera system.

2.2 Principle of operation

The Picoframe I is depicted schematically in fig.2.1. An image formed at the photocathode is reformed onto a fluorescent screen by an electron-optic lens [2]. To isolate the imaging region from the remainder of the tube the anode electrode incorporates a small axial aperture. In the simplist design a single second aperture is located axially on the screen side of the anode aperture. A pair of independent parallel deflectors are positioned after each aperture. These components constitute the 'shuttering mechanism' of the instrument.

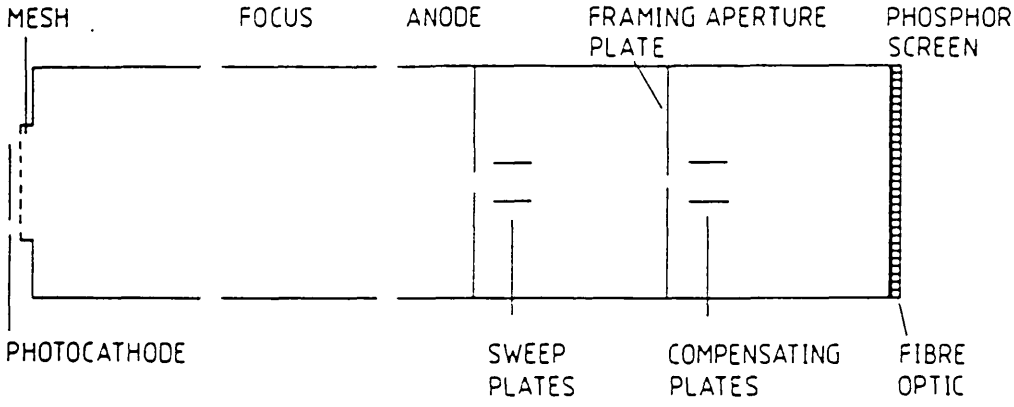

Fig. 2.1 Schematic of the Picoframe I image tube.

The first pair of deflectors (framing or sweep) are located equally disposed about the axis just beyond the anode aperture on the screen side. The second pair of deflectors (compensating), are similarly arranged on the screen side of the second or 'framing' aperture.

In operation, prior to exposure, a DC bias voltage is applied to the framing deflector plates. This deflects the electron beam to a 'shuttered' position either above or below the framing aperture. A time varying linear voltage ramp applied to the framing deflectors sweeps the electron beam across the framing aperture. The transmitted burst of electrons then proceed to form an image on the fluorescent screen. This sweeping action has the effect of imparting a transverse velocity component to the transmitted electrons. If this were to remain uncorrected it would result in a 'smeared' image.

This smearing of the image may be understood by considering two photoelectrons emitted with identical characteristics from a common cathode object point, see fig.2.2. Electrons A and B are emitted at time t_o and $t_o + \delta t$ respectively, where $\delta t < \Delta t$ the time taken to sweep the beam across the framing aperture.

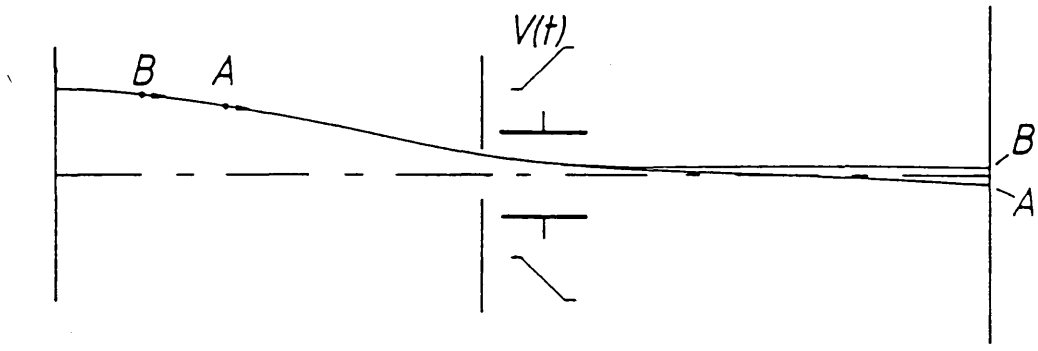

Fig.2.2 The trajectories of two image forming photoelectrons A and B emitted from a common object point.

A linear time-varying voltage ramp V(t) is then applied to the framing deflectors. Provided the correct synchronisation is achieved, both photoelectrons are able to pass unimpeded and contribute to the image formed at the screen. Since the time taken to sweep the beam across the aperture is finite ($\Delta t > 0$), the voltage supplied to the sweep deflectors will change between the passage of electrons A and B. Thus electron B will experience a higher electric field than electron A and so be deflected to a different position on the fluorescent screen (see fig.2.3)

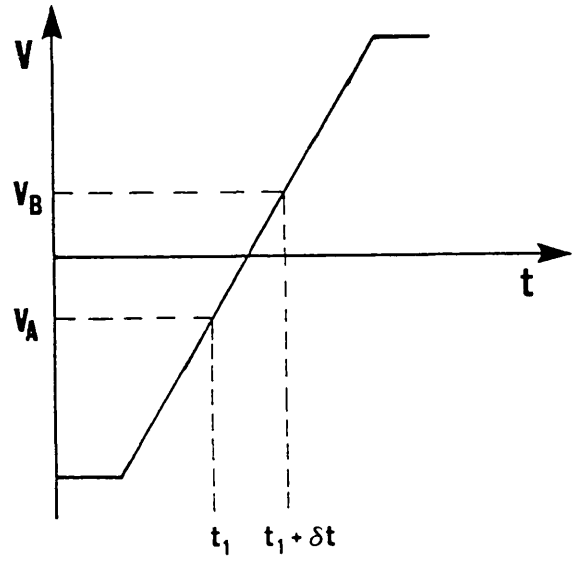

Fig. 2.3. Electrons A and B experience different electric fields at the deflectors.

This effect whereby photoelectrons from a common object

point are deflected to different positions in the image plane results in image blurr. Fortunately the provision of an identical voltage ramp of opposite polarity to a pair of compensation deflectors nullifies the imparted transverse electron velocity. Thus the image 'smear' is removed and well resolved images may be recorded at the screen. The necessary condition for no loss in spatial resolution is that the sensitivities of the two pairs of deflectors must be identical [3]. It can be demonstrated that for an identical driving waveform shape the sensitivities must differ by less than 0.1% to resolve 12.5 lp/mm [4].

2.2.1 Generation of multiple framed images

Several different deflection arrangements were considered to provide a multiple sequenced frame capability [5]. One of these was the provision of a multiplex aperture plate with three framing apertures in place of the one described previously. Each aperture has associated compensation deflectors configured in a manner such that their deflection sensitivity, associated capacitance and inductance are identical to the sweep deflectors. Such an arrangement is illustrated in fig.2.4.

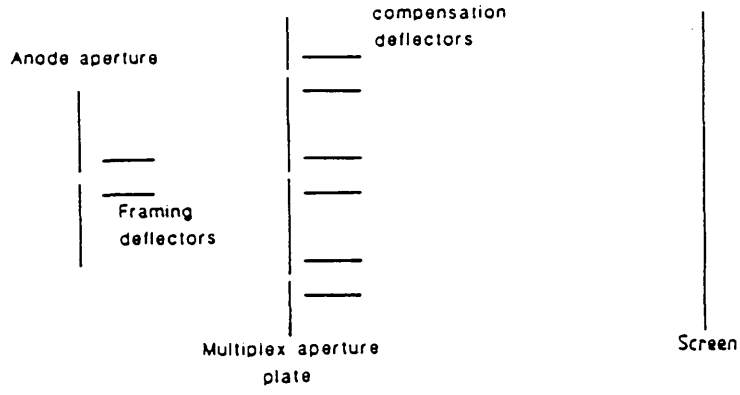

Fig. 2.4 The triple aperture multiplex aperture plate design.

In this design three temporal exposures, a framed 'triplet', would result from a single sweep of the electron beam across the multiplex aperture plate. Again the exact inverse waveform must

be applied to each of the compensator deflectors in order to secure resolvable images. Spatial discrimination of the three images at the screen is achieved by one of two methods.

(i) The provision of separator plates following the outer two compensator deflectors suitably DC biased (see fig.2.5). This approach has the disadvantage that the deflection structure becomes more complex.

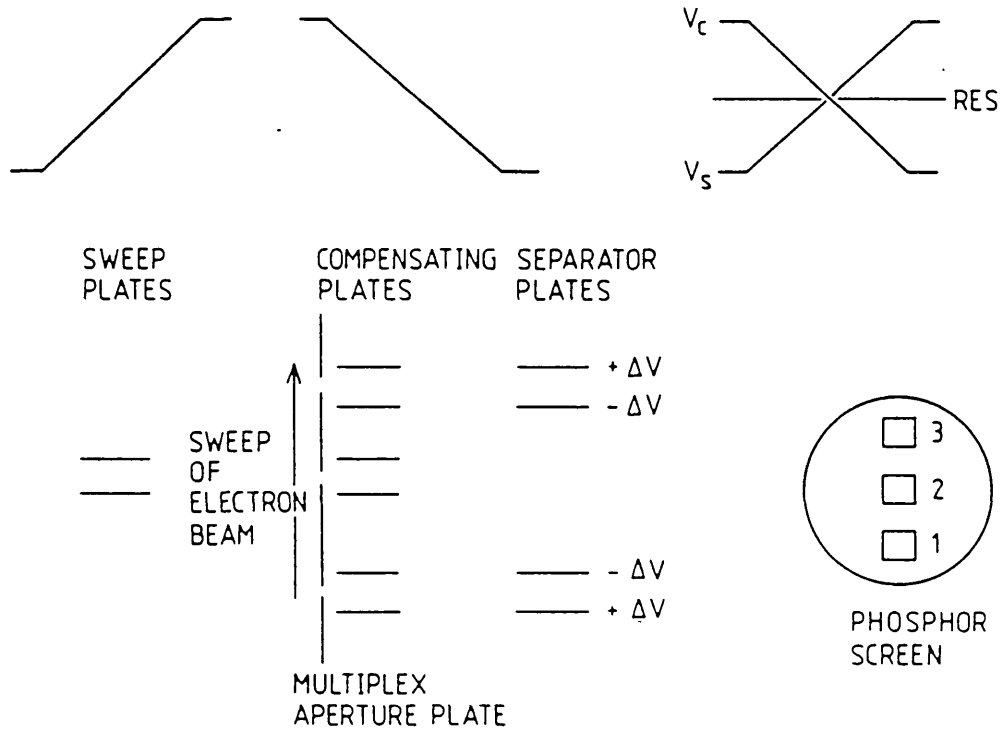

Fig.2.5 Image discrimination in the multiplex aperture plate design by use of DC biased separator plates.

(ii) Careful dephasing of the waveform applied to the compensating deflectors can establish a nett DC bias on the top and bottom deflectors (see fig. 2.6).

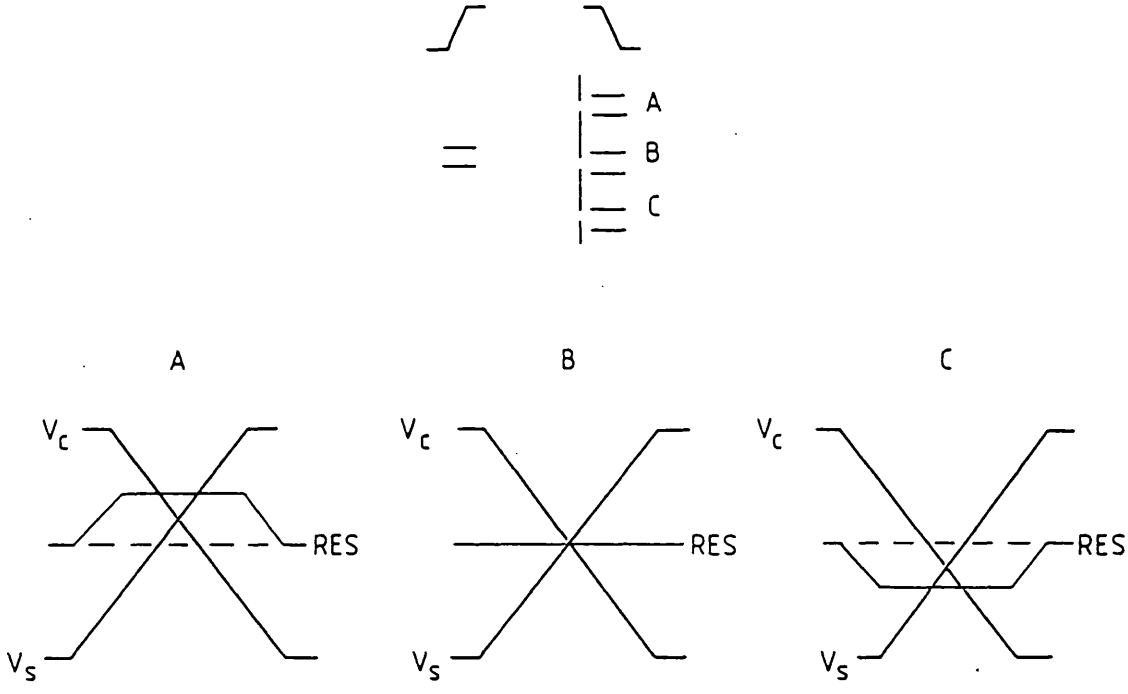

Fig. 2.6 Image discrimination by dephased deflection waveforms

Alternatively exact phasing of the waveforms together with an associated standing DC bias on the outer pairs of deflectors can be used (see fig.2.7).

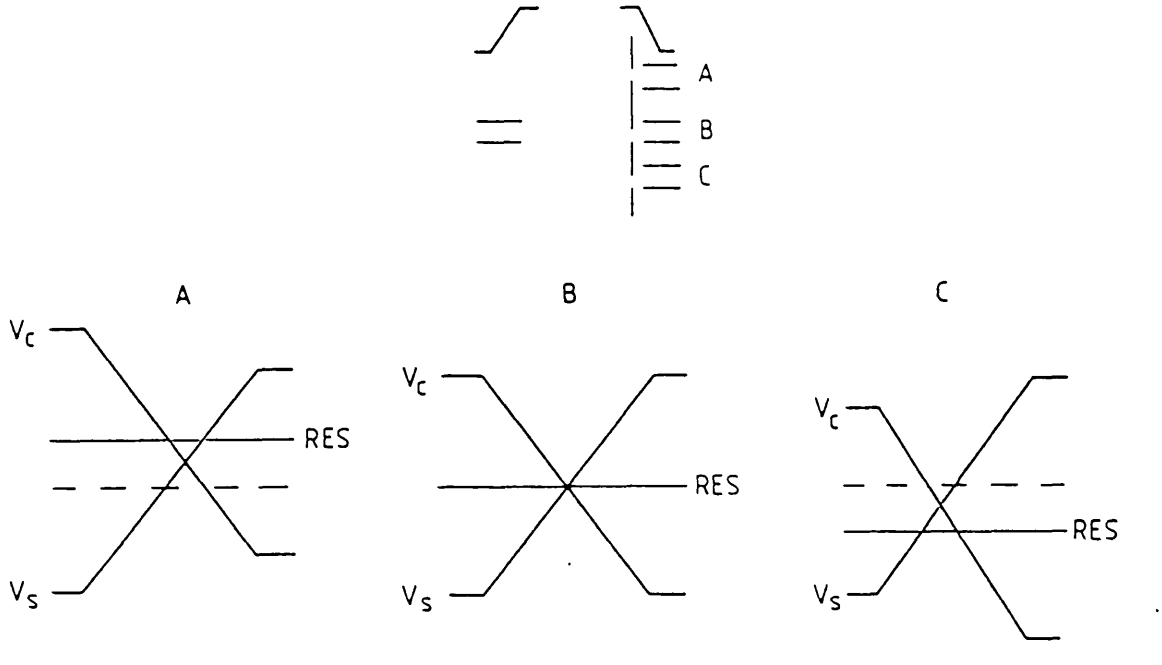

Fig.2.7 Image discrimination by DC bias on the outer pairs of deflectors.

Another approach to multiple sequenced frame imaging using the sweep/compensation technique is multiple sweep operation. Here only a single framing aperture with associated compensation deflectors is employed; this considerably simplifies the deflection arrangement. A symmetrical triangular waveform is applied to the framing deflectors. This provides two transmissions of the electron beam as it is swept across the framing aperture. Again the provision of suitably dephased waveforms (see fig.2.8) results in the discrimination of the framed 'doublet' images formed at the screen.

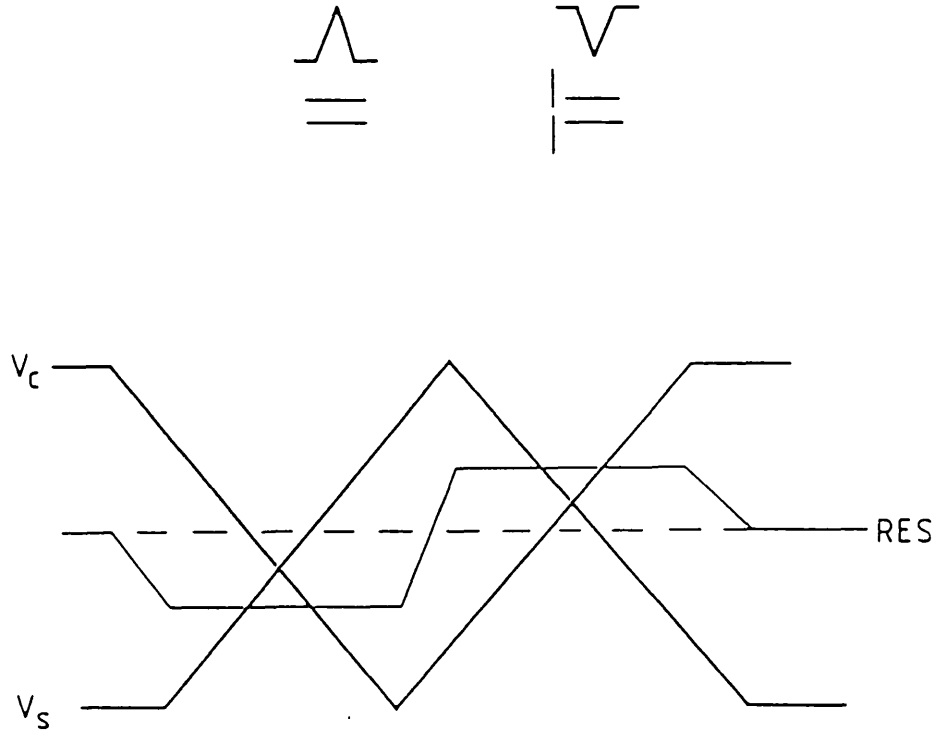

Fig. 2.8 Dephased 'triangular' deflection waveforms for the discrimination of 'doublet' images.

In all these arrangements orthogonally orientated shift deflectors may be employed in conjunction with a staircase type waveform to sequentially shift the images on the screen. A succession of 'triplet' or 'doublet' format framed images may then be produced.

2.3. Design considerations

Consider a tube-varying deflection voltage with a gradient $K = dV/dt$ (V/s). If applied to a pair of framing deflectors of sensitivity S (m/V), the speed at which the electron beam is swept across the framing aperture is given by

$$v = K.S$$

Using parameters defined in fig. 2.9, with an electron beam acceleration potential of V_a, the deflection sensitivity of a pair of parallel plate deflectors is given by [2],

$$S = \frac{l(\frac{1}{2}l + L)}{2V_a d}$$

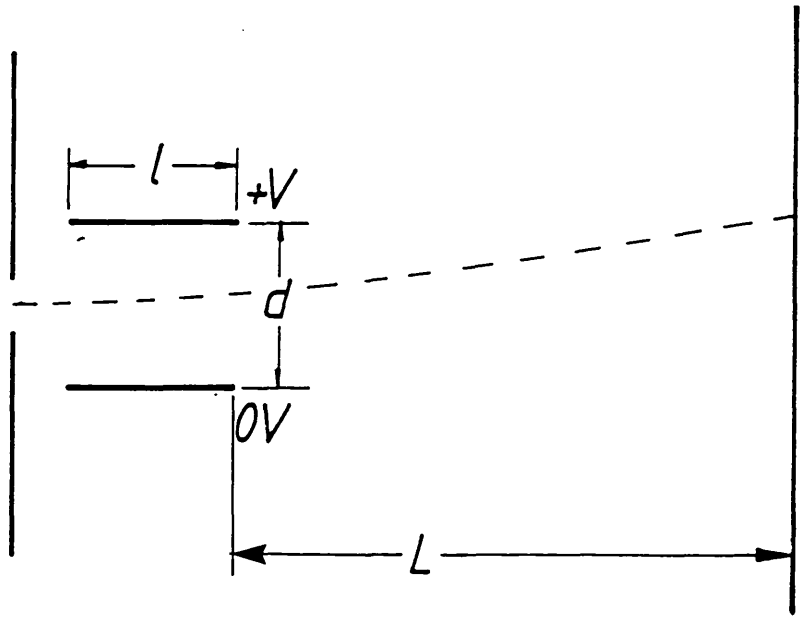

Fig.2.9 A pair of parallel plate deflectors.

Thus the frame exposure duration Δt is defined by the time taken for the beam to traverse the framing aperture of diameter a,

$$\Delta t = \frac{a}{v} = \frac{2V_a d a}{Kl(\frac{1}{2}l + L)}$$

Hence to minimize the temporal exposure it may be concluded [5] that:-

(i) The deflection voltage risetime should be minimized.

(ii) The framing aperture diameter should be minimized.

(iii) The deflection plate separation must be small.

(iv) The distance between the framing deflectors and the aperture plate should be large.

(v) The sweep plates must be as long as possible.

2.3.1 A theoretical image tube design

Conforming to these criteria Sibbett et al [6] proposed a theoretical tube design incorporating a low magnification electron lens with an extended long narrow waist beam profile. A three cylinder lens [7] was adopted with the extraction mesh electrode electrically common to the first cylinder electrode. A photocathode-to-mesh spacing of 2.5mm provides a relatively modest extraction field of 20kV/cm for an applied potential of 5kV. The tube was designed to operate at an overall potential of 15kV, with a focus potential of 2kV yielding a paraxial focus a distance of 434mm from the photocathode. The electron-optical crossover position is located midway between the two aperture plates to facilitate closely spaced deflectors for a high-fidelity response.

The internal diameter of the cylinder electrodes was selected to be 58mm constrained by the commercial availability of non-magnetic stainless steel tube. Cylinder lengths for the combined first/mesh, focus and anode electrodes were determined to be 76mm, 67mm and 29mm respectively by computer aided design optimisation [5]. The inter-electrode separation adpoted was 10mm.

2.3.2 Deflector design

A simplified analysis was employed in designing the deflection assembly (see section 5.4). Considering first the more complex multiplex aperture plate design illustrated in fig. 2.10. The parameter G was selected to be as small as possible within the constraints of constructional viability.

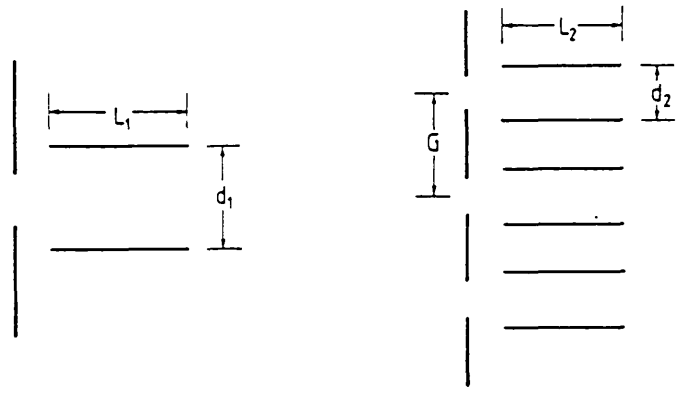

Fig 2.10 The multiplex aperture plate design

An iterative procedure for optimising the deflector dimensions was then undertaken. Initial values for parameters L_1 and d_1 were pre-selected knowing the beam diameter at the anode aperture. The deflection sensitivity of the framing deflectors was evaluated and equated to the sensitivity of the compensation deflectors. By selecting d_2 the value of L_2 was then defined. A series of calculations were carried out pre-selecting d_1 and d_2 and them incrementing L_1. The incremental limit was reached when it was determined that one pair of deflectors had become so long the electron beam was intercepted. Following this analysis the deflector dimensions adopted were; L_1=8mm, L_2=10.6mm, d_1=4mm, d_2=3.8mm. The widths of the deflectors were determined to minimize: (i) the influence of edge effects, (ii) the plate capacitance. Values of 10mm and 7.2mm for the sweep and compensating deflectors respectively result in a deflector capacitance of ~0.2pf (neglecting stray and cross-capacitance effects).

A similar procedure was adopted in evaluating the deflector dimension for the simpler single aperture design. Here the beam had to be deflected a distance of 1.8mm (equivalent to the framing aperture diameter) at the aperture plane to 'shutter' the tube off. The minimum framing deflector separation, dictated by the beam diameter at the anode aperture (3.5mm), was selected to be 4.4mm. Suitable dimensions arrived at after the design analysis were; d_1=4.4mm, L_1=11mm, w_1=11mm and d_2=4.2mm, L_2=14.8mm, w_2=7.8mm. The calculated deflector capacitance, again neglecting stray effects is 0.24pF.

2.4 Theoretical evaluation of static performance

The static imaging performance of the theoretical framing tube design has been analysed computationally using a Modulation Transfer Function (MTF) technique (see section 5.2.3). The two-dimensional spatial imaging characteristics of framing image tubes necessitate that object points covering the whole of the effective cathode area be studied. Axial symmetry however requires that only one quadrant be studied explicitly.

To facilitate analysis a three dimensional cartesian coordinate system is adopted. The cathode is considered to lie in the **x-y** plane, where the origin is centred on the axis of rotational symmetry. This is referred to as the z axis. Object points on the photocathode thus have coordinates (x,y,0), or more usually just (x,y) where z is assumed to be zero at the photocathode. In streak camera terminology the **x** axis is often referred to as the sweep direction and the **y** axis referred to as the slit direction.
The five cathode object points examined explicitly in the theoretical analysis are illustrated in fig.2.11.

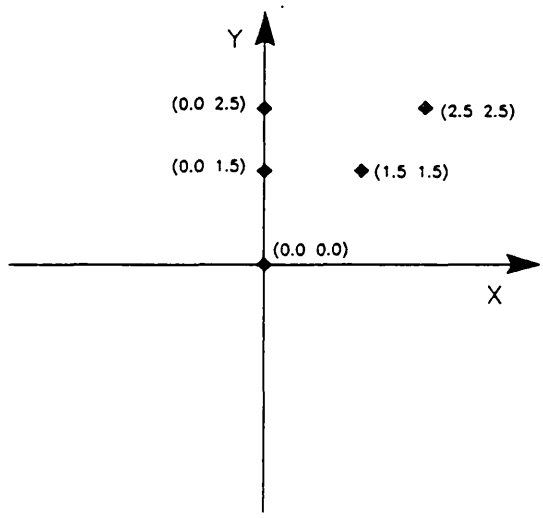

Fig.2.11 Cathode object points considered in the theoretical static evaluation of the framing tube design.

The MTF method characterises fully the performance of a linear imaging system. Using this technique the static (non-swept) imaging capabilities of the lens design were evaluated. It was determined that for cathode object points within a radius of ~3.5mm the limiting spatial resolution at the screen remained above 40 lp/mm. Taking into account the predicted electron-optical magnification of -1.5, this corresponds to a limiting spatial resolution of not less than 60 lp/mm at the photocathode, over a 6mm x 6mm image format. Of course it is to be expected that the dynamic imaging performance will be degraded due to deflection defocusing[5], incorrect image compensation and space-charge effects.

The framing aperture diameter was determined by a compromise between the frame exposure duration and the effective field of view. The trajectories of 1000 electrons emitted from an extreme cathode object point (x=3mm, y=3mm), by an S1 type photocathode were evaluated. Analysing the radial coordinates of each electron path at specific **x-y** planes enabled the number of electrons intercepted for various aperture diameters to be ascertained. Using this technique a framing aperture diameter of 1.8mm situated 60mm

beyond the anode plane was adopted. This resulted in the interception of 8% of the photoelectrons emitted from the extreme object point considered.

2.5 Construction of a prototype image tube

Due to the relatively demanding assembly requirements imposed by the multiplex aperture plate design, the constructionally more simplistic single aperture design was adopted for fabrication of the prototype. A sealed-off, optically sensitive image tube designated 'Picoframe I' was constructed. The internal components (e.g. Lens cylinders, deflection assembly) together with the constructional aids (mandrel, jig and spacers) were fabricated at Imperial College. Tube construction was in collaboration with the Electron Tubes division of Thorn-EMI.*

The three cylinders comprising the electron lens were positioned co-axially with the aid of a mandrel. Axial and concentric tolerances were ~25μm. Each lens electrode was secured by a retaining annulus spot welded to the cylinder. This was then tack welded in between the metal flange ends of two glass envelope pieces. The sub-component so formed then had the metal flanges argon-arc welded together on an industrial jig. Subsequent cylinder electrodes were retained in the same manner until the whole focusing section had been built up. The constructional details are illustrated in fig.2.12.

The deflection assembly comprised two stainless steel side arm supports, secured at one end to the anode aperture plate and to a support annulus at the other. The annulus itself was retained between two metal flanges of the envelope package.

* Thorn-EMI Electron Tubes Division, Ruislip, Middlesex.

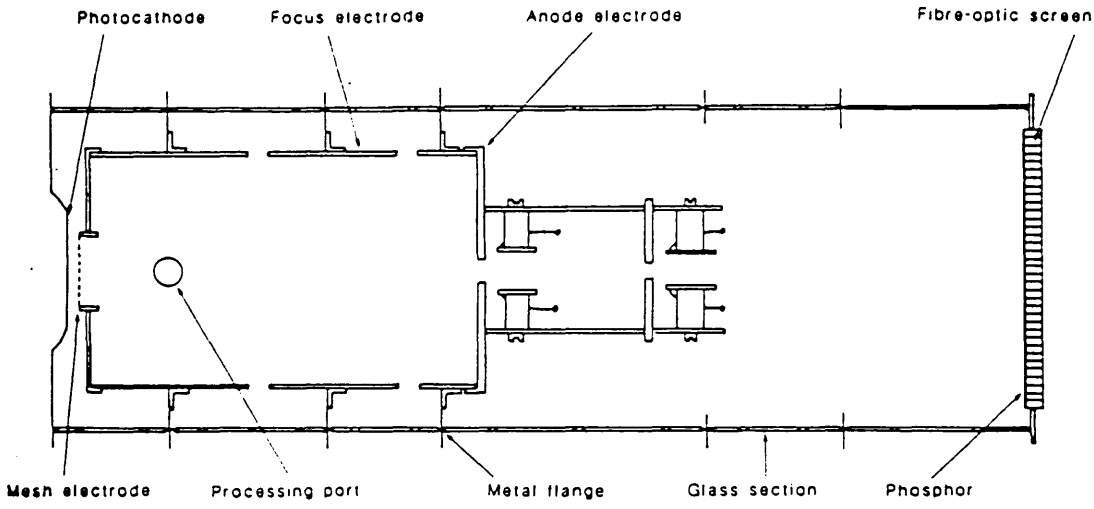

Fig. 2.12 Sectional view illustrating the construction of the Picoframe I.

Each side-arm provided support for the deflectors and the framing aperture plate. The deflector plates were each supported from machinable glass ceramic spacers by means of a threaded stud on the back of each plate. Stainless steel bolts secured each ceramic spacer to the side-arms. The ceramic/steel joint was further retained by a 'gun cement' compound. Before bake-out the positional accuracy of the deflector plates was ~5μm. The aperture plates and side arms were held together by spot welded right-angle sections of molybdenum strip to form a one-piece subcomponent. This was then located and spot welded to the anode cylinder.

Telkoseal * feed-through pins penetrating the glass envelope were electrically connected to the deflection plates with silver plated nickel wire. Short straight lengths were used to minimize inductance. The drift section of the tube was built up using custom made glass sections where necessary to locate the phosphor screen at the optimum focal plane (z=434mm). A P.11 phosphor deposited 49mm fibre-optic face-plate was argon-arc welded onto

* Telkon Metal Co., Crawley.

the back of the tube. To provide a conductive path and enhance light output the phosphor had been vacuum evaporated with aluminium.

The extraction mesh electrode (60 cells per mm copper micromesh) was located in a mesh retaining flange spot welded to the first electrode. An electron transmission of ~30% over the 17mm diameter of the mesh was to be expected. This type of mesh is constructed by sandwiching copper gauze between two support rings which are then spot welded together. In extremely high field applications (e.g. femtosecond streak tubes) the spot weld surface imperfections can result in field emission [8]. However for the relatively modest 20kV/cm field in the Picoframe I no difficulties were envisaged.

Finally a crown glass front window was arc welded in place. This window had a chromium layer vacuum evaporated onto it to provide a conductive substrate for the photocathode when activated. The central 12mm diameter was approximately 50% light transmitting with the remainder opaque.

The constructed tube was baked-out under vacuum at a temperature of 350° - 400°C for a period of about 48 hours. A zinconium 'getter' inside the tube could be 'fired' by application of a large current for a short period (~10 Amps for ~10 sec), to absorb any remaining gas. The final vacuum achieved being better than 10^{-8} Torr. By introducing chemical generators via side processing ports an S20 photocathode was activated through the mesh onto the front window.

2.6 Experimental evaluation of static performance

The image tube operating potentials were derived from a potted voltage divider network, operated from a Brandanburg 807R

high voltage supply unit. Potentiometers were used to derive the variable voltages of -9/-11kV for the mesh electrode and -12/-14kV for the focus electrode. A small mesh rupture was noted soon after manufacture. To relieve stress on the mesh, which might have further propagated the rupture, the operating potentials were scaled down by a factor $\frac{13}{15}$. The tube was successfully operated at a potential of 13kV throughout many of the experimental evaluations.

Focusing was carried out with the aid of a Baum projector [9]. This enabled a test resolution chart to be accurately imaged onto the photocathode. The tube was then optimally focused by adjustment of the variable focus potential whilst observing the screen image with the aid of a microscope. A limiting spatial resolution of around 55 lp/mm at the photocathode in both the **x** and **y** directions was observed. Typical focus potential are shown in table 2.1.

Electrode	Photocathode	Mesh	Focus	Anode
Potential(kV)	-13	-8.6	-11.4	0

Table 2.1 Typical 'reduced' Picoframe I focus potentials.

The electron-optical magnification was measured to be -1.4 (theoretically predicted -1.5) at the focus potentials stated. This discrepancy is due to the reduced operating potentials. The symmetrical DC deflection sensitivity for each pair of deflectors was determined by applying symmetrical bias voltages to one set of plates, with their counterparts maintained at anode potential. Image displacement at the screen was then measured with a travelling microscope. At an anode potential of 13kV the measured sensitivities of the deflectors are shown in table 2.2. It is noted that the sensitivity of the framing deflectors

exceeds that of the compensation deflectors by approximately 7%.

Framing deflectors	2.75mm/100V $\pm$ 0.03mm/100V
Compensation deflectors	2.54mm/100V $\pm$ 0.03mm/100V

Table 2.2 Measured DC sensitivities of the prototype Picoframe I deflectors at an anode potential of 13kV.

Limiting static spatial resolution (referred to the photocathode) as a function of screen position was evaluated by first optimally focusing the test chart on axis. The image was then deflected to different screen positions by application of a symmetrical bias potential to the compensating deflectors. Screen image displacement was measured with the aid of a travelling microscope. The resultant curves of limiting spatial resolution (at photocathode) against screen position for directions **x** and **y** are shown in figs. 2.13 (a),(b). There is particularly close agreement between the theoretically predicted static spatial resolution of 60 lp/mm at the photocathode and the experimental observation.

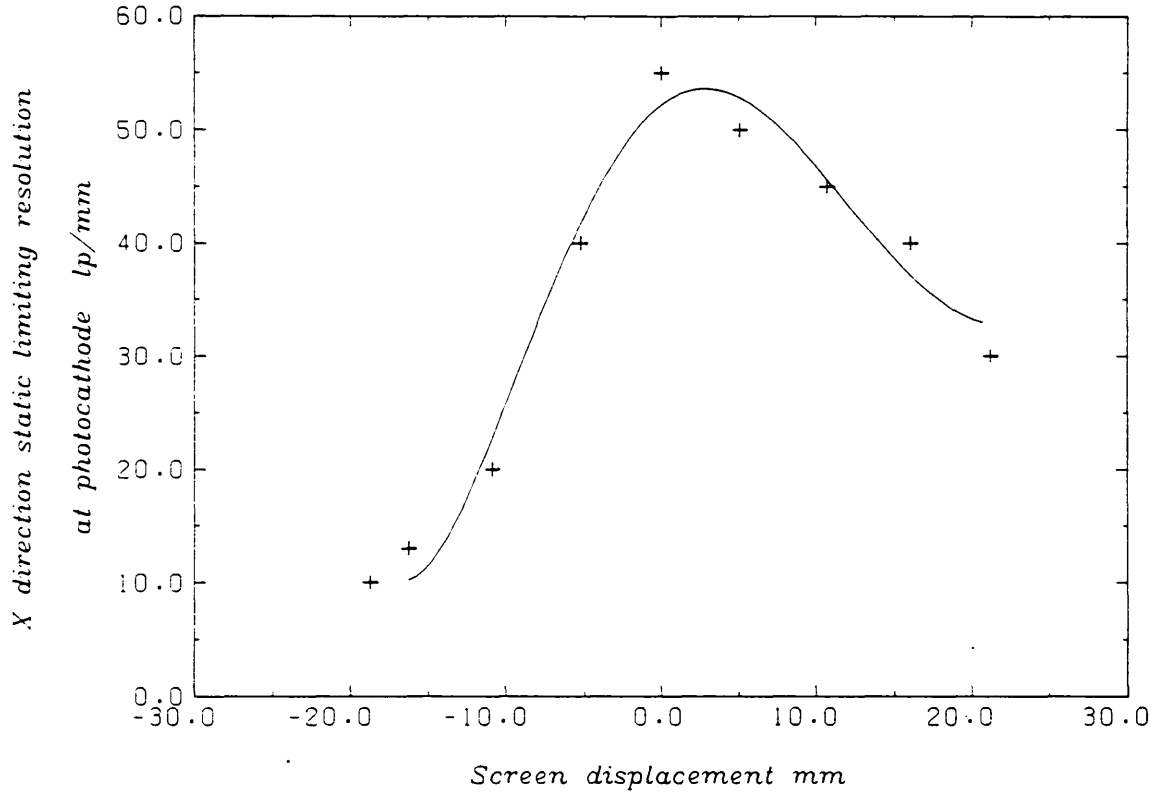

Fig.2.13 (a) Static limiting spatial resolution against screen displacement in the **x** direction.

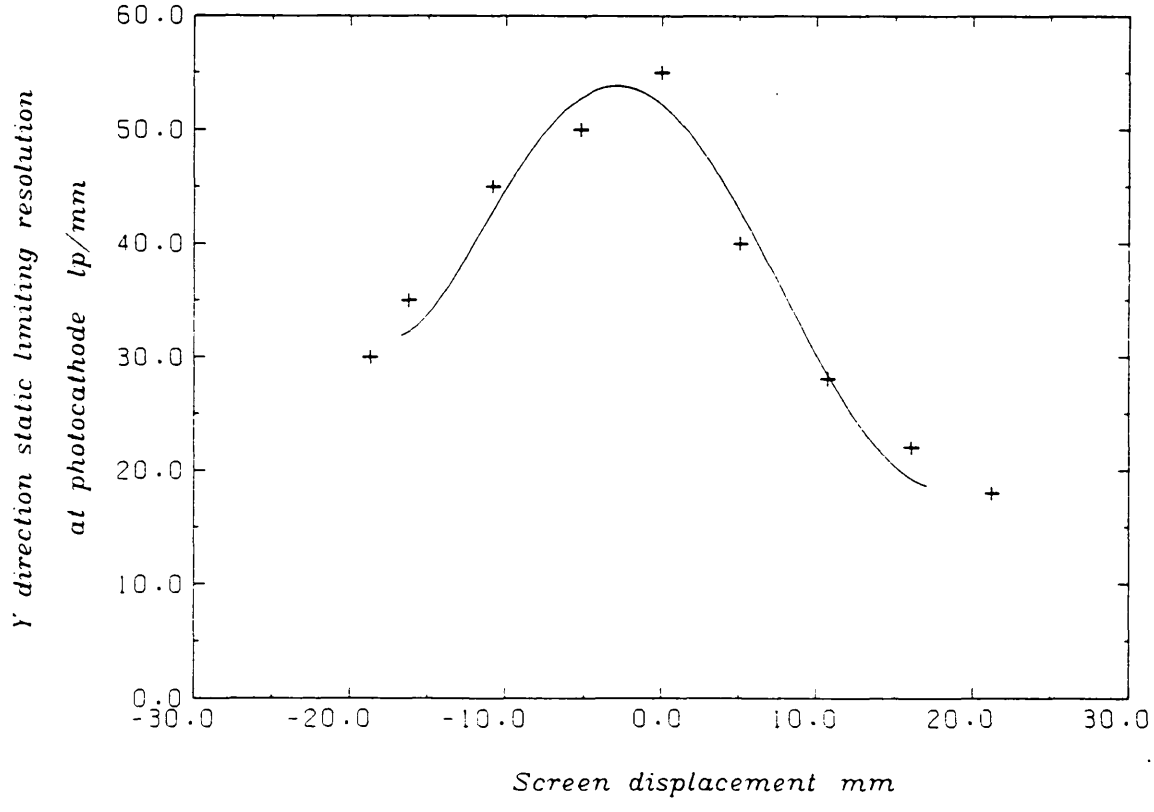

Fig. 2.13 (b) Static limiting spatial resolution against screen displacement in the **y** direction.

It can be seen from fig.2.13 (a), (b) that there is some degree of asymmetric misalignment in the prototype tube. This is probably in the focusing region and can have several causes:-

(1) Misalignment in the axiality and concentricity of the electron lens cylinders. On construction this is good but since the electrodes are supported by the glass-to-metal flanges of the envelope distortions can occur during bake-out.

(2) Cathode and mesh misalignment. The photocathode is particularly susceptable to non-normal axial alignment as it is activated onto the front window of the vacuum enclosure. It is well known that the front window is sucked in and distorts under evacuation.

(3) Phosphor screen misalignment. Positioning of the screen in a non-normal plane relative to the axis results in image distortion.

No single cause can be attributed to the noted image asymmetry in the tube. Due to the nature of the constructional technique used all three effects are likely to be present to some extent.

The limiting spatial resolution is observed to deteriorate off axis. This in common with other imaging systems is due to geometrical aberrations, principally spherical aberration and field curvature. There is also a defocusing effect due to deflection of the electron beam, 'deflection defocusing' [5].

2.7 The experimental Picoframe I camera

The sealed off prototype image tube was mounted into a camera chassis comprising two aluminium end plates, held together

by aluminium spacer rods as illustrated in fig.2.14.

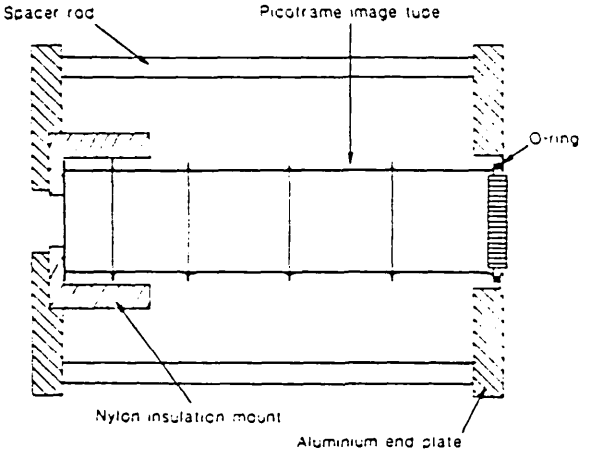

Fig.2.14 Picoframe I camera chassis.

The image tube was operated such that the screen, anode and chassis were maintained at earth potential with the cathode held negative. To provide the necessary electrical insulation the cathode end of the tube was seated into a nylon mount. A copper clad sheet, with a central hole large enough to accept the tube, was held in place at the anode plane via the spacer rods. This facilitated fixing of the deflection circuitry and isolated the imaging and deflection regions of the camera. The whole chassis was then enclosed in an 18 SWG sheet aluminium skin for isolation from RF fields and operator protection.

The prototype image tube was incorporated into a camera configuration illustrated schematically in fig. 2.15.

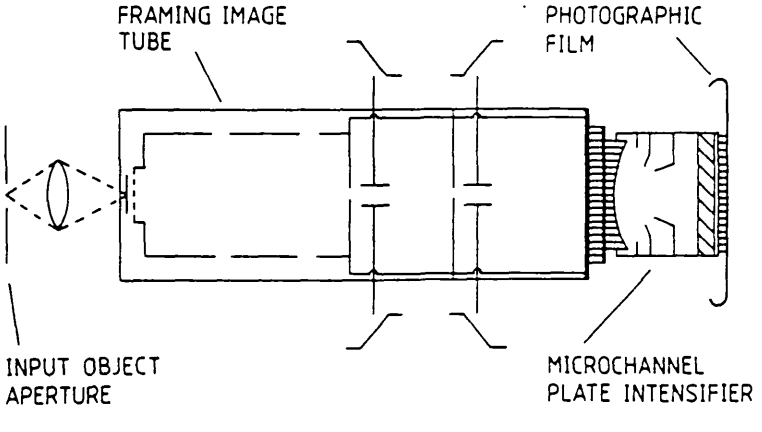

Fig.2.15 Schematic of the Picoframe I camera.

An 80mm focal length f/1.5 input optic was arranged to provide a demagnification of x1.5. Thus the overall magnification between object plane and screen plane was approximately unity. In order to minimize the detrimental effects of space charge defocusing [10] due to excessive photocurrents, a microchannel plate image intensifier (Mullard type XX1330A) was fibre-optically coupled to the image tube. The intensifier had an extended S20 photocathode and a relatively low luminance gain of approximately 250 when coupled to the blue P.11 type phosphor of the tube.

During the experimentation the intensifier was gated on for ~200μs to allow use of optically contacted film recording without undue integrated noise. Image recording was either by Polaroid film or 70mm Ilford HP5 held in intimate contact with the intensifier fibre-optic output. The effect of combining the individual component MTF's (see section 5.2.3) can be seen by the decrease in limiting resolution caused by the addition of each component, see table 2.3

Component	Limiting spatial resolution in x (lp/mm)	
	At screen	At photocathode
Just tube	37	55
Tube + f/1.5 lens	22	31
Tube + f/1.5 lens + Intensifier	10	14

Table 2.3 The effect of combining individual component MTF's

2.8 Conclusion

The principle of operation of a sweep/compensation type electron-optical framing image tube have been discussed. Noting the requirements of laser fusion experiments for a two dimensional

imaging diagnostic, with a temporal resolution of ~100ps and spatial resolution ~10 lp/mm, a theoretical image tube design has been developed. In the design, use was made of computer aided design techniques to produce an electron-optical lens design of low magnification and extended long narrow waist beam profile.

Two proposed deflection schemes have been reviewed. A multiplex aperture plate design incorporating three linear framing apertures, each with an associated pair of compensating deflectors, permits the generation 'triplet' framed images. Three proposals to prevent image overwriting were discussed; (i) discriminator plates, (ii) dephased waveforms, (iii) standing DC bias potentials. A second tube design, greatly simplifying the practical difficulties of construction, incorporates a single framing aperture and pair of compensation deflectors. The action of the tube is similar to that of the three aperture design, but sequenced framed imaging requires multiple sweep operation. A triangular shaped voltage profile allows the electron beam to be swept over the framing aperture twice, resulting in 'doublet' framed images. Frame discrimination is provided by careful dephasing of the applied waveforms such that each image experiences a residual DC bias.

The relaxation in constructional demands resulted in the simplified single aperture design being adopted for fabrication of a prototype tube. The Picoframe I optically sensitive image tube was thus constructed with industrial collaboration. At the centre of the screen the limiting spatial resolution in both the **x** and **y** direction exceeded 35 lp/mm. The image quality was was observed to be asymmetrically degraded as the image was deflected off axis. This asymmetry is attributed to distortions in the electron lens region due to manufacturing tolerances and tube processing.

The static deflection sensitivities of the two pairs of deflectors were observed to differ by around 7%. It is likely that this will result a degradation of the dynamic spatial resolution. Influence of the deflector sensitivities by direct manipulation is of course prohibited by their enclosure inside the vacuum envelope. It is one of the recognised facets of experimentation with sealed-off image tubes that any post processing modifications must be made exterior to the tube.

References - Chapter 2

[1] R Sigel, A G M Maaswinkel and G D Tsakiris,
Proc. 16th ICHSPP, SPIE 491 814 (1984).

[2] O Klemperer and M E Barnett,
'Electron Optics', 3rd Edition
Cambridge University Press (1971)

[3] A E Huston,
Applied Optics, 3(11), 1231 (1964)

[4] F Walters, R A Chippendale and R P Brown,
Proc. 6th ICHSP, p357 (1962)

[5] M R Baggs,
PhD Thesis, University of London (1983).

[6] W Sibbett, M R Baggs, H Niu,
Proc. 15th ICHSPP, SPIE, 348, 267 (1982)

[7] P Grivet,
'Electron Optics', Pergamon Press, Oxford,
2nd English Edition (1972).

[8] S F Essig,
Adv. EEP, 12,73 (1960).

[9] W A Baum,
Adv, EEP, 16, 391 (1962).

[10] H Niu, W Sibbett,
Rev. Sci. Instrum., 52, 1830, (1982)

CHAPTER 3

Single frame operation of the Picoframe I using laser illuminated photoconductive elements

3.1 Introduction

Although the Picoframe I camera system has a multiple frame capability through the provision of shaped deflection waveforms it was felt advisable to first demonstrate the single frame performance of the camera. This relaxed the deflection voltage waveform requirement to the provision of a linear rising ramp. Due to the linearity, fast risetime and earlier success in implementing laser illuminated semiconductor elements in the generation of deflection waveforms for streak cameras, their use was adopted in the initial single frame evaluation of the Picoframe I camera.

Dynamic evaluation of the camera system required that both the temporal and spatial resolution characteristics be evaluated. As the temporal resolution was defined by the time taken to sweep the electron beam across the framing aperture a scheme was devised to evaluate this by operation of the camera in the streak mode. Dynamic spatial imaging characteristics were evaluated by how well the camera could reproduce a test resolution chart imaged at the photocathode. The 1951 USAF test resolution chart was employed during all the dynamic evaluations. A full size version of the test target is reproduced in fig. 3.1.

Each target element consists of two orthogonal sets of three parallel lines whose line width equals the spacing between the lines

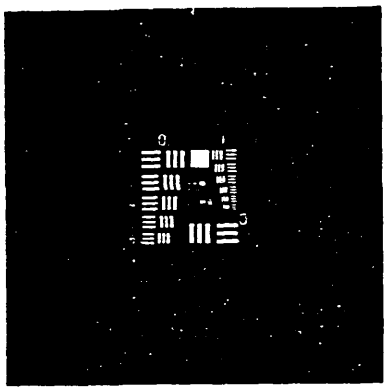

Fig.3.1 The 1951 USAF resolution test chart

Each group consists of six elements labelled 1 through 6. The spatial resolution range covered by a standard size chart is from 1 to 228 line pairs per mm (lp/mm) where each step is separated by a factor of 1.1225.

3.2 Semiconductor photoconductive elements

The transformation of a picosecond optical signal into a picosecond electrical signal by the use of a Semiconductor Photoconductive Element (PCE) was demonstrated by Auston [1] in 1975. He inserted a thin wafer of intrinsic silicon into a transmission line. Applying a voltage to one end of the transmission line and monitoring the other, the PCE could be turned 'on' by illumination with the second harmonic from a Nd: glass laser, and 'off' with the fundamental radiation. Since then PCE's (Auston Switches) have been used for fast switching of Pockels' [2] and Kerr [3] cells, operation of picosecond sampling gates [4] and sychronisation of streak cameras [5].

3.2.1 Description

A simple model of the energy level structure in a semiconductor crystal comprises two allowed bands, valence and

conduction, separated by an energy gap E_g. In a pure (intrinsic) semiconductor at room temperature the valence band is heavily populated, with the conduction band only sparsley so. Electrons in the valence band are shared by all the atoms forming a metallic bond. They are thus unavailable for conduction and the semiconductor exhibits a large resistivity. Promotion of electrons from the valence to the conduction band by absorption of sufficient energy to traverse the band gap, allows the electrons to move freely under the influence of an external electric field forming a current. The vacancy in the valence band so formed is called a 'hole' and may also participate in the conduction of the crystal with an effective charge +e.

In the case of laser illuminated PCE's the absorption of photons is responsible for the generation of charge carriers. If the photon energy exceeds the band gap energy, i.e.

$$h\nu > E_g$$

the single photon absorption occurs, otherwise less efficient multiphoton processes occur. With intense picosecond laser pulses the number of carriers can be dramatically increased and the conductivity modified over several orders of magnitude.

A typical configuration incorporates a semiconductor PCE slab into a microstrip transmission line (fig.3.2). When illuminated by an intense laser pulse the impedance of the PCE drops dramatically due to the rapid creation of electron-hole pairs, allowing the source voltage to be switched into the load. Efficient switching occurs if the PCE impedance drops to very much less than the characteristic impedance of the transmission line (typically 50Ω).

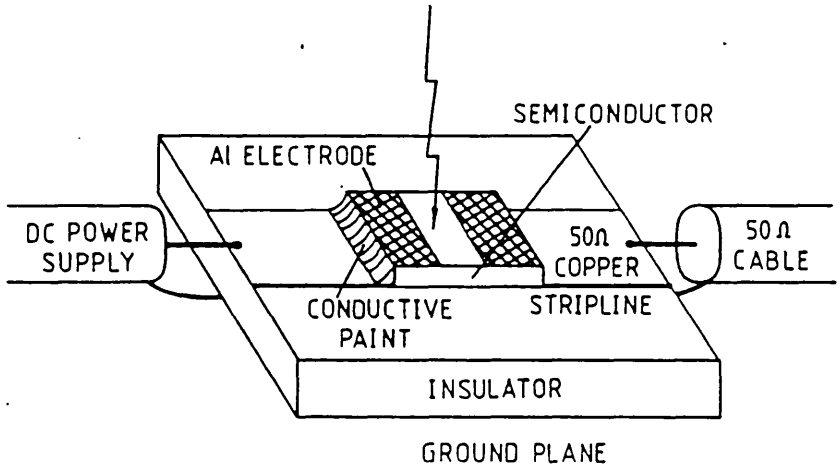

Fig.3.2 PCE in a microstrip transmission line configuration

3.2.2 Gallium Arsenide PCE's

The semiconductor material employed in the fabrication of the PCE's used in work presented in this thesis was semi-insulating chromium doped Gallium Arsenide (GaAs). A III-V semicoductor demonstrated in the picosecond switching role by Lee [6], it can readily be obtained with resistivities 10^8 Ωcm. The chromium dopant concentration is selected during manufacture of the crystal to compensate for the undesirable properties intr-oduced by impurities. The high resistivity of the material enables it to insulate kilovolt bias potentials with very low leakage current, implying good thermal stability.

The recovery time of semi-insulating GaAs PCE's, due to the recombination of photoinduced carriers, has been measured using correlation techniques and found to be between 50-150ps [7,8]. Since the response time of the capacitative deflector plates of a streak or framing tube might be ~1ns, this can present some-thing of a problem. A GaAs PCE incorporated into a 50Ω trans-missions line will start to recover before the deflectors have had an opportunity to respond. This results in low sweep speeds

and limited scan. Margulis [9] devised a novel solution to this problem by incorporating the GaAs PCE between two resistors of much greater resistance than the light impedance of the PCE, but much less than its dark impedance. With a light impedance of ~1Ω and a dark impedance of ~100 MΩ, resistor values of a few MΩ proved satisfactory. The open time of the PCE is thus extended as its impedance must recover to a value comparable with the resistors either side before switching efficiency fails.

The circuit employed in providing the deflection ramps for the experimental framing camera (shown in fig.3.3).

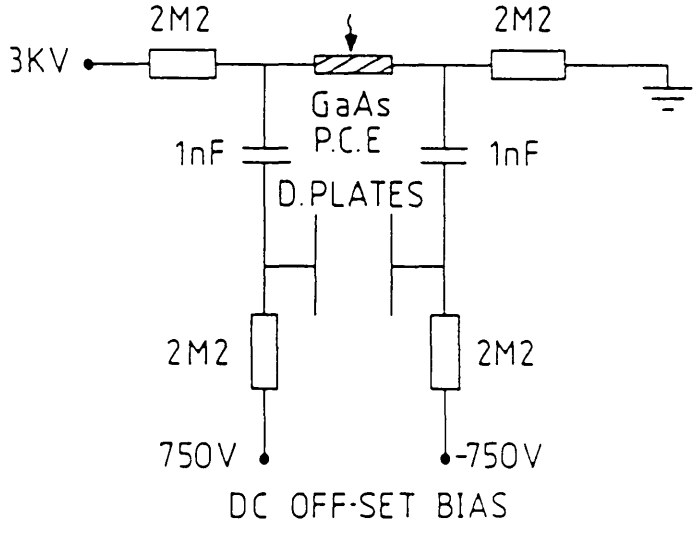

Fig.3.3 GaAs PCE in symmetrical deflection circuit

provided positive and negative going symmetric deflection ramps. The provision of positive and negative bias potentials allowed the fastest section of the voltage ramp to operate over the central region of the screen. Writing speeds as fast as 4×10^{10} cm/s were obtained using this arrangement on a Photochron IIA streak camera, with a typical jitter of < 15ps [10].

3.2.3 Fabrication

A slab of chromium doped GaAs was polished to a thickness of 0.25mm. It was then cut into chips, typically measuring 10mmx2mm using a diamond saw. Each chip was retained on a glass slide by means of optical wax which allowed easy removal by heating with a hot air gun. A 3mm wide strip of aluminium foil was placed centrally across each chip and secured to the glass slide with adhesive tape. The glass slide could then be placed into a vacuum evaporation chamber and a thick aluminium film evaporated over the semiconductor. Once out of the chamber the masking foil was removed, revealing a PCE chip with two aluminium electrodes spaced by 3mm. Other electrode spacings could be obtained by use of different width masking foil.

3.2.4 Operation

The deflection circuit described (fig.3.3), with its associated resistors and capacitors was formed on a small piece of double sided printed circuit board. The back surface of plain copper acted as a ground plane, with 3mm copper tracks etched on-to the front to provide a 50Ω impedance microstrip transmission line. A gap slightly longer than the PCE chip was left in the transmission line. Optical wax then secured the PCE in position with the electrical contact between the aluminium electrodes and transmission line completed by conductive silver paint. The circuit capacitors and resistors were soldered directly to the board to minimize inductance.

When in use care was taken to illuminate not only the whole of the gap but also the electrodes as well. This was found to be important probably because the contacts are not ohmic: an ohmic contact occurs when the conduction bands of metal electrode and

semiconductor overlap permitting easy electron flow in either direction [11]. Effective illumination of the semiconductor - electrode junction produces a large number of free carriers in the semiconductor which transforms the junction characteristics to conductor - conductor rather than semiconductor - conductor.

The activation energy for the PCE is dependent on; photon energy, mobilities of the charge carriers, refractive index of the material and the PCE gap dimensions. Kilovolt pulses have been switched with a few μJ energy [12]. However, for efficient saturated switching of devices of the dimensions described, accounting for optical losses in the system, laser pulse energies of $\sim$100μJ are necessary [5].

3.3 Single - frame operation using the series feed-in configuration

The single fast, linear voltage ramps necessary for single-frame operation of the Picoframe I were generated using a GaAs PCE in the circuit described earlier. To appropriately arrange the timing of the voltage ramps, due account had to be taken of the fact that the photoelectron transit time to the framing deflectors was less than that to the compensating deflectors. This was facilitated by a differential cable delay in the signals applied to the deflectors. For reasons described previously (chapter 2) image 'stationarity' relies upon the correct cancellation of the imparted transverse electron velocity, by the provision of equal but opposite deflection fields. In the first instance this provision was made by driving the two pairs of deflectors in series with the inter-connection between them reversed resulting in operation in the opposite sense. This arrangement is referred to as the series feed-in configuration.

3.3.1 The experimental arrangement

The experimental set-up employed is illustrated schematically in fig. 3.4. Due to the moderately high energy optical pulse requirements for operation of the GaAs PCE use was made of the amplified hypershort pulses for a colliding pulse mode-locked, CW ring dye laser[13] (see section 6.7.1). Optical pulse-widths as short as 200fs were measured for this system using a nonlinear technique.

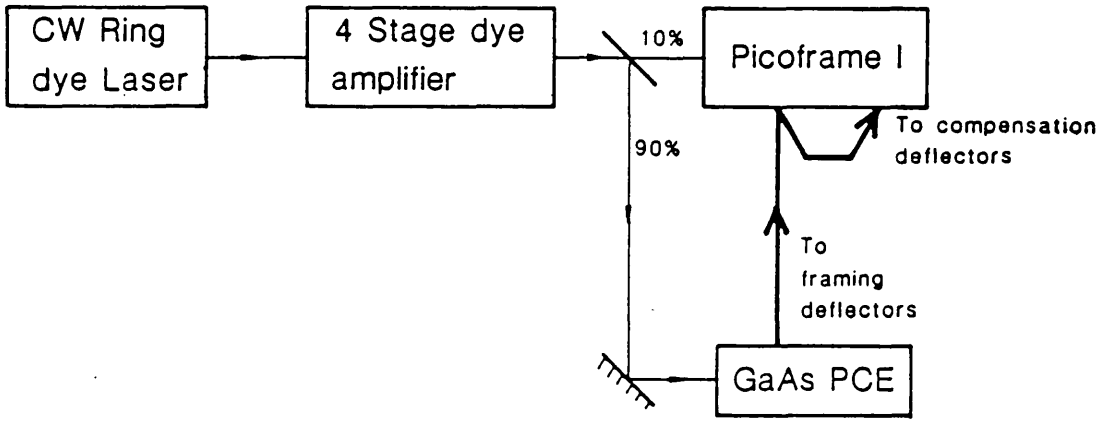

Fig.3.4 Schematic of single-frame operation of the Picoframe I camera using the series feed-in configuration

Low energy (~20pJ) pulses from the CW ring dye laser were amplified in a 4-stage amplifier [10] to energies of ~0.4mJ. The amplifier consisted of three consecutive transversley pumped stages followed by a longitudinally pumped stage. Kiton Red dye was employed in the first stage cell with Rhodamine 101 in each successive cell. To prevent excessive losses due to ASE, each stage was optically isolated from the next by a combination of spatial filtering and saturable absorbers. A 0.3mm thick Schott

RG 630 filter was used between the first and second stages with Malachite Green in ethylene glycol saturable absorber jets between each of the remaining stages. In addition to filtering the ASE the saturable absorbers also helped prevent excessive pulse broadening by sharpening up the leading edges. Each of the four dye cell stages were pumped by the frequency doubled output from a Q-switched Nd:YAG oscillator delivering up to 200mJ optical energy.

The amplified laser pulses were split using a pellicle beam splitter. Approximately 10% was directed by a system of mirrors through a diverging lens to illuminate the camera input. The remaining 90% was directed via an adjustable optical delay line onto the GaAs PCE. A cylindrical lens concentrated the light onto the PCE gap and electrodes. Prolonged operation could be maintained with the PCE biased at 2kV; higher bias voltages over the same gap dimensions often resulted in break-down.

It was necessary to first synchronise the arrival of the framing deflector waveform to the arrival of the image forming electron packet at the deflection plates. This was achieved by means of the adjustable optical delay line, whereby the generation of the voltage ramps could be delayed or advanced with respect to the arrival of the photoelectrons. Sychronisation was carried out in the streak mode, where the compensation deflectors were maintained electrically common with the anode and screen. A single linear voltage ramp was then applied to the framing deflectors only. In this mode the quasi-normal reflections from a calibrated optical delay line illuminated a 40μm slit situated at the camera input. When correct synchronisation was achieved the streaked photoelectrons passed

through the framing aperture and formed a set of slit images at the centre of the phosphor screen.

Due to the limited screen area, restricted by the small framing aperture diameter, only a short time window of between 100 - 200ps existed when anything could be observed at the screen. This corresponded to a delay line change of 3-to-6cm, thus making initial synchronisation difficult. However, due to the picosecond jitter to be expected of laser illuminated PCE's once synchronisation was achieved it was highly reproducible.

3.3.2 Frame duration calibration

Determination of the frame exposure duration was carried out by operating the camera in a streak mode using one set of deflectors. The single input slit, used in setting up the camera synchronisation, was replaced by a mask object illustrated in fig.3.5. It consisted of a combined slit and open area, and was fabricated by masking off half a glass blank and evaporating with aluminium. The masking was then removed and a slit scribed into the evaporated half. When correctly positioned at the input plane of the camera and illuminated, an inverted 'mushroom' shape image was observed at the screen. This was the superposition of the mask image on the circular field of view of the camera, where the field of view was defined by the diameter of the framing aperture (see fig.3.5).

With the camera operated in the streak mode a linear voltage ramp was supplied to the framing deflectors. Six sub-pulses of 20ps temporal separation from a optical delay line were used to illuminate the mask object.

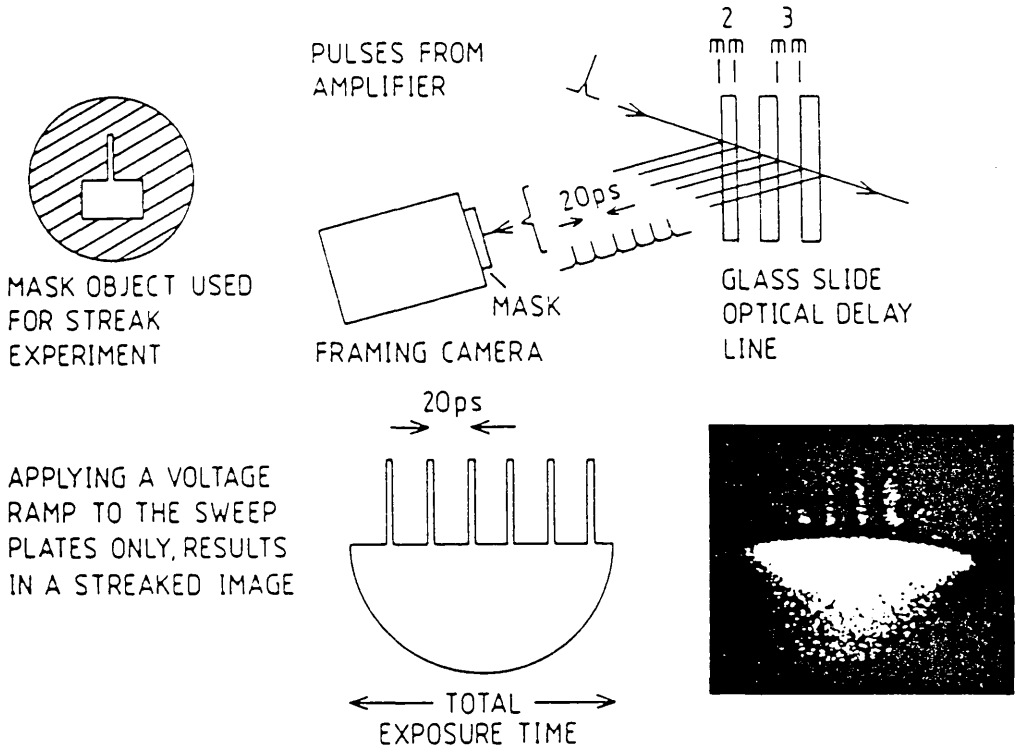

Fig. 3.5 Scheme for streak calibration of frame exposure time. Insert is a reproduction of an experimental result.

When correctly synchronised six displaced images of the mask object were observed at the centre of the screen. The frame duration was then evaluated by comparison of the known streak separation to the diameter of the 'mushroom' head, as the field of view was still defined by the framing aperture diameter. A typical result is shown in fig. 3.5 (insert), which demonstrates a frame duration of 190ps. Shot-to-shot variation in the amplified laser pulse amplitude resulted in an open time variation of $\pm$20ps.

3.3.3. Framing operation

To measure the dynamic spatial resolution of the Picoframe I in single frame mode the mask object used previously was replaced by a standard size 1951 USAF resolution test chart. The test target was then illuminated by a single amplified laser

pulse (i.e. 20ps optical delay line removed). A single GaAs PCE was connected via a 350mm length of 50Ω coaxial cable (UR-M43) to the framing deflector plate feed-through pins. A second length of 50Ω coaxial cable then inter-connected the framing and compensation deflectors in the opposite sense, thus driving the deflectors in series. It was necessary to choose the length of the inter-connecting cable such that the signal transit time matched the electron transit time between the deflectors. The length of cable required was estimated by calculating the electron transit time between the deflectors.

Equating the energy gained by an electron in accelerating to an anode potential V_a to its kinetic energy (assuming it starts from rest, or that the initial energy is negligible) gives:-

$$eV_a = \tfrac{1}{2}mv^2$$

Where m is the rest mass of an electron (relativistic effects can be ignored below acceleration potentials of 20kV), e is the electron charge and v is the electron velocity, then

$$v = \sqrt{\frac{2eV_a}{m}}$$

In the initial tests the anode potential was 12kV, thus substituting for constants e and m gives $v = 6.49 \times 10^7$ m/s. As it is difficult to be sure exactly where the electrons are first influenced by the deflection field, fringing fields will influence the electron before it enters the parallel plate deflectors, the distance between the deflectors was taken as the centre-to-centre distance. For the Picoframe I this distance is 66mm which results in an electron transit time of about 1ns. Since the group velocity in the 50Ω coaxial cable was 0.66c a length of about 200mm was necessary to introduce the required delay.

3.3.4 Results

Slightly different length inter-connecting coaxial cables between the deflectors were employed and framed images for each case recorded on Ilford HP5 film which was push processed using Ilford Microphen developer. Exposures were bracketed by successively stopping down the aperture of the camera input lens. The spatial resolution results obtained are summarised in table 3.1

Cable length(mm)	Limiting spatial res. at photocathode(lp/mm)
180	<1
200	1
224	1.6
233	1.78
239	<1

Table 3.1. Dynamic spatial resolutions for different lengths of inter-connecting cable.

Optimum spatial resolution was obtained using a 230mm length of cable and by fine adjustment of the potential difference across the resistive divider chain by a few hundred volts. This slightly influenced the electron transit time between the two pairs of deflectors with a discernible effect upon the spatial resolution. A single frame recording of the USAF test chart is reproduced in fig.3.6. This does not illustrate the best resolution observed, but shows good contrast with the familiar test target features clearly evident. Close inspection of the original recording reveals a dynamic spatial resolution of 7 lp/mm referred to the photocathode.

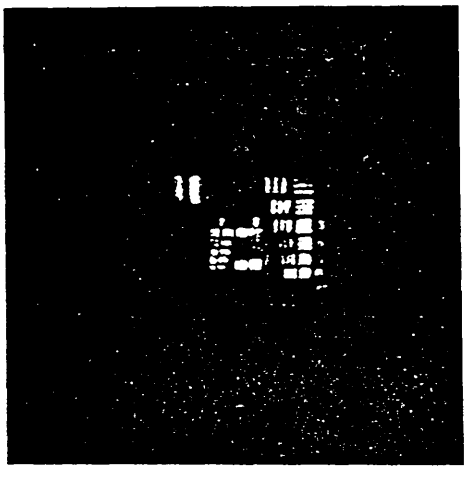

Fig.3.6. A recorded two-dimensional, single frame image of standard size USAF test chart.

The full size USAF chart was a little too large to be conveniently imaged onto the restricted cathode format size with the x 1.5 demagnifying input optic, thus a x2 demagnified copy of test target was substituted. A typical recorded framed image of this format is reproduced in fig. 3.7. It is noted that the images do not suffer noticeably from astigmatism or other spatial distortions. Examination of the original contacted film indicates that it is possible to resolve the sixth element of group one on the x2 demagnified target. This corresponds to a dynamic spatial resolution of 7 lp/mm at the screen. Taking account of the image tube magnification this corresponds to a resolution of 10.5 lp/mm at the photocathode.

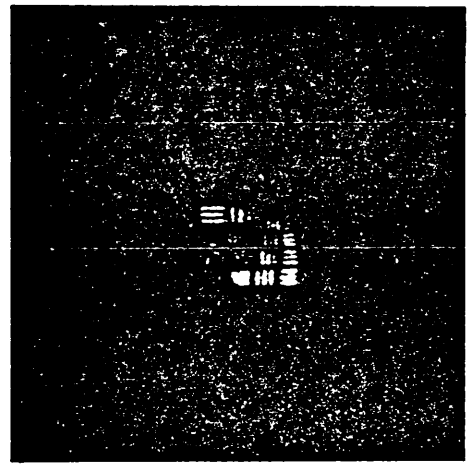

Fig.3.7. A recorded, single frame image of a x2 demagnified USAF test chart object.

3.3.5 Discussion

In this early evaluation it must be emphasized that although the camera had an 'open' time of 190ps, the test target was only illuminated for less than 1ps. This had the consequence of relaxing the constraints on linearity and synchronism of the deflection voltage ramps as a match had only to be achieved over a short timescale. However, for a specific limit of detection (i.e. the film speed) the photocurrent in the tube is inversley proportional to the exposure time [14]. In this case since the illimination period was very much shorter than the tube 'open' time, the exposure duration was governed by the length of the illumination pulse. Thus the space charge effects (see section 1.2.4) associated with high photocurrents were exacerbated. It was likely then that in testing under longer illumination conditions difficulties would be experienced in achieving a good match in the deflection voltage gradients over an extended period and

some loss in dynamic spatial resolution would be observed.

3.4. Framing operation with picosecond illumination

To more fully characterise the dynamic framing performance of the Picoframe I the ~10ps (FWHM) duration pulses from a passively mode-locked Nd: phosphate glass laser [15] were employed.

3.4.1 The experimental arrangement

The experimental set-up used is depicted in fig.3.8

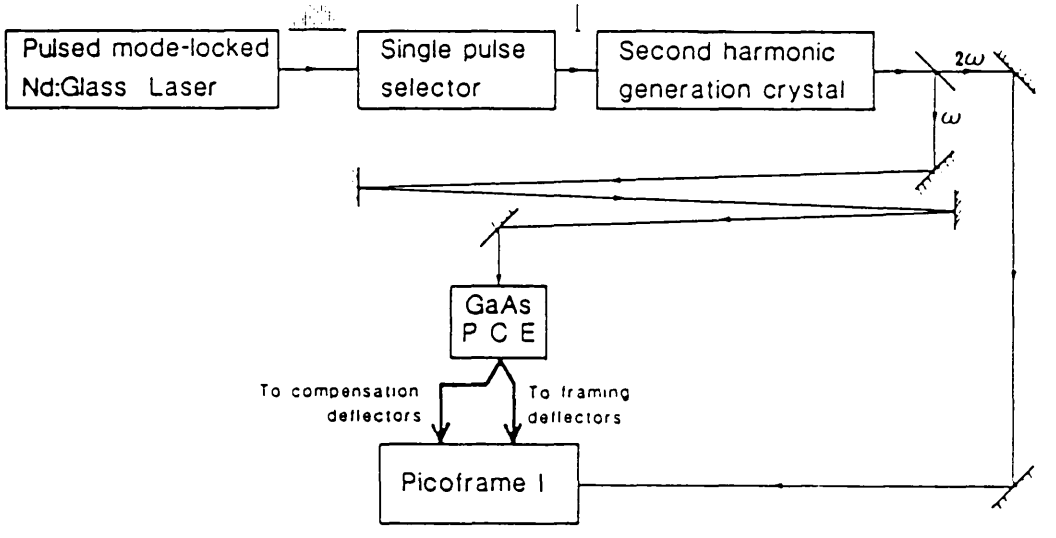

Fig.3.8 Experimental arrangement employed in single-frame evaluation of the Picoframe I using the parallel feed-in configuration

The single-shot Nd:phosphate glass (3.3% doped Hoya LHG5) oscillator had a cavity round trip time of 7ns and produced mode-locked pulse trains at a wavelength of 1.053μm. The laser rod was 166.5mm long with a diameter of 9.5mm and Brewster-angle faces. It was pumped by a single helical xenon flashlamp dissipating

approximately 1kJ of energy stored in a 47μF capacitor charged to around 6kV. A circulating water system around the rod provided cooling, but even so the repetition rate was limited to around one shot per minute. Fresh air pumped into the cavity head displaced the ozone formed by the flashlamp discharge.

Passive mode-locking was by a $2x10^{-5}$ M solution of Eastman Kodak 9860 in 1,2 - Dichloroethane contained in a 250μm cell in optical contact with the 2.0m radius of curvature back mirror. The dye cell window was made of red filter glass to reduce photo-decomposition of the dye by short wavelength flashlamp radiation. No transverse mode selection was employed with completely mode-locked pulse trains obtained at a success rate of around 90%. A typical mode-locked pulse train consisted of between 80 to 100 pulses with a total energy of ~100mJ.

3.4.2 Framing operation

The voltage waveform generated by the laser illuminated PCE deflection circuit comprised a very fast rising edge (risetime limited by the deflection circuit to a few 100's picoseconds) followed by a relatively slow decay (~100ns). High speed framing operation was achieved by sweeping the electron image using the fast rising edge. Since further images would be swept back across the framing aperture during the slow 'reset' period, obscuring any recorded framed image, successive pulses from the mode-locked pulse train were prevented from illuminating the photocathode. This was achieved by selecting a single illumination pulse from the centre of the pulse train, by means of a Pockels' cell located between two crossed Glan-Thompson polarizers in a standard single - pulse - selector (SPS) configuration.

A small percentage of the laser output was incident on a vacuum photodiode which provided a ~10V trigger signal for a hybrid avalanche transistor/Kryton (KN22B) step voltage generator. This was configured in a Blumlein arrangement to provide a 7ns long, 9kV square gating pulse for the Pockels'cell. Reliable pulse selection from the centre of the wave-train was facilitated by positioning a suitable number of neutral density filters in front of the photodiode and by adjusting the trigger signal delay to the hybrid step generator circuit.

The S 20 photocathode activated prototype Picoframe I was insensitive to the fundamental radiation, thus the second harmonic was generated in an angle-tuned crystal of ADP, with a typical conversion efficiency of about 10%. A dichroic beamsplitter (coated for 100% reflectivity at 1.053μm) directed the fundamental via an adjustable optical delay onto the GaAs PCE. It is estimated that due to divergence of the multi-mode beam, optical losses in the SPS and optical delay line that the energy available for PCE activation was between 50μJ to 100μJ. As the photon energy was insufficient to permit single photon excitation in the PCE less efficient multiphoton processes occurred. The transmitted second harmonic radiation was then used to illuminate the test chart. To permit more efficient use of the 6mm x 6mm usable cathode format a f/3.5, 64mm focal length lens operating at an increased demagnification of x2.2 replaced the f/1.5 lens employed previously.

3.4.3 The parallel Feed-in configuration

Initial attempts at framed imaging using the series feed-in configuration employed previously with hypershort pulse illumination proved unsuccessful in recording a truly stationary image,

under longer illumination conditions. It was recognised that mismatch effects arising from the different cable lengths and from the deflector plate connections would cause the voltage ramp to the compensating deflectors to be significantly distorted. As such the gradients may only have matched over a small temporal range.

To overcome this problem a new deflection feed-in arrangement was devised; designated the parallel feed-in configuration. Two separate 50Ω coaxial cables were connected to the output of a single GaAs PCE and used to drive the two pairs of deflector plates. Of course, by necessity, the two cables had to be of different lengths to achieve the correct synchronisation between the electron beam and the deflection ramps. Initial synchronisation of the camera was again carried out in the streak mode using the framing deflector plates only. Framing operation was then carried out and the differential cable length adjusted for optimum dynamic spatial resolution.

3.4.4 Results

The most promising results were achieved using a 350mm length of coaxial cable to the framing deflectors and lengths between 540mm to 560mm to the compensating deflectors. This range was investigated more thoroughly for different anode potentials and deflector bias potentials. Optimum dynamic spatial resolution was achieved using 350mm and 545mm lengths of cable to the framing and compensation deflectors respectively. The overall tube potential was 12kV with a bias of 2kV across the PCE and deflector plate biases of $\pm$325V. A framed image of a full size test resolution target obtained under these conditions is reproduced in fig.3.9.

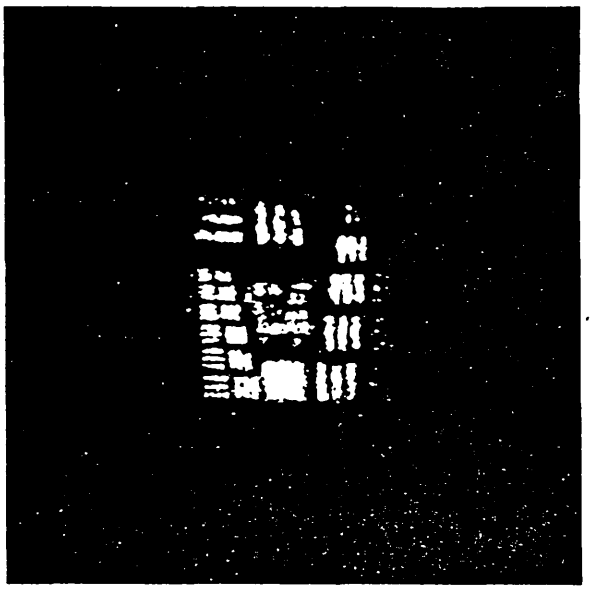

Fig. 3.9 Single-framed image recorded using the parallel feed-in configuration.

Careful inspection can resolve up to group 0, element 6 in both directions, which accounting for the x2.2 demagnification of the input optic, corresponds to a dynamic spatial resolution of 4 lp/mm at the photocathode.

Temporal calibration was carried out in the streak mode using a similar procedure to that described earlier. However, on this occasion a two stage process was adopted. Instead of using a mask object combining an optical slit and open area region, a single slit object was initially employed with the camera in streak operation. Two subpulses temporally separated by 50ps from an optical delay line resulted in two streak images recorded at the screen by optically contacted film. The slit object was then removed and the camera field of view uniformly illuminated. This yielded a shadow image of the framing aperture at the screen again recorded using optically contacted film thus ensuring a direct correspondence between the recorded images.

Provided the sweep speed in the streak and framing evaluations was the same, ensured by maintaining identical experimental conditions, comparison of the shadow image diameter to the calibrated streak separation yields the frame exposure duration. The results presented in fig.3.10 demonstrate a single frame duration of around 150ps for the camera operated in this mode.

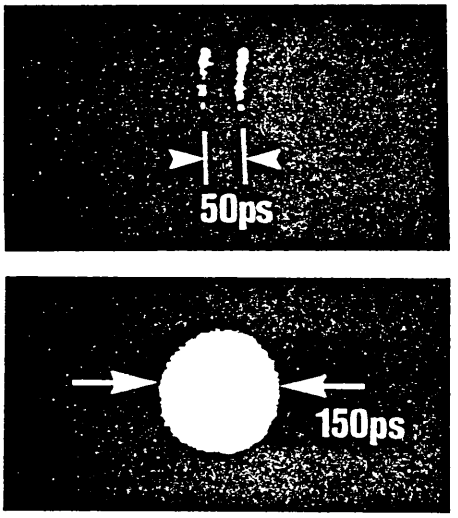

Fig. 3.10 Streak calibration of frame exposure duration of Picoframe I operated with the parallel feed-in configuration.

3.4.5 Discussion

Although it had proved possible to obtain a single framed image of modest spatial resolution with the parallel feed-in configuration, it was evident that the recorded images suffered from incomplete compensation. This was primarily caused by the disparity between the sensitivities of the two pairs of deflectors. It was also realised that dispersion in the unequal lengths of coaxial transmission line might result in discrepancies between the voltage waveforms arriving at the deflectors. This was analysed by propagating a fast risetime step voltage profile

along equivalent lengths of cable to those employed in the experimental set-up. The resultant waveform was monitored at the other end by a fast ($\leq$ 25ps risetime) sampling head (Tektronix type S4). The results illustrated in fig.3.11 show; (a) no cable between the generator and sampling head, just the necessary connections, (b) the cable supplying the framing deflectors, (c) the cable supplying the compensating deflectors.

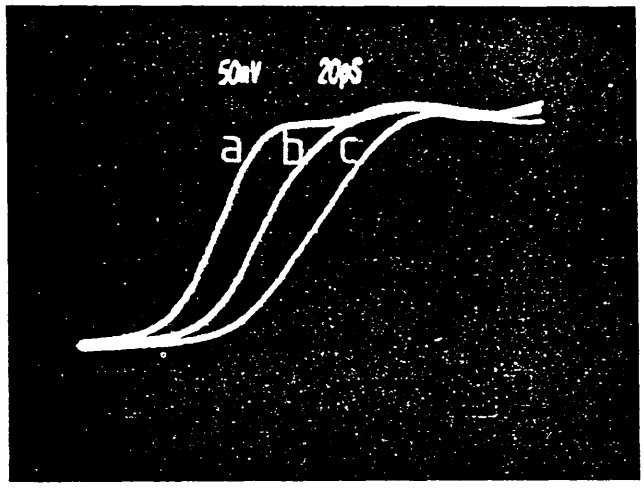

Fig.3.11 Degradation of signal risetime for (a) no cable, (b) 350mm, (c) 550mm lengths.

Inspection of fig.3.11 reveals that the compensation voltage ramp has a 10% - 90% risetime about 10% slower than that of the framing ramp. This effect tended to act in favour of the prototype tube where the sensitivity of the framing deflectors exceeded that of the compensator deflectors by about 7% (see section 2.6). The degraded signal risetime partially offset the disparity in deflection sensitivity thus in this particular instance, probably somewhat fortuitously, it was possible to find a region on the voltage ramp which yielded a moderately well compensated image.

Clearly for longer illumination periods approaching the

frame exposure duration such a fortuitous match in the effective responses of the deflectors cannot be guaranteed. Since manufacturing tolerances and distortions caused by processing are inevitable in this type of tube, it was unlikely that the sensitivities of the deflectors would be identical. Evidently it was desirable to devise a scheme whereby exact compensation of the imparted transverse electron velocity could be achieved, preferably by control of parameters external to the tube. The parallel PCE configuration was a scheme devised to allow external control and is discussed in the next section.

3.5. The parallel PCE configuration

A novel scheme to provide independent control of the deflection voltage gradient applied to each pair of deflectors, thus varying the degree of compensation experienced by the electrons was investigated. Each pair of deflector plates were connected to an independent PCE via identical lengths of 50Ω coaxial transmission line. Independent control of the bias potential applied across each of the switching elements permitted a corresponding control of the voltage gradient applied to the deflectors.

3.5.1 The experimental set-up

Two GaAs PCE chips were cut from the same crystal and had 2mm separation aluminium electrodes evaporated at the same time. Each was mounted onto a circuit board with optical wax; the electrical connection between electrode and microstrip transmission line being made by a conductive silver preparation. Connection to each respective pair of deflectors was made by 350mm lengths of 50Ω coaxial transmission line.

The experimental arrangement is illustrated in fig. 3.12

For fully saturated operation of both GaAs PCE devices optical pulse energies of $\geq$ 200μJ were necessary. To satisfy this requirement the amplified output from a pulsed Nd: YAG mode-locked oscillator operating at a wavelength of 1.06μm in the TEM_{oo} mode was employed. A single pulse of ~35ps (FWHM) duration with an energy of ~0.15mJ was selected from the mode-locked pulse train using a Pockels' cell switched by a triggered spark gap. This was then amplified in a double pass flashlamp pumped amplification stage providing gains of up to x1000, before second harmonic generation in an angle-tuned KDP crystal.

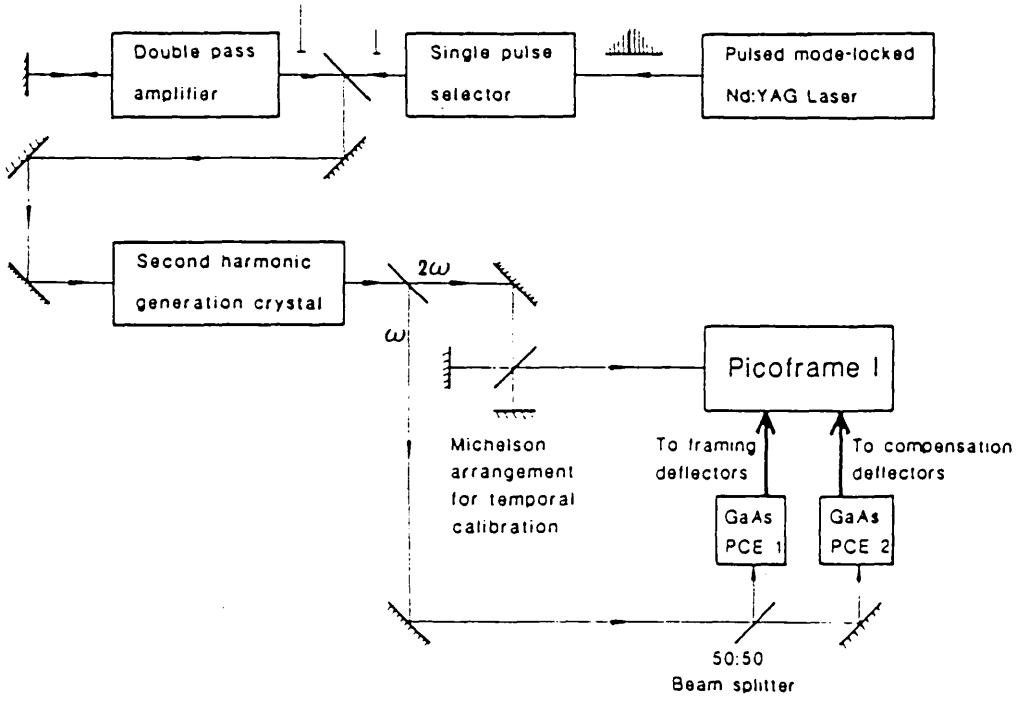

Fig.3.12 Experimental arrangement employed in operating the Picoframe I using the parallel PCE configuration.

Fundamental and second harmonic radiation were separated by a dichroic beamsplitter coated to be 100% reflective for 532nm radiation at 45° incidence. The second harmonic was directed, via a Michelson optical delay arrangement, to illuminate the camera input. Any harmonic leakage was removed by a Schott

RG1000 filter inserted after the beam splitter. The fundamental was then split into two beams of roughly equal intensity by a 50% beam splitter. One beam was directed onto the PCE providing the deflection voltage for the framing deflectors, while the other beam was directed by a 100% reflectivity mirror onto the PCE connected to the compensation deflectors. Both PCE circuits were mounted on translation stages such that their effective separation could be adjusted to advance or retard the relative timings of the deflection ramps. The beam size at the PCE (observed with the aid of an IR image converter) was such that it adequately covered the PCE gap and electrodes. A calorimeter (NPL design type 7471) was used to measure the energy in each fundamental beam incident on the PCE's. Each was determined to be 600μJ $\pm$ 100μJ, which was found sufficient to ensure fully saturated operation of both PCE devices.

Initial camera synchronisation was carried out in the streak mode. Due to the relatively long pulse duration (~35ps FWHM). the optical delay line was adjusted to provide subpulses separated by 100ps for adequate resolvability. As this was close to the expected frame exposure duration the set-up procedure was carried out using the compensation deflectors, with the framing deflectors maintained at anode potential. This greatly increased the viewable time window and considerably eased the synchronisation procedure.

3.5.2 Framing operation

For evaluation in the framing mode one arm of the Michelson delay line was blocked to provide single pulse illumination. The input slit was replaced by a full size USAF test target, and the framing deflectors reconnected to the first PCE. By

differential variation in the positions of the translation stage mounted PCE's, the timings of the deflection waveforms could be synchronised to the arrival of the image forming electron packet at each pair of deflectors. An optical delay of 0.97ns was found to yield the best image 'stationarity' although the spatial resolution was poor. Independent control of the bias potential applied across each of the PCE deflection circuits then enabled the degree of transverse velocity compensation to be varied, such that it was possible to maximize the spatial resolution.

3.5.3 Results

The best spatially resolved image recorded using this scheme is reproduced in fig.3.13. It was achieved while operating the Picoframe tube at an overall acceleration potential of 12kV, with 1.8kV and 2.0kV potential applied across the framing and compensation PCE devices respectively. The deflector plate bias potentials were $\pm$ 600V ensuring sweep operation over the fast, linear central region of the deflection waveform.

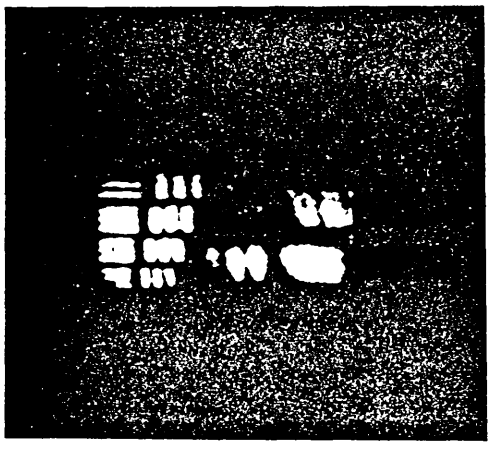

Fig.3.13 Framed image recorded with the parallel PCE configuration.

On inspection of the contacted film recording it is possible to resolve up to group 0 element 6, which corresponds to a dynamic spatial resolution of 4 lp/mm at the photocathode.

Reverting to streak mode operation under identical experimental conditions determined the frame exposure duration. The two stage scheme described in section 3.4.4 was employed to record firstly, the temporally calibrated subpulses from the Michelson delay line arrangement, and secondly the projected framing aperture diameter. The result reproduced in fig.3.14 demonstrates a camera 'open' time of approximately 130ps. This was the shortest duration image recorded during the course of this work.

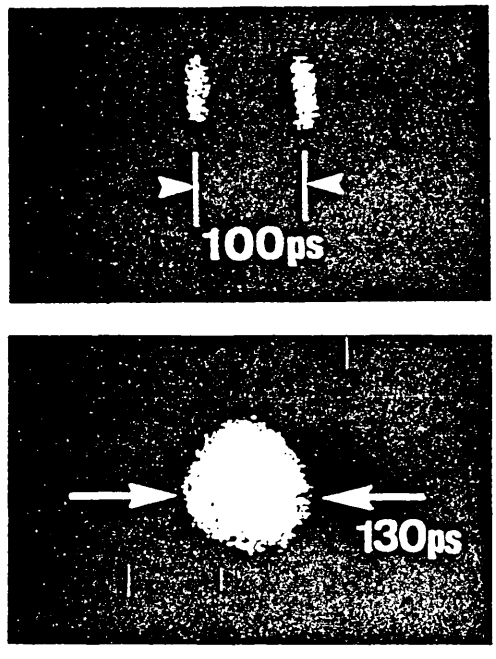

Fig.3.14 Streak calibration of frame exposure duration when operated in the parallel feed-in configuration.

3.5.4. Discussion

Some idea of the criticality in the illumination alignment is apparent from the fact that fig. 3.13 represents the best resolution obtained in many shots. The laser must be extremely reproducible, with any intensity variation in the illumination of the

PCE's resulting in a drastic loss in spatial resolution. Thus although this technique has been demonstrated to be fundamentally sound, the indications are that critical matching of the PCE geometries and use of a highly refined laser system are essential. Generally therefore, this would be a difficult technique to implement into a standard laboratory system. Nevertheless, it has been demonstrated that some form of correction, external to the tube, can compensate for manufacturing tolerances in the sensitivities of the deflectors. In the design proposed by Waters et al, the compensation deflector plate spacing could be externally controlled by means of bellows. This cumbersome added complexity has been shown to be dispensible, if the gradients of the deflection waveforms can be accurately and independently controlled.

3.6 Conclusions

A prototype Picoframe I camera system has been evaluated dynamically in the single frame mode using the high speed, linear voltage ramps generated by laser illuminated PCE's. Chromium doped GaAs PCE chips were prepared from a semiconductor slab, evaporated with aluminium electrodes and incorporated into a symmetrical deflection circuit. The fast recombination time of the material (~100ps) required that the PCE device be located between two high value resistors, to improve the sweep speed and range of scan. Three arrangements employing laser illuminated PCE's in the generation of voltage ramps for the experimental framing camera were evaluated.

In the series feed-in configuration a single GaAs PCE supplied the symmetrical deflection signal for both pairs of deflectors,

connected in series and operating in the opposite sense. Although high quality spatially-resolved images of up to 7 lp/mm resolution at the photocathode were achieved [16], the camera open time of 190ps was very much greater than the illumination period ($\leq$ 1ps). When the experiment was repeated using the longer duration pulses (~10ps FWHM), only very poorly resolved images were obtained. It was thus concluded that under ultrashort pulse illumination the electrons experienced only a very small region of the deflection waveform. Over this it was possible to select a portion where the difference in gradient cancelled the discrepancy in deflection sensitivity, thus generating a well resolved image. When using longer illumination pulses the unpredictable effects of impedance mismatch, made the repetition of such an instance unlikely and only poor reproducibility of results was achieved.

To avoid the unpredictable effects of connecting the deflectors in series, the parallel feed-in configuration was devised. Two coaxial transmission lines, of unequal length to account for the difference in electron transit time to each pair of deflectors, were connected to a single PCE device. In this manner an identical waveform was launched into both cables, and delivered in opposite phase to each pair of deflectors.

Due to dispersion in the transmission line, the risetime of the signal arriving at the compensating deflectors was about 10% slower than that arriving at the framing deflectors. This discrepancy had the somewhat fortuitous effect of off-setting the ~7% difference in the static sensitivities of the deflectors, enabling moderately well resolved images of 4 lp/mm resolution (at the photocathode), with frame durations of ~150ps to be recorded [17]. Realisation that control of the deflection

waveform gradient could be used to effect cancellation of the imparted transverse electron velocity, despite manufacturing tolerances in the sensitivities of the deflectors, resulted in the third configuration evaluated.

In the parallel PCE configuration two independent PCE's were connected via identical lengths of coaxial cable to their respective deflectors. The electron transit time delay between the deflectors was accounted for by an adjustable optical delay between the PCE activation pulses. By varying the voltage applied across each PCE the amplitude of the voltage ramp was changed and the ramp gradient (dV/dt) perturbed, thus permitting accommodation of the response differences of the deflectors. Using this scheme it was possible to generate framed images demonstrating a spatial resolution of 4 lp/mm at the photocathode when the test object was illuminated for at least 35ps [17]. As each PCE device was only required to provide the deflection ramp for one set of deflectors, the current demand was reduced. This permitted the generation of shorter duration framed images, with typical 'open' times of around 130ps.

Unfortunately, although this technique demonstrated the viability of achieving good image compensation by independent control of the ramp gradient applied to the deflectors, there were severe practical problems in ensuring identical operation of two PCE devices. As such the implementation of the camera as a versatile experimental diagnostic would be limited. To ensure a more practical and useful arrangement, it is necessary to develop a more elegant mechanism for achieving control of the waveform gradients and subsequently demonstrate the multiple frame capabilities of the Picoframe design. This is the subject matter of the next chapter.

References - Chapter 3.

[1] D H Auston,
Appl. Phys. Lett., 26, 101 (1975).

[2] P LeFur, D H Auston,
Appl. Phys. Lett., 28, 21 (1976).

[3] M Stavola, J Agostinelli and M sceats,
Appl. Optics 18, 4101 (1979).

[4] J J Weizer, H Merkelo,
Appl. Phys. Lett., 27, 397 (1975).

[5] W Margulis,
PhD Thesis, University of London (1981)

[6] Chi H Lee,
Appl. Phys. Lett., 30, 84 (1977).

[7] S Jayaraman, Chi H Lee,
Appl. Phys. Lett., 20,392 (1972).

[8] V K Mathur, S Rogers,
Appl. Phys. Lett., 31, 765 (1977).

[9] W Margulis, W Sibbett,
Optics Comm., 51, 91 (1984).

[10] P G May
PhD Thesis, University of London (1983).

[11] J Seymour,
'Electronic Devices and Components',
Pitman Publishing Ltd, London (1981).

[12] D H Auston,
Chapter 4,'Ultrashort Light Pulses',
Ed. SL Shapiro, 2nd Edition.
Springer - Verlag (1984).

[13] J P Willson, W Sibbett and W E Sleat,
Optics Comm., 42, 208 (1982).

[14] B R C Garfield, P C Bailey and R Marshall,
Adv. EEP, 33B, 1137 (1972).

[15] J R Taylor, W Sibbett and A J Cormier,
Appl. Phys. Lett., 31(3), 184 (1977).

[16] M R Baggs, R T Eagles, W Margulis, W Sibbett
and W E Sleat,
Adv. EEP. 64B, 627 (1985).

[17] M R Baggs, R T Eagles, W Sibbett and W E Sleat,
16th ICHSPP, SPIE 491, 40 (1984).

CHAPTER 4

Single and double frame operation of a Picoframe camera

4.1 Introduction

A major advantage of the 'Picoframe' framing camera system over a gated image converter tube is the ability to generate multiple framed images. In this chapter two alternative techniques for the generation of 'doublet' framed images are described; (i) the twin aperture Picoframe II, (ii) double sweep operation of the Picoframe I. The Picoframe II is a simplified version of the multiplex aperture plate design discussed in section 2.2.1.

For reasons presented earlier (section 3.1), laser illuminated photoconductive devices were employed in generating the deflection voltage ramps for the Picoframe I camera in the single-frame mode. However, the use of these devices has the disadvantage that moderate energy (~100μJ), picosecond laser pulses are required to efficiently activate them. This might not be a significant limitation in the practical implementation of the camera as a laser fusion diagnostic, where high energy pulses are available, but it can be a disadvantage in preliminary characterisation of the instrument. Where ease of use and only moderate temporal resolution are required, single-shot streak camera systems have successfully utilized electronic avalanche transistor sweep generator circuits [1,2]. In subsequent instrumental evaluations it was thus decided to for-go some degree of sweep speed and proceed with a low trigger energy electronic sweep circuit. It is realised however, that for ultrahigh speed

framing operation (on the sub 100ps timescale), laser illuminated photoconductive devices are currently the only source of the fast, linear voltage ramps required.

4.2 Transistorised sweep generators

Avalanche multiplication in certain types of transistor has formed the basis for high voltage, nanosecond pulse generation for a number of years. This type of generator has been utilized in picosecond streak camera systems with sweep speeds of $\sim 10^{10}$cm/s and trigger jitters of less than $\pm$ 20ps reported [1]. Modest trigger requirements of a few volts can readily be derived from a laser illuminated photodiode for relatively weak optical pulses of around 1μJ energy. Pulse repetition rates are generally low (typically <1kHz), but they readily operate at a few Hertz which is quite satisfactory for framing evaluation.

4.2.1 Avalanche operation

Avalanche action in transistors [3] is due to ionization by collision which creates additional electron-hole pairs within a reversed biased pn-junction. This increases the available current; an action which becomes greater as the collector-base voltage is raised above the normal operating value. The increased electrostatic field across the collector-base junction extends into the base region increasing the width of the depletion layer. Within this extended layer the majority carriers gain sufficient energy to ionise fixed lattice atoms into electron-hole pairs. If the depletion layer is sufficiently wide and the electrostatic field sufficiently strong, these carriers can themselves gain enough energy to cause further ionization. This process is called avalanche breakdown. When it occurs the reverse current

rises rapidly and becomes independent of voltage, generally being limited by the external circuitry.

Not all transistors demonstrate avalanche effects. Usually the most suitable transistors are those designed for high-speed switching which have a thin uniform base region and radial symmetry. Once a promising range of transistors has been chosen, careful selection of devices is necessary to obtain optimal performance due to manufacturing tolerances and impurities.

It is difficult to switch more than a few hundred volts with a single device, so to increase the voltage swing several devices are commonly connected together in series. A trigger signal applied to the base of a transistor at one end of the chain triggers it into avalanche operation. This 'over-volts' the remaining devices causing them to avalanche successively.

4.2.2 An avalanche transistor sweep generator

From work undertaken at Lawrence Livermore National Laboratory USA, it was reported that the National Semiconductor 2N3700 device was highly suited to avalanche operation [4]. A circuit [5] employing two series chains of these transistors was developed by AWRE Aldermaston UK, and has been used in the subsequent work presented in this thesis. The generator was triggered by a fast risetime (~100ps) >10V trigger pulse supplied by a laser illuminated photodiode; there was an intrinsic 10ns delay before avalanche operation. Two chains of transistors provided complementary positive and negative outputs of ~3kV swing about 0V, rising in ~1.5ns. When operated in conjunction with the Picoframe I in a streak mode this circuit provided a sweep speed of 1.2×10^{10} cm/s. The positive and negative ramps

delivered into a 50Ω load and observed using a Tektronix 7904 oscilloscope (700ps risetime) are shown in fig. 4.1.

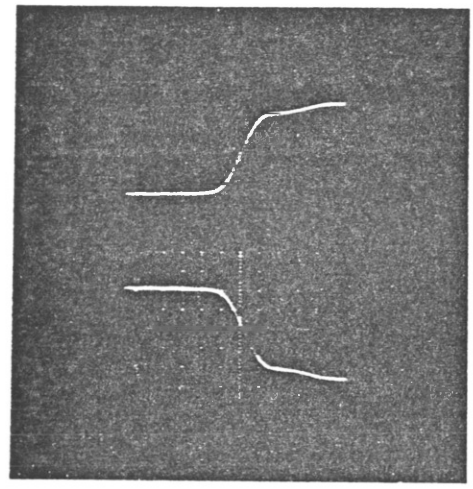

Fig.4.1 Positive and negative output from the avalanche transistor sweep circuit. (1ns/div, 600V/div).

The trigger jitter was evaluated by operating the Picoframe I camera in a streak mode. The compensation deflectors were connected to the sweep generator while the framing deflectors were maintained at anode potential. Sub-pulses from a 100ps calibrated optical delay line were observed at the centre of the screen. Four consecutive streak recordings are reproduced in fig.4.2, demonstrating a trigger jitter of less than $\pm$ 20ps.

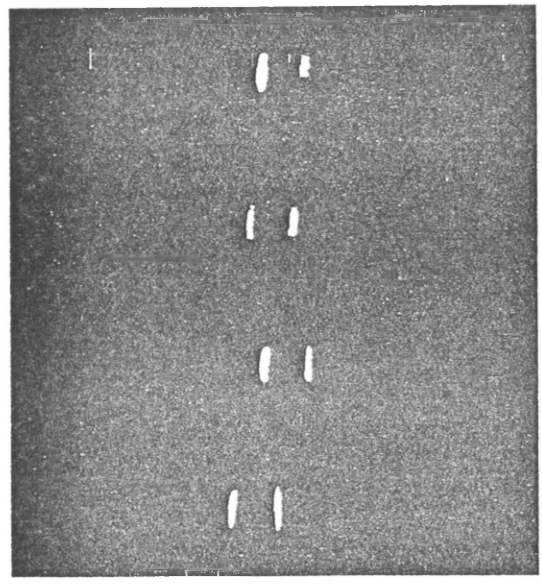

Fig.4.2 Four consecutive streak recordings. Streak separation is 100ps

4.3 Single-frame operation of the Picoframe I camera

In preliminary testing of the prototype camera performance the illuminating laser pulses had durations of 0.25 - 10ps FWHM, while the frame time was determined to be between 150-200ps. Clearly it was necessary to evaluate the instrumental performance with pulse illuminations having durations similar to that of the framed images. This was carried out using the frequency doubled output from a Nd: YAG oscillator.

4.3.1 The experimental set-up

The source of the illumination test pulses was a Q-switched mode-locked Nd: YAG oscillator [6] (modified Quantronix 116 with 351 model Q-switch), with a cavity round trip time of 10ns. It was operated in the prelase mode to allow continuous operation of the mode-locking modulator. Consequently the mode-locked pulses were able to achieve steady-state conditions prior to Q-switched operation. A typical Q-switched mode-locked pulse train consisted of approximately 50 pulses (see fig.4.3), with a peak pulse energy of around 80μJ.

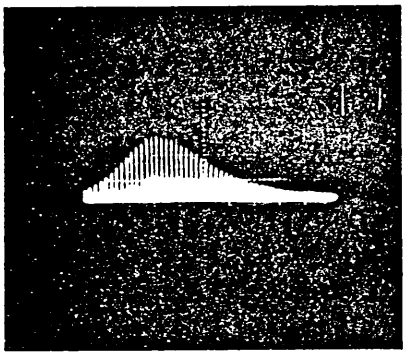

Fig.4.3 Typical Q-switched mode-locked pulse train. 50ns/div.

The output pulses were monitored using a repetitively operating streak camera (S1 activated Photochron I). A typical synchroscan streak record, demonstrating a pulse duration of ~120ps (FWHM) at the fundamental wavelength of 1.06μm, is reproduced in fig.4.4.

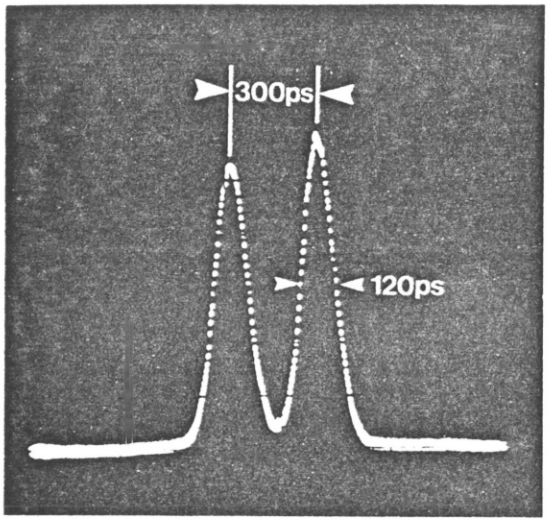

Fig.4.4 Repetitive operation streak recording of the fundamental output pulses from the Q-switched mode-locked Nd: YAG oscillator.

The second harmonic at a wavelength of 533nm was generated in an angle-tuned crystal of KTP with a conversion efficiency of approximately 10%. This resulted in a pulse-width compression of upto a factor of $x1/\sqrt{2}$ [7]. When carrying out setting up and temporal calibration procedures the relatively long laser pulses were temporally compressed to around 3ps prior to second harmonic generation. Compression was by means of self-phase-modulation induced chirp due to propagation in a monomode optical fibre, followed by de-chirp using a dispersive delay line [8].

The experimental arrangement is shown in fig.4.5. Each pair of deflectors were driven symmetrically by dividing both sweep circuit outputs with 50Ω T-piece connectors; such that the four coaxial cables connecting the deflector plates could be driven. To allow for the electron transit time between framing and compensation deflectors, the cable lengths connecting the framing deflectors were deliberately shorter than those connecting the compensating deflectors.

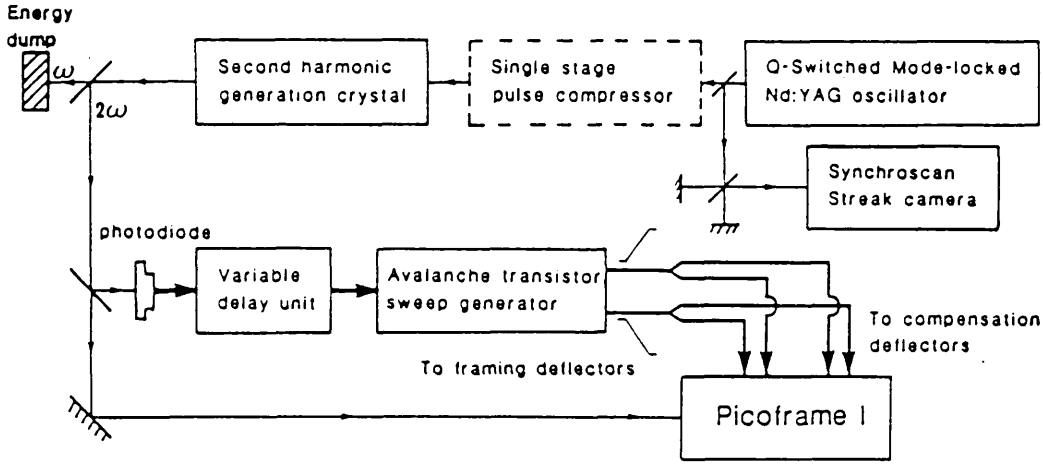

Fig. 4.5 The Experimental configuration used in single-frame operation of a Picoframe I camera illuminated for ~100ps.

Initial synchronisation was carried out in the streak mode using the compensation deflectors to increase the viewable time window and so ease the set-up procedure. Once well centralised streak images were achieved on the screen, the framing deflectors were re-connected and the input slit replaced by a 1951 USAF test chart.

Two 1.0m lengths of 50Ω coaxial cable connected the framing deflectors to the sweep circuit. The correct differential cable delay for effective image compensation was then established by varying the cable lengths connecting the compensation deflectors over the range 0.78m to 0.82m. Although the vague form of the test pattern could be recognised it was not possible to resolve the coarsest bar pattern. Increasing the anode potential from

12kV to 15kV (scaling the other electrode voltages appropriately to maintain focus) resulted in some degree of improvement, but still below the resolution of the coarest bar pattern (2 lp/mm). This effect is most probably due to the decrease in relative difference between the deflection sensitivities of the deflectors and reduced space-charge distortion at higher acceleration potentials.

4.3.2 The capacitative divider

It has been demonstrated in chapter 3 that it is possible to achieve good image compensation, and thus spatial resolution, by independent control of the deflection voltage gradients applied to the deflectors. Since the regulation of the overall PCE potential did not prove particularly convenient, a more elegant approach was devised in which the deflection plate capacitance was incorporated into a capacitative divider.

Consider two series capacitors with capacitances C_1 and C_2 . (fig. 4.6.).

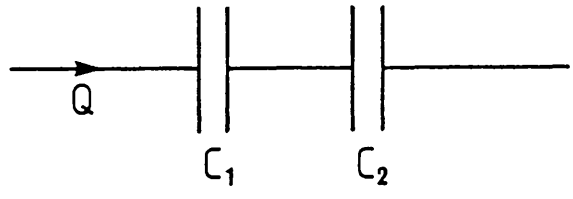

Fig.4.6 Series capacitors C_1 and C_2

By conservation of charge, a charge Q accumulated by the capacitance C_1 will induce and equal charge to be accumulated on capacitor C_2. Thus:

$$Q = V_1C_1 = V_2C_2 \qquad \text{equ.4.1}$$

Where V_1 and V_2 are the voltages developed across C_1 and C_2 respectively. Differentiating equ. 4.1 w.r.t. time yields;

$$\frac{dV_1}{dt} = \frac{dV_2}{dt}.\frac{C_2}{C_1} \qquad \text{equ.4.2}$$

Provided the risetime of the LCR circuit formed by the deflectors is sufficiently faster than the risetime of the driving voltage waveform V(t), the potential across the capacitors will follow that of the driving waveform i.e.

$$V(t) = V_1(t) + V_2(t) \qquad \text{equ.4.3}$$

To justify this assumption it is necessary to evaluate the rise-time of the deflection circuit; this is achieved by analysis of the LCR network.

The deflection plates within an image tube form part of an LCR network where L is the circuit inductance, C is the circuit capacitance and R the resistance (see fig 4.7).

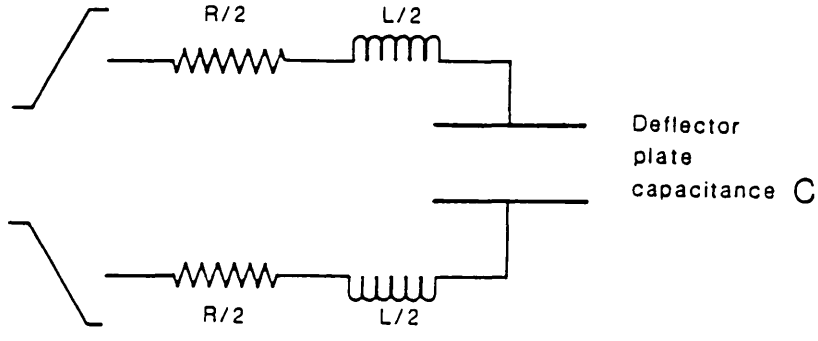

Fig. 4.7 Deflector circuit LCR network

For periods less than twice the round trip time (~6ns) of the connecting coaxial transmission line reflections may be ignored, thus the circuit resistance is given by the characteristic

impedance of the transmission line. During the experimental evaluations two 50Ω characteristic impedance coaxial cables were used to drive each pair of deflectors. Since the coaxial transmission line screen electrode was earthed at either end, the main contribution to the circuit inductance was formed by the parallel feed-in wires between the vacuum feed throughs and deflector plates. The relatively small mutual inductance of the deflector plates could be neglected. For two parallel wires of radius r and separation D in vacuum, the inductance per unit length is given by [9];

$$L = \frac{\mu_o}{\pi} \ln\left(\frac{D}{r}\right)$$

where μ_o is the permeability of free space ($4\pi X10^{-7}$H/m). In the prototype Picoframe I the feed-in conductors are approximately 50mm long with a radius of 0.2mm and a separation of 8mm. Hence the self inductance of the circuit is about 75nH. Similarly the main contribution to the circuit capacitance is presented by the deflector plates; the capacitance of the parallel feed-in wires being negligible. The deflector plate capacitance of the Picoframe I is about 0.2pF (see section 2.3.2).

The transient response of an LCR circuit is determined by solving the ordinary differential equation describing the network (equ. 4.4.) using the Laplace Transform [10], where E(t) is a step impulse.

$$E(t) = \frac{Ld^2q}{dt^2} + \frac{Rdq}{dt} + \frac{q}{C} \qquad \text{equ.4.4}$$

Solving equation 4.4 (Appendix I) it may be shown [4] that the time taken for the capacitor to reach peak voltage (the risetime)

is given by;

$$T_r \simeq \pi\sqrt{LC}$$

Substitution of the calculated values for L and C yields a circuit risetime of 380ps. This is significantly smaller than the driving waveform risetime of 1.5 - 2ns, thus it is concluded that equation 4.3 is valid under these circumstances.

Differentiating equation 4.3 with respect to time gives

$$\frac{dV}{dt} = \frac{dV_1}{dt} + \frac{dV_2}{dt} \qquad \text{equ.4.5}$$

Substituting equation 4.2 into equation 4.5 yields

$$\frac{dV}{dt} = \frac{dV_2}{dt}\left(\frac{C_2}{C_1}\right) + \frac{dV_2}{dt}$$

and hence;

$$\frac{dV_2}{dt} = \frac{dV}{dt}\left(\frac{C_1}{C_1 + C_2}\right)$$

It has thus been shown that within the limitations discussed, the rate of change of voltage across the deflector plate capacitance C_2 can be controlled by the ratio $C_1/(C_1+C_2)$. The capacitance C_1 may be conveniently provided by a miniature series trimmer capacitor located at the vacuum feed-throughs; as close as possible to the deflection system. For biasing purposes a high value resistor (10kΩ) was connected in parrallel with the trimmer capacitor to allow the deflectors to achieve the correct DC bias, see fig.4.8.

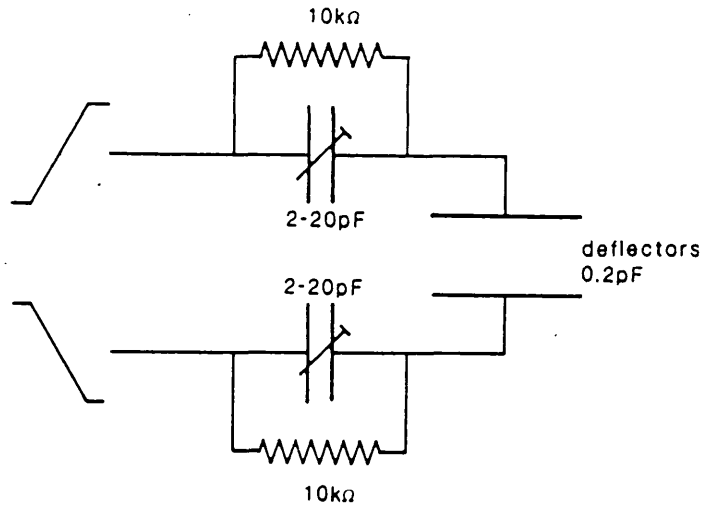

fig. 4.8 The capacitative divider arrangement used with the Picoframe I.

Practical values for the capacitances shown provide for up to a 12% variation in the rate of change of voltage across the deflector plates. As the DC sensitivity of the framing deflectors exceeded that of the compensation deflectors (see section 2.6) the divider arrangement was incorporated into the framing deflector circuit.

4.3.3. Results

The increased signal delay in the trimmer capacitor arrangement required the differential cable delay be correspondingly increased. Optimum results were achieved, providing a well centralised image, with 0.77m and 1.03m cable lengths to the framing and compensating deflectors respectively. With the laser operating at a repetition rate of 3Hz it was possible to carry out quasi-realtime adjustments to achieve optimum dynamic spatial resolution. By this means framed images such as that reproduced in fig.4.9 were obtained. The limiting spatial resolution that was routinely observed under these conditions was 7 lp/mm referred to the photocathode.

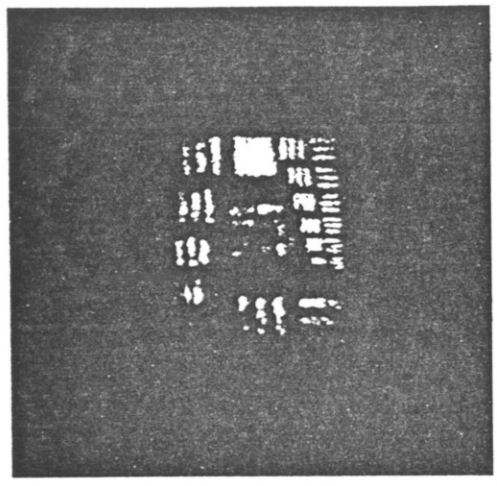

Fig.4.9 Reproduction of a single frame image.

Exposure time calibration was carried out in the streak mode using the compensation deflectors whilst the framing deflector plates were maintained at anode potential. To ensure consistent sweep speed the cables supplying the framing deflectors were disconnected at the tube end, leaving the sweep generator identically loaded. The two stages preocedure described earlier was employed. Temporally calibrated streak images were compared to the projected outline diameter of the framing aperture. The exposure calibration results presented in fig.4.10, recorded directly by a Optical Multichannel Analyser (OMA) (see section 6.7.5), illustrate a frame 'open' duration of 215ps.

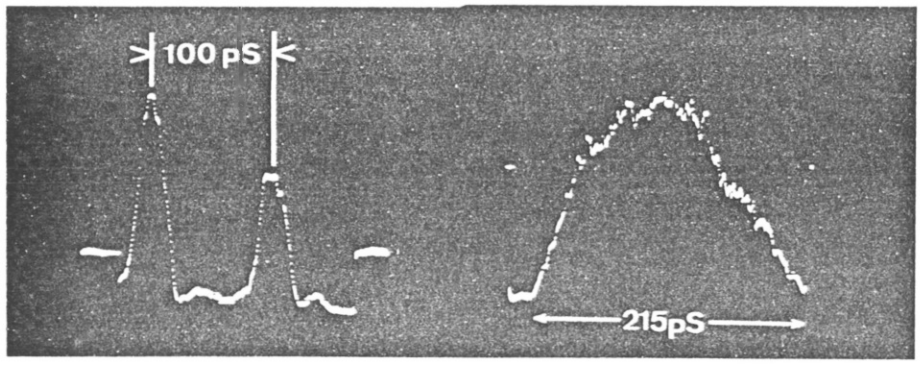

Fig.4.10 OMA recorded streak calibration of frame exposure time

4.4 Techniques for the generation of a sequence of framed images.

Early evaluations of the sweep/compensation framing technique have largely concentrated on demonstrating the soundness of

the basic principle. A major requirement of a practical framing image system is the ability to generate sequenced framed images. Towards this objective two techniques for the production of framed image 'doublets' using the Picoframe design are discussed in this section.

4.4.1 The Picoframe II

The different approaches to achieving a sequence of framed images using the Picoframe camera principle have already been discussed (section 2.2.1). The most direct method is to replace the single framing aperture in the Picoframe I with a series of apertures. As the electron beam is swept across, by application of a linear voltage ramp to the framing deflectors, bursts of electrons form discrete framed images at the screen. This is the so-called multiplex aperture plate design. In the original proposal by Sibbett et al [11] the design incorporated a three aperture multiplex plate for the generation of framed 'Triplet' images. However, the provision of three independent pairs of compensating deflectors of the dimensions envisaged caused severe constructional difficulties. Eventually a modified design, illustrated in fig.4.11, incorporating two framing apertures and pairs of compensating deflectors was adopted.

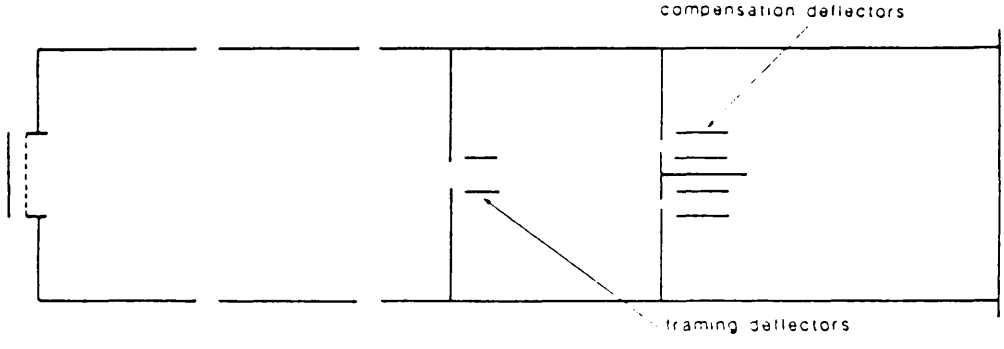

Fig.4.11 The twin aperture Picoframe II tube design.

A prototype twin aperture tube (designated Picoframe II) was

constructed using manufacturing techniques similar to those employed in the fabrication of the Picoframe I. Machinable glass-ceramic spacers provided electrical insulation and mechanical support for the deflection plates. The inner deflector plates were supported from a thin metal plate maintained at anode potential. This also served to screen the interaction between the two deflectors. Outer deflector plates were supported via stainless steel side arms as in the Picoframe I. The tube was 'bakedout' for a period of 48 hours prior to activation with an S25 photocathode.

4.4.2 Picoframe II static evaluation

A Baum projector was used to project an image of a test resolution chart onto the photocathode. As the axial electron path is obstructed in this design of tube, it was necessary to apply a DC bias potential to the framing deflectors to achieve an observable image at the screen. Viewing the screen with the aid of a microscope, at an asymmetric DC bias of + 500V, it was possible to achieve a moderately well focused image. A spatial resolution of 35 lp/mm was obtained at the screen in the **x** direction, but a resolution of only 12 lp/mm was observed in the **y** direction. To allow the electron beam to pass through the other framing aperture an asymmetric DC bias of -1100V was necessary. The quality of this image was extremely poor with an **x** direction resolution of $\leq$ 10 lp/mm and no observable resolution in the **y** direction. Re-adjustment of the focus potential provided a marginally improved resolution in **x** but not so in **y**

4.4.3 Discussion

It is clear that this particular prototype Picoframe II tube suffered severe astigmatism and axial misalignment. This is not perceived to result from a fundamental limitation of the electron lens, as the Picoframe I has demonstrated a static limiting spatial resolution capability of >20 lp/mm in both **x** and **y** directions. An attempt to compensate for any axial misalignment by the careful positioning of a permanent bar magnet failed to improve the imaging performance. Similarly the use of symmetric deflection to reduce the effect of fringing fields near the plates failed to enhance the image resolution.

The prototype tube was not constructed entirely from scratch but incorporated an electron lens structure salvaged from an earlier Picoframe I prototype. It is suggested that in the refurbishment process axial misalignment occurred such that the plane if best focus was not positioned orthogonal to the axis. Coupled with the highly astigmatic nature of the tube this made it impossible to achieve the same focus characteristics for the beam passing through each aperture. It thus had to be conceded that dynamic evaluation of this design of tube would have to be abandoned until a fully operational prototype could be constructed.

4.4.4 Double sweep operation of the Picoframe I

A technique for producing framed 'doublet' images using the single aperture Picoframe I design was discussed in chapter 2. The principle is to supply triangular shaped voltage waveforms to the deflectors. One image is then generated by the sweep on the rising edge with a second image produced by the falling edge

sweep. Suitable de-phasing of the waveforms prohibits over-writing of the images. Successful operation of the Picoframe I in this mode relies upon the generation of triangular waveforms with kilovolt amplitudes and nanosecond rise and fall times.

4.5 Nanosecond electrical pulse shaping

A scheme devised by Ross [12] for a microwave pulse forming network has recently been extended to the picosecond pulse shaping regime by Margulis [13]. In this scheme a series transmission line configuration is able to generate an even number of microwave pulses from a step input. The network consists of a TEM-mode transmission line of characteristic impedance Z_o. A junction with another transmission line branch of impedance $Z_o/2$ and length L is formed, see fig. 4.12

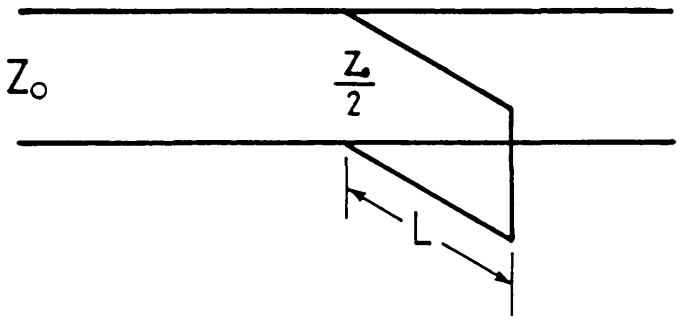

Fig.4.12 Transmission line junction with half impedance branch of length L.

If a step impulse of amplitude V_o is applied to one end (the input) of the first transmission line at time t_o, it will propagate towards the junction at a speed of $v = c(\epsilon_o\epsilon\mu_o\mu)^{-\frac{1}{2}}$.
At the discontinuity the voltage reflection Γ_r and transmission Γ_+ coefficients are given by;

$$\Gamma_r = \frac{V_r}{V_i} = \frac{Z_+ - Z_i}{Z_+ + Z_i}$$

$$\Gamma_+ = \frac{V_+}{V_i} = \frac{2Z_+}{Z_+ + Z_i}$$

Where V_i and V_+ are the amplitudes of the incident and transmitted voltages respectively and Z_+, Z_i are the impedances experienced by the transmitted and incident waveform respectively. When the impulse arrives at the discontinuity the impedances Z_i and Z_+ are given by;

$$Z_i = Z_o$$

$$Z_+ = \tfrac{1}{3}Z_o$$

here Z_o is the characteristic impedance of the input line. Calculating the reflection and transmission coefficients gives;

$$\Gamma_r = -\tfrac{1}{2}$$

$$\Gamma_+ = \tfrac{1}{2}$$

Thus a step potential of $V_o/2$ continues to propagate in the transmission line branch of length L and towards the output. A signal of $-V_o/2$ is reflected back towards the voltage source. If the half impedance branch is short circuited at its end ($Z_+ = 0$), an inverted signal - $V_o/2$ is reflected back towards the junction. At the junction a matched impedance of $Z_o/2$ is experienced so that a signal of $-V_o/2$ is transmitted towards the output and voltage source without reflection. Observing the output a signal $V_o/2$ is followed a time $t = 2L/v$ later by a signal $-V_o/2$.

Although not used in the experimental investigations detailed in this thesis it is noteworthy that if the branch length L is terminated in an open circuit ($Z_+ = \infty$), a reflection of $+V_o/2$ is reflected back. This will appear at the output a time $t = 2L/v$ after the arrival of the first $+V_o/2$ signal, generating a two step staircase type waveform. If further open circuit

branches of increasing length nL (n = 2,3,4...) are joined to the main transmission line at equal intervals, a staircase of 2n steps will be formed. This type of waveform has applications in successively shifting the image to a new screen position by use of orthogonally orientated shift plates. It can also be utilized in the direct production of framed images in some types of framing image tube (see chapter 1).

It is generally most convenient to form the $Z_o/2$ impedance branch by two branches each of length L and impedance Z_o in parallel, a 'cross' arrangement is thus formed. To a first approximation the peak voltage V_p at the output is given by [13];

$$V_p = \frac{V_o}{2}\left(\frac{\delta t}{T}\right)$$

where T is the risetime of the input transient and δt is the branch round trip time. For $\delta t \simeq T$ with a linear rising ramp input a triangular waveform of maximum amplitude $V_o/2$ is generated at the output. This is the type of waveform necessary for double sweep operation of the Picoframe I.

4.5.1 Fabrication of the pulse forming network

The pulse forming network (PFN) was fabricated from 6mm (nominal 0.25 inch) outside diameter plain copper semi-rigid coaxial cable of characteristic impedance $50\Omega \pm 1\Omega$ [14]. This large diameter cable was selected to provide adequate insulation across the slot region for kilovolt potentials. A 360mm length had a 6mm slot milled at the centre to a depth of 3mm. Since only nanosecond risetime signals were to be propagated down the cable the provision of large bandwidth (> 20GHz) connectors were unnecessary and standard BNC connectors were fitted to each end.

To derive a triangular type waveform from a 1.5 - 2.0ns rise-time linear input the branch length must have a round trip time of a similar duration. The transmission line had a velocity factor of 0.66, thus a length of 200mm provided the necessary 2ns delay. A 400mm length was accurately cut and the ends machined flat. To accept the other cable a 6mm width slot was milled at its exact centre to a depth of just less than 3mm.
This ensured good contact when the components were slotted together as in fig. 4.13 (a).

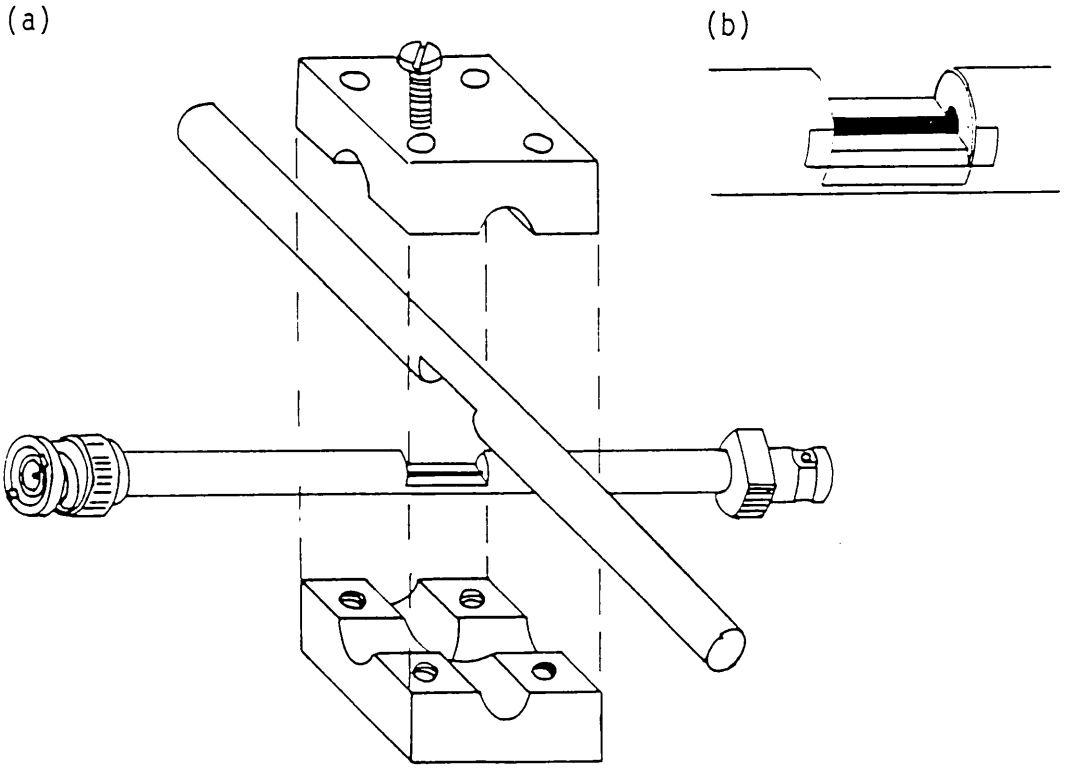

Fig.4.13 Constructional details of a nanosecond PFN.

In order to prevent a short circuit between the central conductor of one cable and the outer conductor of the other, the outer conductor of each was recessed back about 0.2mm as indicated in fig. 4.13 (b).

To securely fix the components together two aluminium slabs 30mm x 30mm x 6mm were bolted together with a 6BA bolt in each corner. Whilst held together two orthogonal 6mm diameter holes

were drilled through the block; forming two bisecting channels symmetrically about the join as shown in fig. 4.13 (a). Once separated one of the halves of the fixing block had a 0.1mm layer machined off the channelled face to ensure the coaxial transmission lines would be securely held together. Once the assembly was fitted together the ends of the stub branches were electrically shorted to ground by application of conductive silver paint to the extremities. Care had to be taken to clean the slot and stub ends of grease deposits and debris that might have caused breakdown and arcing.

4.5.2 Implementation of the pulse forming network

The 3kV output voltage swing of the sweep generator was centred around 0V, positive going from -1.5kV to + 1.5kV and negative vice-versa. This prohibited direct connection of the PFN as it represented a short circuit for DC purposes. To overcome this a 220pF decoupling capacitor was included between the sweep circuit and the PFN. Similarly the deflector plate bias potential was decoupled by a further 220pF capacitor situated between the PFN and deflector plate.

Positive and negative polarity triangular waveforms generated by the PFN's and observed on a Tektronix 7904 fast oscilloscope (risetime 700ps) are reproduced in fig. 4.14. The 2.0ns (FWHM) recorded pulse-width is probably a little pessimistic as the apex of the triangle will be poorly resolved due to the response time of the oscilloscope. Thus the half maximum position shown is likely to be closer to the base than is actually the case.

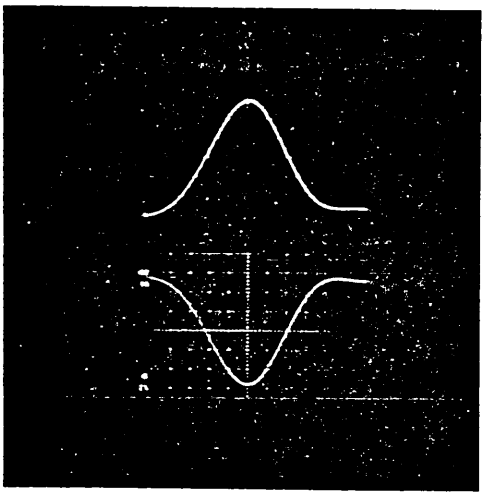

Fig.4.14 Positive and negative 'triangular' waveforms used with the Picoframe I (200V/div and 0.5ns/div).

Although the reflections from the PFN branches experience a matched load at the junction not yielding any reflections, the discontinuity at the deflectors and sweep circuit will result in reflections. This can be seen from the fairly slow timescale oscillogram reproduced in fig. 4.15 (a).

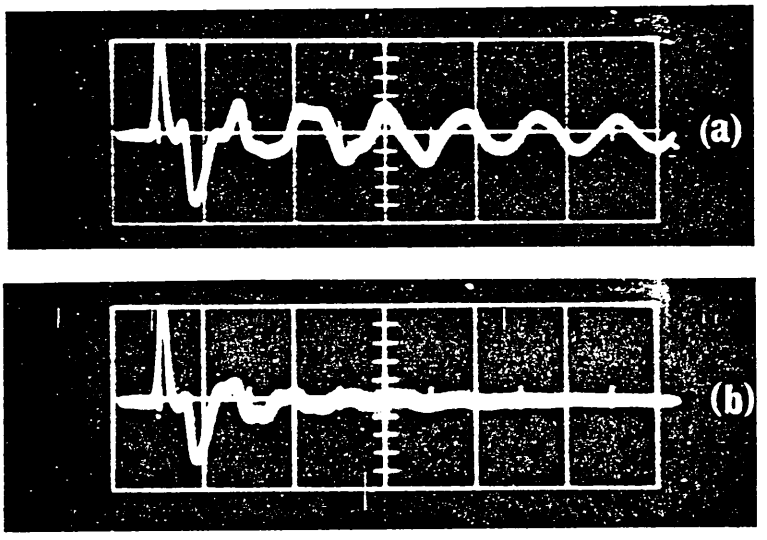

Fig.4.15 Post pulse voltage transients, (a) without protection diodes, (b) with protection diodes. (10ns/div).

Generally this post pulse 'ringing' did not cause undue problems with image overwriting provided the test chart illumination was not allowed to persist (by single-pulse selection from the mode-locked pulse train). However the large inverse polarity transients

did adversely affect the transistors in the avalanche chain, causing complete device failure or damage. It was found to be necessary to minimize the effect of these inverse transients by incorporation of high voltage protection diodes (Mullard BY127) configured to short them to ground. The scheme employed is illustrated in fig. 4.16.

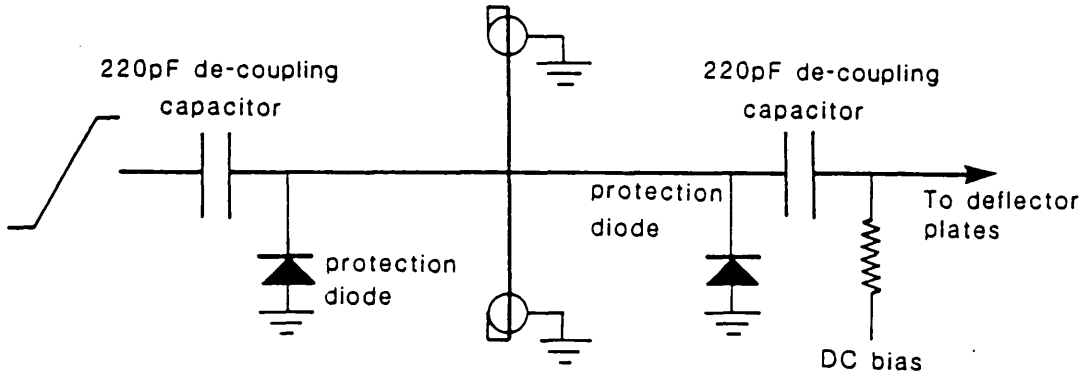

Fig. 4.16 The practical PFN configuration showing the in line decoupling capacitors and protection diodes.

The effect of these diodes is shown in fig.4.15 (b). Unfortunately they were not sufficiently fast to short the first transient but were able to successfully short successive transients. With the protection diodes in place in both positive and negative PFN's no further unwarranted transistor failure was experienced.

4.6 Double frame operation of the Picoframe I

The prototype Picoframe I camera was operated in a 'doublet' frame mode using a double sweep by application of the triangular voltage waveform provided by the PFN's. Initially the single-frame experimental arrangement was retained, with the PFN's inserted between the sweep generator outputs and the cables connecting the deflection plates. This configuration did not prove entirely satisfactory and later two separate sweep generators were operated in synchronism.

4.6.1 Operation with one sweep generator

Two triangular PFN's were employed in conjunction with the avalanche transistor sweep generator used in the earlier evaluations. Each complementary circuit output was connected to one of the networks so as to generate complementary positive and negative going kilovolt amplitude waveforms. The Q-switched mode-locked Nd:YAG oscillator described earlier was used to provide to ~100ps duration test illumination pulses. Increased likelihood of post deflection ringing causing image overwriting effects necessitated the selection of a single illumination pulse from the mode-locked train.

4.6.2 The experimental set-up.

An illustration of the modified experimental configuration used is presented in fig.4.17. The avalanche transistor sweep circuit utilized during the experimental investigations had an intrinsic delay time of around 10ns between being triggered and generation of the voltage ramps. In the previous single frame evaluation the whole pulse train was allowed to illuminate the camera. This resulted in a reduced synchronisation constraint in that the camera could be triggered from one pulse but observe a later one. However, single pulse selection required that the same pulse initiated the sweep generator before embarking on a long optical delay arriving accurately synchronised to illuminate the resolution test chart during the camera exposure. The Michelson type optical delay arrangement used for streak calibration conveniently provided two subpulses for illumination of each framed image.

The triangular waveform output from each PFN was divided using 50Ω T-piece connectors such that four transmission lines, one for each deflector plate, could be connected.

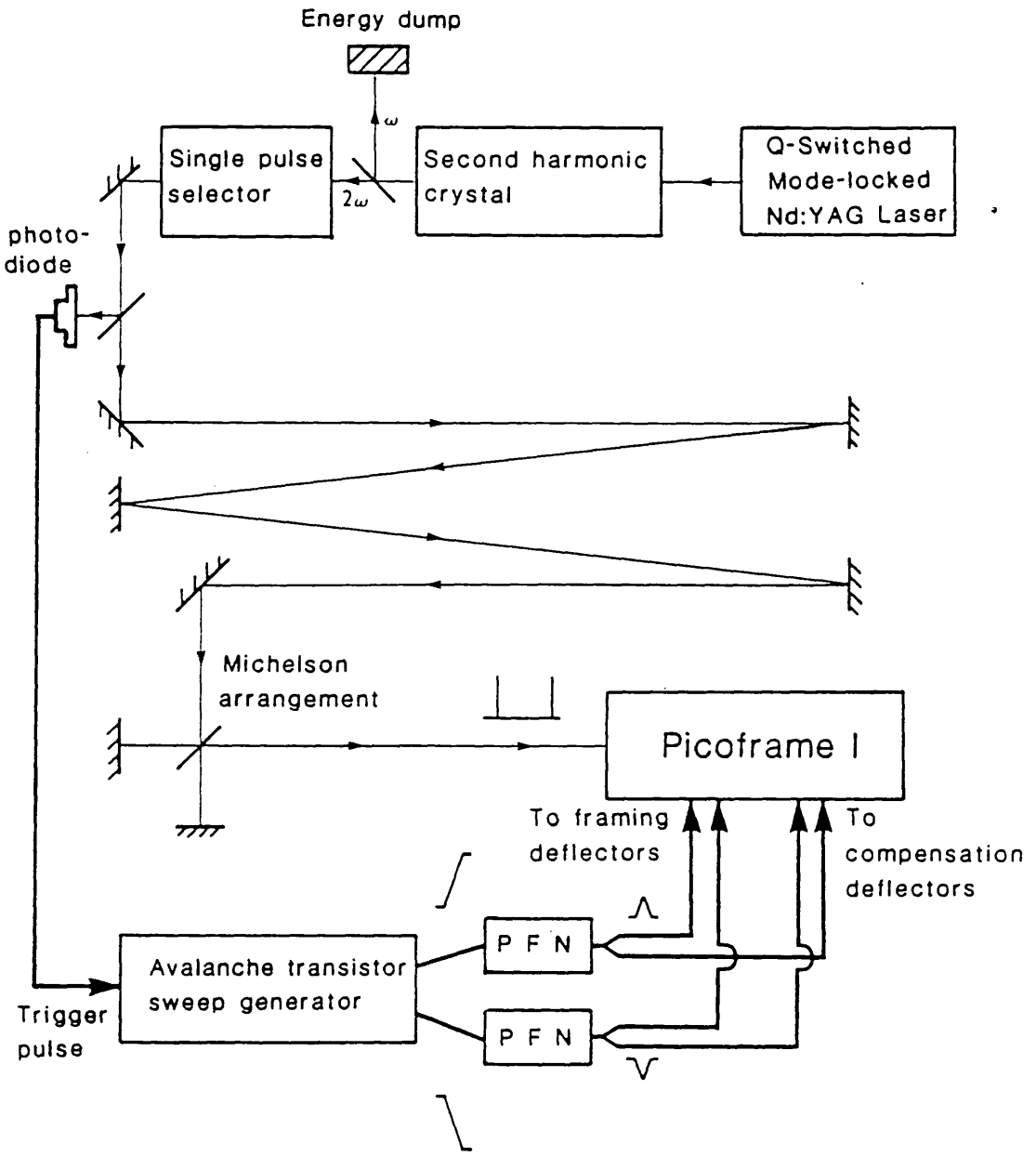

Fig. 4.17 Experimental configuration employed in double sweep operation of the Picoframe I using one sweep generator.

Relative phasing between the deflection waveforms was achieved by varying the cable lengths connecting the deflection plates. The waveform appearing at the deflectors is illustrated by the oscillogram in fig.4.18 (a). The same waveform shown on a longer timescale (fig.4.18(b)) demonstrates the periodic ringing caused by impedance mismatch at the T-piece connector and deflection plates. It can be seen that the back slope of the triangle is perturbed by the impedance mismatch where the signal is divided. This results in degradation of the image produced by its action.

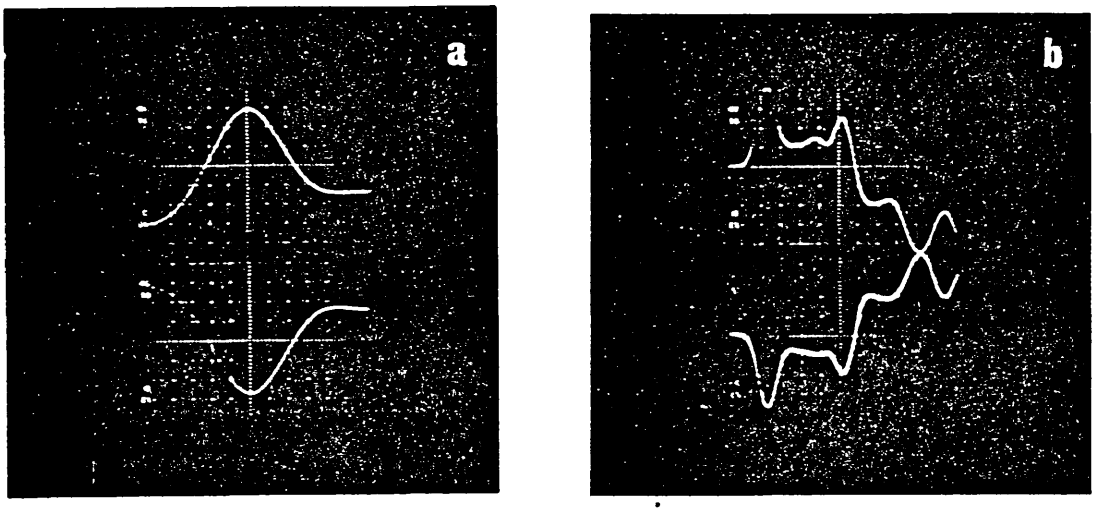

Fig.4.18 Positive and negative 'triangular' waveforms used with the Picoframe I camera, (a) 200V/div and 0.5ns/div, (b) 400V/div and 2ns/div.

The inter-frame time of the camera operated in this mode is governed by the width of the voltage waveform provided by the PFN In the configuration used the branch round trip provided a $\leq$2ns FWHM voltage waveform. To provide object illumination for each frame the Michelson delay line was configured to generate two subpulses temporally separated by 2ns. Q-switched laser operation at a repetition frequency of 3Hz enabled 'real time' adjustment of the sweep circuit trigger delay for initial camera synchronisation. Once framed images, albeit of poor quality, were obtained the trimmer capacitors could be used to optimise the dynamic spatial resolution.

4.6.3 Results

Adjustment of the deflector plate bias potential enabled different regions of the triangular slopes to be used. Too near the base or apex the voltage variation became nonlinear and the spatial resolution deteriorated. However over the central linear region a bias variation of $\pm$ 200V could be tolerated and still generate high quality spatially resolved images. With the viewing region shifted towards the apex of the waveform the inter-frame time was reduced. This could be measured by adjusting the Michelson arrangement for uniform illumination of the images, then measuring the difference in length between the Michelson arms. An inter-frame time of 1.5ns was observed for a bias potential of $\pm$ 400V.

Obstruction of one of the Michelson arms determined which screen image corresponded to the rising and falling edges of the waveform. It was noted that the early image was of slightly better quality than the later image. By careful adjustment of the trimmer capacitors it was possible to achieve a dynamic spatial resolution of up to 10 lp/mm at the photocathode in the early image. However, only 5 lp/mm were resolvable in the later image. With the best compromise position it was possible to obtain 'doublet' framed images with an overall dynamic spatial resolution of 7 lp/mm (at the photocathode). A typical framed image under compromise conditions is reproduced in fig. 4.19.

Streak calibration was carried out using the picosecond pulses from a Nd: phosphate glass oscillator (section 3.4.1). All four cables remained connected to the sweep generator /PFN, although the cables connecting the framing deflectors were

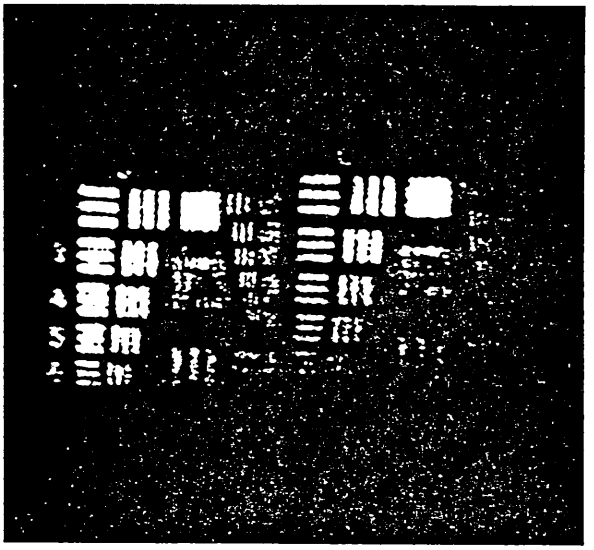

Fig.4.19 Doublet frame format with an overall spatial resolution of 7 lp/mm at the photocathode.

disconnected at the tube end. The triangular waveform was then applied to the compensation deflectors only. A calibrated optical delay stack provided 10 quasi-normal reflection subpluses each separated by 40ps. These illuminated a 50μm slit positioned at the input plane of the camera. Adjustment of the electrical delay between the trigger photodiode and sweep circuit permitted different portions of the voltage waveform to be probed. The top of the triangular waveform could be located by where the streak separation closed up. By adjusting the bias such that this occurred at the centre of the screen (no net deflection) the peak voltage at the plates was estimated to be $\pm$ 750V. Streak images were recorded on the front and back slopes of the wavefront, see fig. 4.20. Analysis of the images suggests the early frame duration to be about 500ps and the latter frame duration to be around 400ps.

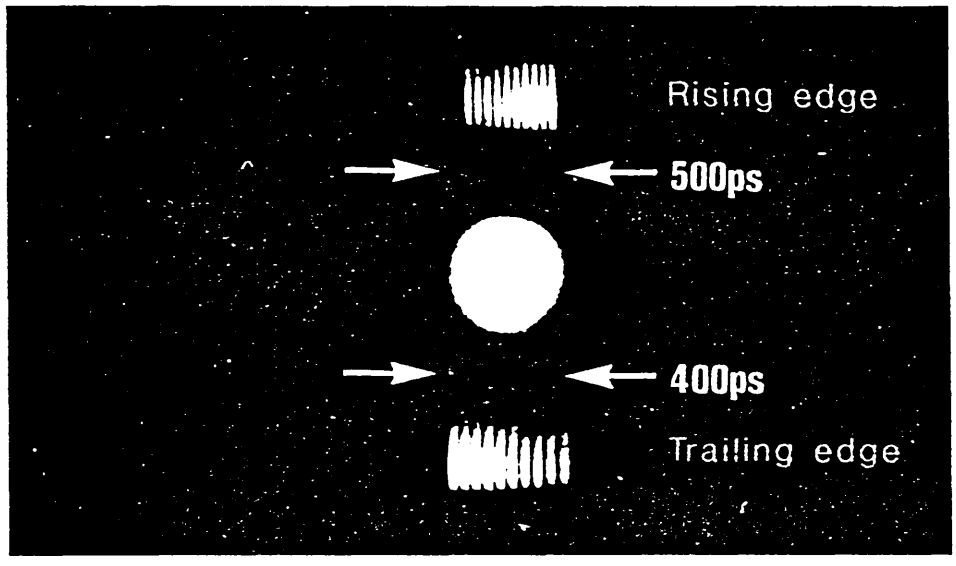

Fig.4.20 Streak calibration of Picoframe I in double sweep mode using one sweep generator.

4.6.4. Discussion

The degraded spatial resolution of the second image compared to the first is due to the restricted linear region on the falling edge of the waveform. This departure from linearity is largely caused by reflections resulting from non-impedance matched signal division. These effects may be avoided by resistivity dividing the waveform at the PFN output.

The exposure duration of the second frame was noted to be shorter than that of the first frame. That is the sweep speed on the falling edge of the triangular voltage waveform is faster than the sweep speed on the rising edge. The cause of this may be understood by analysis of the action of the PFN. An ideal input

waveform is a linear rising edge reaching a constant amplitude plateau. When this is input into the PFN a half amplitude replica of the input is transmitted to the output. A time t later an inverted half amplitude replica of the input is superposed on the output, where t is the branch round trip time (see fig 4.21).

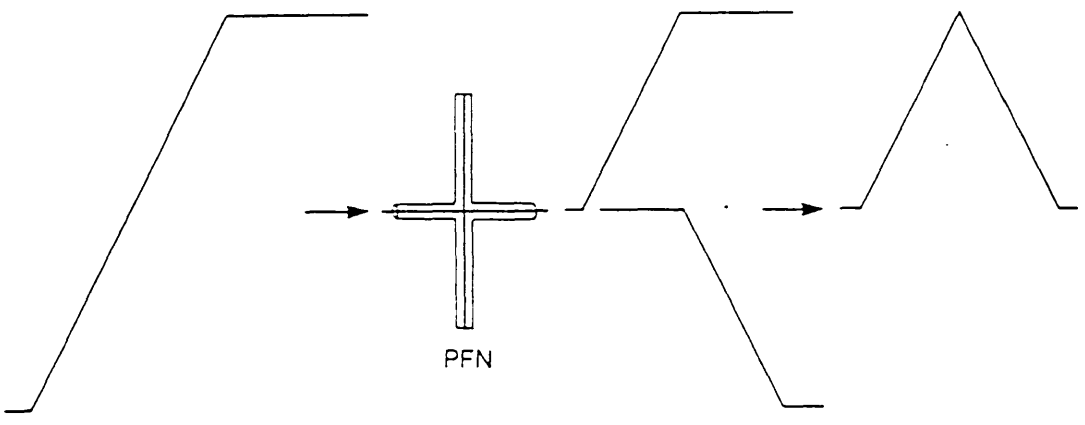

Fig.4.21 Action of the PFN with idealized input waveform.

The output directly from the sweep generator does approach the idealized waveform. However for reasons explained earlier the PFN was capacitatively coupled to the sweep generator by an inline 220pF high voltage capacitor. The effect of this capacitor when driving a 50Ω coaxial cable load 1.5m long was observed using a fast risetime ($\leq$ 25ps) sampling oscilloscope. The oscillogram reproduced in fig.4.22 illustrates that the capacitor is unable to provide sufficient current to maintain the voltage, and the amplitude is observed to fall (trace a).

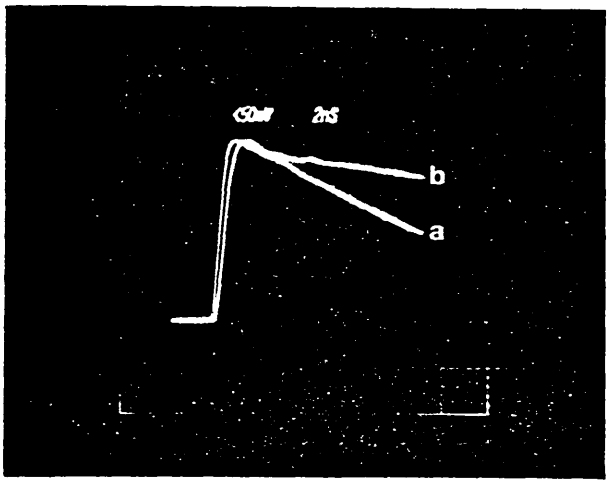

Fig.4.22 Observed waveform input to PFN, (a) with 220pF coupling capacitor, (b) with 1nF coupling capacitor.

When this type of waveform is input into the PFN an inverted reflection of the input is superposed onto the falling edge of the direct signal. This results in a faster falltime than risetime, see fig.4.23.

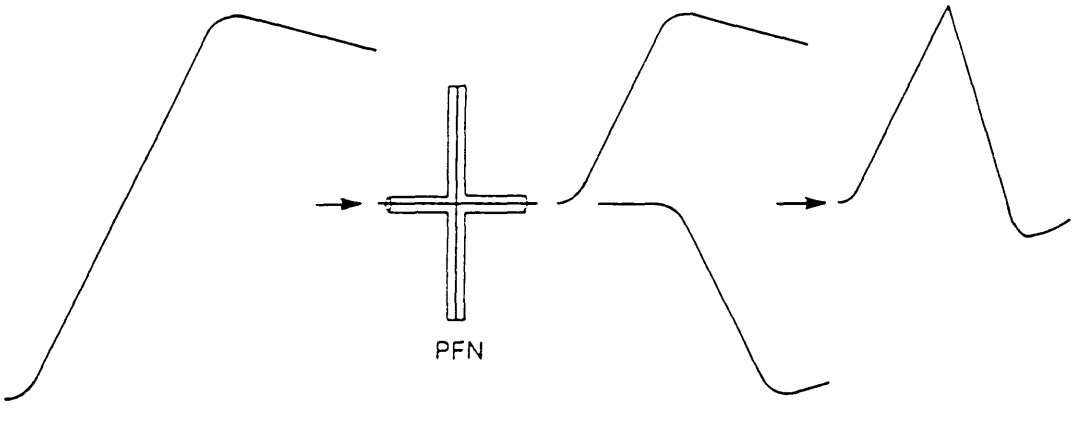

Fig.4 23 Action of the PFN with realistic input waveform.

The decay in amplitude may be reduced by using a larger value decoupling capacitor, figure 4.22 trace (b) shows the effect of a 1nF capacitor. Although the amplitude decays more slowly the risetime is also observed to be slower.

4.6.5 Operation with two sweep generators

Supplying the deflection signal to both pairs of deflectors imposes quite severe operating conditions on the transistor sweep generator circuit. In particular the increased current demand degrades the risetime of the voltage ramps. An attempt to offset this circuit limitation by using higher impedance cable (125Ω) did not present an adequate solution because of the increased capacitative loading effects. Additionally the practical difficulties in connecting the extremely stiff and bulky 125Ω cable to the fragile vacuum tube feed-through pins made its use quite unsatisfactory. To achieve shorter exposure times two independent sweep generators were utilized. This is practical, provided the circuit jitter is much less than the exposure time. The trigger jitter of the circuit employed was measured to be typically less than $\pm$ 20ps (section 4.2.2), which is significantly less than the expected exposure duration of 100-200ps

4.6.6 The experimental set-up

To minimize the trigger jitter between the two circuits caused by the shot-to-shot variation in optical pulse shape, a slave trigger pulse unit was employed. This consisted of a pin photodiode triggered avalanche transistor which provided a 20V subnanosecond risetime voltage pulse when triggered by optical pulse illumination of the photodiode. The trigger pulse was taken directly to the framing deflector sweep generator and via a variable electrical delay to the compensation deflector

sweep generator. This scheme allowed the coaxial transmission lines connecting the deflector plates to be identical in length. The characteristic electron transit time and dephasing features between each pair of deflectors were then facilitated by appropriately selecting the trigger delay.

To rigorously evaluate the camera under realistic experimental conditions, where the duration of the imaged luminous event will in general exceed the frame duration, ~20ns test illumination pulses were utilized. The test source was a frequency doubled Q-switched Nd:YAG oscillator (JK lasers DPLY4 'Hyperyag'). It incorporated a 76 mm x 9 mm rod anti-reflection coated at each end and pumped by a close-coupled twin flashlamp configuration. A typical second harmonic output pulse recorded using an S20 vacuum photodiode and Tektronix 7804 oscilloscope is reproduced in fig. 4.24.

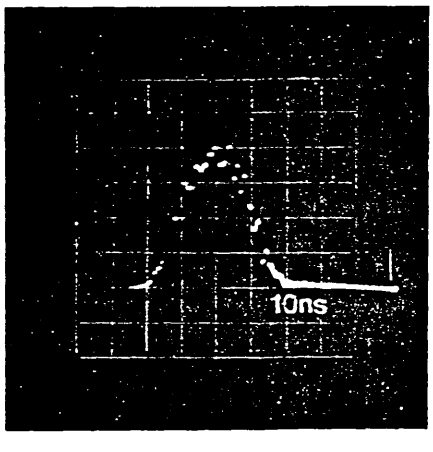

Fig.4.24 Typical duration (~20ns FWHM) second harmonic output pulse from Q-switched Nd:YAG oscillator (5ns/div)

The experimental arrangement is shown schematically in fig. 4.25. Approximately 8% of the second harmonic radiation was directed via a mirror onto the test resolution target located at the camera input. A diverging lens and ground glass diffuser

ensured uniform illumination of the whole chart with the intensity controlled by insertion of neutral density filters. Of the remaining radiation a further 8% was directed onto the pin photodiode of the trigger unit.

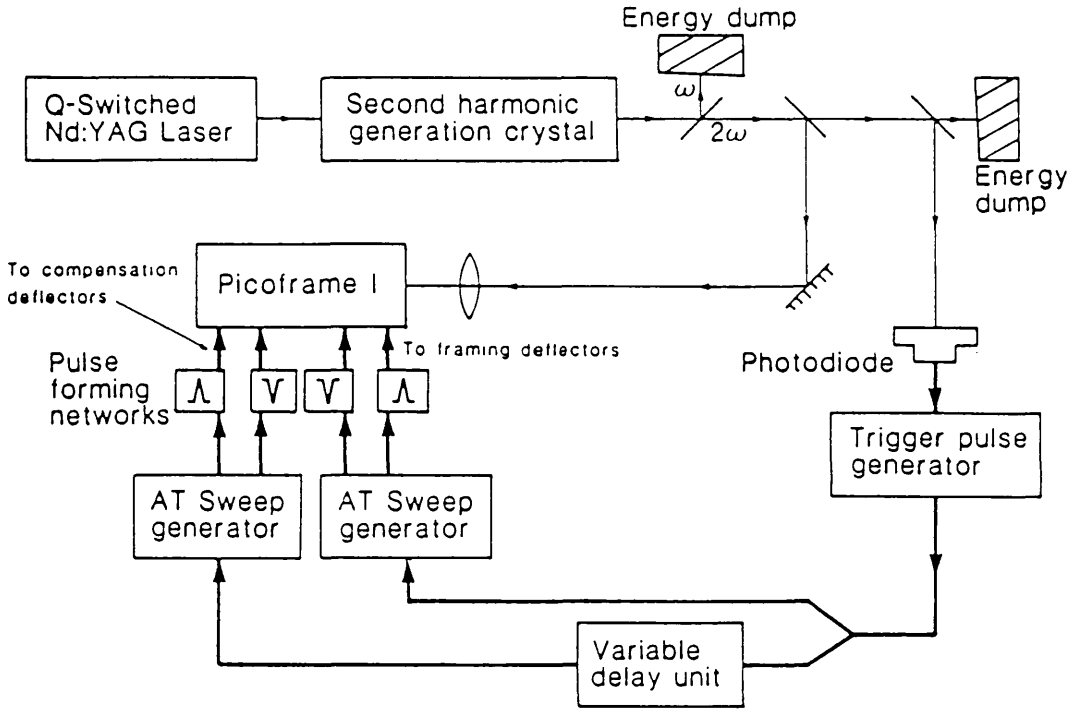

Fig.4.25 Schematic of the two sweep generator experimental configuration.

Due to the long laser illumination pulse, which exceeded the intrinsic sweep generator delay time (~10ns), accurate synchronisation was unnecessary. The sweep generators were triggered on the rising edge of the laser pulse. Thus with the 10ns intrinsic delay plus another 2-3ns cable delay the view time was approximately 13ns into the illumination pulse. Since the laser intensity fell to zero approximately 7-10ns later no undesirable overwriting effects were observed.

4.6.7 Results

Framing operation was readily achieved over a wide range of deflector bias potentials from ± 300V to ± 800V. The camera was generally operated at a high bias, near the triangular waveform apex, in order to reduce the inter-frame time. Operation too near the apex resulted in loss in waveform linearity and consequently degraded spatial resolution. High quality spatially resolved images were obtained by ensuring correct compensation of the transverse electron velocities by adjustment of the capacitative divider arrangement. A typical framed 'doublet' reproduced in fig. 4.26 shows an overall spatial resolution of not less than 7 lp/mm at the photocathode, and up to 9 lp/mm on the early image. This was obtained with a bias potential of ± 700V with the tube operating at an anode potential of 13kV.

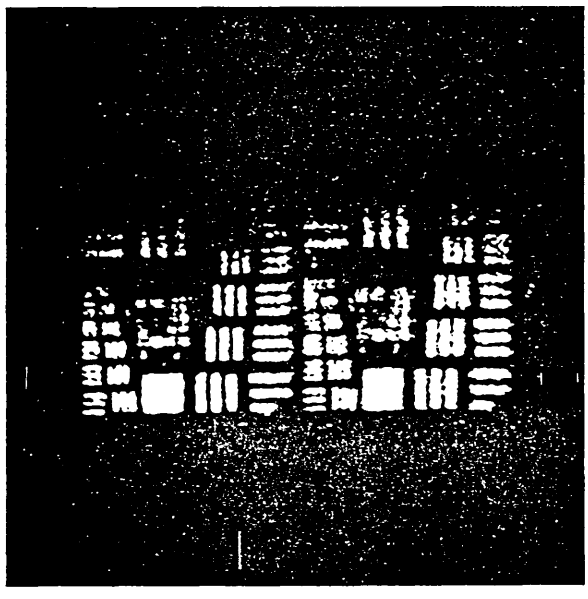

Fig.4.26 Doublet framed image with first (left) and later (right) images.

Streak calibration of the frame 'open' durations were carried out using a single picosecond pulse selected from the train of a passively mode-locked Nd: phosphate glass oscillator (section 3.4.1). Here accurate synchronisation of the camera was

necessary. Quasi-normal reflections from a calibrated stack of glass blanks provided a set of subpulses separated by 40ps. For calibration purposes only one sweep generator with its attendant PFN connected to the framing deflectors was used; the compensation deflectors were maintained at anode potential. The technique described in section 3.3.2 where a series of streaked 'mask' images exposed as the electron beam traversed the framing aperture was utilized. Calibrated streaked slit images in the upper half of the picture when compared to the diameter of the framing aperture shadow provide a direct measurement of exposure time. The two recordings reproduced in fig.4.27, (A) and (B) were recorded on the rising and falling slopes of the waveform and demonstrate a frame 'open' time of 210ps and 180ps respectively. Both recordings were obtained at a bias voltage of $\pm$ 700V and an overall tube potential of 13kV, as used in the framing evaluation.

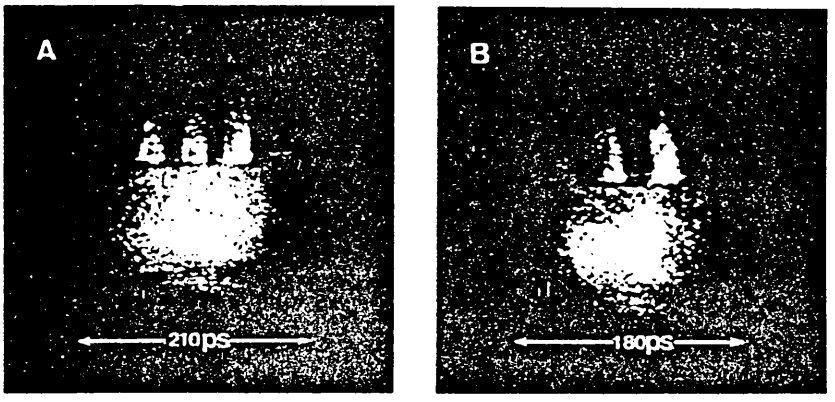

Fig. 4.27 Streak exposure time calibration, (A) on the waveform rising edge and (B) on the falling edge. Streak separation is 40ps.

Variation in the trigger delay to the compensation deflector sweep generator, by means of the variable electrical delay, permitted calibration streaks to be observed on the rising and falling slopes of the waveform. The time delay required to move from the leading to the trailing edge, under identical bias conditions

to those used during framing operation represented the inter-frame time. This was determined to be 1.2ns. By positioning the apex point (minimum streak separation) at the centre of the screen, where there is no net deflection, the peak voltage experienced at the deflector plates was ascertained to be $\pm$ 1100V.

4.6.8 Discussion

It is noteworthy that despite the long photocathode illumination time (~20ns) compared to the frame duration (~200ps) the framed image output is remarkably noise free. This is attributed to the careful positioning of aperture planes within the tube so as to prevent any secondary electrons, emitted by electron bombardment of the tube components, from impinging on the screen.

Again the later image had a shorter exposure time than the early image. The < 200ps 'open' time demonstrates the feasibility of shorter duration framed images with the provision of faster risetime voltage ramps. Slight degradation in the image quality of the later image probably results from some residual ringing from the transient response of the deflectors. These perturbations in the gradient of the falling edge do not cancel exactly and thus deminish the spatial resolution.

4.7 Conclusion

The generation of picosecond framed images with good dynamic spatial resolution using the Picoframe I camera system has been demonstrated under single and 'doublet' framing conditions. Electronic avalanche transistor sweep generators have enabled consistent and reliable operation of the camera in a variety of modes.

Due to the practical difficulties of manufacturing sealed-off image tubes with deflectors possessing identical characteristisc, a procedure for perturbing the deflection risetime to nullify manufacturing tolerances was developed. Incorporation of the deflection plate capacitance into a capacitative divider arrangement permitted the risetime of the deflection signal to be conveniently decreased within limits. In a practical configuration the divider arrangement is incorporated into the deflection circuit exhibiting optimum sensitivity. Single frame generation implementing this scheme demonstrated high quality framed images of 7 lp/mm spatial resolution at the photocathode, with a frame 'open' time of ~200ps.

The problems associated with manufacturing a reliable sealed-off image tube are evident from the difficulties encountered with the twin framing aperture Picoframe II. Poor performance of this prototype is attributed to manufacturing inaccuracies in the axial alignment, and distortions caused during processing. Although evaluation of the prototype proved impractical the basic approach to 'doublet' framed imaging is still considered sound. Ongoing work in this area is confidently expected to yield a usable prototype to allow full investigation of the merits of this design.

A simple but effective pulse forming network was employed in the production of high speed triangular voltage waveforms. The rising and falling edges permitted double sweep operation of the Picoframe I thus generating 'doublet' framed images. It was noted that the fall time of the generated triangular waveform was faster than the risetime. This was attributed to the DC decoupling capacitor being unable to supply sufficient current to maintain a constant amplitude.

Using one sweep generator in conjunction with two PFN's 'doublet' framed images of around 7 lp/mm dynamic spatial resolution at the photocathode with an interframe time of ~1.5ns were generated. Due to the high current demand placed on the single sweep generator relatively long exposure durations of approximately 0.5ns were recorded. A slight degradation in the second framed image was noted in all double sweep evaluations. This was attributed to the superposition of oscillatory transients or ringing on the falling edge of the deflection waveform.

To reduce the frame duration it was necessary to relieve the high current demand imposed on one sweep circuit in supplying all the deflection waveforms. A single dedicated generator with associated PFN's was thus assigned to each pair of deflectors. The transmission line loading of each circuit could then be made identical. Dephasing features were accounted for by an electrical delay in the trigger pulse supplied to the circuit providing the compensation deflector waveform. Employing this arrangement 'doublet' framed images of not less than 7 lp/mm spatial resolution at the photocathode were achieved [15]. Exposure durations of approximately 200ps with an interframe time of 1.2ns were recorded for these frames.

For realistic camera evaluation test chart illumination periods greatly exceeded the frame 'open' time. Under these conditions the high quality sequentially framed images with picosecond exposures were obtained. These results clearly demonstrate the abilities of the Picoframe I camera as a two-dimensional picosecond diagnostic.

References - Chapter 4

[1] Y Tsuchiya et al,
Proc. 16th ICHSPP, SPIE 491, 86 (1984)

[2] G E Philips and S W Thomas,
Proc. 13th ICHSPP, SPIE 189, 508 (1978).

[3] J R A Beale, W L Stephenson and E Wolfendale,
Proc. Inst. Elect. Engrs., 104B, 394 (1957).

[4] S W Thomas, R L Griffith and W R McDonald,
Proc. 16th ICHSPP, SPIE 491, 101 (1984).

[5] M C Jackson, R D Long, D Lee, N J Freeman,
Laser and Partide Beams, 4(1), 145 (1986).

[6] M D Dawson, A S L Gomes, W Sibett and J R Taylor,
Optics Comm., 52(4), 295 (1984).

[7] D H Auston, chapter 4,
'Ultrashort Light Pulses', Ed. S L Shapiro, Second Edition,
Springer - Verlag (1984).

[8] ASL Gomes, W E Sleat, W Sibbett and J R Taylor,
Optics Comm., 57 (4), 257 (1986).

[9] See for instance 'Electromagnetism',
I S Grant and W R Philips,
John Wiley & Sons (1980).

[10] S Goldman,
'Transformation calculus and electrical transients',
Prentice - Hall Inc, New York (1949).

[11] W Sibbett, M R Baggs and H Niu,
Proc. 15th ICHSPP, SPIE 348, 267 (1982).

[12] G F Ross,
IEEE Trans. Microwave Theory Techn.
MTT - 13, 704 (1065).

[13] W Margulis and R Persson,
Rev. Sci Instrum. 56 (8), 1586 (1985).

[14] Coaxitube Technical literature,
Precision Tube Co. Inc., North Wales, PA19454, USA.

[15] R T Eagles, W Sibbett and W E Sleat,
Optics Comm., 57(6), 423 (1986).

CHAPTER 5

A modified x-ray sensitive framing camera design

5.1 Introduction

In laser fusion experiments microballoon fuel pellets are heated by laser energy impinging on the outside of the sphere. As the resulting hot plasma expands outwards a compression wave is generated which propagates towards the centre of the pellet thus compressing the core. Thermal conduction from the hot corona raises the temperature of the core to several keV. If thermonuclear burn of a significant fraction of the fuel is achieved, temperatures may rise to ~50keV. Thus the photon emission spectrum from such a target includes optical, VUV, soft and hard x-rays. Much useful information is contained in the x-ray emission spectrum and considerable effort has been devoted to the development of x-ray sensitive diagnostics [1-3].

X-ray streak cameras [4] currently provide the best temporal resolution of x-ray phenomena. These are usually modified forms of optical cameras incoprorating an x-ray sensitive photocathode in place of the optical photocathode. Filter packs are often positioned along the slit length to provide spectral resolution, with a typical temporal resolution of around 15ps [5].

Often it is desirable to supplement the one-dimensional spatial information derived from a streak camera with other diagnostics. Of particular interest is the aquisition of two-dimensional time resolved x-ray images which are useful in the study of implosion symmetry and Rayleigh Taylor instabilities

[6,7]. Where just a single exposure of an x-ray opaque object from a specific viewpoint is required, flash x-radiography using conventional pin-hole optic imaging may be employed [8]. Here an x-ray image is formed at a film plane using a pin-hole. A short duration (~50ps) x-ray burst from a point source behind the object provides the exposure.

If the object is x-ray self luminous a shutter must be introduced into the system to prevent blurring. Use is often made of a gated Microchannel plate (MCP) proximity focus intensifier (see section 1.2.9). An intermediate image is formed at the photocathode of the MCP which is incorporated into a transmission line configuration. Final image recording is by photographic film held in intimate contact with the MCP fibre-optic output. Propagation of a shaped voltage pulse onto the photocathode enables the device to be shuttered for periods as short as ~100 ps [9]. Several such devices may be arranged to operate successively, providing a sequence of images. By necessity there will be a parallax error between each viewpoint, each device being able to record only one image. A further complication is the close proximity of the phosphor screen to the photocathode. The MCP does not itself provide sufficient attenuation of highly energetic x-rays which tend to penetrate to the phosphor screen and obscure any photographic image formed by the electrons. This problem may be overcome by placing the whole tube in a strong axial magnetic field which confines the electrons to tight helices. The electrons then follow curved trajectories while the x-ray paths remain unchanged.

The problem of multiple viewpoints may be avoided if each successive image may be located in a different position on the

recording medium. The Picoframe framing camera provides a mechanism for achieving this. Additionally the remoteness of the phosphor from the photocathode and the location of aperture plates along the tube axis minimizes the problems associated with x-ray penetration. An x-ray luminous event must be imaged onto a suitably sensitive photocathode. This may be achieved using pin-hole optics [10], grazing incidence x-ray mirrors [11] and Fresnel zone plate imaging [12].

It might be thought that by merely replacing the optical photocathode in the standard Picoframe framing camera design, with a suitable x-ray sensitive photocathode, would yield a device capable of recording an imaged x-ray luminous event. However the electron optics of the design are not optimised to image the photoelectrons emitted by an x-ray photocathode. The principal difference in response between optical and x-ray photocathodes is the increased spread in secondary electron energy of the latter. The secondary electron energy spread of a gold photocathode under soft x-ray illumination is about 3.8eV (FWHM) [13] compared to around 0.3eV (FWHM) for an S1 type photocathode illuminated by light of wavelength 1.06μm [14].

The effect of this increase in secondary electron emission energy is demonstrated by computing the trajectories of 0.3eV and 3.0eV energy photoelectrons through the Picoframe design. Three cathode object points are considered y = -2, 0, +2mm with emission angles ±45°, yielding six trajectories. The trajectories for 0.3eV and 3.0eV energy photoelectrons are illustrated in fig. 5.1 (a) and (b) respectively. Radial dimensions have been scaled by a factor of two for clarity.

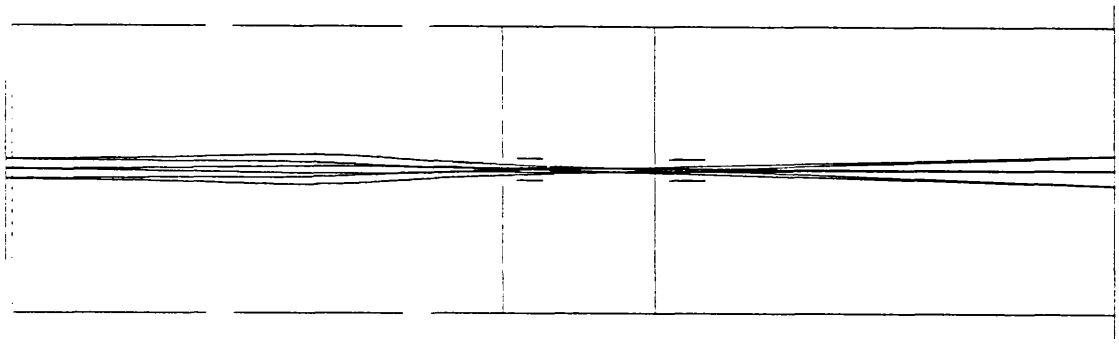

Fig.5.1 (a) 0.3eV energy electron trajectories in the Picoframe I

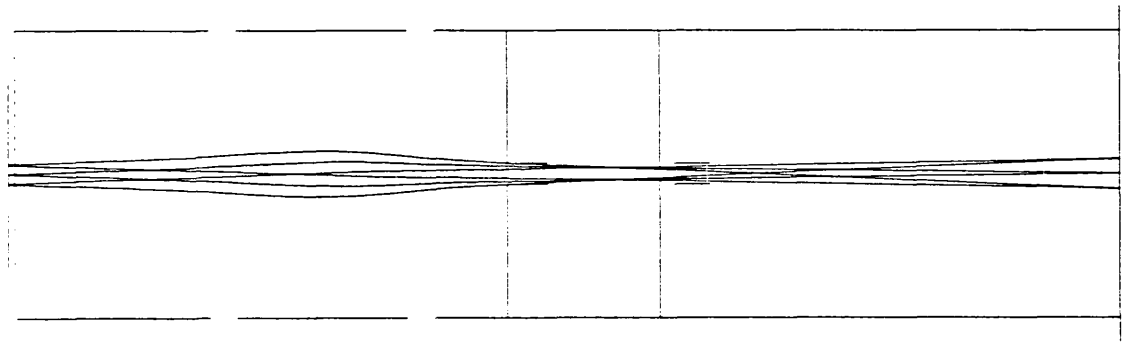

Fig. 5.1 (b) 3.0eV energy electron trajectories in the Picoframe I

It is obvious from Fig.5.1 (b) that the crossover diameter has increased, and that electrons through the lens follow paths which stray a considerable distance from the axis, so suffering

increased geometrical distortions. Since the principle of operation of this type of tube is such that to form an image the electron beam must pass unimpeded through two axially separated apertures and two sets of deflectors, it is necessary to maintain a long narrow waist beam profile. The standard tube design employed in the x-ray sensitive mode would have a severely restricted usable cathode area as electrons from off axis cathode positions are intercepted by the anode and framing apertures. Consequently it is necessary to redesign the imaging characteristics attempting to limit the radial spread of the photoelectrons, retain the narrow waist beam profile and modify the deflector plate design to accommodate the increased beam diameter whilst maintaining sensitivity. The aims of the design modifications were:

1) Minimize beam waist diameter
2) Minimize beam divergence or magnification
3) Prevent electrons intercepting the deflection plates

5.2 Computer aided design

To evaluate the imaging characteristics of an electrostatically focused system it is first necessary to establish the potential distribution in the system. Early techniques for achieving this relied upon analogue simulations. These included mechanical simulations such as the rubber membrane [15] and electrical simulations such as the use of conductive paper [16], the electrolytic tank [17] or resistance networks [18].

With the advent of modern digital computers these analogue techniques have been superseded by the application of numerical analysis techniques to solve electric field distributions and

evaluate electron trajectories. In recent years these techniques have been widely used in the field of electron-optics [19,20] and, more particularly in the design of electron-optical ultra-high time resolution cameras [21,22,23]. Considerable early work in this field was carried out by C.V.Weber [24] at Philips Research Laboratories, Eindhoven. Using similar techniques a suite of computer programs have been developed [23] in the Laser Group, Imperial College to assist in the design of electron-optical streak and framing image tubes. These programs have been employed in modifying the Picoframe design for x-ray sensitivity.

5.2.1 Computational techniques

Only electrostatically focused systems which can be mapped onto a two-dimensional grid may be analysed using the suite of programs. Thus rotationally symmetric systems (e.g. focusing region of an image tube) and systems possessing two-dimensional symmetry (e.g. electrostatic deflection regions) may be modelled; three dimensional systems are excluded. The test region is mapped onto a uniform 'square mesh' grid; for rotationally symmetric systems the cross-section will be a meridian plane and only the upper half need be considered. The potential at each grid point is obtained by solving a finite difference form of Laplace's equation iteratively, using an accelerated successive over-relaxation routine [25]. For a numerical solution of Laplace's equation the system must be totally closed, thus for each boundary point the potential must be defined. This is achieved by extending existing electrodes or by using linear or logarithmic interpolation between them. In practice these

approximations are distant enough from the region of interest so as not to influence the results.

Once the potential at each grid point has been established the electric field at each point may be found by solving

$$E = -\text{grad}(V)$$

This is accomplished using Lagrange interpolation and numerical differentiation [26]. Both the axial (z) and radial (r) electric field components are evaluated at each grid point. In general of course the position of an electron during its trajectory through the region will not coincide exactly with a grid point. It is thus necessary to be able to evaluate the electric field at any position within a grid square. The electric field components E_z, E_r, are two dimensional functions of parameters r and z, thus a two-dimensional Lagrange interpolation routine [27] is employed using 16 grid points surrounding the position of interest.

5.2.2 Calculation of electron trajectories

To evaluate the trajectory of an electron through an electrostatic region the equations of motion must be solved. For an electron possessing charge -e and mass m these may be written in cartesian co-ordinates as;

$$\frac{d^2x}{dt^2} = -\frac{eE_x}{m} = -\frac{e}{m}\frac{x}{r}E_r$$

$$\frac{d^2y}{dt^2} = -\frac{eE_y}{m} = -\frac{e}{m}\frac{y}{r}E_r$$

$$\frac{d^2z}{dt^2} = -\frac{eE_z}{m}$$

The trajectory evaluation is usually broken down into a number of distinct stages. For reasons described section 1.2.3 , most ultrahigh time resolution electron-optical instruments and all those described in this thesis, incorporate a fine mesh electrode close to the photocathode. In cases where the cathode and mesh are planar and parallel the equations of motion have analytic solutions in that region. All that is necessary is that the initial conditions at the photocathode are defined. This is covered in detail later, but essentially the emission co-ordinates, energy and angular spread must be defined. Thus the electron trajectories may be evaluated up to the mesh.

The mesh electrode forms the start of the rotationally symmetric focusing region. Here the electric field is not an analytic function of electron position, so the equations of

motion must be solved by numerical integration. The position, velocity and transit time t_o at the mesh electrode are used as the starting conditions from which the position and velocity at time t_o + dt are computed. These values form the starting conditions for the next step. This procedure is repeated until the electron reaches the end of the modelled region.

Where the electrons are to undergo simulated deflection a second two-dimensional data region containing the deflector plates is butted onto the focusing region. Here the anode aperture plane forms the first column of the deflection region. Application of a linear time varying deflection voltage means that the fields and potential distribution within the region are not static. To model this situation the data region is set up with a unit voltage difference between the deflector plates, i.e. 0V and 1.0V for asymmetric deflection and -0.5V to +0.5V for symmetric deflection. Once the potential distribution has been solved using Laplace's equation the time dependence is introduced as a multiplicative time varying scaling factor. Trajectories can then be calculated up to the end of the deflection region using a third-order Runge-Kutta scheme.

Finally trajectories from the end of the deflection region up to the phosphor screen through the field free drift region may be computed analytically. Where no deflection simulation is undertaken (i.e. when analysing static performance) the trajectories may be computed analytically from the end of the focusing region onwards.

The suite of electron trajectory evaluation programs have been implemented in the computation of electron paths through

various modified Picoframe configurations. This theoretical analysis accurately models the performance of each design, enabling critical evaluation to be carried out without recourse to expensive and time consuming prototype construction.

5.2.3 The MTF Method

Evaluation of the photoelectron trajectories through an electro-static imaging system despite providing useful data such as paraxial focus, magnification and image distortions, does not directly yield data such as the spatial and temporal resolution. The temporal resolution of streak image tubes has in the past been obtained using a method based on the Gaussian approximation (see section 1.2.3), in which it has been assumed to be composed of a number of discrete, independent factors of equal weight. With the evolution of ultra-high time resolution instruments, particularly in the sub-picosecond regime, this technique has been found wanting [28] and a more accurate method of analysis sought. The Optical Transform Function (OTF) developed from communication theory and incorporating diffraction theory has for sometime been applied in the evaluation of the spatial response of imaging systems [29]. However it is only relatively recently that this method has been employed in the evaluation of spatial resolution [30], and more importantly temporal resolution [28,31] of electron-optical devices.

To fully describe the properties of a linear imaging system it is desirable to test the response at all spatial frequencies. If an input signal has a sinusoidal variation of spatial frequency f_{in}, the output will also be sinusoidal but with a spatial frequency modified by the magnification M of the system such that $f_{out} = f_{in}/M$. In general the image has a lower contrast

and may suffer a phase shift, displacing it with respect to the object. The modulation at this frequency is defined as the image to object contrast ratio and defines the performance at that frequency. If this process is continued for a whole range of spatial frequencies the variation against spatial frequency of the Modulation and Phase represent respectively the Modulation Transfer Function (MTF) and the Phase Transfer Function (PTF). They each form part of the complex Optical Transfer Function (OTF), where the MTF is the modulus of the OTF and the PTF is the imaginary part. The OTF is evaluated by determination of the Point Spread Function (PSF) and the Line Spread Function (LSF) of the linear imaging system under investigation.

The PSF is the surface generated by plotting intensity as a function of position (x and y) in the image plane, and represents how well the imaging system can reproduce an infinitesimal point object. A line integral carried out over this surface yields the LSF. This is equivalent to replacing the infinitesimally small point object with an infinitesimally narrow line object and plotting the intensity at the output plane against the distance in a direction normal to the length of the object. Realizing that the delta function line object for the LSF contains equal amplitude sine waves at all spatial frequencies it may be deduced that the LSF is related to the OTF. In fact the OTF is defined as the Fourier transform of the LSF. Both the MTF and PTF may be determined from the OTF. However because the magnitude and phase may vary for each frequency interpretation of the PTF is difficult and thus only the MTF is usually evaluated.

It is a property of the MTF that if a number of incoherently linked systems are used together the combination MTF is determined by the product of the individual component MTF's [32].

This enables the combined response of the ancillary optics (e.g. input lenses, image intensifiers) to be evaluated easily.

Although the MTF fully describes the performance of a linear imaging system it is still useful to retain the concept of limiting spatial resolution. Limiting resolution is taken to be the spatial frequency at which the modulation has fallen to a value of 5%. This is around the modulation limit for the human eye [33].

5.2.4 A simplified Analysis Method.

Due to the large number of electron trajectory computations necessary to evaluate the MTF, the method is not particularly well suited to the preliminary investigation of prototype designs. It had been concluded from earlier work that the crude evaluation of parameters such as focus, crossover position and magnification using just a few electron trajectories provided a satisfactory method of testing early designs. This procedure was adopted in the initial stages of modifying the Picoframe design. More rigorous evaluation using the MTF method was then applied to the more promising designs.

5.2.5 Initial conditions of the Photoelectrons

As already stated accurate analysis of an imaging system using the MTF method requires the computation of a large number of electron trajectories (usually 1000). The initial conditions of the electrons are determined to simulate as closely as possible the characteristics of the proposed photocathode. The angular distribution of photoelectrons is assumed to be Lambertain, imposing a cosine law function in the radial angle [34]. Simulation of the initial energy distribution is more

difficult as it is not an analytic function, but must be determined for a particular photocathode under specific illumination conditions.

Since not all combinations of emission angle and energy can be considered, the energy and angular distributions are divided into a number of equally spaced strips. A single electron trajectory can then be used to represent a particular strip by application of a suitable weighting factor. The energy distribution is split into five strips, the radial angle θ ten and azimuthal angle φ twenty strips. Angles θ and φ are as defined in fig. 5.2

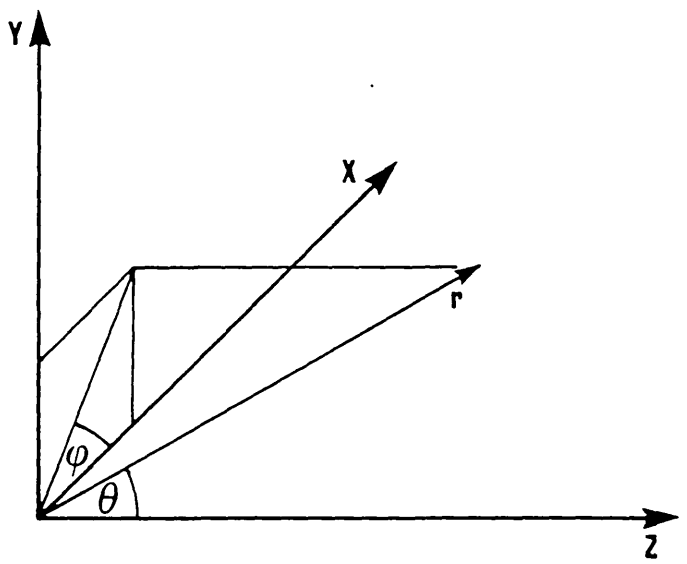

Fig. 5.2 Definition of angles and axes

The radial angle θ can vary from 0° to 90°. Division into ten strips gives a width $\Delta\theta = 9°$ with each strip described by its midpoint (4.5°, 13.5°...85.5°). The number of electrons emitted into the range θ_1 to $\theta_2 = \theta_1 + \Delta\theta$ is given by the emission probability multiplied by the area of the range [23]. For a unit sphere it can be shown to be proportional to:

$$\cos\theta dA = 2\pi\int_{\theta_1}^{\theta_2} \cos\theta.\sin\theta d\theta$$
$$= \sin(\Delta\theta).\sin 2\theta_{av}$$

The appropriate weighting factor for each angular strip is thus given by:-

$$WF(\theta) = N\sin\theta_{av}\cos\theta_{av}$$

Where θ_{av} is the electron emission angle used in the sumulation and $\Delta\theta$ is a constant.

The number of electrons emitted within the energy range E_1 to $E_2 = E_1 + \Delta E$ is similarly given by:-

$$\int_{E_1}^{E_2} N(E)dE$$

where N(E) is the number emitted with energy E. This expression cannot be integrated analytically since N(E) is not an analytic function. Instead the experimentally determined energy spectrum is divided into five equal width slices ΔE each with a midpoint energy E_{av}. The integral is then approximated to $N(E_{av}).\Delta E$.

As described earlier x-ray photocathode materials possess a broader spread in emission energy than typical IR/visible sensitive photocathodes. This increases the electron beam waist diameter necessitating design modifications. Obviously minimizing this energy spread by careful photocathode selection

will impose less severe operating conditions on the design With this in mind caesium iodide was selected as the photocathode material due to its comparatively low energy spread ΔE = 1.5eV (FWHM), compared to ΔE = 3.8eV (FWHM) for gold and ΔE = 4.2eV (FWHM) for aluminium; two commonly used x-ray/VUV photocathode materials. The secondary electron emission distribution for caesium iodide determined by Henke et al [13] was divided into five 1.0eV width strips, with each midpoint energy appropriately weighted. The discrete energies and corresponding normalised weighting values are given in Table.5.1.

E Midpt.(eV)	0.5	1.5	2.5	3.5	4.5
$N(E_{av})$	0.518	0.277	0.111	0.055	0.037

Table 5.1 Normalised energy weighting values

5.2.6 Design criteria for a modified imaging region

Photoelectrons emitted from a cathode with zero energy would be focused by a perfect electron lens to a point cross-over. The finite diameter of the beam waist is primarily caused by the finite transverse energy distribution. This distribution causes transit time dispersion in streak tubes, and necessitates the incorporation of a mesh electrode close to the photocathode surface (see section 1.2.3). The rapid axial acceleration to relatively high electron energies reduces the effect of the transverse energy spread. Thus increasing the mesh potential will reduce the diameter of the beam waist. This may be understood by evaluation of the photoelectron entry angle into the electron lens. As the angle tends to zero the photoelectron is emitted

normal to the photocathode and is brought to a point crossover.

Consider a photoelectron emitted along the cathode surface with an energy eV in electron volts. If a planar electric field region is maintained by a potential Φ on the mesh electrode, as illustrated in fig. 5.3 (a), the electron will follow a parabolic trajectory up to the mesh.

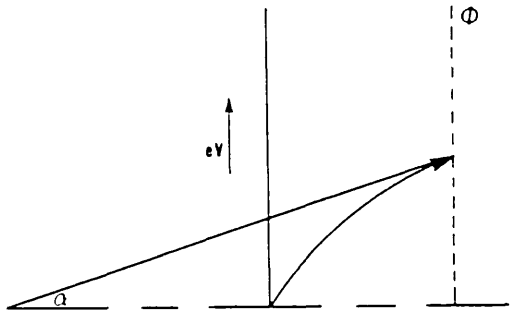

Fig.5.3 (a) Parabolic trajectory of a photoelectron up to the mesh electrode.

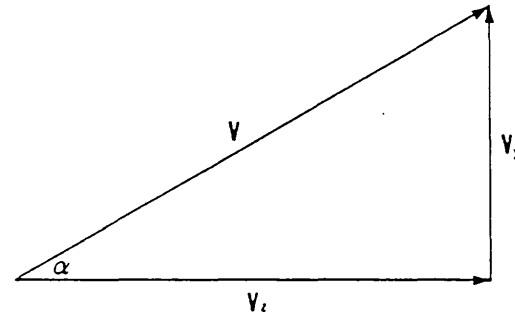

Fig.5.3 (b) Velocity triangle

Constructing the velocity triangle (fig.5.3 (b)), the angle of entry into the lens is given by:-

$$\alpha \simeq \frac{V_y}{V_z} = \sqrt{\frac{V}{\Phi}} \qquad \text{equ.5.1}$$

The mesh potential in the Picoframe design is 5kV applied over a distance of 2.5mm. Hence a factor of two decrease in angle α would require an increase from 5kV to 20 kV. Unfortunately although this has the desired effect of reducing the beam waist diameter, it also has the undesired effect of increasing the lens magnification.

The Lagrange Helmholtz relation [35] (equ.5.2) describes the

characteristics of paraxial electrons in an electrostatic lens. Parameters are as illustrated in fig.5.4, where Φ_o , Φ_i are the object and image plane potentials respectively.

$$\frac{h_i}{h_o} \cdot \frac{\alpha_i}{\alpha_o} \cdot \sqrt{\frac{\Phi_i}{\Phi_o}} = 1 \qquad \text{equ.5.2.}$$

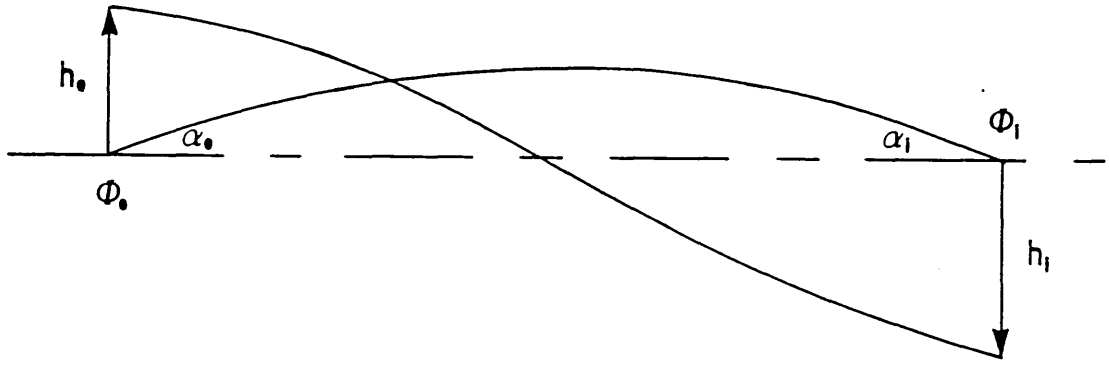

Fig.5.4 Paraxial electrons in an electrostatic lens

This relationship has the consequence that the angle of entry (related to radial spread) and magnification (h_i/h_o) cannot be controlled independently.

One way of ensuring the electron trajectories in an x-ray sensitive design are identical to the trajectories in the optically sensitive design is to scale the electrode voltages up by the same factor as the increase in emission energy spread. For instance an increase in energy spread from 0.3eV (FWHM) to 3.0eV (FWHM) would require scaling the lens electrode voltages by factor of ten. Unfortunately this solution is impractical, for a number of reasons including;

(1) The deflection sensitivity of the deflectors would be reduced by the same scaling factor so increasing the camera open time.

(2) There would be severe practical difficulties in ensuring adequate insulation between the lens electrodes.

Of course if such a design procedure were to be adopted the equations of motion would have to be modified to account for the relativistic electron mass, as the electrons would be travelling at relativistic velocities. Electron velocities in the standard design are about 0.25c, hence relativistic effects are negligible.

5.3 A modified imaging region

The computational techniques discussed were employed in modifying the Picoframe imaging region in a manner now described.

5.3.1 Modification procedure

The approach to modification was to retain the basic Picoframe lens structure as a proven design but modify specific parameters such as electrode voltages, lengths and spacings. A complete re-design of the deflection system was necessary to increase the deflector plate spacing to accommodate the increased beam diameter.

The effect of changing the mesh potential whilst maintaining the same cathode extraction field, by appropriately altering the cathode-mesh spacing was studied. The focus voltage was modified to preserve the Picoframe I focal plane of z = 434mm from the photocathode, so that valid comparisons could be made of the magnification. A particular photoelectron trajectory, with initial parameters y = 2mm, θ = 45°, E = 3eV, was analysed.

The axial distance between the anode aperture and the point where the electron trajectory strayed 2mm off axis was defined as parameter D. This ascribed a figure of merit to the divergence of the beam waist. The variation of D against mesh potential at constant electric field and anode potential is shown in fig.5.5

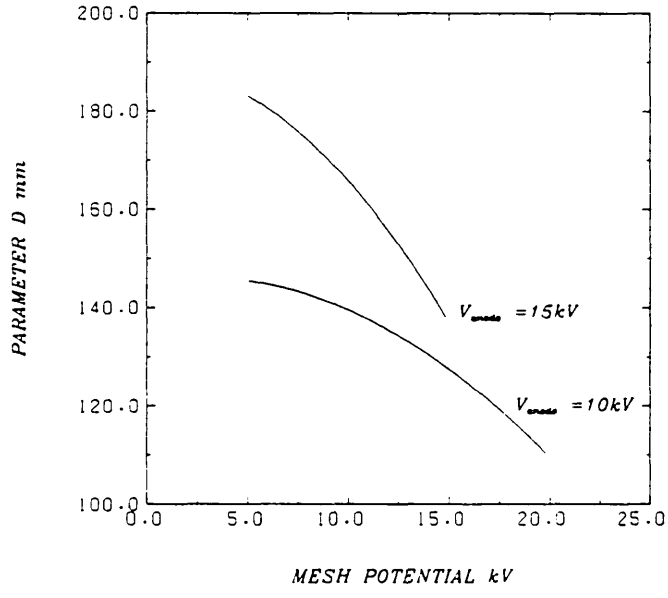

Fig.5.5 Variation of D against mesh potential

The value of parameter D is largest (i.e. the beam diverges least and the magnification is small) at low mesh potentials and high anode potentials.

Another parameter studied was the variation in beam waist radius with mesh potential. Photoelectrons from object points y = 0mm, y = 2mm (x = 0mm) with initial angular values θ = 0°,10°, $\pm$ 90° and initial energy 3eV were used. The trajectories were evaluated through a number of test regions and the crossover position located. The beam radius was determined at this point and plotted against mesh potential (Fig.5.6) under conditions of constant cathode electric field and at an anode potential of 15kV.

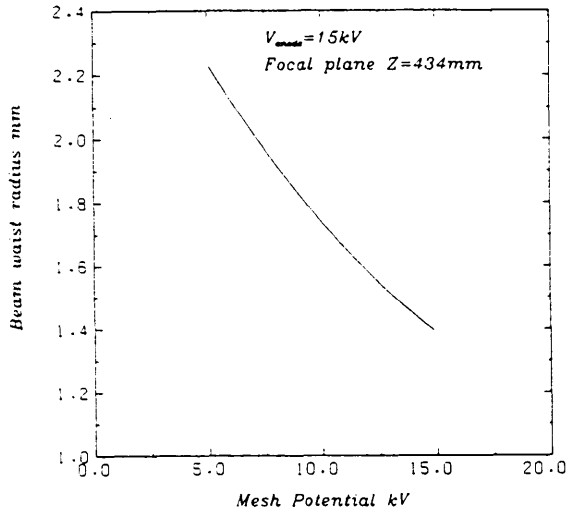

Fig. 5.6 Beam waist radius against mesh potential

Analysing image magnification against mesh potential (fig. 5.7) maintaining the focal plane at z = 434mm, demonstrates clearly the increase in beam divergence with increasing mesh voltage. This can however be counter-acted by increasing the anode potential to maintain the ratio $\sqrt{\Phi_i/\Phi_o}$. The focus electrode potential must be changed with increasing mesh potential to provide a stronger lens in order to focus the increasingly energetic photoelectrons at the same image plane.

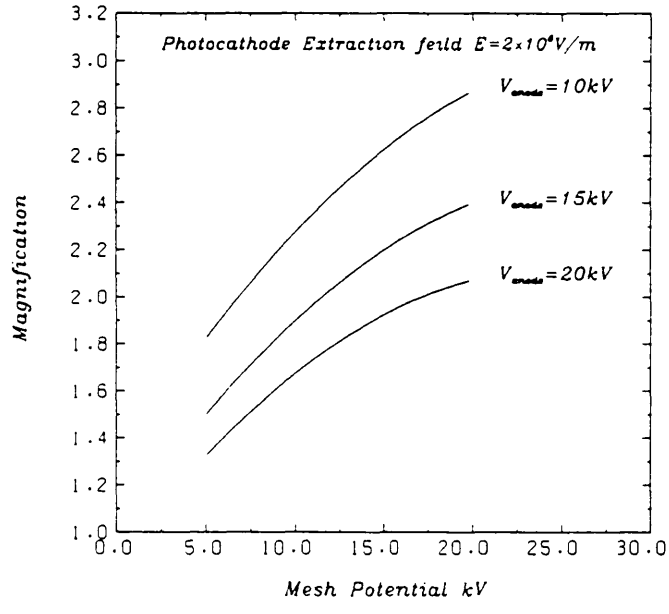

Fig 5.7 Image magnification versus mesh potential

Variation in the electric field at the photocathode has only a weak effect upon the beam waist radius and magnification. Photoelectron trajectories with the same initial conditions used in the previous analysis were evaluated through data regions with different cathode extraction field strengths. The mesh potential was maintained at 10kV and the cathode-mesh spacing varied (2,5,8,10mm), again the beam waist radius was located and determined.

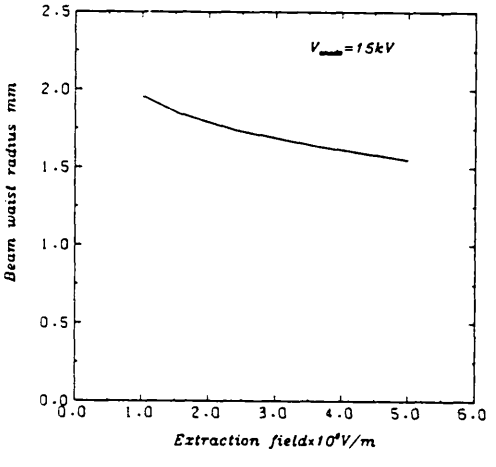

Fig.5.8 (a) Beam waist radius versus Electric field

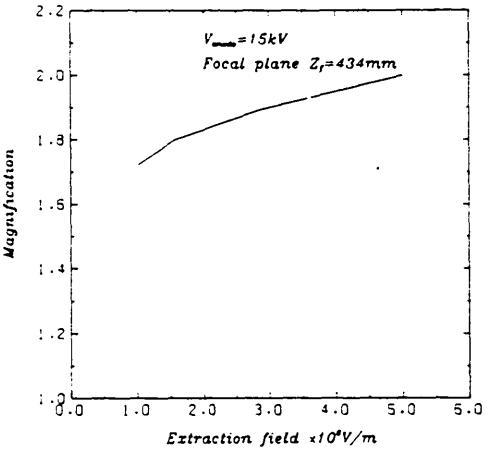

Fig.5.8 (b) Magnification versus Electric field

It is clear from fig.5.8 (a) that there is a small decrease in beam waist radius with increasing electric field. The variation in magnification with electric field shown in Fig.5.8 (b) was determined by analysis of the electron trajectory from y = 2mm with θ = 10°. A small increase in magnification is noted with electric field.

5.3.2 Discussion

As predicted by equation 5.1 the beam waist radius is observed to decrease with increasing mesh potential. However the electron optical magnification is increased as predicted by the Lagrange Helmholtz relation. It is this combination of

effects which makes the implementation of the Picoframe design into an x-ray sensitive role problematic. Since not only is it desirable to achieve a small crossover diameter but also a long narrow waist beam profile, or low magnification. From the preceding analysis these objectives are demonstrated to be incompatible. This conflict does not arise to the same extent when implementing an optically sensitive streak camera design into an x-ray sensitive mode, as the beam waist minimum may be conveniently located at the single aperture plane. Also the constraint on usable cathode area is of less importance as the cathode area is often deliberately restricted to minimize dynamic slit curvature (see section 1.2.5). Maximum usable cathode area and high temporal resolution are two of the most important factors in a practical framing camera design. However these conflicting requirements must inevitably result in compromise.

5.3.3 Design considerations

In order to adequately excite the phosphor the anode potential should be greater than 10kV, but too large a potential will reduce the sensitivity of the deflectors and increase the exposure time for a given sweep speed. The design specification Picoframe I value of 15kV is a good compromise. (It should be noted that the Picoframe I could satisfactorily be operated down to an overall potential difference of 12.5kV to improve the sensitivity of the deflectors.) It is desirable to maximize the parameter D, resulting in a long narrow waist beam profile, thus the mesh potential should be less than 15kV. Increasing the mesh potential from 5kV to 10kV only decreases D by 8%, but reduces the beam waist radius by 27%. The magnification of the tube is increased from -1.5 to -1.9 if the cathode extraction

field if maintained at $2x10^6$ V/m.

The imaging section of the Picoframe design has been modified retaining a similar electrode geometry with the mesh potential increased to 10kV and the cathode-to-mesh spacing doubled to 5mm. The focus potential is modified to V_f = 2.46kV to maintain the focal plane at z = 434mm from the photocathode, at an anode potential of 15kV. A more detailed evaluation of the static performance of the modified imaging section design was undertaken using the PSF to examine the beam waist.

The Picoframe I was designed with the electron-optical cross-over positioned midway between the anode and framing aperture planes. Using the PSF routine different z planes were examined in this region to determine the beam waist characteristics. In particular the anode plane and planes +50mm, +55mm, +60mm relative to it. The minimum requirement for the image format is 5mm x 5mm at the photocathode, thus the PSF of object point (2.5mm, 2.5mm) was examined specifically. It was established that due to the increased beam divergence in the modified design, the 60mm axial separation specified in the Picoframe I design was no longer appropriate as it would have been necessary to enlarge the framing aperture significantly. A reduction in the length of the anode electrode cylinder from 30mm to 20mm was made to introduce a relative shift in the crossover position away from the anode towards the framing aperture. The inter-aperture separation was decreased to 55mm further enhancing this effect and thus allowing the framing aperture diameter to be minimized. This inevitably required an increase in the anode aperture diameter, but this was considered preferable and was found to be minimal.

The percentage loss of photoelectrons emitted from the most distant off-axis point (2.5mm, 2.5mm) against aperture radius at the anode and framing aperture planes are illustrated in fig.5.9 (a), (b).

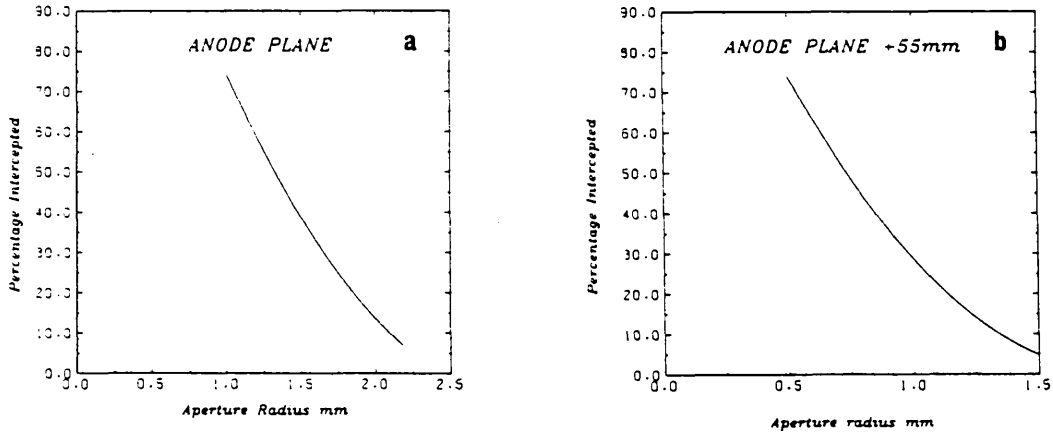

Fig. 5.9 Percentage of intercepted photoelectrons from object point (2.5mm, 2.5mm); (a) for anode aperture plane, (b) for anode plane + 55mm.

An anode aperture diameter of 4.0mm was selected resulting in a photoelectron loss of 12%. A framing aperture daimeter of 2.0mm, an increase of 10% compared to the Picoframe I, was adopted with a resultant photoelectron loss of 27%. The PSF's for object point (2.5mm, 2.5mm) at the anode aperture and framing aperture plane are shown in fig 5.10 (a), (b).

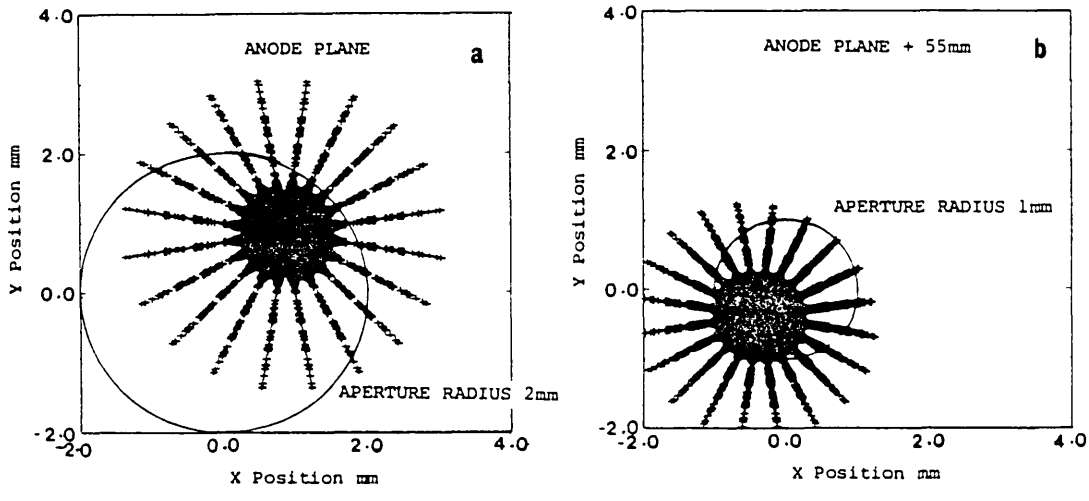

Fig. 5.10 (a) PSF at anode plane, (b) PSF at anode plane + 55mm.

5.3.4 Static MTF results

The static (undeflected) performance of the modified Picoframe imaging section was evaluated for different points in the object field using the MTF method described in section 5.2.3. Since the framing camera images in two spatial dimensions object points from the whole cathode area must be considered. However due to axial symmetry it was only necessary to study one quadrant. Five object points were selected; (0.0,0.0), (0.0,1.5), (1.5,1.5), (0.0,2.5), (2.5,2.5), where these represent (x,y) in mm.

Static limiting resolution in the x direction was plotted against axial position z for each of the studied object points (fig. 5.11).

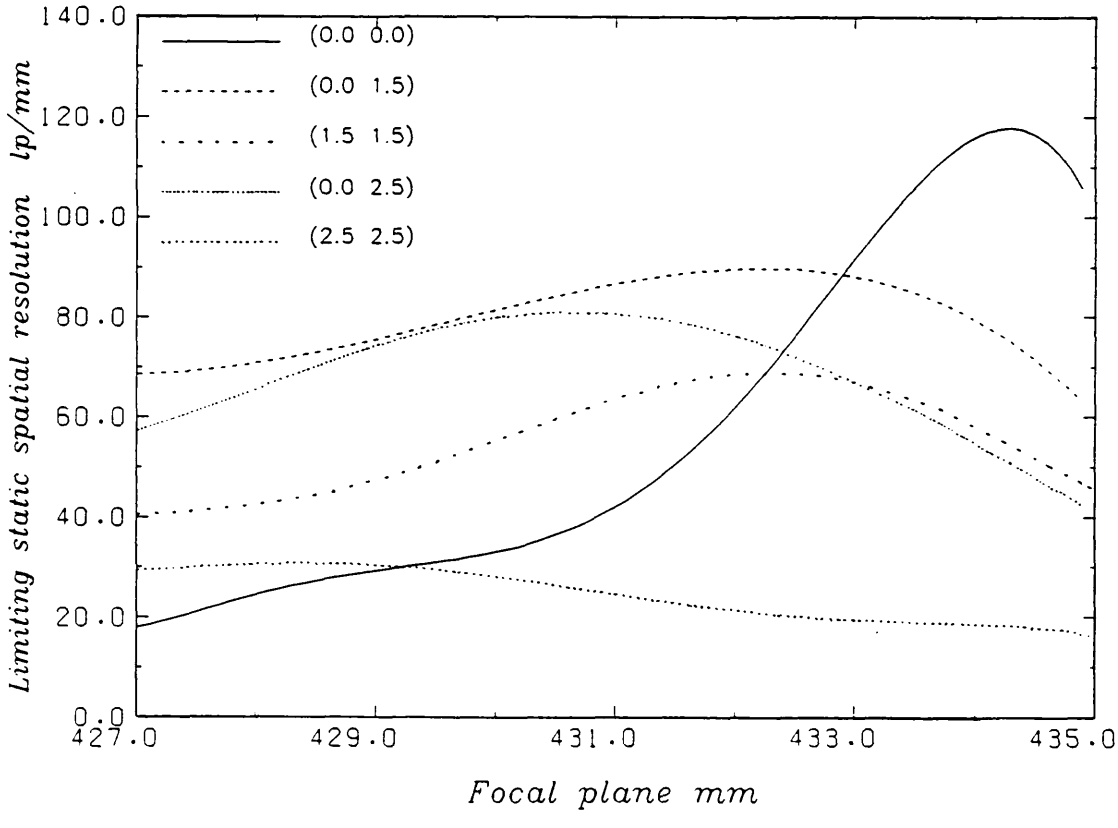

Fig 5.11 Variation of static limiting resolution with axial position

The effect of electron-optical aberrations in degrading the image quality for off-axis points is obvious. In particular the effect of field curvature is clear from the gradual movement of peak resolution towards the cathode as object points further off axis are considered.

If point (2.5, 2.5), is neglected the optimum focal plane is z=432mm (from the photocathode) with a limiting spatial resolution of 69 lp/mm (at the screen). Inclusion of point (2.5,2.5) brings the resolution down to 24 lp/mm (at screen). Taking into account the magnification of the tube this corresponds to an overall spatial resolution of 47 lp/mm referred to the photocathode. This compares well with the theoretically predicted limiting spatial resolution of 55 lp/mm (at photocathode) of the Picoframe I over a 6mm x 6mm cathode format. Static MTF curves for the optimal focal plane z=432mm for the object points considered are shown in fig.5.12. The modified design, designated Picoframe-X has an increased electron-optical magnification of -1.9.

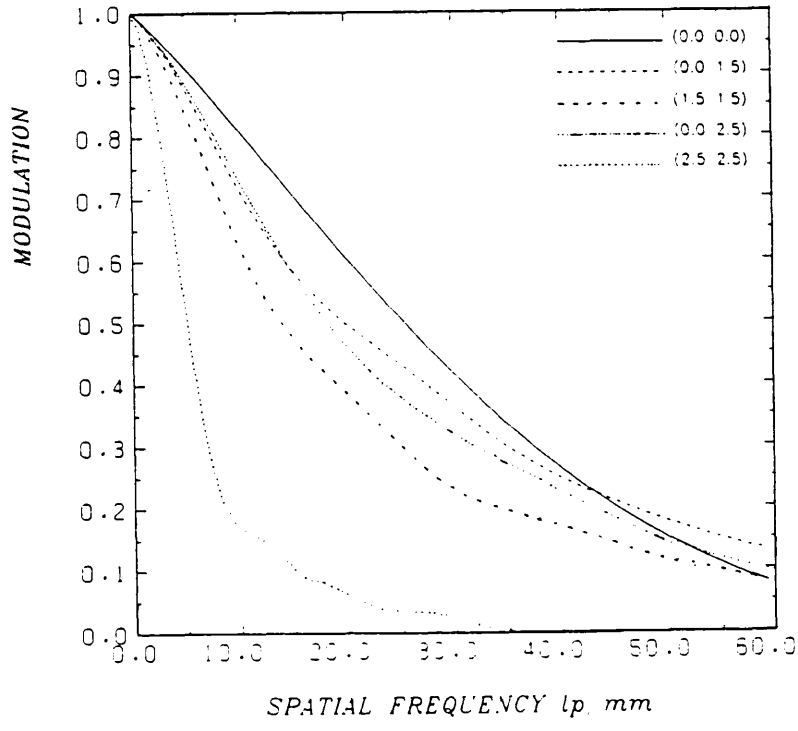

Fig.5.12 Static MTF curves at optimum focal plane of z=432mm.

5.4 Design of Deflectors

The increased electron beam diameter in the Picoframe-X design necessitated a complete redesign of the Picoframe deflection assembly to prevent the electrons being intercepted by the deflection plates, or passing so close that fringing fields could no longer be ignored. Additionally the repositioning of the framing aperture closer to the anode aperture decreased the effective sensitivity of the framing deflector plates. Thus to maintain similar exposure times in the modified design the overall sensitivity of the deflectors had to be improved.

Two deflector designs are presented. The first analogous to the Picoframe I incorporates a single framing aperture, permitting double frame generation by shaping of the deflection voltage waveform. The second design, modelled on the Picoframe II uses two framing apertures equally disposed about the tube axis. 'Doublet' images are generated by provision of a simple linear voltage ramp. While a 'quadruplet' format option is available by using a shaped voltage pulse in conjunction with a pair of orthogonally orientated separator plates driven with a staircase waveform. The original proposal for a triple aperture multiplex aperture plate [35] is extremely difficult to fabricate with current constructional techniques, but may become viable with the advent of new assembly procedures.

5.4.1 The Picoframe X-I design

A similar analysis to that employed in the earlier design of the Picoframe I deflectors was undertaken. The parameters used are defined in fig. 5.13

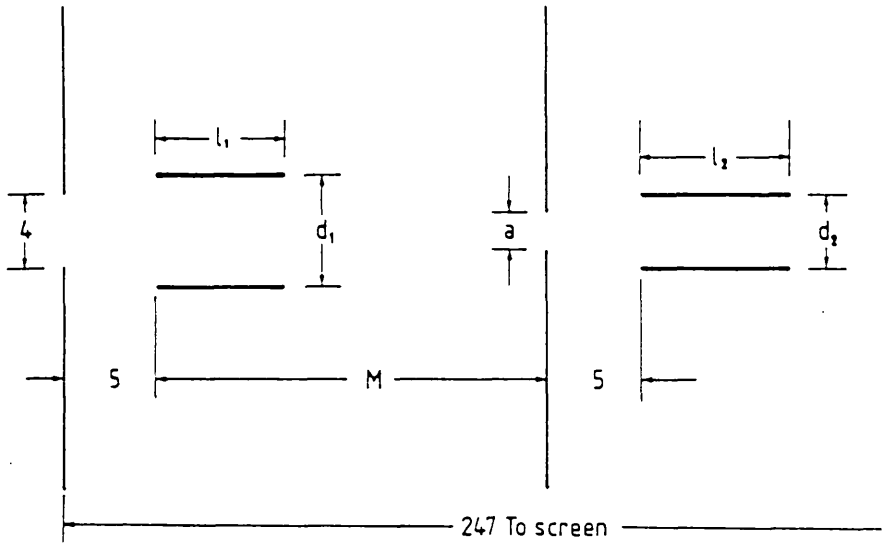

Fig 5.13 Picoframe X-I deflector design parameters (Dims in mm)

A framing aperture diameter of 2mm was adopted from earlier analysis (see section 5.3.3). Thus a transverse beam deflection of 2mm is required to shutter the tube off. This is achieved by deflecting with the framing deflectors. The voltage V required for the requisite deflection is calculated from equ.5.3 where V_a is the overall acceleration potential of the electron tube; in this case V_a = 15kV.

$$V = \frac{2aV_a d_1}{l_1.(M - \frac{1}{2}l_1)} \qquad \text{equ.5.3}$$

Calculating the deflection produced at the screen Y_{screen} by similar triangles, then yields the deflection sensitivity S_1(in mm/V) of the framing deflectors at the phosphor screen. (equ.5.4)

$$S_1 = \frac{Y_{screen}}{V} \qquad \text{equ.5.4}$$

For frame 'stationarity' this must be identical to the sensitivity of the compensating deflectors. Inserting S_1 into equ.5.5, having first preselected parameter d_2 yields the compensating deflector length l_2

$$l_2 = M - \sqrt{M^2 - 4S_1V_ad_2} \qquad \text{equ.5.5}$$

Provided the beam is not intercepted by the compensating plates this value of l_2 is acceptable, otherwise d_2 is incremented and l_2 re-evaluated. This analysis provided a range of deflector dimensions and sensitivities, from which a suitable design could be selected.

A number of assumptions are implicit in this analysis.

(i) The axial velocity V_z of the electrons is constant.

(ii) The diameter of the electron beam is small compared to the deflection plate separation.

(iii) The electric field between the plates is uniform and there are no fringing fields.

(iv) The deflector plate widths extend to infinity, i.e. the simulation is explicitly two-dimensional.

The minimum size of d_1 is governed by the diameter of the anode aperture (4.0mm). However to reduce the chance of beam interception and to justify assumption (ii) above, a plate spacing d_1 of 5.8mm was adopted. Since the fabrication and accurate positioning of very small plates is difficult, the the minimum length l_2 was defined as 10mm. Some of the resulting values of l_2, deflection sensitivity (at phosphor screen), l_2 and d_2 are presented in Table 5.2.

l_1(mm)	Def.Sen.(cm/kV)	l_2(mm)
13	1.75	14.2
14	1.9	15.35
15	2.0	16.5
16	2.16	17.66
17	2.29	18.80
18	2.43	20.00
19	2.56	21.20

Fig.5.2 Dimensions for d_1 = 5.8mm and d_2 = 4.8mm

In order to maximize the deflector sensitivities a framing plate length of 19.0mm was selected. The individual plate widths were chosen to equalise the capacitance of the deflectors, using equ. 5.6

$$\frac{l_1 . W_1}{d_1} = \frac{l_2 . W_2}{d_2} \qquad \text{equ. 5.6}$$

Where W_1 and W_2 define the plate width for the framing and compensating deflectors respectively. With the compensating deflector plate width selected to be 10mm the framing deflector width was determined to be 13.3mm, with a resulting deflector plate capacitance of 0.38pF. This is almost double that of the Picoframe I design but it is likely to be similarly limited by the stray capacitance of the connector/electrical feed-in arrangement. Thus a loss in deflector response time compared to that of the Picoframe I is not anticipated. The deflector dimensions for the Picoframe X-I design are presented in Table 5.5

d_1 = 5.8mm	d_2 = 4.8mm
l_1 =19.0mm	l_2 =21.0mm
W_1 =13.3mm	W_2 =10.0mm

Table 5.5 Deflector dimensions for the Picoframe X-I

5.4.2 The Picoframe X-II design

The design analysis of the twin aperture tube was carried out in a similar manner to that described for the single aperture design. Practical constructional constraints dictated that the framing aperture separation was a minimum of 8mm. If this is equally disposed about the axis a beam deflection of 4mm is required at the aperture plate to generate an exposure. The constraints on the framing deflector dimensions are identical to those in the previous case with the same initial values of d_1 and l_1 chosen. There is an extra constraint on d_2, which should be minimized so as to reduce any cross coupling effects between the two compensating deflectors. The values of l_1, deflection sensitivity (at phosphor) and l_2 for d_1 = 5.8mm and d_2 = 4.8mm are presented in Table 5.6. Parameter Y is the distance of closest approach the beam makes to the compensating deflector plate. This is of value in deciding which dimensions to select in order to maximize sensitivity yet reduce the possibility of beam interception.

l_1(mm)	Def.Sen.(cm/kV)	l_2(mm)	Y(mm)
10	1.35	9.9	0.88
11	1.48	10.92	0.79
12	1.62	11.95	0.7
13	1.75	13.0	0.61
14	1.87	14.0	0.51
15	2.02	15.06	0.42
16	2.16	16.12	0.33
17	2.30	17.18	0.23
18	2.43	18.24	0.14
19	2.56	19.31	0.04

Table 5.6 Dimensions for d_1=5.8mm and d_2=4.4mm

In order to maximize the sensitivity yet retain the compactness of the Picoframe I deflector design l_1 and l_2 were chosen to be 16mm, 16.12mm respectively. The plate widths were again calculated to equalise the deflector capacitance. Sweep and compensation deflector plate widths of 13.3mm and 10.0mm respectively result in a deflector capacitance of 0.32pF, neglecting cross capacitance effects. However, as indicated earlier, this value would probably be limited by connector capacitance effects. The deflection system dimensions for the Picoframe X-II design are illustrated in fig.5.14.

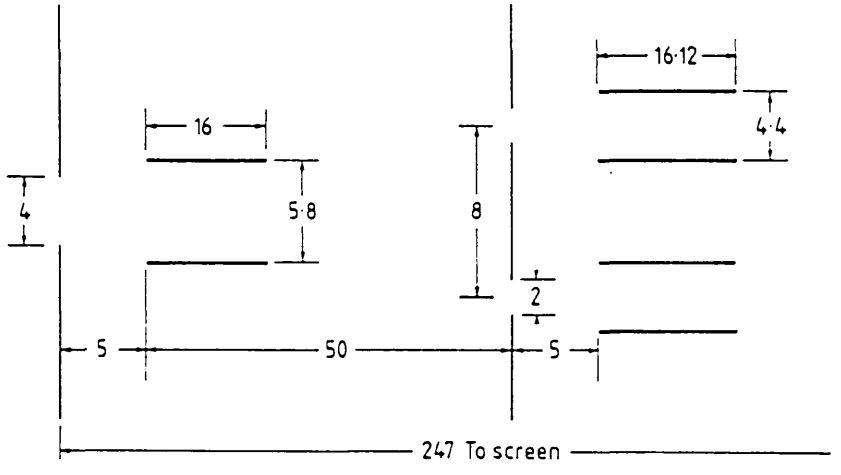

Fig.5.14 Picoframe X-II deflector design (Dims in mm).

The design dimensions of the orthogonally orientated shift deflectors, for provision of multiple framing, need not be modified from the optically sensitive Picoframe design. A set of plates 25mm long, 20mm wide separated by 20mm and positioned 20mm from the end of the compensating deflectors would provide a deflection sensitivity of about 9mm/kV at the phosphor screen.

5.5 Frame exposure duration

Since the sensitivity of the deflectors and the framing aperature diameter have been modified, the exposure durations attainable are now re-evaluated.

5.5.1 Exposure duration in Picoframe X-I design

The deflection sensitivity of the sweep plates at the framing aperture is 4.42mm/kV. Using an avalanche transistor sweep circuit it has been possible to generate voltage gradients of 2×10^{12}V/s (see section 4.3). Thus this design should be capable of 220ps frame exposures when operated in this configuration. The fastest voltage gradients available at present are provided by laser illuminated semiconductor switches (section 3.2). A rate of rise of 3×10^{12}V/s was achieved in the Picoframe I tube with such a device (section 3.4.4). Consequently a frame exposure time of about 150ps, only slightly longer than the 130ps shortest duration achieved with the Picoframe I, should be attainable.

The inter-frame time with this design is dependent upon the width of the triangular voltage waveform. In the voltage pulse-forming arrangement used with the Picoframe I (section 4.5). this was limited to around 2ns (FWHM). However if the waveform has sufficient amplitude and linearity the region of operation

may be shifted towards the apex to reduce the inter-frame time. Recent technological improvements in solid state electronic pulse generators have enabled the reliable production of kilovolt triangular pulses with durations as short as 200ps (FWHM) [37]. Hence inter-frame times of <800ps would be realistic with this type of design.

5.5.2 Exposure duration in Picoframe X-II design

In this design the sensitivity of the sweep plates is 3.9mm/kV at the multiplex aperture plate. When used in conjunction with the avalanche transistor circuit frame exposure times of 260ps are predicted. With the faster voltage ramps available from semiconductor switching devices ($dV/dt = 3x10^{12}V/s$) the frame exposure duration would be around 170ps. The inter-frame time: exposure time ratio is entirely set by the geometry of the design. In this case the ratio is 3:1, dictating an inter-frame time of ~780ps or ~500ps for the two cases cited above.

5.5.3 Discussion - Modified Design

For comparison, the six x-ray photoelectron trajectories studied in through the standard Picoframe I design were re-evaluated through the Picoframe X-I design. The resulting trajectory plots are illustrated in fig.5.15 where again the radial dimension is scaled up by a factor of two for clarity. It is clear that the photoelectrons follow an unimpeded path through the modified design without collision with either deflector assembly. The photoelectron crossover is positioned close to the framing aperture plate permitting the aperture diameter to be minimized for optimally short exposure durations.

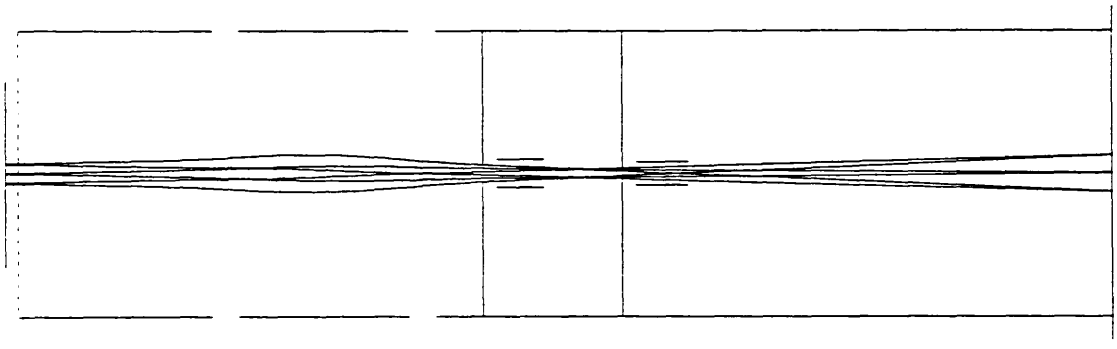

Fig. 5.15 3.0eV electron trajectories in Picoframe X-I

5.6 Conclusions

The large amount of information available in x-ray luminous events in the field of laser induced thermonuclear fusion has made the development of ultrahigh time resolution x-ray sensitive imaging diagnostics a necessity. The Picoframe framing tube design, capable of producing multiple two-dimensional framed images, has been modified to operate more efficiently with the energetic secondary photoelectrons emitted by x-ray photocathodes.

In particular the action of a caesium iodide x-ray photocathode has been modelled. This was adopted because of the relatively low energy spread in its secondary electron emission spectrum. Gold and aluminium are in more common usage as x-ray/VUV photocathode materials but suffer from a relatively large energy spread in their emission spectrum. The effect of this has been demonstrated to cause an increase in radial spread of the photoelectron trajectories through the imaging electron optics. This has the consequence of reducing the effective cathode area as photoelectron trajectories are rapidly obstructed as more

distant off-axis emission points are considered. Despite the design model using caesium iodide, alternative x-ray photocathode materials might prove acceptable if a further reduction in usable cathode area can be tolerated. Due to the obstruction of off-axis electrons some degree of vignetting will be inevitable, with the central portion of an image bright but the periphery less so.

The Picoframe-X has been developed from the Picoframe design by increasing the extraction potential on the combined mesh/first electrode to 10kV constraining the photoelectrons to follow more paraxial paths than they would do in the conventional design. The length of the anode electrode is shortened by 10mm and the distance between the anode aperture and framing aperture reduced from 60mm to 55mm. This has the effect of relocating the crossover position closer to the framing aperture plate, and allows the framing aperture to be only 10% larger than in the standard design despite the increased beam waist diameter. The potential loss in sensitivity of the sweep deflectors by repositioning the framing aperture plane is compensated for by increasing the plate length so permitting the deflection field to act upon the photoelectrons for a longer time. The modified design has a predicted electron-optical magnification of -1.9 and a predicted static spatial resolution of around 50 lp/mm at the photocathode over a usable cathode area of 5mmx5mm.

Two deflection system designs are presented, a single aperture version the Picoframe X-I, and a twin aperture version the Picoframe X-II. The first relies upon shaping the deflection voltage into a triangular form. This configuration, because of its great simplicity, has proved highly successful in the Picoframe I. New fast transistorised pulse generators should enable

framed doublet images of around 100-200ps duration, separated by ~ 500ps to be generated. The Picoframe X-II has a more complex twin aperture, twin compensator configuration but the voltage waveform requirements are reduced to the provision of a simple linear rising ramp for equivalent 'doublet' image formation. Provision of the same speed transistor generated voltage ramps used with the Picoframe I would produce frame duration of 260ps separated by around 700 ps. However, constructional difficulties and cross-coupling effects between the two pairs of compensating deflectors may make this design somewhat more difficult to operate in practice.

Under dynamic conditions the spatial resolution performance of the image becomes degraded due to deflection-distortion effects, space charge, and incorrect matching of the framing and compensating voltage waveforms. It has been shown experimentally with the Picoframe I operated with a voltage ramp of $2x10^{12}$V/s, that a dynamic spatial resolution of ~10 lp/mm is achievable. Similar results are to be expected from the modified Picoframe-X design.

References - Chapter 5

[1] H N Kornblum and V W Slivinsky,
LPAR-77, LLNL, Livermore, CA.,
3-63/3-64 (1977).

[2] L N Koppel and J D Eckels,
LLNL, Livermore, CA.,
UCRL-79781 (1977).

[3] H G Ahlstrom et al,
J. Opt. Soc. Am, 68, 1731 (1978).

[4] L W Coleman,
Proc. 16th ICHSPP, SPIE 491, 51 (1984).

[5] R L Kauffman, G Stradling and H Medecki,
Proc. 15th ICHSPP, SPIE 348, 752 (1982).

[6] A J Cole et al,
Nature (London), 299, 329 (1982).

[7] A J Cole et al,
J Phys. D 15, 1689 (1982).

[8] D L Fehl and J Chang,
Rev. Sci. Instrum. 54(16), 665 (1983).

[9] A K L Dymoke - Bradshaw, J D Kilkenny and J Westlake,
Adv EEP, 64B, 531 (1985).

[10] D T Attwood,
LLNL, Livermore, CA.,
LPAR - 76, pp6-8 to 6-12 (1976).

[11] H Wolter,
Ann. Phys. 10, 94 (1952).

[12] N M Ceglis,
LLNL, Livermore, CA.,
LPAR -78, pp6-30 to 6-36 (1978).

[13] B L Henke, J P Knauer and K Premarante,
J Appl Phys 52(3), 1509 (1981).

[14] N A Soboleva, A G Berkovsky, N D Checnik and R E Eliseev,
'Photoelectronic Devices', Science, Moscow (1965).

[15] G Alma, C Diemer and H Groendijk,
Philips tech. Rev., 14, 336 (1952).

[16] W Clausnitzar and H Heuman,
Z. Angew. Phys., 2, 443 (1950).

[17] M Bowman-Manifold and F H Nicoll,
Nature, 142, 39 (1938).

[18] D C DePackh,
Rev. Sci. Instrum., 18, 798 (1947).

[19] 'Image processing and computer aided design in electron optics' Ed. P W Hawkes,
Academic Press, London (1973).

[20] P W Hawkes,
J Phys. E, 14, 1353 (1981).

[21] M R Alpern
Proc. 9th ICHSP, 207 (1970).

[22] V P Degtyareva et al,
Proc. 14th ICHSPP, 354 (1980).

[23] M R Baggs,
PhD Thesis, University of London (1983).

[24] C V Weber,
'Analogue and digital methods for investigating electron-optical systems',
Philips research reports supplements (1967).

[25] B A Carre,
Comput. J., 4, 73 (1961).

[26] W E Milne,
'Numerical calculus', Princeton University Press,
New Jersey (1949).

[27] C F Gerald,
'Applied numerical analysis', 2nd Edition,
Addison - Wesley (1978).

[28] H Niu, W Sibbett and M R Baggs,
Rev. Sci. Instrum, 53 (5), 563 (1982)

[29] K R Barnes,
'Monographs on applied optics No. 3',
Hilger, London (1971).

[30] J C Richmond,
Adv EEP, 40B, 519 (1976).

[31] V N Platanov,
Proc. 14th ICHSPP, 357 (1980).

[32] W T Welford,
Optica Acta, 18, 401 (1971).

[33] A Rose,
'Vision, human and electronic',
Plenum Press, New York (1974).

[34] O Klemperer and M E Barnett,
'Electron Optics', 3rd Edition,
Cambridge University Press (1971).

[35] P Grivet,
'Electron Optics', 2nd English Edition,
Pergamon Press (1972).

[36] W Sibbett, M R Baggs and H Niu,
Proc 15th ICHSPP, SPIE 348, 267 (1982).

[37] J D Hares,
Private Communication.

CHAPTER 6

Repetitive operation of a Photochron IV-M Streak camera at 300 MHz

6.1 Introduction

The Photochron family of streak tubes; I *, II [2]. IIA [3], III [4]. IV [5] follows the progress in electron-optical streak tube evolution over the past 20 years. Photochron IV, the lastest addition was developed with the aid of computational design techniques [6], as a femtosecond resolution instrument. Finding applications in the direct duration measurement of hypershort mode-locked laser pulses [7], time-resolved spectroscopic studies [8] and plasma kinetics in the picosecond regime [9]. The design features maximized electric fields and axial potentials throughout the overall photocathode to anode region, so optimising the temporal resolution and dynamic range [10,11]. Extensive theoretical studies have been carried out on the design and estimates for the spatial resolution, temporal resolution, temporal distortion and dynamic range for operation at UV/visable/NIR and x-ray wavelengths presented [12].

6.1.2 Description of Photochron IV

The electrode configuration of the Photochron IV streak image tube is shown schematically in Fig.6.1. Six electrodes constitute the re-deflection section including a planar photocathode and mesh arrangement and four coaxial equidiameter lens cylinders.

* The Photochron I streak tube is an adaption of the English Electric Valve Company tube type P856, which is itself a variant of the tube described by Butslov et al [Ref.1]

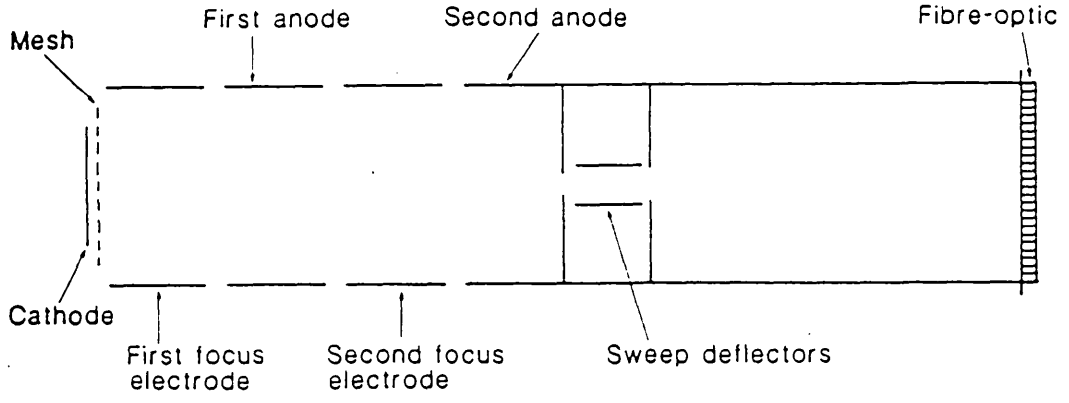

Fig.6.1 Photochron IV electrode configuration

These are designated in sequence from the mesh as the first focus electrode (FFE), first anode (FA), second focus electrode (SFE) and second anode (SA), with assigned potentials (in kV); -18, -8, -10, +6, -13 and 0V respectively. The photocathode to mesh separation is 2mm providing an electric field of 50kV/cm at the photocathode. This ensures the emitted photoelectrons are rapidly accelerated to a high velocity to minimize temporal dispersion but necessitates the interacting 'dual-lens' configuration to focus the 'rigid' electron beam. The electron optical crossover is positioned close to the anode aperture, allowing a closely spaced deflector design arrangement to give a high-fidelity response to fast time varying linear deflection voltages. Additionally the anode aperture diameter may be small so that the detrimental interaction effects of the deflection fringing field with the focusing field may be minimized.

It has been shown [13] that an optimum streak speed of $3x10^{10}$cm/s exists for this tube. Analysis using the Modulation Transfer Function method (section 5.2.3) and assuming an initial photoelectron energy spread of 0.6eV suggests a temporal resolution of about 0.5ps [13]. For illumination of a photocathode at a wavelength just short of the cut-off or threshold wavelength,

where the initial energy spread is around 0.2eV, a limiting temporal resolution of < 300fs is predicted.

6.2 Synchronous operation of a streak camera

Synchronous operation is achieved by locking the phase of the deflection waveform to that of the repetitive luminous event. The deflection waveform is usually sinusoidal where the central half of the peak to peak amplitude is linear to within 5%, and lasts for approximately one sixth of the period. The frequency and amplitude of the applied voltage determines the streak velocity of the photo-electrons at the phosphor screen, and the period over which quasi-linear recordings may be made (1/6th period). The repetition frequency of the deflection waveform may be a sub-harmonic or higher harmonic of the luminous phenomena. In the latter case the time axis is reversed every half cycle so care is required in interpretation of the images.

When the luminous event is produced directly, or indirectly by a synchronously pumped CW laser, where mode-locking is by active modulation of an inter-cavity component, the deflection signal may be derived from the RF modulating oscillator. This configuration was used with a synchroscan Photochron II streak camera where the overall resolution was 13ps, limited by jitter between the argon ion pump laser and the pumped dye laser [14]. Recently a Photochron II repetitively operating streak camera has demonstrated a temporal resolution of 4ps when observing the temporally compressed pulses from a synchronously mode-locked CW Nd: YAG oscillator [15].

When a passively mode-locked CW laser is employed as the luminous source the streak camera deflection waveform must be derived directly from the mode-locked pulse train. This is

generally achieved by directing part of the laser output onto a fast photodiode which provides synchronised trigger pulses for a tunnel diode [16] oscillator biased for monostable operation.

6.2.1 The tunnel diode oscillator

The characteristic curve of the tunnel diode device used is shown in Fig.6.2. When incorporated into an oscillator circuit and biased for monostable operation the device load is selected such that only the stable operating point is at position **A**. An incoming current pulse supplied by the illuminated photodiode will shift the operating point to position **B**, which is on the negative resistance portion to the curve and therefore unstable. The field collapse in a series inductance provides the necessary voltage to rapidly shift the operating point to position **C**, from where it moves down the characteristic curve towards position **D**, as the current decays. At the valley point D, the operating position makes a further rapid transition to position E and then returns to the monostable position **A** to await the next trigger pulse. The relaxation time, and hence the free run frequency of the oscillator, is largly determined by the series inductance and is chosen to be close to that of the trigger frequency.

To increase the streak writing speed for a given amplitude the frequency is usually doubled . This can be achieved by driving a class C amplifier with the fundamental, and then selecting out the second harmonic with a tuned circuit. The Photochron IIA was operated at 164 MHz in conjunction with a passively mode-locked Rhodamine 6G CW colliding pulse dye laser with a cavity frequency of 82 MHz. A temporal resolution of 5ps was reported [17].

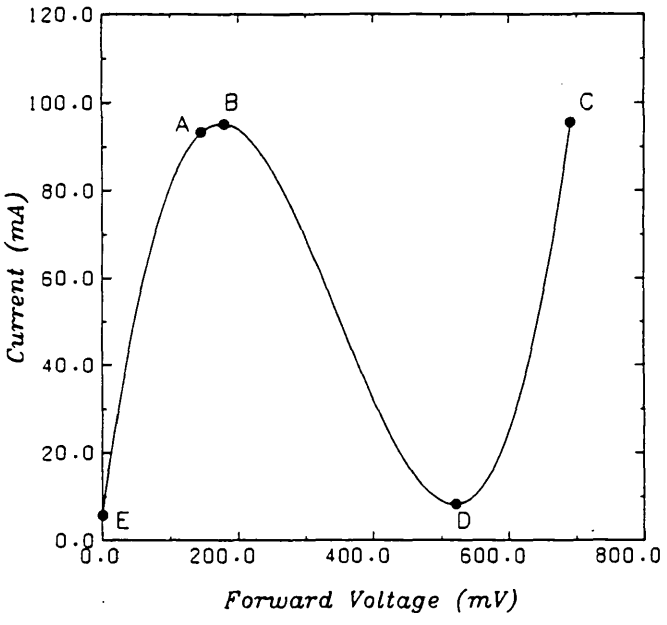

Fig.6.2 Characteristic curve of tunnel diode

6.3 The experimental Photochron IV camera

Two camera configurations have been assembled and evaluated under dynamic conditions. In one case a repetitively operating or 'Synchroscan' mode of operation was investigated. In the other case a single-shot streak mode was operated. The prototype sealed-off tube used in both these configurations had a deliberately modest extraction electric field of 25kV/cm (10kV across 4mm) maintained between an S20 photocathode and copper micromesh electrode (600 cell/cm). The measured electron optical magnification was -2.1 and a static spatial resolution of 33 lp/mm was observed on the P.11 phosphor screen. This corresponds to a spatial resolution of 70 lp/mm at the photocathode.

6.3.1 Photochron IV synchroscan camera

The repetitively operating synchroscan principle was discussed in Chapter 1. It suffices to say here that it relies upon the application of a periodic linear deflection voltage ramp in

synchronism with the incident luminous signals from a repetitive source; such as a mode-locked CW laser. Low intensity streaks, with correspondingly low photocurrents, are superposed millions of times on the phosphor screen thereby accumulating streak images of a recordable intensity level without the need for image intensification. A schematic of the synchroscan Photochron IV camera configuration is shown in Fig.6.3. The input lens operating at a demagnification of x4 imaged a 30μm optical slit onto the photocathode, streak recording was either by film or preferably a lens coupled (x4 mag) optical multichannel analyser with ancillary VDU and chart recorder for hard copy. The laser source was a passively mode-locked CW Rhodamine 6G dye laser operating at a wavelength of 617nm producing pulses of <200fs duration with a periodicity of 83 MHz [18].

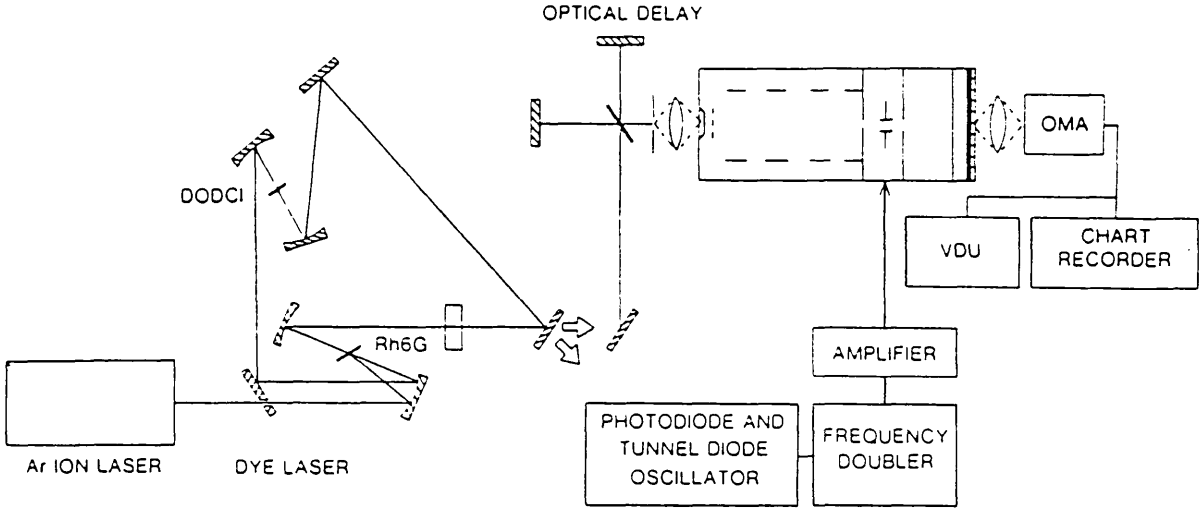

Fig.6.3 Photochron IV repetitive operation configuration

Of the two output beams available from the cavity one was directed with appropriate attenuation via a calibrated optical delay onto the input slit of the camera, the other provided the optical trigger to the photodiode/tunnel-diode oscillator (section 6.7.4). The output from this tunnel-diode oscillator was frequency doubled before being amplified to a power of ~12W. This signal was then inductively coupled into a high-Q circuit incorporating the streak deflectors.

The shortest recorded duration of 1.7ps (FWHM) demonstrated [19] at a streak speed of 6.5×10^9 cm/s is shown in Fig.6.4

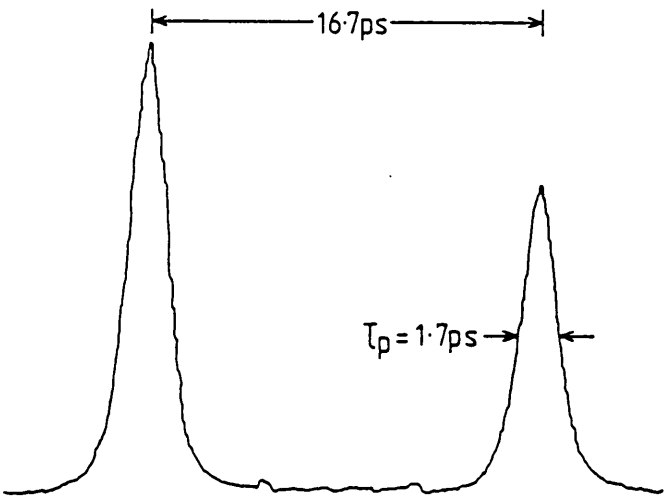

Fig. 6.4 Shortest recorded repetitive operation pulse-width

A computational simulation of the tube performance under the above experiment conditions predicted the camera resolution to be ~1ps. The difference in experimental and theoretical resolution can probably be attributed to trigger jitter arising through slight variations in the amplitude of the laser pulse (see section 6.7.6)

6.3.2 Photochron IV single-shot camera

Due to the detrimental effects of high photocurrents on the spatial and temporal characteristics of this type of camera, it

is necessary to limit the photocurrent by the provision of a high gain intensification stage when operated in the single-shot mode. This may be provided either internally or externally. In this case the provision was external in the form of an inverting, self-focusing microchannel plate intensifier (Philips type 21XX '20/30') having a nominal luminance gain of 10^5, and limiting spatial resolution of 45 lp/mm at its photocathode. This was coupled to the faceplate of the streak tube by a 20mm long fibre optic cylinder. The overall limiting spatial resolution of the camera was measured to be 32 lp/mm at the photocathode of the streak tube, due to the combined MTF [20] characteristics of the imaging components. An input optic operating at a demagnification of x2 imaged a 16μm slit onto the photocathode. Image recording was as described in section 6.3.1.

The high speed deflection voltages for single shot operation were provided by a laser illuminated photoductive element (see section 3.2). Due to the activation energy requirement of about 100μJ the pulses from the passively mode-locked CW ring dye laser were amplified by a four-stage dye amplifier [21] producing pulses of duration 250fs (FWHM), with energies of $\sim$0.4mJ at 10Hz repetition rate. Approximately 90% of the pulse intensity was used to irradiate the GaAs PCE, the remaining light was directed via a calibrated delay line onto the camera slit. Attenuation was provided by neutral density filters in front of the slit.

The best streak result obtained under single-shot conditions is shown in Fig.6.5

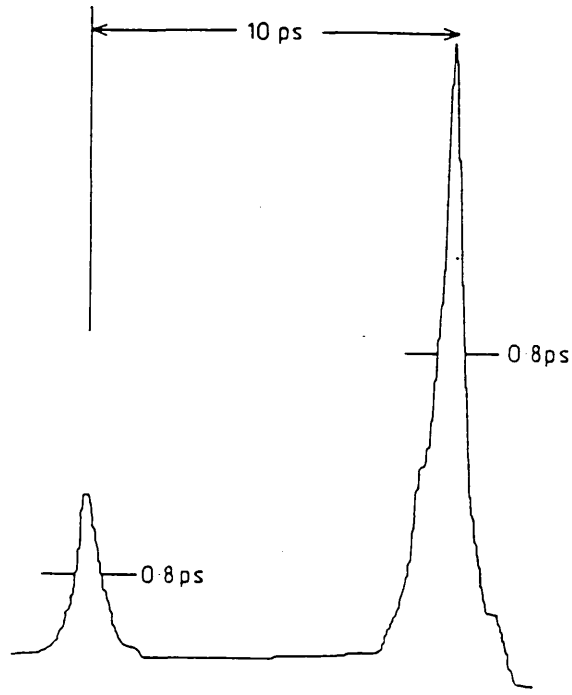

Fig. 6.5 Shortest recorded single-shot pulse-width

With the OMA spatial resolution limit deconvolved, assuming the Gaussian approximation [22,23] a camera instrumental function of ~0.7ps is implied. This is in agreement with theoretically predicted value of 0.7ps for the observed streak velocity of $2x10^{10}$ cm/s [24].

6.4 A Miniaturised Photochron IV (Photochron IV-M)

In circumstances of limited diagnostic volume, such as an evacuated x-ray target chamber, the physical size of the Photochron IV (over 400mm long) might prove restrictive. For this reason a scaled down version was developed [25]. Designated Photochron IV-M, it is essentially a three quarter size version of the standard design.

Applying the standard un-scaled voltages to the miniaturised design resulted in too short a focal length. Repositioning of the paraxial focus approximately 300mm from the photocathode by changing the second focus electrode potential to -12.4kV, so yielding a weaker lens, had the undesirable effect of increasing the field curvature. To reduce the field curvature the first

focus electrode voltage was changed to increase the power of the first of the coupled lenses. This moved the crossover position and focal plane closer to the cathode. However the focal plane could readily be reset to around 300mm by a further slight decrease in the power of the second coupled lens.

Unfortunately this had little effect on the repositioning of the crossover position which remained around z=119mm with the anode plane located at z=154mm. It is desirable to minimize the distance between the crossover and anode plane to allow the use of high sensitivity, closely spaced deflectors. It was discovered that reducing the length of the second anode electrode had little effect on the field curvature and absolute crossover position, but had the effect of reducing the relative separation between crossover and anode aperture as the anode plane was moved closer to the crossover.

The modified Photochron IV-M design consists of four cylinder electrodes of 30mm diameter, the first three 30mm in length with the second anode reduced to 22mm in length. The inter-electrode separation is 8mm and the tube has an overall cathode to phosphor length of 306mm (around 120mm shorter than the standard Photochron IV), with a slightly increased magnification of -2.2. The new electrode potentials (in kV) from the cathode onwards are -18, -8, -10.5, +6, -12.3,0 respectively.

Theoretical evaluation presented in full by Baggs [26] indicates the overall performance of the tubes to be similar with a limiting temporal resolution (cathode illuminated close to threshold of sensitivity) of <200fs for both tubes. The temporal dispersion of the Photochron IV-M is smaller and increases more slowly with slit height. This is due to the reduced cathode-anode distance giving rise to a smaller transit time dispersion.

Temporal distortion (see chapter1) resulting in dynamic slit curvature is more severe in the scaled down design. The electrodes being closer to the axis gives rise to the equipotential lines in the axial region being more curved. This problem can be alleviated by restricting the slit height on the cathode.

The TRL dynamic range of both Photochron IV designs has been evaluated [27] assuming an input pulse duration of 3ps and a camera response of 2ps. The decreased mesh to anode distance and increased confinement of the low potential region in the focusing section of the miniaturised design gives it an enhanced dynamic range of 1700. This compares to the standard design dynamic range of 900 under identical conditions. Space charge effects which are the main cause of limited dynamic range are most prevalent where the electrons are moving slowly. That is in regions of low potential.

6.5 The experimental Photochron IV-M

Two experimental versions of the Photochron IV-M have been constructed (i) a demountable version. (ii) a sealed-off version.

6.5.1 UHV Demountable Photochron IV-M

A demountable version of the Photochron IV-M has been constructed by Philips [28]. This was used in the evaluation of test photocathode materials fabricated in an ultrahigh vacuum (UHV) chamber. The constructional details are illustrated in Fig.6.6

The observed spatial resolution was determined to be in excess of 51 lp/mm at the photocathode, limited by the range of the UV-sensitive test chart. Dynamic evaluation in the synchroscan mode was carried out using test illumination pulses from a synchronously mode-locked Rhodamine B CW dye laser. Output pulses of ~1ps duration [29] were passed through a calibrated optical delay line

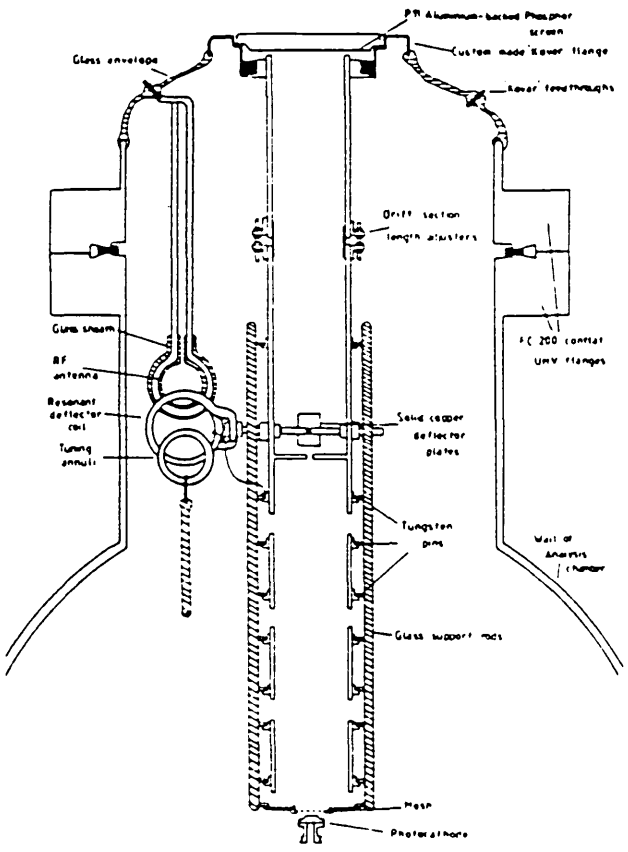

Fig.6.6 Experimental Photochron IV-M demountable streak tube

producing two sub-pulses of 100ps separation and then directed onto a 5μm slit focused at the photocathode. For calibration purposes a synchronously operating sealed-off Photochron II streak camera (resolution $\leq$ 2ps [2]) was similarly illuminated by the subpulses. The RF deflection waveform for both cameras at a frequency of 138.8 MHz was derived from the mode-locked pulse train by frequency doubling the output from a photodiode triggered tunnel diode oscillator. Once amplified and inductively coupled to the deflection plates a streak speed of 1.8×10^9 cm/s was observed at the phosphor of the Photochron IV-M.

The recorded pulse-width was 18ps for both cameras [28]. Due to the proven picosecond resolution of the Photochron II camera the degradation in instrumental function was attributed to jitter arising in the laser, camera or through mutual

interference effects. Thus the achieved resolution is taken to represent only a pessimistic upper limit, with a subpicosecond instrumental resolution achievable under conditions of subpicosecond jitter.

6.5.2 Construction of a sealed-off Photochron IV-M streak tube

Transportation difficulties prohibited the UHV demountable Photochron IV-M undergoing extensive tests on different laser systems. For this reason a sealed-off version was constructed. All the internal components; cylinder electrodes, aperture plates and deflection system were designed and fabricated at Imperial College. The components, once degreased and vacuum stoved, were incorporated into a glass/metal flange envelope by Thorn-EMI, Electron Tubes Division, in a manner similar to that described in section 2.5. Although desirable to utilize fully the compact design features by incorporation into a scaled down glass envelope, component availability dictated the use of standard 76mm diameter glass sections. The tube was vacuum pumped and stoved for 48 hours prior to being activated with an S20 photocathode.

6.5.3 Photochron IV-M static evaluation

The electrode voltages for the Photochron IV-M were derived from a resistive divider chain potted into an insulating rubber compound. Two high voltage power supply units were necessary to provide the maximum positive and negative voltages. When operated at the design specification overall potential difference of 18kV severe glow discharge occurred around the glass-to-metal flanges supporting the SFE and SA electrodes. Light from the discharge illuminating the photocathode introduced a high background noise level on the phosphor screen. Consequently it was necessary to operate the tube at an overall potential difference

of 12kV where no glow discharge was noted.

A Baum [30] projector was used to image a resolution test chart onto the photocathode. The variable voltages on the FFE and SFE were adjusted to achieve maximum undeflected static spatial resolution observed at the screen with the aid of a microscope. A typical set of focus potentials are shown in table 6.1.

Electrode	Cathode	Mesh	FFE	FA	SFE	SA
Voltage(kV)	-12.4	-6.26	-7.0	3.0	-8.34	0.0

Table 6.1 Reduced Photochron IV-M focus potentials.

The static spatial resolution referred to the photocathode was measured to be 60 lp/mm in the **x** direction, and 50 lp/mm in the **y** direction. An electron-optical magnification of -2.0 was measured in **x** and **y**. This is lower than the theoretical value of -2.2 [26] due to the reduced mesh potential (see section 5.3.1)

With the focus potentials unchanged the variation of limiting spatial resolution with screen position was analysed by applying symmetrical deflection voltages $\pm V$ to the deflector plates. The results are illustrated in fig. 6.7 (a), (b) where **x** and **y** are the streak and slit directions respectively.

The asymmetry about the screen centre (displacement = 0mm) position indicates some degree of misalignment in the focusing section. Reasons for this have been discussed in section 2.6. The tube is slightly astigmatic as evidenced by the **y** direction spatial resolution being lower than the **x** direction resolution (the tube was set up for optimum focus in the **x** direction). The faster fall off in resolution with increasing displacement in the **x** direction is probably due to some degree of deflection distortion, as the electrostatic deflection field operates in **x** not **y**.

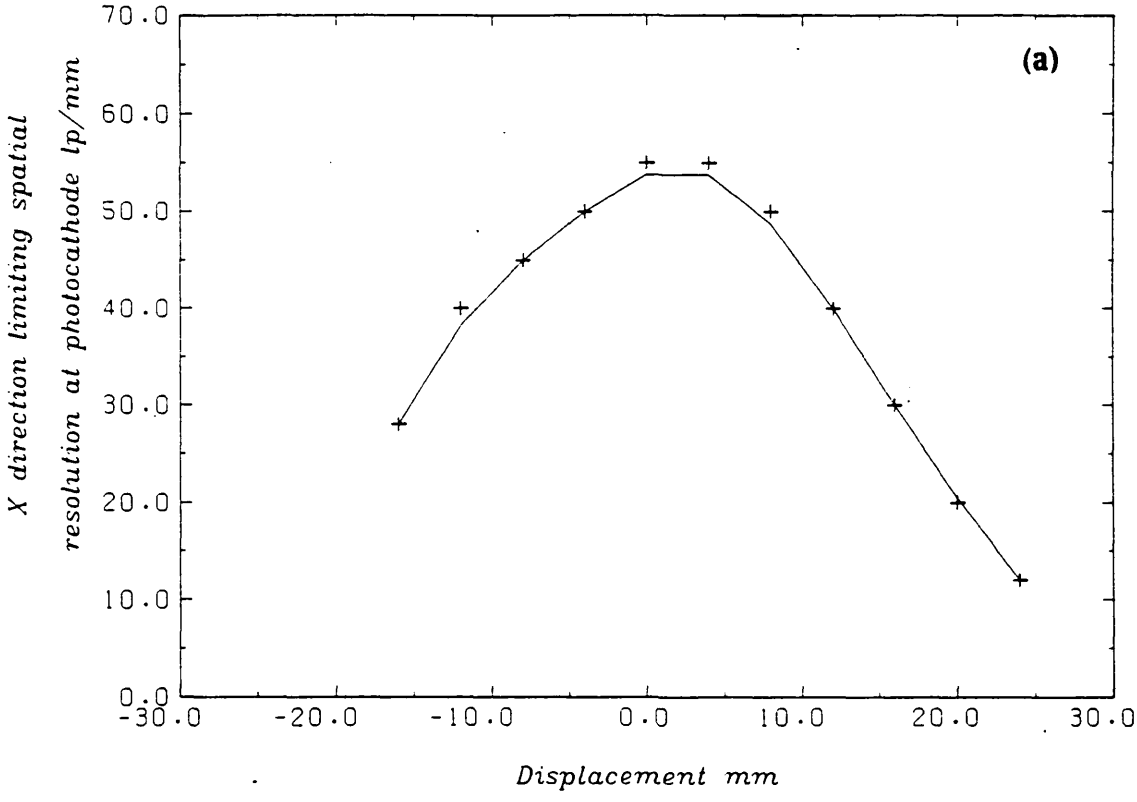

Fig.6.7(a) Static spatial resolution in x-direction as a function of screen position

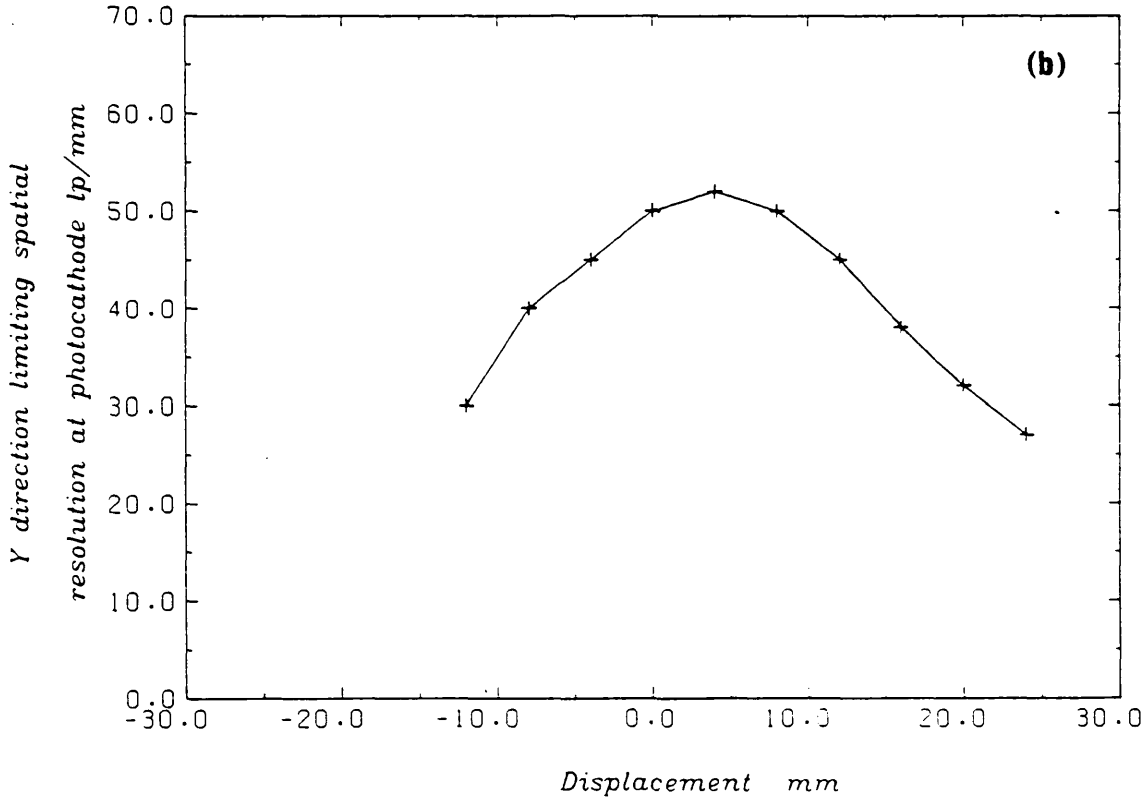

Fig.6.7(b) Static spatial resolution in y-direction as a function of screen position

For a streak camera the important region is the central 20mm of screen, as non-linearity in the deflection waveform restricts the usable time window. Over this region the static spatial resolution is $\geq$ 40 lp/mm referenced at the photocathode.

An advantage of operating the tube under reduced voltage conditions is the increase in sensitivity of the deflection plates. At the operating potentials stated the static deflection sensitivity of the photochron IV-M was measured to be 4cm/kV.

6.6. Theoretical Evaluation

It was realised that due to operating the Photochron IV-M under conditions of reduced electrode potentials, the theoretically predicted resolution of 0.5ps might not be achievable. This is due to increased temporal dispersion of the photoelectrons as they pass through regions of low potential. The time resolution limited dynamic range will also be degraded as detrimental space-charge effects become more important in regions of low potential. For these reasons a realistic assessment of the temporal performance characteristic of the tube was made using the experimental electrode voltages.

The MTF method discussed previously (section 5.2.3) provides a complete characterisation of the performance of a linear imaging system. In work described earlier in this thesis the spatial resolution performance was of prime interest so the spatial MTF was studied. In a streak camera however, one of the two spatial dimensions available for the recording of information is transformed into a temporal dimension. This is achieved by the provision of a slit image which is swept by application of a linear time varying signal. In a similar manner the spatial MTF in the streak direction may be transformed by multiplication of a constant,

the streak speed. The resulting transformed curve is called the Temporal Modulation Transfer Function (TMTF) and may be used to predict the temporal resolution in a similar manner used to predict the spatial resolution with the MTF.

The TMTF curve for the simulated Photochron IV-M was determined by evaluating 1000 electron trajectories through the focusing region modelled using the experimental electrode potentials. Some small adjustment ($\sim$200V) in the second focus potential was necessary to locate the image plane at a position representative of the phosphor screen plane. This discrepancy was probably due to errors in the determination of the electrode potentials using a Brandenburg high voltage meter (model 88M). The electrons were modelled from a cathode slit position (x=0mm, Y=0mm) assuming an initial energy spread of 0.6eV, with a Lambertain cosine Law distribution in radial angle θ and a uniform spread in azimuthal angle φ between 0 and 2π (see section 5.2.5).

Once evaluated for the focusing region the trajectories were calculated through the deflection region modelled onto a two dimensional grid. To facilitate easy calculation one plate was assigned +0.5V and the other -0.5V. Each grid point potential was then evaluated to an accuracy of 10 μV. Trajectories could be calculated through the region under symmetric deflection conditions by multiplying each potential by a scaling factor. This was determined by the rate of change of the applied voltage, and was updated each time step. At the end of the deflection region each trajectory was plotted under field-free conditions to the image plane.

The PSF and LSF could then be evaluated as described in section 5.2.3. Transforming the LSF and multiplying the spatial frequency

axis by the streak speed at the image plane, yields a curve of Modulation against frequency, the TMTF. Limiting resolution, analogous to the spatial frequency case, is defined by the 5% Modulation point. The resulting TMTF curve for the Photochron IV-M under realistic conditions at a streak speed of $5x10^9$cm/s is shown in fig. 6.8. At this speed a limiting temporal resolution of ~1ps is predicted.

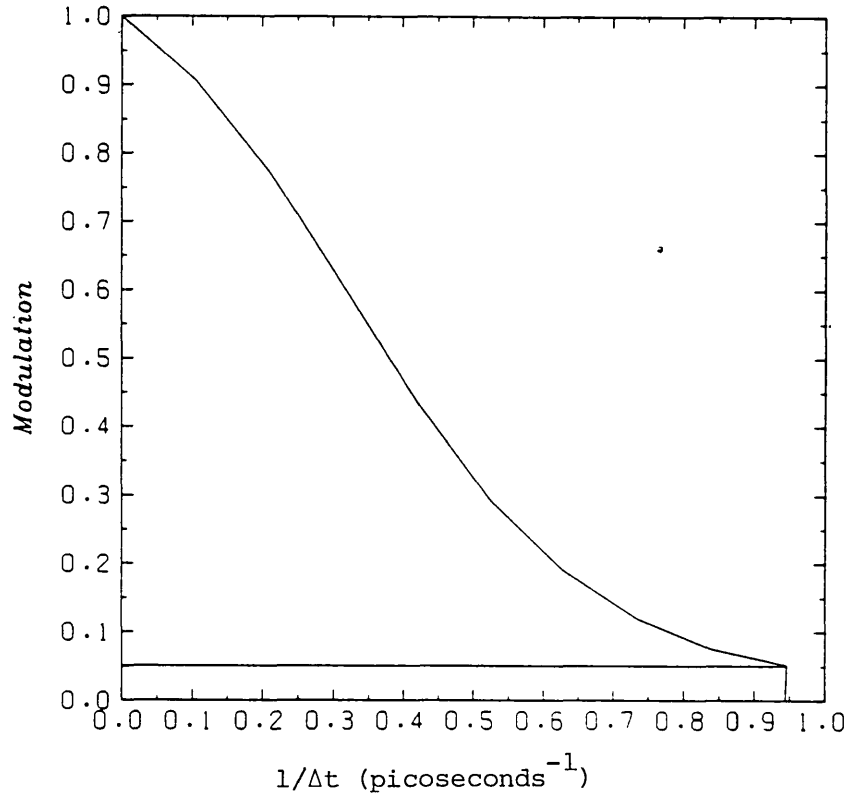

Fig.6.8 Theoretical TMTF curve for experimental Photochron IV-M

6.7. Repetitive operation of an experimental Photochron IV-M at 300 MHz

As stated earlier synchronous repetitive operation may be carried out at a sub or higher harmonic of the luminous event. The advantage of working at higher harmonics is the increase in streak speed for a given amplitude. Because the linear region of the sinusoid is approximately one sixth of the period, this extra streak speed is achieved at the expense of the available time window. For ultrashort optical pulse measurement this is not a major limitation and operation at higher harmonics is advantageous.

If the ouput from the tunnel diode oscillator has the form of a crude square wave it will be rich in odd harmonics, i.e. third, fifth, seventh ... etc. It is thus a simple matter to select out the desired frequency with a tuned filter before amplification and application to the streak camera. This approach was adopted with the Photochron IV-M synchronously operating streak camera where two tuned filters operating at the third harmonic cavity frequency of 300MHz were employed.

It is worth noting here that recent work has demonstrated that the tunnel diode oscillator may be replaced by a laser-illuminated photoconductive element in series with a pulse forming network similar to that used in section 4.4. The round trip time of the stub lines is made short ~50ps; the device then takes the acronym PEPS (Picosecond Electrical Pulse Shaper). Output from the PEPS is a series of electrical pulses at the laser cavity frequency. This signal is again rich in harmonics. One of which may be selected with a tuned filter and amplified. The potential advantage of this scheme is that if sufficient laser energy is available to fully saturate the PCE device, a constant amplitude signal will be derived from the PEPS so eliminating intensity dependent trigger jitter (section 6.7.6)

This scheme was investigated using the optically compressed pulses from a frequency doubled CW mode-locked Nd:YAG laser [31] A Photochron II camera was driven from the amplified 3rd harmonic electrical signal but only demonstrated a relatively poor resolution of 13ps. [32]. This is attributed to insufficient optical second harmonic beam energy to fully saturate the PCE. In principle with intensity dependent trigger jitter minimized, subpicosecond resolution should be obtained if this is matched by

the technical resolution of the camera.

6.7.1 The Ring dye laser

The test illumination source for this work was a colliding pulse, passively mode-locked CW ring dye laser [18] as used in section 6.3.1 in the evaluation of the full size Photochron IV. When used for this work the laser system had been modified to support a cavity length of 3.0m and hence a cavity frequency of 100MHz. The gain medium was a $1.5x10^{-3}$M solution of Rhodamine 6G (Rh6G) and the saturable absorber was $2x10^{-4}$M solution of DODCI (3,3 diethyloxadicarbocyanine iodide) both dissolved in ethylene glycol. Each dye jet was positioned at the focus of a folding section made up of two 100% reflecting, 10cm focal length dielectric mirrors. Two cavity mirrors were 100% reflecting, while the output coupler had a reflectance of 98%. The Rh 6G was pumped by an unmode-locked CW argon ion laser (Spectra Physics Model 170). The DODCI jet was positioned one quarter of the way around the cavity from the gain jet so that the counter-propagating pulses passed through the gain medium a maximum distance apart. This allowed the Rh 6G time to recover adequately between pulses [7]. A tuning wedge was provided in the cavity to constrain laser action to the peak of the absorption wavelength of the DODCI photoisomer, in this case around 617nm for the concentration used. The laser pulse-widths were measured using a SHG autocorrelation technique (see chapter 1) with a 250μm thick ADP crystal. Although pulse durations of <200fs [21] were achieved with the un-modified configuration, the shortest duration pulses achieved while this work was in progress were around 250fs (FWHM) However more generally pulse-widths of around 350fs (FWHM) were recorded. A typical autocorrelation trace is shown in Fig.6.9.

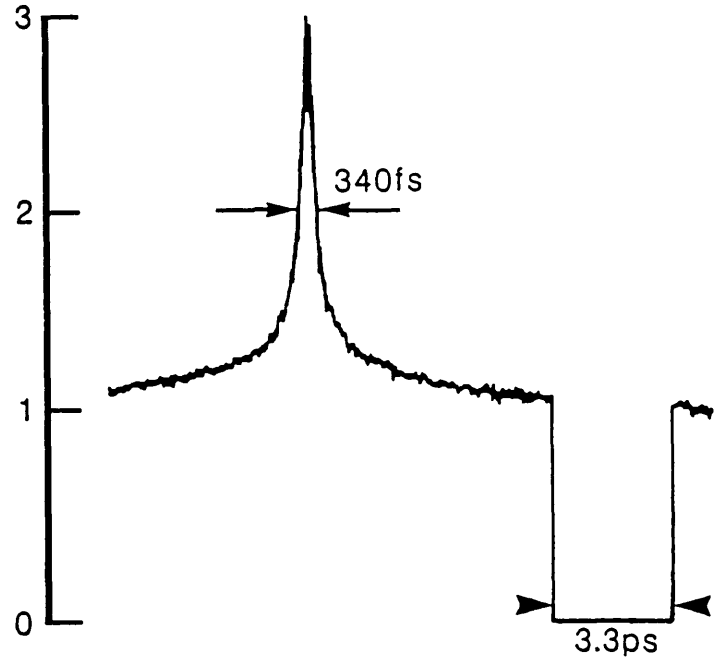

Fig.6.9 Typical autocorrelation pulse measurement

6.7.2 Design of 300MHz filters

Two types of high quality bandpass filters were employed; (i) High-Q cavity resonator, (ii) Interdigital bandpass. The design and construction of these filters are dicussed.

6.7.2.1 High-Q cavity resonator

The bandwidth of this type of filter [33] is very small, but it is ideally suited to this application operating at the fixed third harmonic laser cavity frequency of 300MHz. The filter (shown in Fig.6.10) consists of an inner conductor made of a length approaching a quarter wavelength at the centre frequency of 300MHz, with end capacitance tuning.

The length of the inner conductor was made 0.2m long, a little short of the 0.25m quarter wavelength at 300MHz. The precise diameter at the filter is not critical, but the ratio of the inner conductor OD, and the outer conductor ID determines the characteristic impedance of the line.

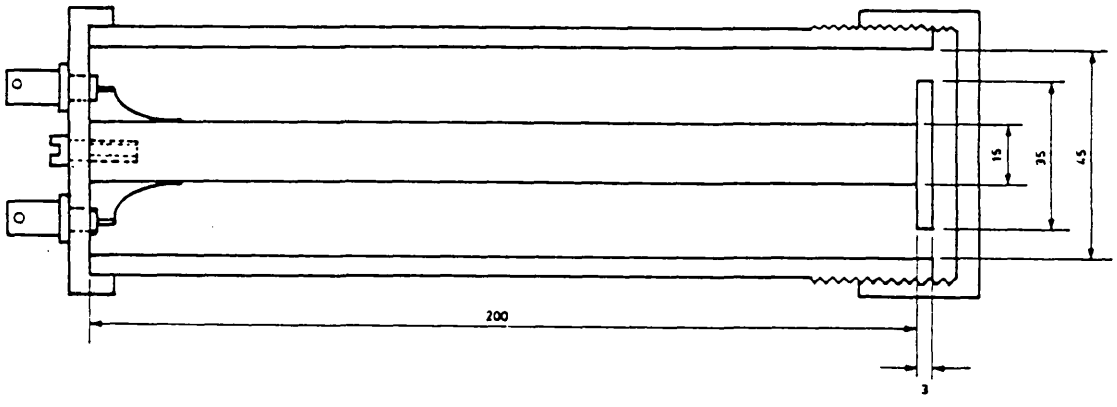

Fig.6.10 Design dimensions of the High-Q cavity resonator (Dimensions in mm)

Other workers have indicated [34] that the lowest loss, highest unloaded Q resonators have a characteristic impedance of around 70Ω. In this case the actual diameter ratio of the conductors was dictated by material availability to be 3:1, resulting in a characteristic impedance of 66Ω.

At resonance the inductive reactance (x_L) is precisely balanced by the capacitative reactance (x_c). To evaluate the capacitance required to tune the slightly short quarter wavelength resonator to resonance at 300MHz the inductive reactance at the open end of the line was determined to be $x_L = j203.3$ using a Smiths' chart [35]. Hence the capacitance required for resonance at a frequency f is given equation 6.1

$$C = \frac{1}{2\pi f x_c} \qquad \text{equ.6.1}$$

Inserting the calculated values into the above equation yields a capacitance of 2.6pF. This is provided by the adjustable parallel plate capacitor at the end of the resonator, which is used for

final tuning. Input and output coupling is made by wire loops adjusted for optimum matching efficiency, by minimizing the reflected standing wave ratio when terminated with a 50Ω resistive load.

The filter was made of brass with silver solder around the component joints and silver plated for optimal performance. The response function of the filter is shown in Fig.6.11, it has a -3dB bandwidth of 2.4MHz and a particularly high Q value of 125. A 1dB attenuation is exhibited at 300MHz.

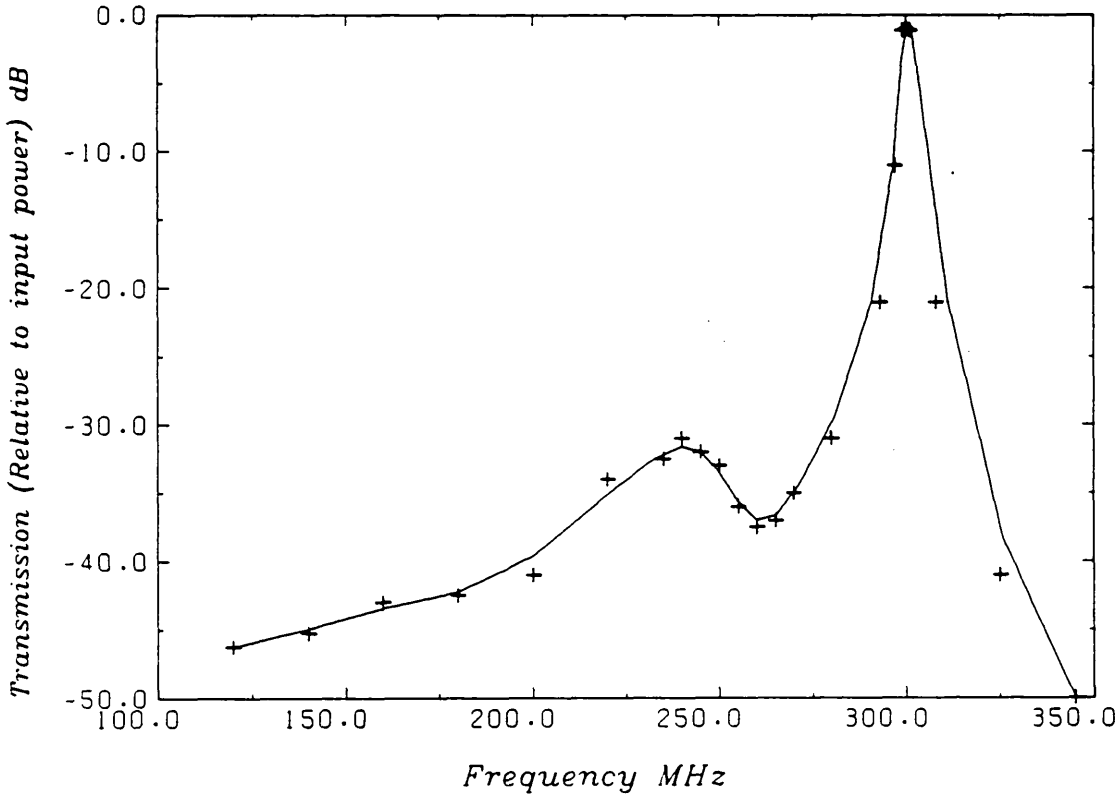

Fig.6.11 Response function of High-Q cavity resonator

6.7.2.2 300MHz Interdigital bandpass filter

In order to remove any unwanted harmonic leakage from the first filter and attenuate any harmonic distortion in the preamplifier stages a second 300MHz bandpass filter was employed. An interdigital bandpass filter was adopted. This has the advantage of flatter passbands, steeper skirts and better attenuation in the stopband than the previously described filter. This type

of filter is generally difficult to design but an analysis by Dishal [36] led to a simplified design precedure [37] under certain conditions (i.e. limited bandwith). The design procedure is still somewhat complex and covered in great detail in Ref.37. The filter is basically composed of a series of approximately quarter wavelength 'resonators', alternately mounted on opposite sides of a fully enclosed box, like interlinking fingers of opposite hands (hence name 'interdigital'). The number of resonators determines the shape factor (the more resonators the steeper the skirts) and commonly ranges from 2 to 4.

The basic steps in Dishal's algorithm are to first choose the centre frequency and -3dB frequencies, thus defining the fractional bandwidth w as;

$$w = (\text{-3dB bandwidth})/(\text{centre frequency}).$$

Then select the required stopband performance (i.e. the frequency bandwidth at 40dB attenuation). This determines the number of resonators required. Look up the coupling and Q-factors of each resonator, (supplied in Dishals' procedure) and adopt a specific rod diameter d and box height h. These should be in the approximate ratio 1:2; in the design used d = 9.7mm and h = 19.5mm. The inter-rod spacing is then calculated. Each rod length is 0.95 of the quarter wavelength at the central frequency, with fine tuning provided by trimmer capacitance formed by the variable gap at the end of each rod (in a similar manner to that described for the cylinder filter previously). Finally the input and output tapping point positions are calculated to provide matched 50Ω impedances.

This procedure was followed and the filter (Fig.6.12) constructed in brass. Again all metal joints were soldered to ensure good connections. To minimize insertion loss the top and bottom surfaces of the box were securely screwed to the body. The filter

was designed to have a -3dB bandwidth of 10MHz and a stopband (-40dB) bandwidth of 25MHz. A response curve for the filter is shown in Fig.6.13; the -3dB bandwidth is 11MHz yielding a Q-factor of around 27. The transmission at 300MHz is -1dB

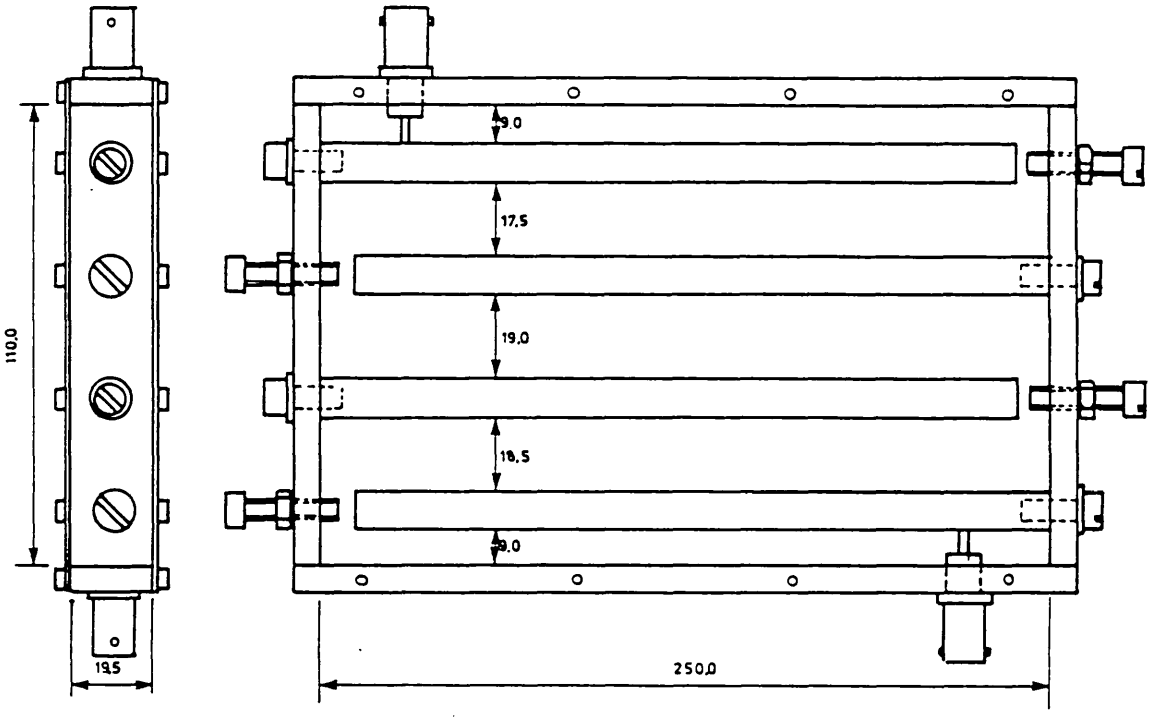

Fig.6.12 300MHz Interdigital filter (Dimensions in mm)

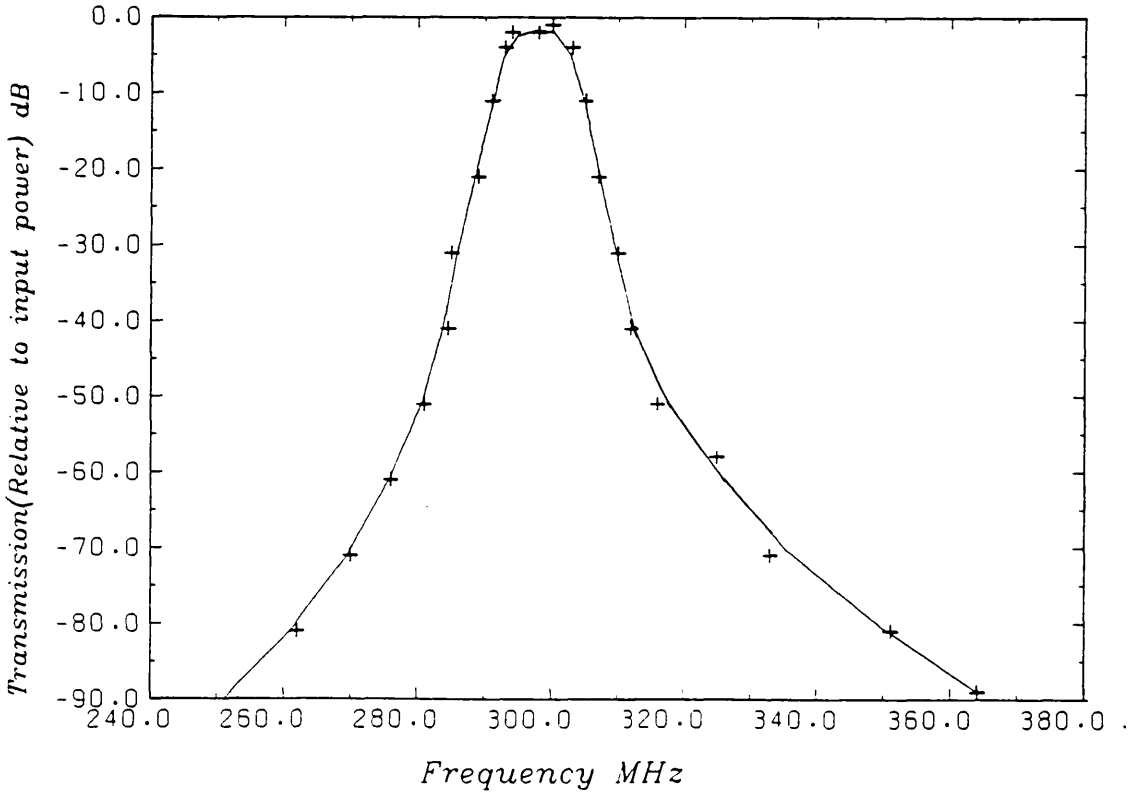

Fig.6.13 Frequency response of the 300MHz interdigital filter

The effect of the two filters can be seen from the oscillogram presented in Fig.6.14. The upper trace shows the output directly from the tunnel diode oscillator, the lower trace shows the filtered 300MHz signal.

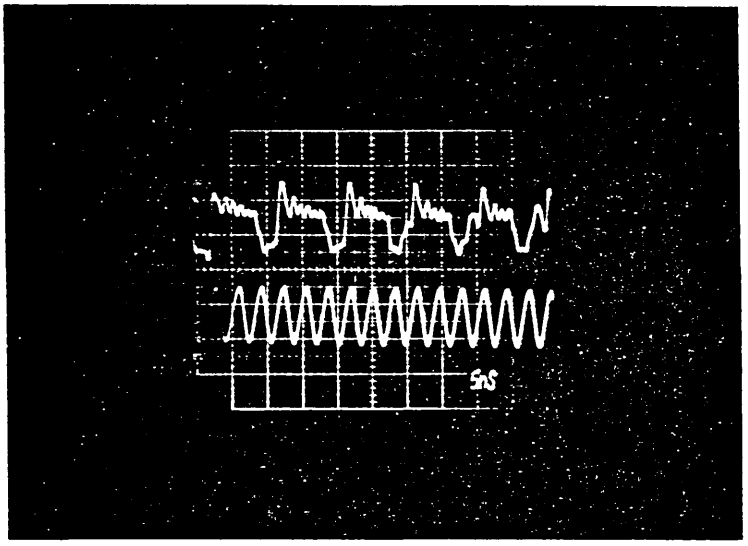

Fig. 6.14 Unfiltered and filtered tunnel diode output. Upper trace 200 mV/major div, lower trace 20mV/major div.

6.7.3 Experimental configuration

The experimental arrangement for synchronous repetitive operation of the Photochron IV-M Streak camera is shown in Fig. 6.15. The tunnel diode employed in the oscillator circuit was a General Electric TD266A, which has a peak current ability $I_p \simeq 100mA$ and a risetime $T_r \simeq 22ps$. This was connected in close proximity to a fast p-i-n photodiode (AEG - Telefunken BPW28) via an etched 50Ω stripline. When illuminated by the dye laser pulse train the photodiode produced a train of electrical pulses of ~250ps (FWHM) duration at a repetition rate of 100MHz with a peak amplitude of approximately 400mV.

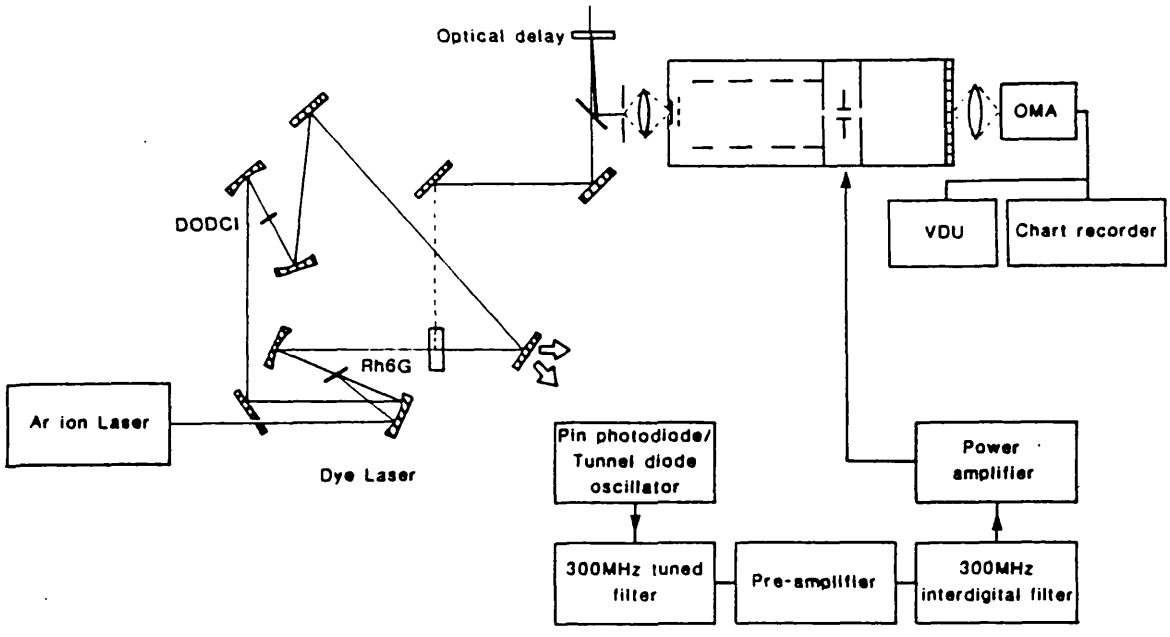

Fig.6.15 Experimental lay-out of Photochron IV-M synchronously operating streak camera and passively mode-locked CW ring dye laser.

The oscillator circuit used (Fig.6.16) had a variable 0-25V power supply for convenient biasing of the tunnel diode to the mono-stable operating **A** (see section 6.2.1). The output waveform was a heavily distorted 100MHz sine wave with an average power of $\sim$ 0.3mW (into 50Ω load).

The cylindrical 300MHz filter was connected directly to the tunnel diode oscillator which gave a $\sim$ 40mV ppV third harmonic signal, approximately 8μW into a 50Ω load. This was then amplified to around 400mW by two TRW* CA2820 wide band linear hybrid amplifiers, operating in tandem. Each amplifier had a gain of 30dB with a bandwidth of 1-520MHz.

* TRW RF Semiconductors, 14520 Aviation Blvd., Lawndale CA902 USA

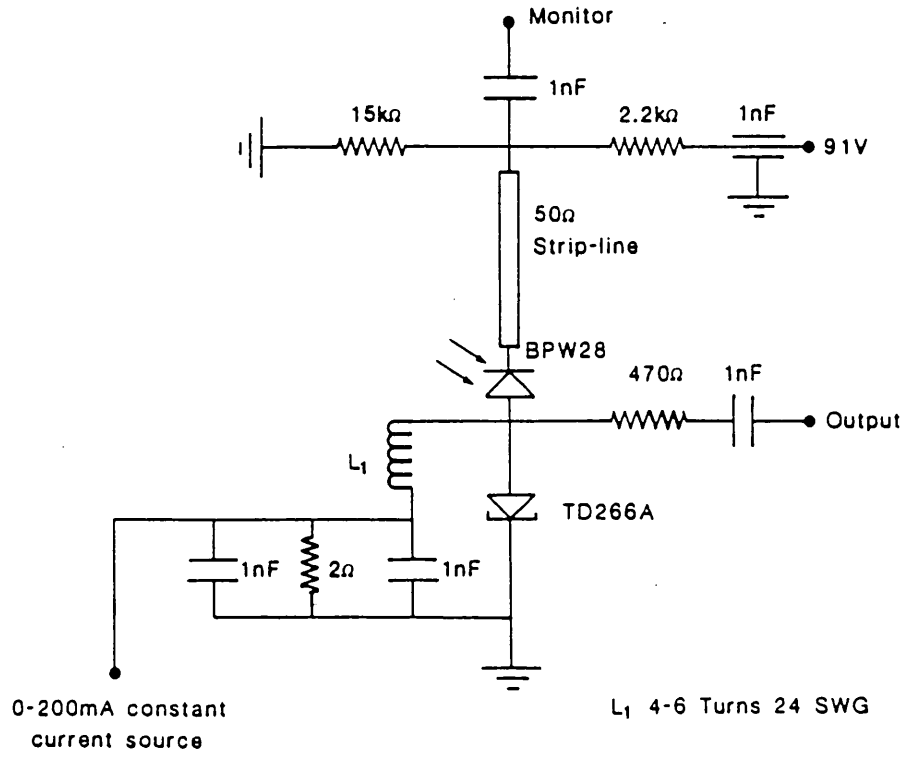

Fig.6.16 Tunnel diode oscillator circuit

Any necessary signal attenuation was provided by 50Ω in-line attenuators inserted at the amplifier inputs. The bandpass 300MHz interdigital filter was inserted between the preamplifiers and the power amplifier to reduce any second harmonic distortion. The power amplifier was a Microwave Modules Ltd. MML432/100, Linear power amplifier modified to operate at 300MHz with a minimum power gain of 20dB providing up to 40W RF power. Generally it was operated in the 10-30W range by insertion of suitable attenuation in the preamplifier stages.

The RF signal was coupled into the deflection plates using a high-Q network illustrated in Fig.6.17. Each arm, of approximately one eighth wavelength, was made from 1.5mm diameter tinned copper wire formed into a rectangular structure of approximate dimensions 14cm x 2cm. One loop was driven by a closely coupled 25mm diameter aerial coil connected to the power amplifier. The plate capacitance was then situated in a balanced circuit between the driven and 'ideller' inductance loops.

The inductance of a single turn loop is given by equation 6.2 [38].

$$L = \mu_o a \left[\ln\left(\frac{8a}{b}\right) - \frac{7}{4} \right] \qquad \text{equ.6.2}$$

where a is the radius of the loop and b the radius of the conductor. Thus for the values used (average radius a = 5cm, b = 0.75mm) the inductance of a single loop is 2.85×10^{-7} H. The resonant frequency of a LC circuit is given by equation 6.3.

$$f = \frac{1}{2\pi\sqrt{LC}} \qquad \text{equ.6.3}$$

Inserting the calculated total inductance of 1.42×10^{-7} H for both loops, resonance of 300MHz requires a capacitance of ~2pF. This is provided by the deflection plate capacitance (~ 1pF) and the stray capacitance of the feed-throughs and connectors. The deflection network was earthed for DC purposes via a 10kΩ RF isolation resistor at the nodal point.

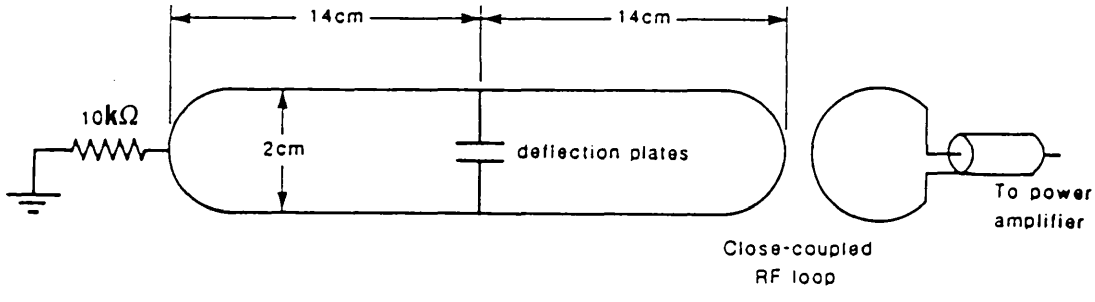

Fig. 6.17 High Q deflection circuit

The streak tube was fully enclosed in an aluminium alloy case with a BNC socket connection for provision of the RF power, and flying leads for the HT connections.

The phosphor screen, drift region and anode were electrically common to the chassis at earth potential; the cathode being operated at -12.4kV. Effective RF screening was provided between the focusing and deflection sections of the tube by incorporation of a double sided copper laminate board. A hole large enough to allow the tube to pass through was cut into the board, which was then positioned at the anode aperture plane completely dividing the aluminium enclosure. Good electrical contact was ensured between the chassis, screening laminate board and anode electrode.

6.7.4 Multipactor discharge

When RF power exceeding ~2W was applied to the tube a glow discharge was observed around the deflection region, resulting in the screen being saturated with light due to cathode illumination by the discharge. This effect known as multipactor discharge has been noted in earlier work and by other workers [39,40].

It is postulated that stray low energy electrons between the deflection plates are accelerated towards the deflection plates by the RF field. At high enough powers they collide with the deflection plates generating secondary electrons. The effect builds up as more and more secondaries are produced by continued electron bombardment. Eventually a sufficient electron flux is built up to ionise stray gas molecules and alkali metal contaminants (due to photocathode activation)from the deflector plate surfaces. The resulting luminescence illuminates the photocathode and swamps any signal under investigation. Additionally the ionization can degrade the photocathode, reducing the life of the tube.

It has been shown [40] that with careful fabrication

techniques alkali metal vapour contamination of the deflector surfaces can be minimized, and the discharge eliminated. Unfortunately these techniques cannot be readily applied to the Photochron IV and a certain degree of contamination of electrode surfaces is probable.

A small electric field in the deflection region, acting parallel to the tube axis so extracting the stray electrons, can eliminate the discharge without noticeable influence on the high energy electrons [41]. The procedure was adopted in the Photochron IV-M, with the anode held at +200V with respect to the zero potential drift region and phosphor screen. This tended to make the image astigmatic but with careful refocusing a static spatial resolution of 50 lp/mm (referred to the photocathode) could still be achieved in the streak direction at the expense of the slit direction. The DC connection between the laminate screening board was replaced by three 1nF (1kV) ceramic capacitors to provide an RF path.

6.7.5 Evaluation of temporal resolution

The input slit (30 μm x 3mm) was coupled onto the photocathode with a 50mm f/2.8 lens arranged to provide a demagnification of x2. Similarly a lens operating at a x 1.3 magnification coupled the streaked image onto an Optical Multi-channel analyser (OMA). The OMA employed was a B & M Spectronik OSA 500 vidicon with WP1 and WP2 data processing and display units. Up to thirty 500 channel memories were available on the WP2 microprocessor - contolled terminal which incorporated data processing capabilities. The OSA head employed a silicon intensified target 12.5mm long by 10mm high composed of 500 diodes separated by 25 μm. Read out

time was variable between 10-80ms but it was generally set to the default value of 32ms. Real-time read out of the target image was available on a cathode ray tube VDU, with hard copy of memory contents available via chart recorder or XY plotter.

Leakage light from the cavity tuning wedge was directed onto a 3.45mm thick disc of Spec. B fused quartz (n =1.457). The quasi-normal front and back reflections provided two calibrated sub-pulses temporally separated by 33.5ps for calibration purposes. These sub-pulses were steered onto the camera slit, suitably attenuated with neutral density filters as necessary. Under static conditions the OMA recorded a slit width of 6 channels. Applying 15W of RF power and optimising the synchronisation by adjustment of the cable delay between the pre-amplifier and power amplifier stages for maximum streak separation, demonstrated a temporal resolution of 3ps (Fig.6.18) The dynamic streak separation was 78 channels with a dynamic slit width of 7 channels; a small increase of 1 channel over the static slit width. In an effort to reduce the static contribution to the streak width the input lens demagnification was increased to 3:1, and with careful refocusing a static slit width of 4 channels was obtained.

At an increased RF power of 18W the dynamic slit width had increased to 7 channels with a streak separation of 87 channels demonstrating a temporal resolution of 2.7ps (Fig.6.19) at a streak speed of 5×10^9cm/s. Increasing the streak speed to 6.4×10^9cm/s by increasing the RF power to 30W provided a slit width of 9 channels and streak separation of 111 channels, with a corresponding temporal resolution of 2.7ps again. This would imply that the camera resolution is not set by the intrinsic

limiting temporal resolution of the tube as this has been shown to vary with streak speed [13].

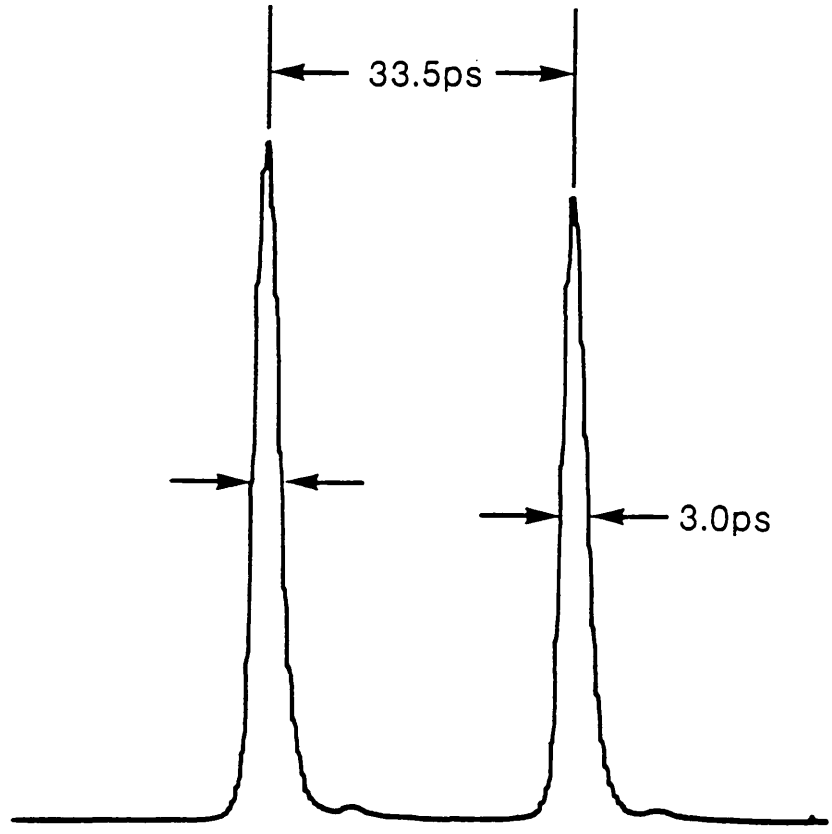

Fig. 6.18 Synchronous streak record with a static slit width of 6 channels

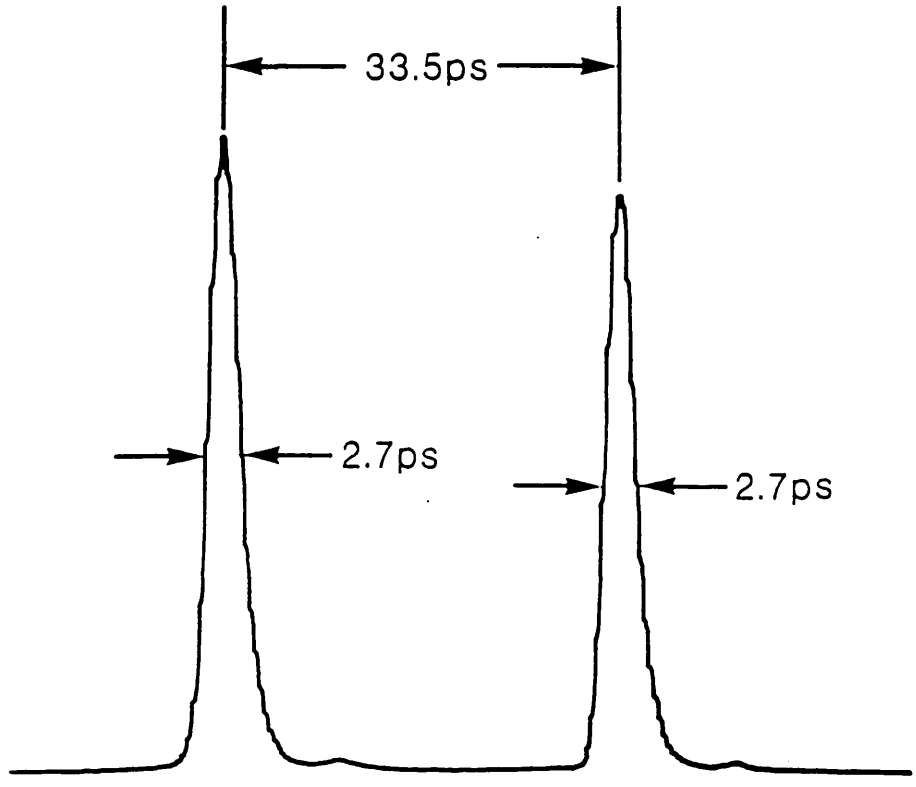

Fig. 6.19 Synchronous streak record with a static slit width of 4 channels

6.7.6 Intensity dependent trigger jitter

The degradation in temporal resolution was, at least in part, attributed to jitter due to the fluctuating laser output. Monitoring the p-i-n photodiode output with an oscilloscope on a millisecond timescale revealed a periodic amplitude fluctuation in laser intensity, showing ~10% modulation (Fig.6.20).

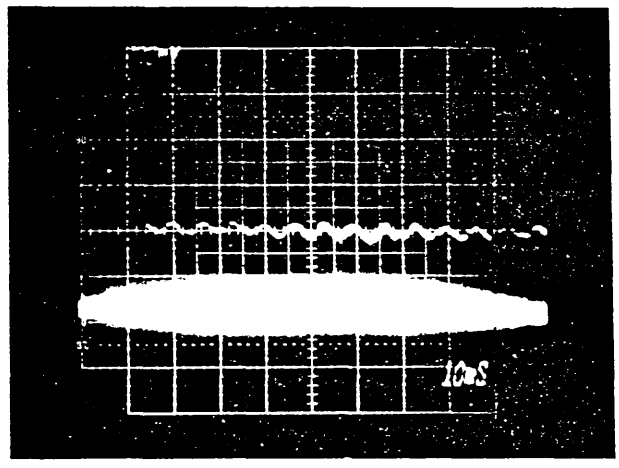

Fig. 6.20 Fluctuating laser intensity on a millisecond timescale

This was traced to be three phase mains ripple leakage to the pump beam through inadequate smoothing of the argon ion power supply. The resulting time error in triggering (jitter) the tunnel diode oscillator will degrade the temporal resolution of the instrument.

To quantify this jitter it may be assumed that the mode-locked laser emits pulses of constant repetition rate but fluctuating intensity. The photodiode then produces pulses of risetime T_r, which trigger the tunnel diode at a voltage level V_t. Electrical pulses from the photodiode are assumed to have a linear rising edge and a peak voltage amplitude given by the product of the photodiode sensitivity S and the laser pulse intensity I. A laser pulse of intensity I incident on the photodiode at time

t=0 would trigger the tunnel diode at time t_1, given by equation 6.4 [42],

$$t_1 = D + \frac{V_+ T_r}{SI} \qquad \text{equ.6.4}$$

where D is the delay of the signal in the cables. If the illumination is fluctuating in intensity by (1-F) I, where F is the fractional deviation from average intensity, the trigger time would be;

$$t_2 = D + \frac{V_+ T_r}{SI} \qquad \text{equ.6.5}$$

the intensity dependent trigger jitter Δt is then given by the difference between equ.6.4 and equ.6.5,

$$\Delta T = t_2 - t_1 = \frac{F V_+ T_r}{(1-F)SI} \qquad \text{equ.6.6}$$

this is illustrated in Fig. 6.21. For the BPW28 photodiode the product SI is $\sim$400mV and the risetime T_r $\sim$ 200ps. Assuming a tunnel diode trigger level V_+ of $\sim$20mV this gives an intensity dependent trigger jitter of $\sim$1ps.

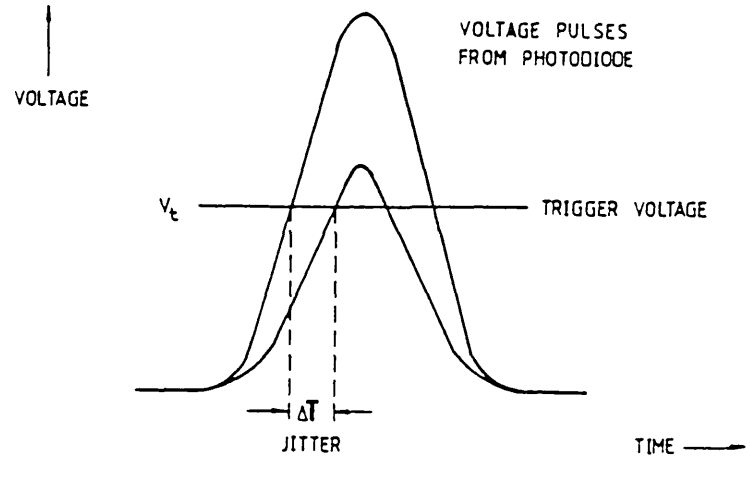

Fig.6.21 Intensity dependent trigger jitter

6.7.7 Results

To minimize the effects of the intensity modulation of the laser beam a mechanical shutter was introduced in front of the camera, with the purpose of selecting out a portion of the pulse train over which the intensity did not fluctuate appreciably. Although desirable to use a shutter speed of 1/1000th second the leakage light from the tuning wedge was not of sufficient intensity to achieve a high enough signal to noise ratio to make satisfactory recordings at this speed. Thus in practice a shutter speed of 1/500th second was employed. The shutter provided a +5V trigger pulse to activate the OMA to readout the image on the vidicon. The vidicon was scanned up to four times to improve the signal to noise ratio by taking advantage of the phosphor screen decay time. [43]

With this arrangement an improved temporal resolution of 2.3ps (Fig.6.22) was achieved at a streak speed of 5×10^9cm/s with 20W of RF power. The static slit width was 4 channels with a streak separation of 95 channels giving a technical time resolution of 1.4ps. Again operation at different streak speeds failed to provide any further improvement in temporal resolution.

6.8 Discussion

The static slit width is close to the spatial resolution limit of the vidicon, which is limited by charge leakage between adjacent channels. In order to take full advantage of the high spatial resolution of the Photochron IV design it would be necessary to increase the magnification onto the vidicon target. Unfortunately before the opportunity arose to do this a serious fault in the argon ion pump laser prohibited further investigation.

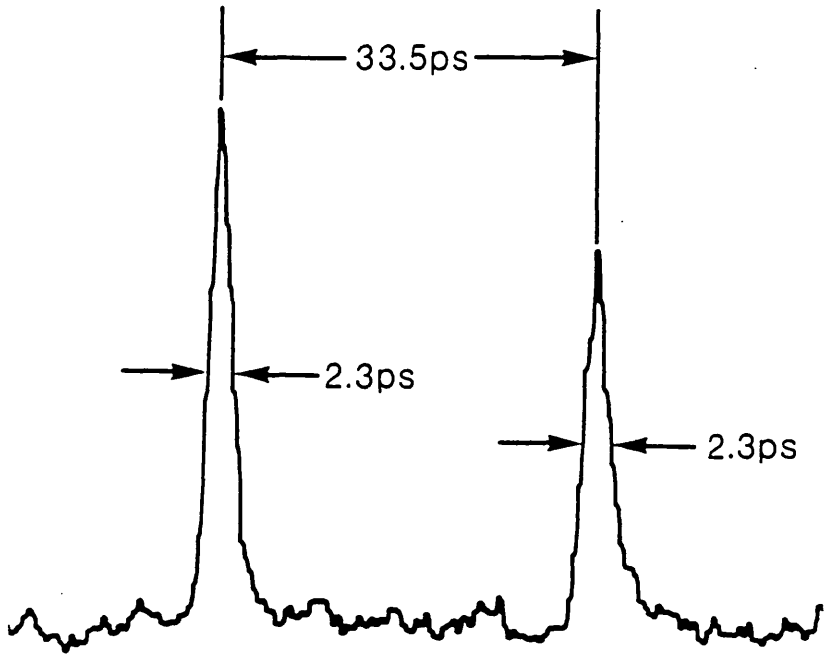

Fig. 6.22 Best recorded synchronous streak record shuttering for 1/500th second

The limitations imposed upon the Photochron IV-M streak camera are two fold: intensity dependent trigger jitter and vidicon spatial resolution. The first may be remedied by improving the laser stability, which may be difficult, or by operating the mechanical shutter at a faster speed. Shorter duration shutter periods would require more efficient use of the available laser intensity. This might be achieved by replacing the quartz blank optical calibrator (4% efficient) with a Michelson type arrangement (25% efficient).

The second limitation may be overcome by increasing the magnification onto the vidicon target. Up to x4 magnification has been used in previous work. The viewable screen size is correspondingly reduced to ~3mm and this can present a problem during the set up procedure. Particularly at high RF powers where

resistive heating of the deflection circuit causes the loop resistance to change. This results in the streak image drifting across the screen and out of the vidicon field of view. Perhaps the best hope for the future is a technological improvement in the spatial resolution limit of readout devices to match the high spatial resolution now being obtained with state-of-the-art streak image tubes.

6.9 Conclusions

Direct and indirect hypershort pulse generation techniques have enabled pulse durations of less than 30fs to be produced (see chapter 1 and Refs. therein). The ability to generate these pulses of only a few optical cycles has far exceeded the ability to apply linear measurement techniques to them. The development of a femtosecond resolution streak tube would enable direct linear time-domain studies in the femtosecond region for the first time. The Photochron IV image tube has been designed to meet this increasingly pressing requirement. By maximizing electric fields and maintaining high axial potentials throughout the imaging region, photoelectron transit time dispersion has been minimized providing a theoretical limiting temporal resolution ~200fs when the photocathode is illuminated close to threshold. The predicted temporal resolution when operated in a more practical regime (not at the cathode threshold) is ~0.5ps. A sub specification Photochron IV with modest photocathode extraction field of 50% the design value, has been constructed and demonstrated to have a deconvolved instrumental function of 0.7ps when operated in the single shot mode. When operated in the repetitive mode, where the deflection waveform is synchronised to the repetitive luminous event, a temporal resolution of 1.7ps has been demonstrated, limited by intensity

dependent trigger jitter.

In certain situations such as limited space the physical size of the Photochron IV might prove preclusive, so a three quarter size scaled down version Photochron IV-M has been developed. It was found necessary to modify the focus potentials and reduce the second anode electrode length in order to achieve an optimal focus plane with acceptable field curvature, and anode aperture situated close to the electron-optical crossover position. Theoretical studies suggested the temporal resolution to be similar to the standard size tube. The electron temporal dispersion is decreased due to the reduced cathode-anode distance, and the TRL dynamic range enhanced due to the increased confinement of low potential regions.

Two experimental versions of the Photochron IV-M have been constructed. A UHV demountable version was operated in a repetitive mode at a frequency of 138.8MHz in conjunction with a synchronously mode-locked Rhodamine B laser. A temporal resolution of 18ps was demonstrated, limited by jitter between the pump and dye laser pulses. A more versatile 'sealed-off' version of the tube has been fabricated and activated with an S20 photocathode. Glow discharge on the glass envelope around the high potential difference region between SFE and SA, prohibited the tube being run at the full specification potentials. When optimally focused the tube had a static spatial resolution of 60 lp/mm in the x-direction (streak) and 50 lp/mm in the y-direction (slit), as referred to the photocathode. The electron-optical magnification was -2.2 and the deflectors demonstrated a static deflection sensitivity of 4 cm/kV.

Evaluation of the instrumental resolution of the Photochron

IV-M streak camera system was carried out using a colliding pulse, passively mode-locked CW ring dye laser producing pulses of ~350fs (FWHM) duration at a frequency of 100 MHz.
To eliminate the use of a frequency conversion circuit the sinusiodal deflection waveform required for repetitive operation of the camera was derived directly from a laser pulse triggered tunnel diode oscillator. The third harmonic signal was selected using two series 300 MHz tuned filters. The filtered signal was amplified to a power ~20W and applied to a closely coupled high-Q deflection circuit incorporating the sweep plates. A temporal resolution of 2.7ps was obtained at streak speeds of 5×10^9 cm/s and 6.4×10^9 cm/s, demonstrating that this did not represent the limiting temporal resolution of the tube design.

A theoretical analysis of the tube under the experimental conditions imposed, indicated an instrumental function of ~1ps. The discrepancy between achieved and predicted temporal resolution was attributed in part to intensity dependent trigger jitter. Fluctuating laser intensity causes the tunnel diode to trigger with a time error of about 1ps. This fluctuating intensity was traced to the three phase mains ripple from the argon ion laser power supply. It was possible to reduce the effect of this ripple by use of a mechanical shutter set to 1/500th second, so limiting the amount of intensity variation experienced by the camera. Using this scheme the temporal resolution was increased to 2.3ps at a streak speed of 5×10^9 cm/s. Limiting the exposure to 1/500th second still represented the accumulation of 2×10^5 pulses retaining the repetitive operation principle. A further limitation was imposed by the spatial resolution of the vidicon target, caused by charge leakage between adjacent channels.
A reduction in the static slit width contribution to the dynamic

width could have been achieved by increasing the magnification onto the vidicon.

The Photochron IV design has been developed to provide a high spatial resolution at the screen. To fully utilize this feature requires a similar capability in the associated readout device. A dynamic spatial resolution of 20 lp/mm at the screen would require a single picture element resolution of 25μm, for a 1:1 magnification onto the readout device. Charge leakage effects limit the resolution of typical vidicon devices to ~100μm, hence the requirement for magnified coupling. These considerations are of particular importance with the current trend of intimate mating of charge coupled device (CCD) readout sensors directly onto the streak camera [44], to produce truly integrated data aquisition and processing camera systems.

The temporal resolution of the Photochron IV-M camera system has been shown to be 2.3ps limited by intensity dependent trigger jitter and vidicon charge leakage effects. Ongoing evaluation with an improved stability laser and better utilization of the high spatial resolution available with this design, is confidently expected to reduce the instrumental function to a value at least equal to the standard size design. Fabrication of Photochron IV image tubes meeting the full design specification can be expected to realize the reality of a truly femtosecond resolution linear diagnostic.

References - Chapter 6

[1] M M Butslov, E K Savoiskii, A G Plahov, G E Smalkin and S D Franchenko,
Proc. 4th ICHSP

[2] P R Bird, D J Bradley, W Sibbett,
Adv, EEP, 40A, 51 (1976).

[3] W Sibbett, W E Sleat, J R Taylor and J P Willson,
Proc. 15th ICHSPP, SPIE 348, 217 (1982)

[4] D J Bradley, K W Jones,
Proc. 15th ICHSPP, SPIE 348, 237 (1982).

[5] W Sibbett, H Niu and M R Baggs,
Rev. Sci Instrum, 53(6), 758 (1982).

[6] D J Bradley, K W Jones and W Sibbett,
Proc. 13th ICHSPP, SPIE 189, 451 (1978).

[7] R L Fork, B I Greene and C V Shank,
Appl. Phys. Lett. 38, 671 (1981).

[8] C V Shank, E P Ippen, R L Fork, A Migns and T Kobayashiv,
Philos. Trans. R Soc London, Ser A298, 303 (1980).

[9] M H Key,
Philos. Trans. R Soc London, Ser A298, 351 (1980).

[10] D J Bradley, S F Bryant, J R Taylor and W Sibbett,
Rev. Sci. Instrum. 49(2), 215 (1978).

[11] P Dooley, V I Little, S Sim and S Majumdar,
Proc. 12th ICHSPP, SPIE 97, 80 (1976).

[12] W Sibbett, H Niu and M R Baggs,
Rev. Sci Instrum. 53(6), 758 (1982).

[13] H Niu, W Sibbett and M R Baggs,
Rev. Sci. Instrum. 53(5), 563 (1982).

[14] W Sibbett,
Proc. 15th ICHSPP, SPIE 348, 15 (1982).

[15] A S L Gomes, U Osterberg, W Sibbett and J R Taylor,
Optics Comm., 54 (6), 377 (1985).

[16] S P Gentile,
'Basic theory and applications of tunnel diodes',
D Van Nostrand Co. Inc. (1962).

[17] M C Adams, W Sibbett and D J Bradley,
Adv. EEP, 52, 265 (1979).

[18] J P Willson, W Sibbett and W E Sleat,
Optics Comm., 42, 208 (1982)

[19] M R Baggs, R T Eagles, A E Hughes, W Margulis, C C Phillips, W Sibbett and W E Sleat,
Proc. 16th ICHSPP, SPIE 491, 212 (1984)

[20] W T Welford.
Optica Acta, 18, 401 (1971)

[21] P G May,
PhD Thesis, London University (1983).

[22] V V Korobkin, A A Maljutin and M Ya Schelev,
J Photog. Sci., 17, 179 (1969).

[23] R Kalibjian, C F McConaghy and L W Coleman,
Rev. Sci. Instrum., 45, 776 (1974).

[24] M R Baggs, R T Eagles, W Margulis, W Sibbett and W E Sleat,
Adv. EEP, 64B, 617 (1985).

[25] W Sibbett, H Niu and M R Baggs,
Proc. 15th ICHSPP, SPIE 348, 271 (1982)

[26] M R Baggs,
PhD Thesis, London University (1983).

[27] H Niu, W Sibbett,
Rev. Sci. Instrum., 52 (12), 1830 (1981).

[28] C C Philips,
PhD Thesis, London University (1983).

[29] P G May, W Sibbett, K Smith, J R Taylor and J P Willson,
Optics Comm., 42, 285 (1982).

[30] W A Baum,
Adv. EEP, 16, 391 (1962).

[31] A S L Gomes, W Sibbett and J R Taylor,
IEEE J. Quant. Electron. QE 21, 8 (1985)

[32] A S L Gomes, A S Gouvera-Neto, W Margulis and J R Taylor,
To be published in Rev. Sci. Instrum.

[33] See for instance 'VHF/UHF Manual',
Radio Soc. of Great Britain.

[34] W H Hayward,
'Introduction to Radio frequency design',
Prentice Hall Inc. (1982).

[35] P H Smith,
'Transmission line calculator',
Electronics, 12 (1939).

[36] M Dishal,
IEEE Trans, MTT - 13, 696 (1965).

[37] I White,
Radio Communication, 120 (Feb 1984)

[38] See for example, W T Scott,
'The Physics of Electricity and Magnetism', second edition,
John Wiley & Sons, New York (1966)

[39] A J Hatch,
Nucl. Inst. and Methods, 41, 261 (1966).

[40] K Kinoshita, K Shinoda and Y Suzuki,
Proc. 15th ICHSPP, SPIE 348, 227 (1982)

[41] M C Adams, M R Baggs, W Sibbett and W E Sleat,
U K Patent Application, Agents Ref No. PQ20 925 (1983)

[42] M C Adams,
PhD Thesis, London University (1979)

[43] W E Sleat, W Sibbett J R Taylor and D J Bradley,
Optics Comm. 45(6), 411 (1983)

[44] C Cavailler et al,
Proc. 16th ICHSPP, SPIE 491, 693 (1984)

CHAPTER 7

General Conclusions

The importance of developing thermonuclear fusion as an alternative energy source for the next century has prompted extensive research activity. Experiments in inertial confinement fusion by the laser compression of matter, has resulted in a requirement for an ultrahigh time resolution, two-dimensional imaging diagnostic. A new framing camera system has been developed to fulfil this demand, and complement the one-dimensional imaging characteristics of streak cameras.

Electron-optical devices have been adopted in the field for some years due to the femtosecond response times of photoemissive materials. Early design techniques utilized analogue simulations, but this approach was found insufficient to fully characterise the current generation of ultrahigh time resolution instruments. To facilitate a more complete analysis, numerical techniques have been developed into computer codes which permit comprehensive evaluation of theoretical designs. These techniques have been employed in the design of the Picoframe I & II framing image tubes and the Photochron IV femtosecond streak tube.

The Picoframe framing tube design utilizes a weak electrostatic focusing lens, with a long narrow waist beam profile. One of three independent deflection assemblies may be combined with the imaging section to yield various framed image formats. Constructional simplicity of the single framing aperture version resulted in its adoption for construction of an experimental prototype.

A sealed-off prototype Picoframe I has demonstrated a static spatial resolution of around 55 lp/mm at the photocathode. Manufacturing inaccuracies and distortions caused during processing, resulted in the sensitivities of the two pairs of deflectors differing by ~7%. The experimental image tube was implemented into a camera system, incorporating an input optic and external, fibre-optically coupled MCP intensifier. This was necessary to limit the detrimental space charge effects caused by excessive photocurrents in the tube.

Initial evaluation in the framing mode was carried out using hypershort (~200fs) and ultrashort (< 10ps) optical pulses to illuminate a resolution test target. The necessary high speed, linear voltage deflection ramps were derived from a laser illuminated photoconductive element (PCE). Two schemes for connecting the deflectors were initially assessed. Results using the series feed-in configuration proved inconsistent, probably due to impedance mismatch effects at the deflectors. The parallel feed-in configuration was more successful. Dispersion effects in the connecting coaxial transmission line degraded the signal risetime. This tended to compensate for the manufacturing inaccuracies in the sensitivities of the deflectors. Using this scheme moderately well resolved images, demonstrating 4 lp/mm spatial resolution at the photocathode were recorded. Streak mode operation of the camera determined the frame exposure duration to be between 150-200ps.

It was realised that effective control of the deflection ramp gradient could be utilized to nullify manufacturing inaccuracies in the sensitivities of the deflectors. This was more fully investigated in the third, parallel PCE, configuration. The two pairs of deflectors were each connected to operate in the opposite

sense to separate PCE devices. Both PCE's were illuminated by sub-pulses from an optical delay line to provide the necessary synchronisation features. Gradient control was facilitated by regulation of the applied PCE bias potential. Again moderately well resolved images of up to 4 lp/mm spatial resolution at the photocathode were recorded. However the use of relatively long object illumination periods of ~40ps, and a reduction in the frame exposure duration to 130ps represented improved performance.

The practical difficulties of ensuring identical illumination characteristics for both PCE devices, made the parallel PCE configuration unsuitable for implementation into a standard laboratory diagnostic system. A more elegant approach to the control of the deflection ramp gradient was devised. The deflection plate capacitance was incorporated into a capacitative divider arrangement. By use of a miniature series trimmer capacitor, the gradient of the ramp supplied to the deflectors exhibiting optimum sensitivity could be conveniently perturbed. This arrangement provided a method for real-time optimisation of the framed images.

Initial dynamic mode evaluations were of single framed images. For double/multiple frame evaluation a second, more complex, dual framing aperture sealed-off image tube was fabricated. Extensive static evaluation of this prototype Picoframe II revealed severe image distortion probably due to misalignment in the imaging section caused during processing. This prevented effective evaluation in the dynamic mode. Due to the intricacy of the dual aperture design it would probably be more appropriate to utilize a demountable vacuum system in further investigations.

It is always questionable whether it is more appropriate to

use sealed-off or vacuum demountable tubes in prototype evaluation. The former has advantages of portability, compactness, wide spectral coverage (IR/visible/uv) through activated photocathodes, and may be readily isolated from other equipment which might influence the spatial resolution. Its main disadvantage is that any post processing modification of internal components is prohibited. The latter has the principal advantage that the internal components are readily accessible. However, such systems are generally cumbersome, bulky, only uv/x-ray sensitive and difficult to isolate from stray electromagnetic fields generated by vacuum eqipment. Nevertheless, the intricate nature of multiple aperture deflection assemblies demand the convenience of accessibility conferred by a demountable system.

The viability of multiple sequenced framing operation was assessed by operation of the Picoframe I in a dual sweep mode. A simple pulse forming network was employed to derive a 'triangular' shaped voltage deflection waveform. Applied to the sweep deflectors this permitted the electron beam to be swept across the framing aperture twice. To relieve stringent experimental demands a low trigger energy avalanche transistor sweep generator replaced the PCE device employed previously. Using a separate sweep generator/pulse forming network for each pair of deflectors, framed doublet images demonstrating $\leq$ 8 lp/mm resolution at the photocathode were recorded. The frame open time was measured to be ~200ps with an inter-frame time of 1.2ns.

It was noticed that the spatial resolution observed for the second framed image was always poorer than that of the first image. This is attributed to the superposition of oscillatory transients or ringing on the falling edge of the waveform. Improvements in

the transient response of the deflectors may alleviate this problem. A future design might include travelling wave deflection [1] structures. Here the deflection signal is propagated in a travelling wave network such that the deflection signal is synchronised to the passage of the electrons through the network. This has the advantage of increasing the sensitivity of the deflectors. Additionally such a network may be conveniently made of an impedance to match the characteristic impedance of the connecting transmission line. Thus the deflection system may be incorporated into a matched transmission line. This would permit any detrimental ringing effects to be postponed until after the passage of image forming electrons.

It is likely that improvements in the design of electronic sweep circuits, coupled with enhanced sensitivity deflectors will permit the generation of ~100ps duration framed images. However for truly sub-100ps durations it will probably be necessary to revert to laser illuminated PCE's for provision of the necessary high speed deflection ramps. The generation of multiple framed 'doublet' images using a single aperture design would necessitate the incorporation of orthogonally orientated shift deflectors, and the production of complex deflection waveforms [2]. Alternatively, utilization of vacuum demountable technology should make the fabrication of multiple aperture designs viable. Nevertheless it may ultimately be the case that it is easier to derive complex deflection waveforms than fabricate intricate deflection assemblies.

The modest temporal resolution of framing image tubes (~100ps) results in a correspondingly modest peak photocurrent. As such this type of tube is probably more suited to incorporation

of an internal MCP intensification stage [3]. Incorporation of internal intensification into streak tubes has been found to limit the dynamic range [3]. Thus despite the convenience and compactness conferred by this option, it is probably not suitable for single-shot femtosecond streak tubes. However there might be advantages for internally intensified repetitively operating streak cameras for observing particularly weak optical phenomena.

The wealth of diagnostic information available from x-ray imaging of imploding microballoon targets, has resulted in a modified x-ray sensitive Picoframe image tube design. Computational simulation of the photoelectrons emitted from an x-ray sensitive photocathode, revealed that the broad initial energy spread caused the beam waist diameter to expand. By doubling the mesh potential, whilst maintaining the same extraction field and reducing the anode electrode length, the degree of beam waist spread could be minimized. Two new deflection assemblies compatable with the modified conditions have been proposed. It is likely that evaluation of a prototype x-ray sensitive vacuum demountable camera will be carried out using the UV frequency quadrupled output from a Nd:YAG oscillator [4].

The generation of ultrashort and hypershort optical pulses has provided a valuable tool for probing many ultrafast physical, chemical and biological phenomena (see chapter 1). Due to its sensitivity, linearity of response and broad spectral coverage the electron-optical streak camera has found wide usage as a picosecond diagnostic. Current research is aimed at extending the temporal resolution to effectively cover the femtosecond regime, whilst maintaining a useful dynamic range.

In this thesis two modes of streak camera operation have been discussed, single-shot and repetitive of 'Synchroscan'. A sealed-off miniaturised version of the Photochron IV, developed for use in circumstances of limited diagnostic volume, has been operated at a repetition frequency of 300MHz for the first time. This instrument demonstrated a temporal resolution of 2.3ps operated in this mode. Limited by intensity dependent trigger jitter and the spatial resolution of the read-out device. Further refinement of the temporal resolution in the repetitive mode would require the use of a highly stable mode-locked laser system. Additionally due attention must be given to the provision of a suitably matched image read-out device. The enhanced spatial resolution characteristics of the Photochron IV and IV-M necessitate a correspondingly high performance from the image sensor. Consideration must be given to the overall shape of the MTF curve of ancillary optics, intensifiers and sensors; not just the figures pertaining to limiting resolution.

Relatively recent advances in the field of laser induced compression of matter has provided the impetus to develop picosecond framing camera systems. As such there is scope for further instrumental improvement to fully complement the one-dimensional imaging capabilities of the current state-of-the-art femtosecond streak camera systems. The Picoframe I camera has provided a valuable contribution to the development of picosecond two-dimensional imaging diagnostics.

References - Chapter 7

[1] R G E Hutter,
'Advances in image pickup and display',
Ed. B Kazan,
Academic Press, New York, Vol.1, p183 (1974).

[2] W Margulis and W Sibbett,
Optics Comm., 51, 91 (1984).

[3] W Sibbett, W E Sleat, J R Taylor and J P Willson,
15th ICHSPP, SPIE 348, 217 (1982).

[4] P D Rockett,
Appl. Optics, 23,176 (1984).

Appendix I

Solution of the transient response of an LCR network

A constant voltage E is applied at time t = 0 to a series circuit of inductance L, capacitance C and resistance R, the initial current and charge being zero. The differential equation describing such a circuit is

$$E = \frac{Ld^2q}{dt^2} + \frac{Rdq}{dt} + \frac{q}{C} \qquad a.1$$

where q is the charge on the capacitor. If $V_c(t)$ is the instantaneous voltage across the capacitor then

$$\frac{V_c(t)}{E} = \frac{\frac{q}{C}}{\frac{Ld^2q}{dt^2} + \frac{Rdq}{dt} + \frac{q}{C}} \qquad a.2$$

Transforming equation a.2 using the Laplace transform:

$$\frac{V_c(p)}{E} = \frac{\frac{q}{C}}{qp(p^2L + pR + 1/C)}$$

or

$$\frac{V_c(p)}{E} = \frac{1}{p(p^2LC + pRC + 1)} \qquad a.3$$

Transforming equation a.3 into its partial fractions gives

$$\frac{1}{p(p^2LC + pRC + 1)} = \frac{a}{p} + \frac{bp + c}{p^2LC + pRC + 1}$$

expanding and equating coefficients of p^n yields

$$a = 1 \ , \ b = - LC \ , \ c = -RC$$

$$\therefore \quad \frac{1}{p(p^2LC + pRC + 1)} = \frac{1}{p} + \frac{- pLC - RC}{(p^2LC + pRC + 1)}$$

Again transforming the right hand side into its partial fractions

$$\frac{pLC + RC}{p^2LC + pRC + 1} = \frac{pLC + RC}{(p + \alpha)^2 + \beta}$$

expanding and equating coefficients of p^n gives

$$\alpha = \frac{R}{2L} \qquad \beta = \left[\frac{1}{LC} - \frac{R^2}{4L^2}\right]^{\frac{1}{2}}$$

$$\therefore \quad \frac{1}{p(p^2LC + pRC + 1)} = \frac{1}{p} - \frac{(p + R/L)}{(p + \alpha)^2 + \beta^2}$$

$$= \frac{1}{p} - \frac{(p + \alpha)}{(p + \alpha)^2 + \beta^2} - \frac{\alpha}{(p + \alpha)^2 + \beta^2}$$

$$= \frac{1}{p} - \frac{(p + \alpha)}{(p + \alpha)^2 + \beta^2} - \frac{\beta}{\frac{\beta}{\alpha}(p + \alpha)^2 + \beta^2} \qquad \text{a.4}$$

Inverting equation a.4 for $\beta^2 > 0$ yields

$$\frac{V_c(t)}{E} = 1 - e^{-\alpha t}\left[\cos \beta t + \frac{\alpha}{\beta}\sin \beta t\right] \qquad \text{a.5}$$

The Q of an LCR circuit is defined:

$$Q = \frac{1}{R}\sqrt{\frac{L}{C}}$$

Hence define parameter A such that

$$A = \sqrt{4Q^2 - 1} = \sqrt{\frac{4L}{R^2C} - 1}$$

Then $$\alpha A = \frac{R}{2L}\sqrt{\frac{4L}{R^2C} - 1} = \sqrt{\frac{1}{LC} - \frac{R^2}{4L^2}} = \beta$$

Equation a.5 may then be written

$$\frac{V_c(t)}{E} = 1 - e^{-\alpha t}\left[\cos A\alpha t + \frac{\sin A\alpha t}{A}\right] \qquad a.6$$

Differentiating equation a.6 with respect to time gives

$$\frac{\dot{V}_c(t)}{E} = \frac{4Q^2\, e^{-\alpha t} \,.\, \sin A\alpha t}{A} \qquad a.7$$

The circuit risetime (T_{rise}) is then determined by equating equation a.7 to zero and solving for t

Hence $$T_{rise} = \frac{\pi}{\alpha A}$$

$$= \frac{\pi}{\frac{R}{2L}\sqrt{\frac{4L}{R^2C} - 1}}$$

$$= \frac{\pi}{\sqrt{\frac{1}{LC} - 1}}$$

$$\therefore \quad T_{rise} \simeq \pi\sqrt{LC}$$

Acknowledgements

I would like to thank my supervisor Professor W Sibbett for his supervision and tireless encouragement throughout this project. Thanks are due also to Dr. Martin Baggs for his help and guidance during the early work.

I gratefully acknowledge the help and advice of all the members of the Laser Group at Imperial College, in particular: Drs. Walter Margulis and Bill Sleat for their assistance with the experimental evaluations; Dr. Eric Munro for his advice during the computational work and Mr. C F Chen for his assistance in evaluating the Photochron IV-M.

My thanks also go to the technical staff of the Optics Section and Dr. Martin Adams and Mr. Phil Grigg of Thorn-EMI Electron Tubes Division, for their assistance in the construction of prototype image tubes.

Special thanks are due to my Mother, Mrs. Edna Eagles, for the hours spent typing and proof-reading this thesis.

Finally, I am indebted to; the Science and Engineering Research Council, Thorn-EMI Electron Tubes Division, Ruislip and AWRE, Aldermaston for their financial support during this work.

Publications

SINGLE-FRAME AND DOUBLE-FRAME OPERATION OF A PICOSECOND FRAMING CAMERA

R.T. EAGLES, W. SIBBETT [1] and W.E. SLEAT [1]

Optics Section, Blackett Laboratory, Imperial College, Prince Consort Road, London SW7 2BZ, UK

Received 29 November 1985

The operation of an ultrafast, electron-optical framing camera which has been designed to provide single or sequential, doublet image formats is described. Individual frame exposures of approximately 200 ps were measured and the interframe periods for the doublets were 1.2 ns. High quality images were recorded from which it could be deduced that the spatial resolution at the photocathode of the camera was in excess of 7ℓp/mm.

1. Introduction

The requirement for a framing camera which can provide a rapid sequence of picosecond, two-dimensional images has already been extensively discussed [1,2]. It suffices to mention here that such an instrument offers data which complements those taken from one-dimensional, time-resolved streak images. This is of primary relevance in studies that include, for example, plasma studies of laser-irradiated microballoon targets [3]. For this type of application an X-ray sensitive version of our camera is being developed but the results presented here relate to an experimental visible-sensitivity S20 "Picoframe I" system.

2. Description of camera

The Picoframe I camera system illustrated schematically in fig. 1 incorporates an image tube that has been designed specifically for ultrafast framing [1,2]. In brief, its operation relies upon the rapid sweeping of a narrow photoelectron beam across a small aperture to ensure an optimally short exposure time. A time-varying linear voltage ramp of opposite sense

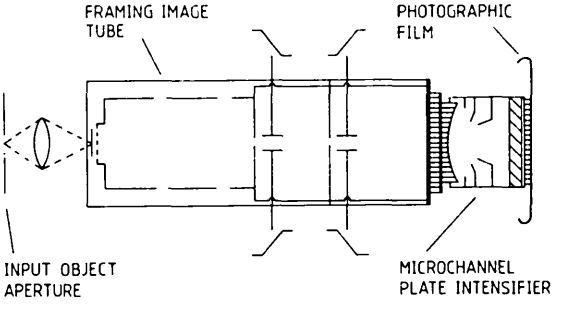

Fig. 1. Schematic of "Picoframe I" camera with deflection waveforms for single-frame operation.

supplied to the so-called compensation deflectors cancels the induced swept motion in the transmitted beam so that a stationary image can be displayed on the phosphor screen. To obtain this image with sufficient intensity for photographic recording at appropriately modest photocurrent levels the output of the framing tube is fibre-optically coupled to an image intensifier. By this means space-charge induced defocusing effects within the framing tube can be largely avoided. The intensifier used for these particular performance evaluations employed a Mullard type XX1330A microchannel plate tube having an "extended-red" S20 photoresponse and a relatively low luminance gain of approximately X250 when receiving light from the blue P11-type phosphor. During

[1] Present address: Physics Department, University of St Andrews, North Haugh, St Andrews, Fife KY16 9SS, Scotland.

0 030-4018/86/$03.50

our studies the intensifier was gated on for 200 μs to limit the integrated noise while ensuring that the majority of the signal photons were received from the screen of the framing tube.

The image of an illuminated resolution test chart was relayed onto the framing tube photocathode with an $f/3.5$, 64 mm focal length lens arranged to provide a demagnification of X2.2. The final image recording was on photographic film held in intimate contact with the fibre-optic face-plate of the image intensifier.

In initial evaluations of the performance of this Picoframe I camera [2] laser-illuminated photoconductive elements [4] were used to produce the deflection voltage ramps and exposure times as short as 130 ps were obtained [5]. However, the rather high optical pulse energy required to ensure proper saturation of this type of optoelectronic switch, having gap widths consistent with the required deflection voltage amplitudes, imposed severe practical constraints on the laser that was employed to test the camera. Consequently in the work reported here avalanche transistor sweep circuits with extremely low trigger energy requirements have been preferred. The circuitry actually employed comprised two synchronised chains of transistors which were capable of providing complementary outputs of plus and minus 3 kV in 1.5 ns into a 50 ohm resistive load. Naturally there is appreciable degradation in this rate of rise/fall of voltage when due account is taken of the deflection plate capacitances, the inherently inductive tube connecting leads and the 50 ohm coaxial drive cables.

3. Single-frame operation

In preliminary tests of the performance of the camera reported earlier [2,5] the illuminating laser pulses had durations ~0.25–10 ps FWHM while the frame time was determined to be 150–200 ps. Clearly it was necessary to evaluate the instrumental functions with pulse illuminations having durations exceeding the frame exposures. This has been done by using the frequency-doubled output from a Q-switched Nd : YAG laser which produced ~20 ns FWHM pulses at a repetition rate of 3 Hz. A portion of the beam intensity was directed onto a photodiode such that with suitable neutral density filters, the sweep circuit was triggered on the rising edge of the optical pulse. The intrinsic delay time of the sweep circuit, approximately 10 ns, meant that the latter half of the Q-switched pulse illuminated the camera during its framing operation.

To appropriately arrange the timing of the voltage ramps, due account had to be taken of the fact that the photoelectron transit time to the framing deflectors was less than that to the compensating deflectors. For the present design this time difference was approximately 1 ns and a corresponding allowance in length of coaxial feed cable was included. Each avalanche transistor circuit provided two opposite polarity ramp voltage outputs which were shared between the pairs of deflectors to provide balanced deflection. Precise compensation demands that the rate of deflection of the electron beam exciting the compensation plates is zero. It is to be expected that there will be some variations in the applied electrostatic deflections due to non-ideal coaxial cable parameters and also to the fact that the plates will respond slightly differently to the supplied signal as a result of manufacturing tolerances. With our prototype Picroframe I tube, it was found that the framing plates had a d.c. sensitivity which exceeded that of the compensation plates by 5%. To correct for this and any signal degradation in the feed cables etc. the voltage ramps to the framing plates were reduced by adding a pair of series variable capacitors (2–20 pF) which acted as capacitive dividers in conjunction with the capacitance of the deflectors. These "trimming" capacitors were bypassed for d.c. bias purposes by 12 kΩ resistors.

To evaluate the camera performance in this single-frame mode of operation a 1951 USAF resolution test chart, which was uniformly illuminated by the frequency-doubled pulses from the Q-switched Nd : YAG laser, was imaged onto a the tube photocathode to a 5 mm X 5 mm format size. At the repetition rate of 3 Hz it was possible to carry out quasi-realtime adjustments to achieve the optimum dynamic spatial resolution. By this means, framed images such as that reproduced in fig. 2 were obtained. The limiting spatial resolution that was routinely observed under these conditions was 7 ℓp/mm referred to the photocathode.

The exposure time for such a frame was determined by operating the camera in streak mode. In this configuration the resolution test chart was replaced

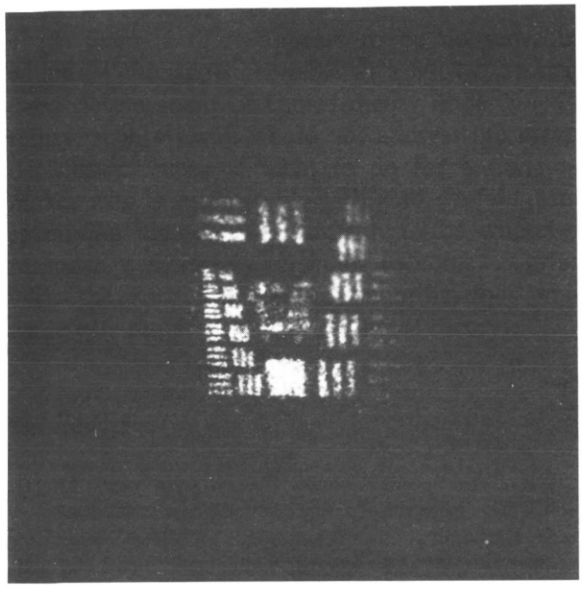

Fig. 2. Reproduction of single frame image, exposure time is 215 ps.

by a slit and only the framing deflectors were driven. For slit illumination using a constant intensity light source the observed scan on the output screen indicated the limits imposed on the transmission of the photoelectron beam by the geometry of the framing aperture. The slit was then illuminated by a series of delay-calibrated, picosecond, mode-locked laser pulses and the subsequent images streaked across the screen using the ramp generator. It is probably worth remarking that if the camera has been optimally adjusted for framing then by driving either the framing or compensation deflectors the streak speed could be deduced. From these two measurements the frame exposure time can be determined.

A more direct method for obtaining frame exposures that we now generally employ involves replacing the simple slit with the mask object illustrated in fig. 3. When the ramp voltage is applied and the mode-locked laser pulses are incident on this mask, a projected image of the outline of the framing aperture together with delay-line calibrated streak images are simultaneously presented on the phosphor screen.

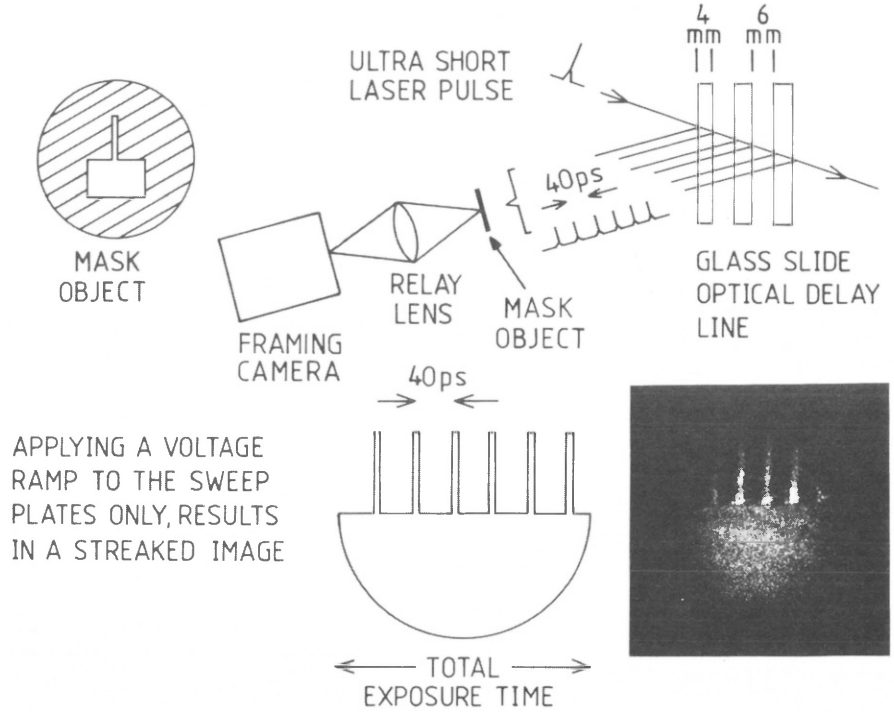

Fig. 3. Temporal calibration scheme. Inset shows experimental result for measured exposure time of 215 ps.

Thus the exposure time can be measured in a single operation.

For these calibration purposes we used the frequency-doubled output of a passively mode-locked flashlamp pumped Nd : YAG laser or more recently the temporally-compressed pulses [6] from a Q-switched, mode-locked cw Nd : YAG laser [7]. The latter had the convenience advantage that with its shorter pulse train (~300 ns) there was no requirement to select single pulses in an effort to avoid the over-writing that results from the relatively slow "reset" sweep back of the ramp generator. By this means it was established that the exposure time for the framed image reproduced in fig. 2 was 215 ps and the range of exposures was 200–230 ps.

4. Multiple-frame operation

Substantial research effort has been directed towards the design and operation of gated image intensifiers in an effort to achieve effective ultrafast operation. While some success has been reported for subnanosecond gating procedures [e.g. 8, 9] these devices have the major disadvantage of producing single frames only. In contrast, Picoframe cameras can be designed to provide a sequence of triplet [1] or doublet [2] framed images.

In the present prototype tube which has only one framing aperture and no shift deflectors then a double-frame operation can be achieved by applying triangular framing/compensating voltage profiles. The

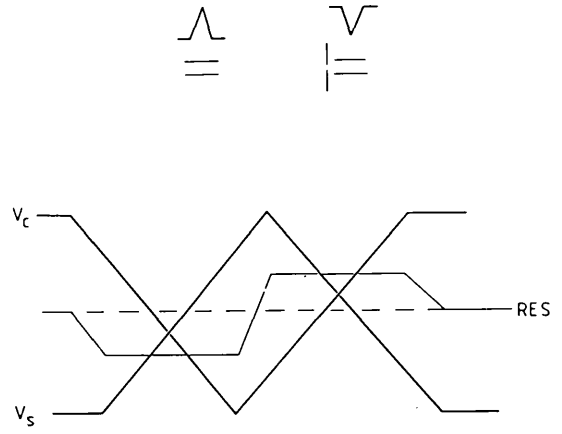

Fig. 4. Appropriately phased, ideal "shuttering V_s" and "compensating V_c" deflection waveforms.

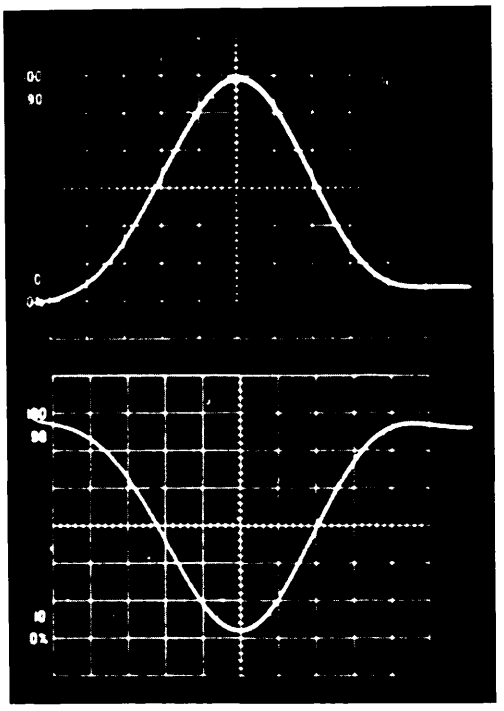

Fig. 5. Positive and negative "triangular" waveforms used with Picoframe I camera (200 V/div and 0.5 ns/div).

photoelectron beam can therefore be shuttered once on the positive-going edge and once on the negative-going edge of the waveform. When an opposite-polarity compensating wave-form is applied with non-zero phase relationship to the framing waveform as illustrated in fig. 4 then a spatially distinct doublet image format can be produced on the screen.

An appropriate triangular waveform was derived by propagating a ramp voltage profile into a simple pulse-forming network. The arrangement used which has already been described in some detail [10] comprised a pair of equal length shorted stubs placed on a transmission line. When the round-trip time of the voltage signal in each stub is less than or comparable to the signal risetime then a triangular pulse having half or less of the input ramp amplitude will be available at the output. For the stub lengths (~20 cm) used during this work, the round-trip time was 2 ns and the triangular profiles had FWHM durations of approximately 2 ns as shown in fig. 5.

5. Double-frame operation

Initial evaluations of the camera performance in a double-frame mode of operation, involved the supply of triangular voltage waveforms produced from one avalanche transistor drive circuit. This was accomplished by coupling a pulse-forming network to the opposite polarity outputs of the ramp generating circuit used earlier for single-frame evaluations. Each output was subsequently shared via two separate coaxial cables to provide the framing and compensating deflection signals, suitable phasing being achieved with appropriate cable feed lengths. The test object was again a USAF resolution test chart which was illuminated by frequency-doubled pulses (~100 ps duration) from a mode-locked and Q-switched Nd : YAG laser. By including a Michelson type optical-delay arrangement in the experimental set-up it was conveniently possible to provide a pair of subpulses of variable separation from each laser pulse. With this scheme we could also readily distinguish the framed image that resulted from the leading edge of the sweep waveform from the "partner" image that was produced during the trailing edge. In fact it was observed that the frame derived from the leading edge was always more clearly resolved than that of the subsequent frame associated with the trailing edge of the waveform. However, with careful adjustment of the cable delays and trimming capacitors and spatial resolution corresponding to 8 ℓp/mm for the early image and 5.5 ℓp/mm for the late image at the input photocathode was observed. The degradation in the later image was due to waveform distortion caused by nonimpedance matched splitting of the signal from the pulse forming network.

Supplying the deflection signal to both sets of deflectors imposes quite severe operating conditions on the transistor drive circuit. In particular the requirement of increased current delivery results in a degraded rate of rise for the voltage ramps and this was evidenced by the measured frame durations. These were actually determined to be 550 ps and 480 ps for the first and later frames respectively and the interframe period was measured with the optical-delay calibrator to be 1.5 ns. Offsetting this circuit limitation by the use of higher impedance coaxial feed cable did not represent a practical solution because of the attendent capacitive loading effects of the pairs of deflectors. Thus to achieve shorter exposure times two independent sweep generators were employed. This was possible because the measured triggering jitter of the avalanche transistor circuits used was typically less than ±20 ps which was much smaller than the frame exposure times.

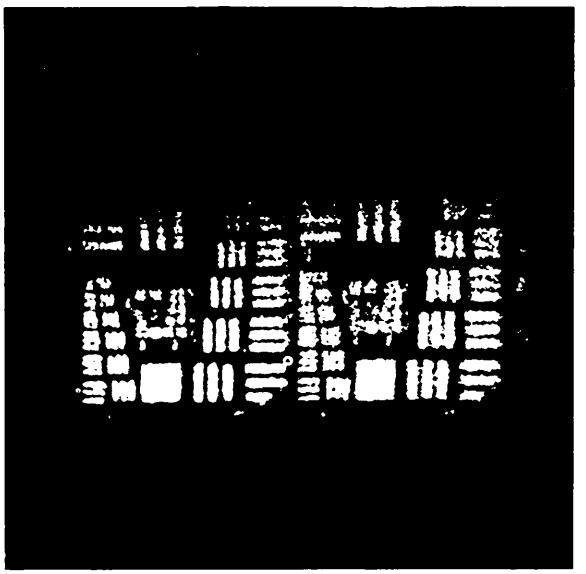

Fig. 6. Doublet frame format with first (left) and later images. Exposure times are 215 ps, 175 ps with interframe time of 12. ns.

For the work reported here, a p-i-n photodiode–avalanche transistor pulse generator was used to trigger the two sweep circuits. This pulse provided a subnanosecond risetime voltage impulse having an amplitude of approximately 20 V regardless of the intensity profile of the incident optical pulse so that shot-to-shot variations in the trigger times of the sweep generators (caused by changes in the optical pulse shape) were minimised. The trigger pulse was taken directly to one sweep generator and via a variable electrical delay line to the second sweep generator. Thus all the coaxial cable lengths could be made equal and the characteristic electron transit time and dephasing features between the sets of deflectors being allowed for by appropriate adjustment of the trigger delay to the second circuit.

Observations indicated that the image quality of the leading frame was again superior to that of the subsequent frame. In fact, an optimum spatial resolution of 10 ℓp/mm (referred to photocathode) could

be achieved for the leading frame while the second frame had a spatial resolution of just 5 ℓp/mm. The best compromise adjustment gave a recorded spatial resolution of 7 ℓp/mm maintained over both images. Exposure times for these images (reproduced in figure 7) were 215 ps and 175 ps for the first and second frames respectively with an interframe time of 1.2 ns which represents a substantial improvement over those measured for the single ramp generator arrangement described earlier.

6. Conclusion

The results presented here serve to indicate that this design of framing camera offers the realisation of ultrafast single or multiple format exposures. We expect that more refined electrode configurations currently being investigated will provide further enhancements of the observed spatial and temporal resolution characteristics for this family of Picoframe cameras.

Acknowledgement

Regular interactions and discussions with Dr. John Freeman (AWRE, Aldermaston) during the course of this work contributed substantially to its progress. One of us (RTE) was supported by an SERC "CASE" postgraduate studentship in collaboration with Thorn-EMI, Electron Tubes Division, Ruislip, Middlesex, England. The funding by the Paul Instrument Fund of The Royal Society, the Science and Engineering Research Council and AWRE Aldermaston is also gratefully acknowledged.

References

[1] W. Sibbett, M.R. Baggs and H. Niu, Proc. 15th Intern. Contress on High speed photography and photonics (San Diego) SPIE 348 (1982) 267.
[2] M.R. Baggs, R.T. Eagles, W. Margulis, W. Sibbett and W.E. Sleat, Advances in Electronics and Electron Physics 64B (1985) 627.
[3] H.G. Ahlstrom, Diagnostics of experiments on laser fusion, Vol. II, Lawrence Livermore National Laboratory, Livermore, Ca. UCRL-53106 (1982).
[4] W. Margulis and W. Sibbett, Optics Comm. 51 (1984) 91.
[5] M.R. Baggs, R.T. Eagles, W. Sibbett and W.E. Sleat, Proc. 16th Intern. Congress on High speed photography and photonics (Strasbourg) SPIE 491 (1984) 40.
[6] A.S.L. Gomes, U. Osterberg, W. Sibbett and J.R. Taylor, Optics Comm. 54 (1985) 377.
[7] M.D. Dawson, A.S.L. Gomes, W. Sibbett and J.R. Taylor, Optics Comm. 52 (1985) 295.
[8] A.K.L. Dymoke-Bradshaw, J.D. Kilkenny and J. Westlake, Advances in Electronics and Electron Physics 64B (1985) 531.
[9] G.J. Yates, N.S.P. King, S.A. Jarmillo, J.W. Ogle, B.W. Noel, N.N. Thayer, Proc. 15th Intern. Congress on High speed photography and photonics (San Diego) SPIE 348 (1982) 422.
[10] W. Margulis and R. Persson, Rev. Sci. Instrum. 56(8) (1985) 1586.

ADVANCES IN ELECTRONICS AND ELECTRON PHYSICS, VOL. 64B

Subpicosecond Chronoscopy Using a Photochron IV Streak Camera

M. R. BAGGS, R. T. EAGLES, W. MARGULIS, W. SIBBETT, and W. E. SLEAT

The Blackett Laboratory, Imperial College of Science and Technology, London, England

INTRODUCTION

At the Sixth Symposium on Photoelectronic Image Devices we described a Photochron II streak image tube which when later incorporated into a camera system was demonstrated to have a limiting time resolution of just less than 1 psec.[1] During the couple of years that followed the 1974 Symposium, generation of subpicosecond light pulses by applying passive mode-locking techniques to continuous wave (CW) rhodamine 6G dye lasers was reported[2] and this laid the foundation for time-resolved spectroscopy on a subpicosecond time scale. This development vividly highlighted the need for further improvements to the performance of electronoptical streak cameras and in anticipation of yet shorter duration laser pulses we embarked on a research program to design a femtosecond resolution streak image tube.

The era of femtosecond time-domain spectroscopy has now arrived because pulse durations ~55 fsec[3] have been produced directly by passively mode-locking CW ring dye lasers and amplified 90-fsec pulses have been compressed to 30-fsec durations by a sequence of imposed nonlinear frequency broadening in an optical fiber followed by spectral compression using a dispersive delay line.[4] The durations of such hypershort pulses are usually deduced from measurements taken using refined autocorrelators[4] or cross-correlators.[5] Although this technique offers excellent time resolution (<30 fsec), the nonlinearity of response leads to insensitivity to pulse shape and low intensity background detail. The streak camera, on the other hand, has a linear response together with a wide spectral coverage for a particular photocathode and in addition has the facility for simultaneous recording of any spectral information dispersed along the slit. Consequently, a streak camera having optimized time resolution offers the best combination of diagnostic assets for use in time-domain spectroscopic studies in the femtosecond regime. Current topical applications

ISBN 0-12-014724-6

include the investigation of the carrier dynamics in multiple quantum well semiconductor structures,[6] phase transitions in semiconductors,[7] and detailed observations of molecular dynamics in liquids.[8]

Photochron IV Streak Tube Design

In streak image tubes which are intended for use in femtosecond streak cameras it is of basic importance to minimize the transit time dispersion which arises from the initial distribution of energy and angle of the electrons emitted at the photocathode. It must also be emphasized that quantitative time-resolved data can be inferred only when a particular instrumental function is maintained over a useful range of incident light intensity. Therefore, before a new, improved design could be devised, it was necessary to establish a thorough understanding of the factors which limit the performance of existing streak tubes. We did this for the Photochron systems for which a good deal of experimental data were already available. From a detailed theoretical analysis of space-charge effects in Photochron cameras we showed for the first time that the predictions of an appropriate model[9] were in close agreement with experimental results which illustrated intensity-dependent temporal broadening of recorded streak durations.[10] In addition, the temporal and spatial resolutions of Photochron streak cameras were calculated by using a method based on modulation transfer functions which provides a physically realistic appraisal of their characteristics.[11] The salient inferences drawn from these analyses for the Photochron II streak tube were that (1) for initial photoelectron energy $\gtrsim 0.15$ eV the temporal dispersion in the mesh-to-deflector region exceeded that of the photocathode-to-mesh section, (2) at operational current densities the intensity-dependent broadening effects (i.e., limiting dynamic range) were particularly evident in the relatively low voltage, low electric field, mesh-focusing cone section of the electron lens, and (3) that an optimum range of streak velocities existed.

A provisional tube design (designated the Photochron III)[12] appeared to have a predicted limiting time resolution ~200 fsec when its performance was evaluated under the idealized conditions of low initial photoelectron energy spread (0.1 eV) and high streak velocity (5×10^{10} cm sec^{-1}) in the absence of space charge and deflector network effects. It was concluded, however, that on the basis of the results of our theoretical studies[9,11] a more extensive design study had to be applied to ensure adequate subpicosecond resolution from a camera operating under much less favorable, practical conditions. This work led to the development of the Photochron IV streak tube[13] which has the electrode configuration shown in Fig. 1. The overall design concept is based on the provision that optimally high

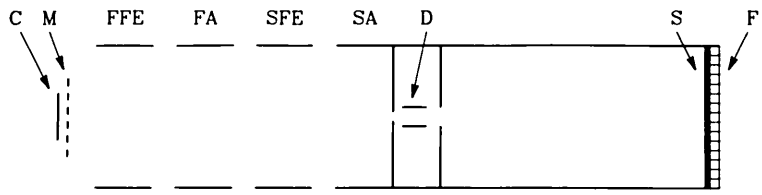

FIG. 1. Electrode configuration of Photochron IV streak tube: photocathode (C), mesh (M), first focus electrode (FFE), first anode (FA), second focus electrode (SFE), second anode/screen (SA/S), deflectors (D), fiber optic (F).

voltages and electric fields be maintained in the photocathode-to-deflector region. For this region the original 0.5-mm photocathode-mesh separation of the Photochron II has been increased in the Photochron IV configuration to 2 mm and the applied accelerating mesh potential increased from 1 to 10 kV. To adequately manipulate the more energetic photoelectron signal, the Photochron IV has a "doublet" focusing electron lens constituted by the four cylindrical electrodes. For focus, the voltages applied to the photocathode, mesh, first focus electrode, first anode, second focus electrode, and second anode/screen are -18, -8, -10, $+6$, -13 kV and 0 V, respectively. In our present experimental version a modest electric field of 25 kV cm^{-1} is maintained between the S · 20 photocathode and the copper micromesh (600 cell cm^{-1}) electrode by deliberately selecting a 4-mm separation. (Later Photochron IV tubes will have 2-mm separation.) The measured electronoptical magnification is -2.1 and the spatial resolution observed on the P · 11 phosphor screen (is 33 lp mm^{-1}).

DYNAMIC PERFORMANCE OF PHOTOCHRON IV STREAK CAMERA

Two camera configurations have been assembled and preliminarily tested under dynamic (i.e., streaking) conditions. In one case a repetitively operating or "Synchroscan" mode of operation is used while the other is a single-shot streak operation. The details of the camera systems and associated experimental evaluations of their performance are presented in the following two sections.

Photochron IV Synchroscan Camera

The Synchroscan streak principle has been discussed in detail elsewhere[14] so it suffices to say here that the basic idea relies upon the application of a periodic linear, deflection voltage ramp (such as the central half amplitude of a sinusoidal waveform) in synchronism with incident

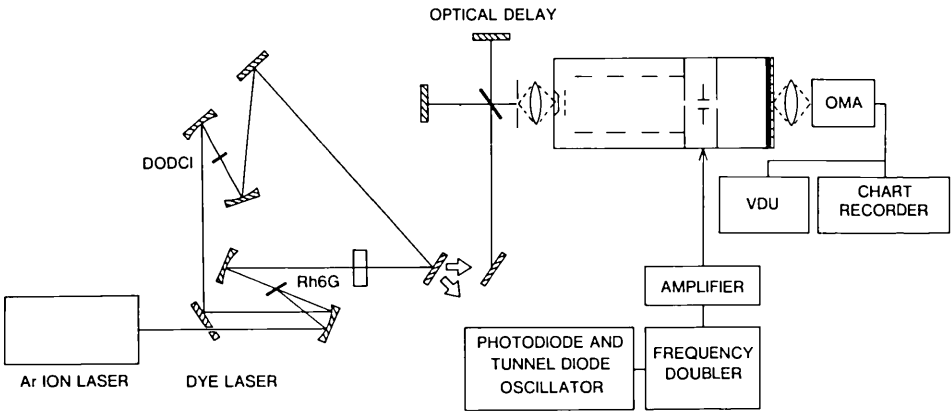

FIG. 2. Experimental lay-out of Photochron IV Synchroscan streak camera and passively mode-locked CW ring dye laser.

light signals from a repetitive source such as a mode-locked CW laser. Low-intensity streaks (with correspondingly low photoelectron currents) are thereby accumulated at the streak tube phosphor screen and recordable intensity levels are available without recourse to additional image intensification.

The Synchroscan Photochron IV camera arrangement is shown schematically as part of Fig. 2. The input optics comprised a 30-μm optical slit, the image of which was relayed by a lens operating at a demagnification of $\times 4$. The streak output image could be recorded either directly onto photographic film or with an electronic readout system. In general, the latter has been preferred and we have used a lens-coupled ($\times 4$ magnification) optical multichannel analyzer (B & M Spektronik, OSA/WP2) for detection and display. Permanent records of the streak intensity profiles are taken using a chart recorder as indicated. Also included in Fig. 2 are the schematic representations of the laser source of hypershort test light pulses and the electronics by which the synchronized RF deflection voltage sinusoid was derived. The laser is a passively mode-locked CW rhodamine 6G ring dye laser which when operated at a wavelength of 617 nm reliably produces pulses having durations of less than 200 fsec at a repetition rate of 83 MHz.[15] Two output beams are available for this cavity configuration and one was directed with appropriate attenuation via a calibrated optical delay to the input slit of the camera while the other provided the optical trigger to the photodiode/tunnel-diode oscillator. The output of this tunnel-diode oscillator was frequency doubled, amplified to a power $\sim$12 W, and supplied to the tube deflector network which has

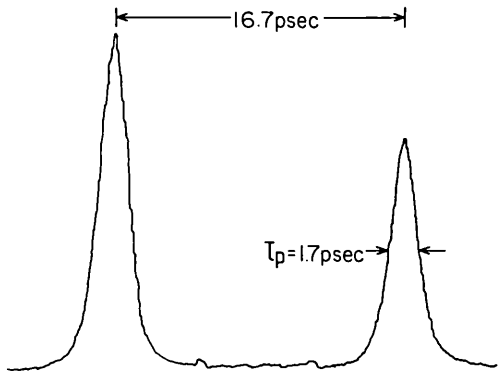

FIG. 3. Intensity profiles of streak images recorded with Synchroscan streak camera.

been designed to be compatible to the application of RF signals as well as single voltage ramps.

The 1.7-psec recorded durations (FWHM) shown in Fig. 3 are the shortest that we have obtained so far for the Photochron IV in this synchronous mode of operation. It must be remembered, however, that this streak duration is a convolution of the camera instrumental function with the laser pulsewidths and any jitter that exists between the arrival times of the laser pulses and the deflection voltage ramps. For the observed streak velocity of 6.5×10^9 cm sec^{-1} the estimated camera resolution is 1 psec so there is reasonable agreement between the theoretical prediction and the experimental result. The most probable explanation for the difference is that there is likely to be some jitter which arises through slight variations in the triggering instants due to appreciable (~5%) intensity fluctuations in the laser pulses.

Photochron IV Single-Shot Camera

In single-shot streak operation it is essential to ensure that photocurrent densities do not reach levels where space charge and related problems degrade the spatial, and more particularly, the temporal characteristics of the streak image tube.[9,10] For this reason, high gain intensification is provided in either external[10] or internal[16] configurations. Each has relative merits; for example, convenience, lack of intensifier photocathode background noise, and elimination of geometrical aberrations are in favor of an internal proximity-focused intensifier whereas an external intensifier module has the advantage of flexibility and also that gain saturation effects[10] in the microchannel plate are less problematical for submillisecond phospho-

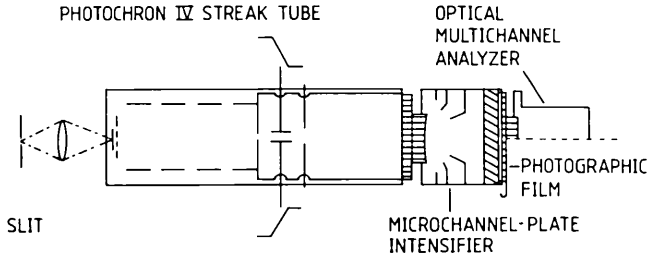

FIG. 4. Schematic of Photochron IV single-shot streak camera.

rescent image signals than for subpicosecond electron images. Both schemes have been investigated with the Photochron II[1,10] and Photochron IIA[16] streak cameras and similar studies are planned for the Photochron IV counterparts. So far, however, preliminary experimental results have only been obtained for a camera which incorporates an external intensifier as depicted schematically in Fig. 4. The intensifier (Philips-type 21XX, "20/30") was an inverting, self-focusing microchannel plate unit having a nominal luminance gain of 10^5 and a measured spatial resolution of 45 lp mm^{-1} at the photocathode. It was coupled to the screen faceplate of the streak tube via a 20-mm-long fiber optic cylinder and under static focus conditions the spatial resolution at the photocathode of the single-shot camera has been measured to be 32 lp mm^{-1}. The input optics and the OMA recording arrangement were the same as those already described for the camera in the Synchroscan operation.

The experimental set-up used in the evaluation of the single-shot streak performance is outlined in the block diagram of Fig. 5. Because of our decision to employ a laser-activated GaAs photoconductive element (PCE) with which to generate the fast deflection voltage ramps[17] we used amplified pulses from the passively mode-locked, colliding pulse CW ring dye laser referred to earlier. The durations of these amplified pulses were typically 250 fsec with energies ~0.4 mJ produced at the 10-Hz repetition rate of our four-stage-dye amplifier.[18] Approximately 90% of the pulse intensity irradiated the GaAs PCE in the circuit network which provided

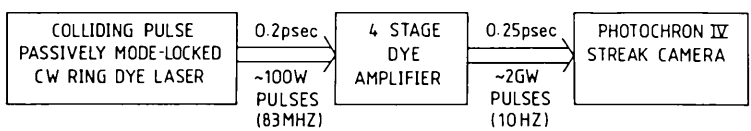

FIG. 5. Block diagram of experimental configuration used for dynamic tests on single-shot streak camera.

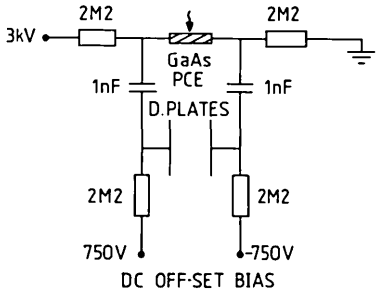

FIG. 6. Deflection voltage ramp generator circuit.

the symmetrical streak deflection (see Fig. 6). Of the remaining intensity part illuminated a second PCE circuit which provided the 15-V OMA electrical trigger and the rest was directed to the streak camera by way of a calibrated optical delay. In this instance, quasi-normal reflections (temporally separated by 10 psec) were taken from the front and back faces of a 1-mm-thick glass disk.

The best indication to date of the subpicosecond temporal resolution capability of the Photochron IV single-shot camera can be deduced from the streak result shown in Fig. 7. When the OMA spatial resolution limit is

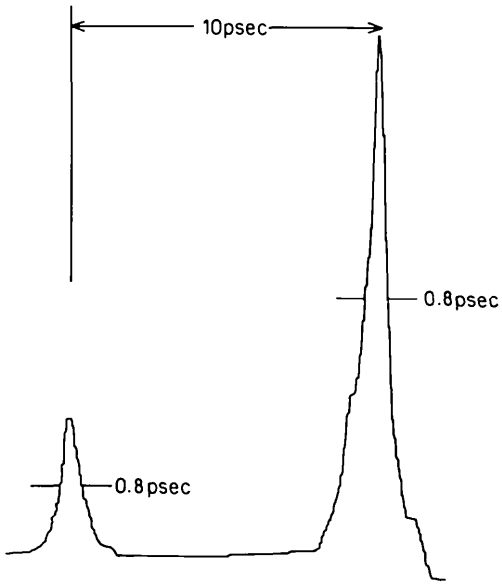

FIG. 7. Intensity profiles of streak images recorded with single-shot camera.

deconvolved then a camera instrumental function ~0.7 psec is implied, in excellent agreement with the theoretically predicted value of 0.7 psec for the observed streak velocity of 2×10^{10} cm sec^{-1}. It is therefore expected that for a streak tube having an applied extraction electric field of 50 kV cm^{-1} and an optimum sweep velocity of 3×10^{10} cm sec^{-1}, the estimated camera resolution of 0.4 psec will be realized in practice. Moreover, when illuminated at wavelengths close to the cathode photoemission threshold then the limiting temporal resolution ~0.2 psec should be achieved.

Conclusions

The experimental results presented here indicate that even in its present state of development the Photochron IV camera can provide subpicosecond resolution in the single-shot mode of streak operation. When our next experimental streak tube is constructed to meet all the design specifications and when tested dynamically with a fully optimized mode-locked CW ring dye laser, we are confident that improved, subpicosecond time resolution will be demonstrated in both single-shot and Synchroscan camera systems.

Related research activities include the evaluation of UHV demountable and sealed-off miniaturized versions of a Photochron IV tube (designated Photochron IV-M)[13] and the incorporation of improved near infrared-sensitive (Pd-Ag-O-Cs) photocathodes.[19] With these ongoing and planned developments the prospect of direct time-domain spectroscopic studies in a femtosecond regime is clearly a practical reality. Subpicosecond chronoscopy is therefore expected to find new applications in fundamental aspects of photophysics, photochemistry, and photobiology.

Acknowledgments

The financial support of the Paul Instrument Fund of The Royal Society and the Science and Engineering Research Council is gratefully acknowledged. One of us (R.T.E.) is supported by an SERC CASE Studentship in collaboration with Thorn-EMI, Electron Tubes Division, Ruislip, Middlesex, and another (M.R.B.) has financial support from AWRE, Aldermaston. We would also wish to give special thanks to Dr. M. C. Adams and Mr. P. Grigg (Thorn-EMI) for their major contributions in the construction of the experimental Photochron IV streak tube and to Dr. P. G. May for assistance with the mode-locked CW dye laser and amplifier system.

References

1. Bradley, D. J. and Sibbett, W., *Appl. Phys. Lett.* **27,** 382 (1975).
2. Ruddock, I. S. and Bradley, D. J., *Appl. Phys. Lett.* **29,** 296 (1976).
3. Halbout, J. M. and Tang, C. L., *IEEE J. Quantum Electron.* **OE-19,** 487 (1983).

4. Fork, R. L., Shank, C. V., Yen, R., Stolen, R. H. and Tomlinson, W. J., *Appl. Phys. Lett.* **40,** 761 (1982).
5. Fork, R. L., Shank, C. V., Yen, R. T. and Hirlimann, C., *Springer Ser. Chem. Phys.* **23,** 10 (1982).
6. Shank, C. V., Fork, R. L., Yen, R., Shah, J., Greene, B. I., Gossard, A. C. and Weisbach, C., *Solid State Commun.* **47,** 981 (1983).
7. Shank, C. V., Yen, R. and Hirlimann, C., *Phys. Rev. Lett.* **50,** 454 (1983).
8. Kalpouzos, C., Kenney-Wallace, G. A., Kroger, P. M., Quiteris, E. and Wallace, S. C., *Springer Ser. Chem. Phys.* **23,** 221 (1982).
9. Niu, H. and Sibbett, W., *Rev. Sci. Instrum.* **52,** 1830 (1981).
10. Bradley, D. J., Bryant, S. F. and Sibbett, W., *Rev. Sci. Instrum.* **51,** 824 (1980).
11. Niu, H., Sibbett, W. and Baggs, M. R., *Rev. Sci. Instrum.* **53,** 563 (1982).
12. Bradley, D. J. and Jones, K. W., *In* Proc. of 15th Int. Conf. on High Speed Photography and Photonics, p. 237 (1982).
13. Sibbett, W., Niu, H. and Baggs, M. R., *In* Proc. of 15th Int. Conf. on High Speed Photography and Photonics, p. 271 (1982).
14. Sibbett, W., *In* Proc. of 15th Int. Conf. on High Speed Photography and Photonics, p. 15 (1982).
15. Willson, J. P., Sibbett, W. and Sleat, W. E., *Opt. Commun.* **42,** 208 (1982).
16. Sibbett, W., Sleat, W. E., Taylor, J. R. and Willson, J. P., *In* Proc. of 15th Int. Conf. on High Speed Photography and Photonics, p. 217 (1982).
17. Margulis, W., Sibbett, W. and Taylor, J. R., *Opt. Commun.* **35,** 153 (1980).
18. May, P. G., Ph.D. Thesis, London University (1983).
19. Hou, X., Sibbett, W. and Weekley, B., *Rev. Sci. Instrum.* **52,** 1487 (1981).

ADVANCES IN ELECTRONICS AND ELECTRON PHYSICS, VOL. 64B

A Picosecond Framing Camera for Single or Multiple Frames

M. R. BAGGS, R. T. EAGLES, W. MARGULIS, W. SIBBETT, and W. E. SLEAT

The Blackett Laboratory, Imperial College of Science and Technology, London, England

INTRODUCTION

The electronoptical framing camera, capable of producing two-dimensional single frames or preferably a sequence of framed images, is an important and versatile diagnostic tool with direct application in several fields of research but notably in experiments on laser-induced thermonuclear fusion and more general laser plasma interactions.[1] Currently available commercial cameras have a time resolution limit ~1 nsec and interframe periods ~2 nsec with modest (~4 lp mm^{-1}) spatial resolution.[2] To adequately supplement the time-resolved data obtained from NIR/visible, UV, VUV, and X-ray sensitive streak cameras there is a present need to develop a picosecond framing camera. Its primary features must include (1) frame exposure times $\leq$100 psec, (2) interframe periods $\leq$250 psec, (3) dynamic spatial resolution $\geq$10 lp mm^{-1} (at the photocathode), and (4) X-ray/NIR spectral coverage using appropriate photocathodes. Considerable effort has already been directed toward such a development and a variety of distinct approaches have been reported.[3-8] In this article we summarize the principle of operation and design of a Photochron framing image tube which we believe should fulfill the rigorous requirements mentioned above. Preliminary results are also included to illustrate the static and dynamic performance characteristics of an experimental S·20 version of this picosecond framing camera.

THE FRAMING IMAGE TUBE

The basic electrode configuration of the Photochron framing tube is shown schematically in Fig. 1. The photoelectron signal is initially accelerated in a planar-geometry, photocathode-to-mesh region before entering a single, weak electrostatic lens consisting of three cylindrical electrodes. The constraints which are imposed upon the design of this lens have been described in detail elsewhere[9] and it suffices to mention here

ISBN 0-12-014724-6

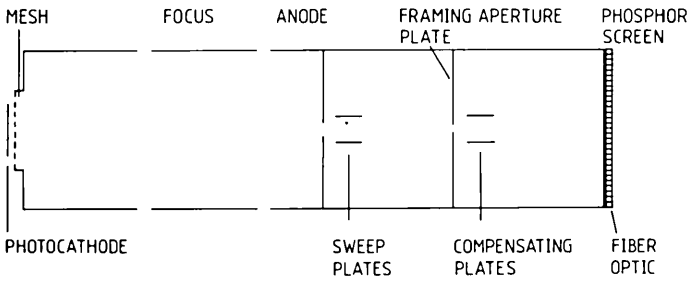

FIG. 1. Schematic of framing image tube.

that the electron beam is confined to a long, narrow waist in the crossover region which coincides with the deflection section of the tube. The electronoptics of this arrangement have been optimized by analyzing computer-generated electron trajectories with a modulation transfer function program[10] and for the operating electrode potentials given in Table I, a magnification of -1.5 is predicted. Also, from the MTF curves given in Fig. 2 for the spatial resolution expected at the phosphor screen corresponding to a number of object points on the photocathode, it can be seen that the limiting static resolution should exceed 40 lp mm^{-1}.

SINGLE AND MULTIPLE FRAME GENERATION

The method of frame generation can be understood by considering Fig. 3. A fast time-varying linear voltage ramp applied to the sweep deflector plates streaks the electron beam across the aperture in the framing aperture plate and thus a single temporal transmission of photoelectrons is defined. The transmitted electrons have an imposed transverse velocity which must be cancelled so that two-dimensional spatial resolution infor-

TABLE I

Operating voltages for photochron framing image tube

Electrode	Voltage (kV)
Photocathode	−15
Mesh	−10
Focus electrode	−12.8
Anode	0
Screen	0

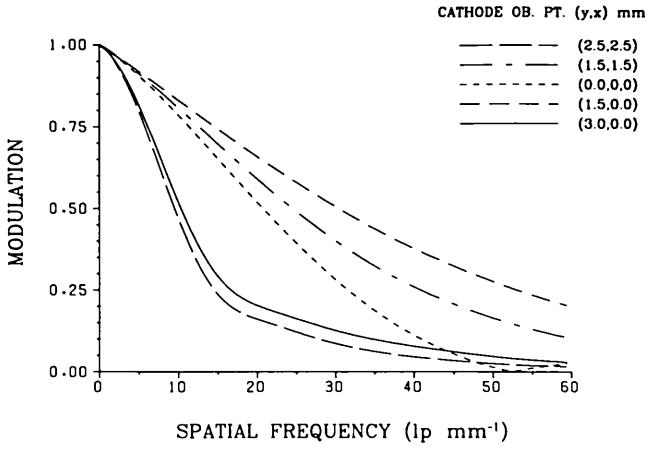

FIG. 2. MTF curves for static mode operation.

mation can be secured. This is achieved by applying an inverted-polarity duplicate voltage ramp to the compensating deflector plates which have the same deflection sensitivity as the sweep plates. It is of course imperative to accurately synchronize these two voltage ramps.

The frame exposure time, T, is given by,[9]

$$T = 2Vad/[Kl(\tfrac{1}{2} + L)]$$

where the physical parameters are as indicated in Fig. 4, V is the anode

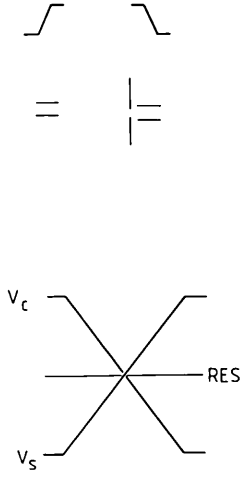

FIG. 3. Scheme for single frame generation.

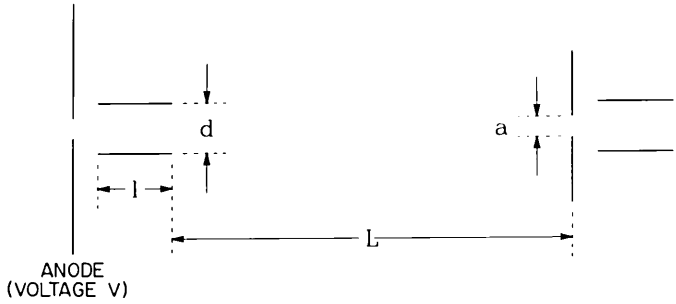

FIG. 4. Deflectors/aperture geometry.

voltage, and K is the slope of the voltage ramp. Frames having the shortest exposure times will therefore be produced by minimizing the diameter of the framing aperture and maximizing the rate of change of deflection voltage.

When the linear voltage waveforms applied to the sweep and framing deflectors cancel precisely a single frame is positioned at the center of the screen. For multiple-framing operations several techniques can be used,[9] but only one method which is compatible with the tube configuration of Fig. 1 will be outlined here. A triangular voltage pulse is suitably dephased from an inverted-polarity duplicate such that their combined effect is to produce two frames at discrete locations on the screen. By then applying an appropriate staircase voltage waveform to a pair of shift plates,[9] oriented orthogonally to sweep and compensating deflectors, a series of "frame doublets" can be generated.

THE EXPERIMENTAL FRAMING CAMERA

A framing image tube has been constructed with an S · 20 photocathode and the P · 11 phosphor screen has been deposited on a fiber optic faceplate. The performance characteristics of the tube under static operating conditions which are presented in Table II are in good agreement with the theoretical predictions. These data confirm that the deflection sensitivities of the sweep and compensation deflectors are well matched and that a relatively large image format (8 mm × 8 mm at the photocathode) can be accommodated.

This framing tube has been incorporated into the camera arrangement illustrated schematically in Fig. 5. The luminous event under study is imaged onto the photocathode by an $f/1.5$, 80-mm focal length lens with a demagnification of ×1.5. There is therefore an overall magnification of

TABLE II
Static performance characteristics of framing tube

Characteristic	Value
Electronoptical magnification	−1.5
Static spatial resolution at screen	37 lp mm^{-1}
Deflection sensitivity of sweep plates	2.6 cm kV^{-1}
Deflection sensitivity of compensating plates	2.5 cm kV^{-1}
Usable area on cathode	8 mm × 8 mm

unity between the optical input at the object plane and the image produced at the phosphor screen. With the nonoptimized input optics used in these preliminary evaluations, the static spatial resolution at the screen has been measured to be 23 lp mm^{-1}. A microchannel plate image intensifier (Mullard, type XX1332) was fiber optically coupled to the screen of the framing tube to ensure that excessive photocurrents which induce deleterious space charge effects[11] were not drawn during the framing operation. The intensifier was gated on for 200 μsec just prior to camera illumination and provided a modest gain ~250 and the output image was recorded on Ilford HP5 photographic film in intimate contact with its fiber optic faceplate.

EVALUATION OF FRAMING PERFORMANCE

In our preliminary evaluation of the camera dynamic performance, the basic single-frame operation was selected. The experimental set-up has

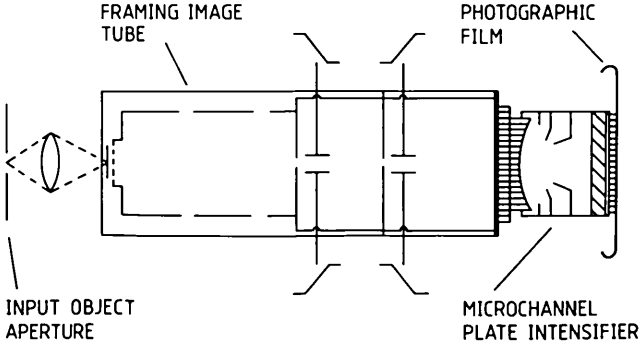

FIG. 5. Schematic of experimental framing camera.

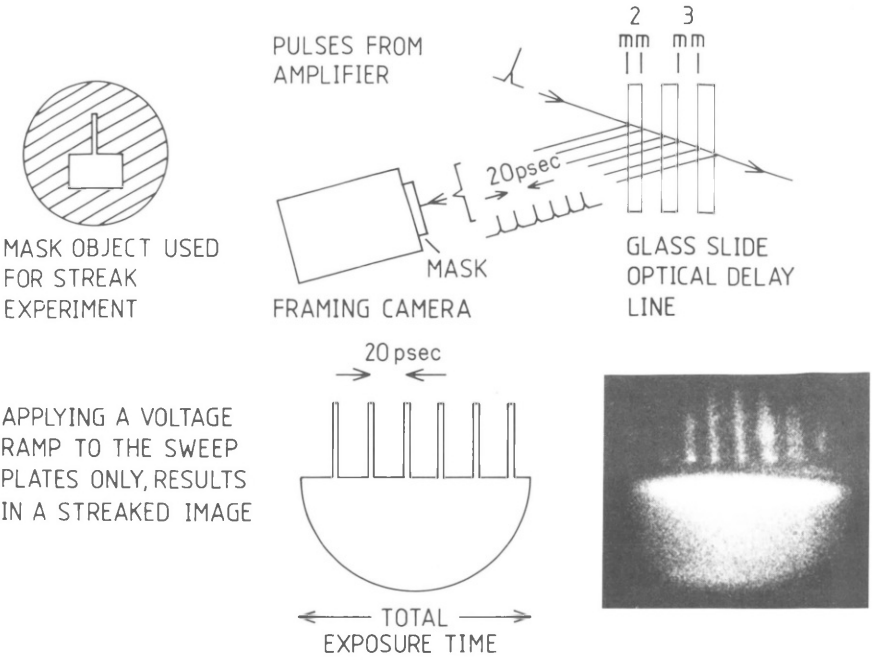

FIG. 6. Scheme for streak calibration of frame exposure time. Inset is a reproduction of an experimental result.

been described elsewhere.† Laser pulses were used both to illuminate a test object and to irradiate the photoconductive switch which was used to produce the linear voltage deflection ramps. A passively mode-locked CW ring dye laser generated pulses having durations below 200 fsec at 617 nm (Willson *et al.*[12]) which were then amplified to powers ~2 GW by a four-stage dye amplifier operating at a 10-Hz repetition rate.[13] Approximately 10% of the amplified, hypershort laser pulse was directed onto the semiinsulating, Cr-doped GaAs photoconductive element[14] which was maintained with a 2-kV dc bias voltage.

To determine the frame exposure time the camera was operated in a streak mode where the compensation deflectors were made electrically common with the anode and screen and a single linear voltage ramp was applied to the sweep deflectors. Thus the photoelectrons which pass through the framing aperture form a streaked image at the screen, the width of which is directly related to the total exposure time of a frame.

The mask object shown in Fig. 6 was positioned at the camera input so

† See p. 617.

that half the photocathode was illuminated by a slit object while the other half was uniformly illuminated. For calibration purposes, part of the intensity of each amplified laser pulse was directed through an optical delay line which produced six subpulses each separated by 20 psec. With these subpulses incident on the camera, six photoelectron pulses were produced and swept across the aperture plate to produce a streak image at the framing tube screen. The expected and experimentally recorded streak images are both included in Fig. 6 where the exposed "shadow" of the lower half of the framing aperture contains data relating to the total exposure time while the upper half displays the temporal calibration. From this record the exposure time was calculated to be 190 psec, although shot-to-shot variations in the voltage ramp profile arising from amplitude fluctuations in the amplified laser pulses led to observed exposures slightly below and above this value.

The spatial resolution in the single frame has also been measured for this dynamic mode of framing operation. For this part of the work the slit mask object used in the streak calibration described above, was replaced by a standard USAF resolution test pattern which was illuminated directly (i.e., no optical delay line) by a portion of the amplified laser pulse intensity. A single GaAs photoconductive element was used to generate the voltage ramps applied to the sweep and compensation deflectors. The inverted polarity ramp for the latter was obtained by taking the voltage waveform from the sweep plates via a 50-Ω transmission line arrangement to the opposite plates of the compensation deflectors. The dependence of the recorded spatial resolution on the length of this transmission line has been found to be critical to within ± 5 mm although the spatial resolution can be optimized by fine tuning the overall image tube voltage through ~ 500 V.

A single frame recording of the USAF chart made under these dynamic conditions is reproduced in Fig. 7a. Although this does not represent the best spatial resolution that we have observed, the image has good contrast and the familiar features of this resolution chart are clearly visible. To encompass the entire format of the USAF test pattern a $\times 2$ demagnified copy was used as the object and the associated framed recording is included as Fig. 7b. It can be seen from these results that the image does not suffer noticeably from astigmatism or other spatial distortions. Examination of the original recordings on the photographic film indicates that it is possible to resolve the sixth element of group one on the demagnified chart which corresponds to a dynamic spatial resolution of 7 lp mm^{-1} at the screen (i.e., 10.5 lp mm^{-1} at the photocathode) of the framing image tube.

It must be emphasized, however, that for the single frames recorded to

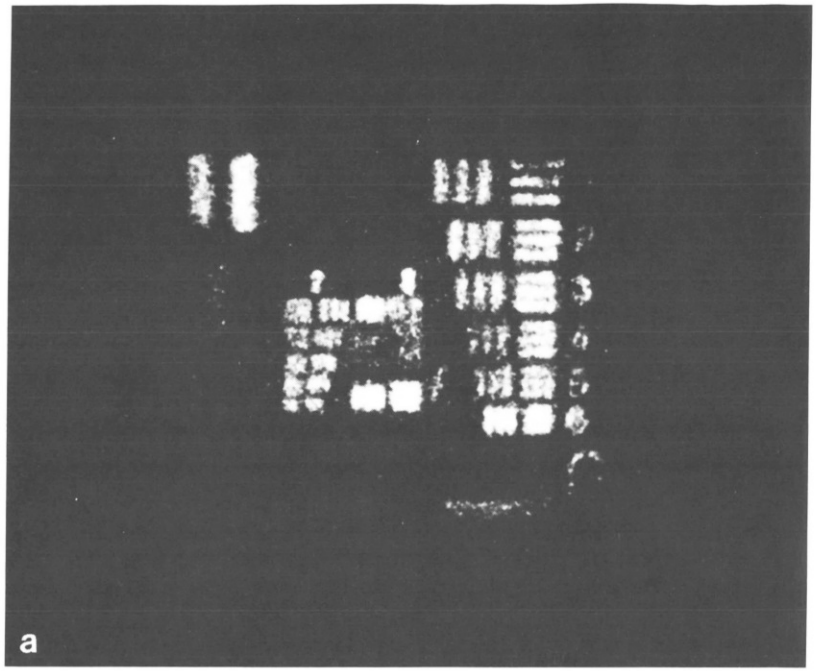

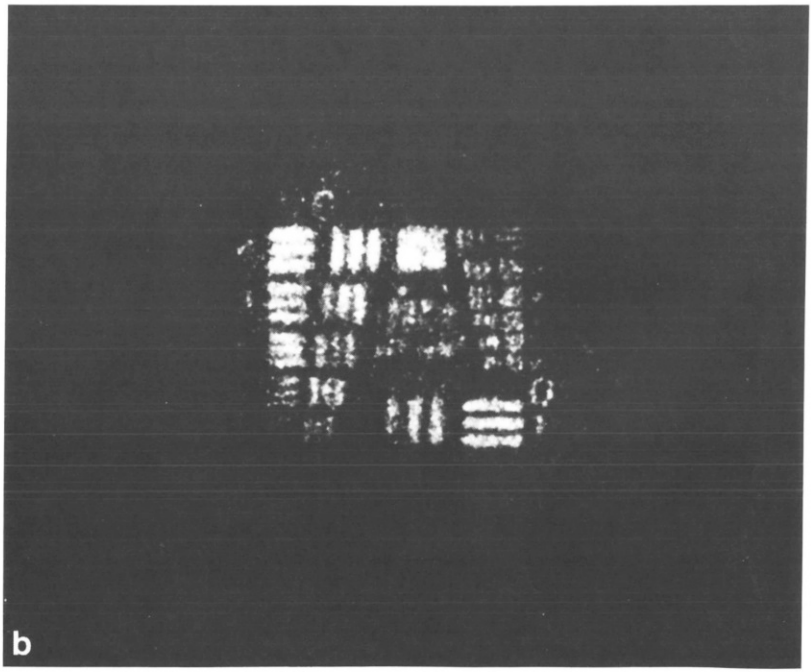

FIG. 7. Recorded two-dimensional, single frame images of (a) standard size USAF test chart object and (b) ×2 demagnified USAF test chart object.

date the camera has been illuminated with single light pulses having subpicosecond durations. So, although the framing aperture effectively remains "open" for ~190 psec the duration of the photoelectron signal is much shorter. This has the practical consequence of relaxing the constraints upon the linearity and synchronism of the deflection voltage ramps but exacerbating space charge problems[11] arising through the high photocurrents necessary to produce recordable image intensities. It must be conceded, therefore, that the dynamic spatial resolution may be slightly lower than that reported here when the camera is illuminated for longer durations (100 to 200 psec).

Conclusions

The results obtained so far relating to the static and dynamic performance of our Photochron framing camera indicate that it offers the facility for picosecond exposure times (<200 psec), good spatial resolution (~10 lp mm^{-1} at the photocathode), and low image distortions. In a future design the aperture diameter will be reduced from 1.9 to 1.5 mm while still retaining an acceptable cathode image size of at least 5×5 mm^2. When this modification is combined with the application of faster deflection speeds the frame exposure times are expected to be reduced to less than 100 psec. Other design aspects being considered include an X-ray version of the framing camera and the incorporation of an internal microchannel plate intensification stage similar to that in the Photochron IIA streak camera.[15] Evaluation of these and the multiple-frame operation of the present camera are the subject of our ongoing research in this area.

Acknowledgments

The financial support of the Paul Instrument Fund of The Royal Society and the Science and Engineering Research Council is gratefully acknowledged. One of us (M.R.B.) is supported by AWRE, Aldermaston, and another (R.T.E.) is supported by an SERC CASE studentship in collaboration with Thorn-EMI Electron Tubes Division, Ruislip, Middlesex. Particular thanks are due to Dr. M. C. Adams and Mr. P. Grigg of Thorn-EMI Electron Tubes Division for their major contributions toward the construction of the experimental framing image tube. We would also wish to thank Dr. P. G. May for his assistance with the dye laser/amplifier system during the evaluation of the camera performance.

References

1. Key, M. H., *Philos. Trans. R. Soc. London, Ser. A* **300**, 599 (1981).
2. Imacon 675 Technical Data Sheet, Hadland Photonics, Ltd., Bovingdon, Herts.
3. Cheng, J. C., Multhauf, L. G. and Tripp, G. R., *In* Proc. of 12th Int. Conf. on High Speed Photography and Photonics, p. 218 (1976).

4. Kalibjian, R. and Coleman, L. W., *In* Proc. of 13th Int. Conf. on High Speed Photography and Photonics, p. 447 (1978).
5. Lieber, A. J. and Sutphin, H. D., *Appl. Opt.* **18,** 745 (1979).
6. Laviron, E. and Delamare, C., *In* Proc. of 9th Int. Conf. on High Speed Photography and Photonics, p. 198 (1970).
7. Niu, H., Chao, T. and Sibbett, W., *Rev. Sci. Instrum.* **52,** 1190 (1981).
8. Hall, T. A., Kler, C. and McGoldrick, E., Rutherford Appleton Laboratory Report RL-83-043, Section 1.7.1 (1983).
9. Sibbett, W., Baggs, M. R. and Niu, H., *In* Proc. of 15th Int. Conf. on High Speed Photography and Photonics, p. 267 (1982).
10. Niu, H., Sibbett, W. and Baggs, M. R., *Rev. Sci. Instrum.* **53,** 563 (1982).
11. Niu, H. and Sibbett, W., *Rev. Sci. Instrum.* **52,** 1830 (1981).
12. Willson, J. P., Sibbett, W. and Sleat, W. E., *Opt. Commun.* **42,** 208 (1982).
13. May, P. G., Ph.D. Thesis, London University (1983).
14. Margulis, W., Sibbett, W. and Taylor, J. R., *Opt. Commun.* **35,** 153 (1980).
15. Sibbett, W., Sleat, W. E., Taylor, J. R. and Willson, J. P., *In* Proc. of 15th Int. Conf. on High Speed Photography and Photonics, p. 217 (1982).